Gabriela Sarti Kinker

Causas e consequências da heterogeneidade celular intratumoral
e o papel do sistema melatonérgico em tumores cerebrais

Causes and consequences of intratumoral cellular heterogeneity
and the role of the melatonergic system in brain tumors

São Paulo

2019

Gabriela Sarti Kinker

Causas e consequências da heterogeneidade celular intratumoral e o papel do sistema melatonérgico em tumores cerebrais

Causes and consequences of intratumoral cellular heterogeneity and the role of the melatonergic system in brain tumors

Doctoral Dissertation presented at the Institute of Biosciences, University of São Paulo, to obtain the title of Doctor of Sciences in the field of General Physiology.

Advisor: Pedro Augusto Carlos Magno Fernandes, PhD

São Paulo

2019

Judging Committee

_____
Prof. Dr.

_____
Prof. Dr.

_____
Prof. Dr.

_____
Prof. Dr.

To my family and friends.

*"Life isn't as serious as the mind
makes it out to be."*

Eckhart Tolle
(A New Earth: Awakening
to Your Life's Purpose)

Acknowledgments

To my family: I would first like to express my immeasurable gratitude to my parents for providing me a privileged childhood and an impeccable education. I am grateful for all their love and care, and for the financial and emotional support. I thank my mother Marcia for patiently introducing me to study techniques when I was under 10 years old, and for being such a fearless woman. I thank my father Walter for being an example of how to handle pressure and for always reminding me not to worry too much. Words simply cannot describe how grateful I am to my sister Camilla and my husband Iuri for being at my side every step of the way, making my life lighter, filling it with so much love and joy. I am also greatly appreciative of my grandparents, aunts, uncles and cousins.

To my advisors: I am deeply thankful to my mentors Dr. Pedro Fernandes and Prof. Regina Markus for sharing with me their creativity, love to science, and for sparing no efforts to help me grow as a scientist. I would like to express my gratitude to the time and resources they have invested in my training. I thank Pedro for always being available, encouraging me to think out of the box, and teaching me humanistic values. I thank Regina for all her enthusiasm and trust in my work, and for helping me build confidence and become a stronger woman. I am also greatly appreciative of my mentor Dr. Itay Tirosh, who has given me an amazing opportunity and taught me so much in a short period of time. I thank Itay for his constructive criticism, which has been significantly pushing my intellectual development in a very positive way.

To my friends and colleagues: Appreciation is due to all of those who have contributed to this journey. I thank all young scientist from the Department of Physiology (IB-USP) who have positively impacted my first steps in the lab, specially Dr. Sandra Muxel and Dr. Claudia Carvalho de Sousa, who I genuinely admire. I would like to knowledge my gratitude to Luiza Ostrowski, Debora Santos, Ray Takiguchi and Paula Ribeiro, who started as enjoyable co-workers and later became great friends. I am also grateful for all my friends at the Weizmann Institute of Science, Israel, specially Rony Chanoch and Alissa Greenwald, who I miss daily. I also thank Beatriz Brandt, Karina Otsuka and Luciana Verissimo for the decades of truthful friendship. Lastly, I am appreciative of my mentors Cecilia Oliveira and Lu Favoreto who have taught me transcending lessons through dance and provided me moments of mental escape.

Resumo

A plasticidade e heterogeneidade das células malignas têm papel fundamental sobre a progressão tumoral e o desenvolvimento de resistência terapêutica. Nos últimos anos, com o advento de tecnologias de sequenciamento de células individuais (scRNA-seq), estudos com diferentes tipos de câncer revelaram que um único tumor pode conter subpopulações de células malignas com perfis transcricionais distintos. Com isso, tornou-se necessário estabelecer modelos experimentais que permitam o estudo da relevância biológica e clínica dessa diversidade celular, bem como os mecanismos moleculares subjacentes. Nesse sentido, geramos dados de scRNA-seq para 198 linhagens celulares (22 tipos de câncer) e caracterizamos sistematicamente a heterogeneidade da expressão gênica. Descobrimos que a coexistência de subpopulações altamente distintas em uma mesma linhagem celular é rara. Por outro lado, padrões contínuos de heterogeneidade de expressão gênica, representados por espectros de estados celulares, são comuns, recorrem em diferentes linhagens, estão associados a múltiplos processos biológicos e são geralmente independentes da diversidade genética. Notavelmente, apesar de condições *in vitro* não possuírem um microambiente nativo e espacialmente variável, muitos dos padrões contínuos de heterogeneidade observados nas linhagens recapitulam aqueles encontrados em amostras tumorais clínicas, indicando que a plasticidade epigenética intrínseca tem papel fundamental na geração da heterogeneidade intratumoral. Os dados gerados também nos permitiram identificar as linhagens mais adequadas para o estudo da plasticidade celular. Como exemplo, selecionamos duas dessas linhagens modelos e demonstramos a dinâmica temporal e relevância terapêutica de um programa de heterogeneidade recorrente associado à senescência epitelial. Além disso, considerando os meios pelos quais as células malignas se comunicam, isto é, via interações físicas célula-a-célula e secreção de fatores solúveis, também buscamos explorar novas redes de sinalização autócrina/parácrina que possam ser exploradas clinicamente. A melatonina, mais conhecida como "hormônio da pineal", é uma molécula pleiotrópica produzida em diversos tecidos e que vem sendo cada vez mais reconhecida como um agente antitumoral. A melatonina atua por meio de vários mecanismos biológicos, incluindo a eliminação direta de radicais livres e a ativação de receptores de alta afinidade acoplados à proteína G (MT1 e MT2). Na última década, nosso grupo forneceu diversas evidências de que o ajuste fino da produção extrapineal de melatonina durante a inflamação aguda é crítico para a manutenção da homeostase tecidual. Entretanto, nosso conhecimento sobre o papel fisiopatológico da melatonina local em processos malignos é muito limitado. Interessantemente, demonstramos que, em gliomas, a capacidade das células de sintetizar e acumular melatonina correlaciona-se negativamente com o grau malignidade tumoral. Utilizando dados de expressão gênica, desenvolvemos um modelo preditivo do conteúdo de melatonina no microambiente tumoral, o índice ASMT:CYP1B1, o qual se mostrou um fator prognóstico positivo, independente do grau e subtipo histológico dos gliomas. Por fim, buscamos fornecer suporte adicional para o uso racional da melatonina e análogos no tratamento de cânceres cerebrais. Revelamos que em gliomas e meduloblastomas os receptores de melatonina MT1 e MT2 desempenham papéis opostos sobre o controle da progressão tumoral. Notavelmente, compostos que simultaneamente ativam MT1 e inibem MT2 exibiram um efeito antitumoral robusto *in vitro* e *in vivo*, destacando o potencial de tais receptores como alvos terapêuticos.

Palavras-chave: heterogeneidade celular intratumoral, plasticidade epigenética, Eixo Imune-Pineal, melatonina extrapineal, receptores de melatonina, gliomas.

Abstract

Tumor cell plasticity and heterogeneity are key features underlying disease progression and therapeutic resistance. Recent advances of single-cell RNA-seq (scRNA-seq) technologies have highlighted the co-existence of transcriptionally distinct subpopulations of malignant cells within single tumors of different lineages. Thus, there is now a need to establish frameworks to better understand the biological and clinical relevance of such cellular diversity, as well as its underlying molecular mechanisms. To address this issue, we generated scRNA-seq data for 198 cell lines (22 cancer types) and systematically characterized intra-cell line expression heterogeneity. We found that co-existence of highly distinct subpopulations within the same cell line is rare, while continuous patterns of expression heterogeneity, represented by spectra of cellular states are common, recur across different cell lines, are associated with multiple biological process, and are usually independent of genetic diversity. Notably, despite the absence of a native and spatially-variable microenvironment in vitro, many of the continuous programs observed in cell lines recapitulate those found in clinical samples, suggesting a prominent role of intrinsic epigenetic plasticity in generating intratumoral heterogeneity. The data also allowed us to prioritize specific cell lines as model systems of cellular plasticity. As an example, we selected two of such models to demonstrate the temporal dynamics and vulnerabilities associated with a cancer senescence program observed both in cell lines and in human tumors. Additionally, given the means by which malignant cells communicate in the tumor bulk, i.e. physical cell-to-cell interactions and secretion of soluble factors, we also aimed to explore new autocrine/paracrine signaling networks that could be exploited clinically. Melatonin, best known as the "pineal hormone", is a pleiotropic molecule produced by many extrapineal tissues and increasingly recognized as a tumor suppressor agent. Melatonin acts through several biological mechanisms, including direct scavenging of free radicals and activation of high-affinity G-protein coupled receptors (MT1 and MT2). Over the past decade, our group has provided compelling evidences that fine-tuning the extrapineal production of melatonin during acute inflammation is critical for the maintenance of tissue homeostasis. However, our knowledge about the pathophysiological role of local melatonin in malignant processes is very limited. Interestingly, here we demonstrated that the ability of gliomas to synthesize and accumulate melatonin negatively correlates with their overall malignancy. Using gene expression data, we designed a predictive model of the content of melatonin in the tumor microenvironment, the ASMT:CYP1B1 index, which was shown to be a positive prognostic factor, independent of glioma grade and histological subtype. Finally, as we sought to provide further support for the rational use of melatonin and analogous in brain cancer therapy, we demonstrated that in gliomas and medulloblastomas MT1 and MT2 melatonin receptors play opposite roles in disease progression. Remarkably, compounds that simultaneously activate MT1 and inhibit MT2 displayed a robust antitumor effect in vitro and in vivo, highlighting the potential of such receptors as therapeutic targets.

Keywords: intratumoral cellular heterogeneity, epigenetic plasticity, Immune-Pineal Axis, extrapineal melatonin, melatonin receptors, gliomas.

Contents

Introduction

Tumors as complex ecosystems

Cancer is increasingly recognized as a community in which malignant and non-malignant cells interact over time in a dynamic and often tumor-promoting manner (Balkwill et al., 2012). The diversity of these cells is a fundamental feature of tumor ecosystems and ultimately governs disease progression and clinical outcome (Binnewies et al., 2018; Hanahan & Coussens, 2012; Quail & Joyce, 2013). Tumors are infiltrated with different cell types, including fibroblasts, immune and endothelial cells, which collectively form the tumor microenvironment (Balkwill et al., 2012). In addition, malignant cells are themselves heterogenous, what poses a significant challenge to cancer therapy, as subpopulations of treatment resistant cells may underlie tumor recurrence and metastasis (Marusyk et al., 2012; McGranahan & Swanton, 2015; Pribluda et al., 2015). Various factors contribute to intratumoral heterogeneity, including genetic diversity, as subclonal mutations accumulate during tumor evolution (Gerlinger et al., 2012); spatial variability from extrinsic factors (e.g. oxygen and nutrients; Berglund et al., 2018); and intrinsic epigenetic plasticity related to developmental pathways, like those linked to stem cell differentiation (Tirosh, Venteicher, et al., 2016).

The comprehensive characterization of all cellular elements in the tumor ecosystem has been limited by technical reasons. Although methods such as standard multicolor flow cytometry/immunohistochemistry might allow the identification of distinct subpopulations of cells, they can hardly profile more than 10 proteins simultaneously (Dixon et al., 2015; Pedreira et al., 2013). Conventional DNA and RNA sequencing, on the other hand, provide genome-wide data and have shaped much of our current understanding of human tumors. However, protocols require bulk samples as input material, thereby revealing average cellular patterns (Ren et al., 2018; Tirosh & Suvà, 2019). Recent advances in single-cell sequencing have led to a paradigm shift in cancer research by allowing the study of human tumors at the resolution of individual cells. Over the past decade, single-cell high-throughput technologies have improved considerably from the initial proof-of-principle studies using chips or plates with limited cell numbers (Tang et al., 2009). For instance, recently developed systems based on droplet microfluidics that enable the profile of an

order-of-magnitude-more cells in each batch are gradually becoming standard in the field (Macosko et al., 2015). Despite the dramatic advances, substantial limitations and challenges still exist, including the requirement of fresh tumor samples and highly optimized processing protocols to maximize cell viability and data quality, and the reduced sequencing coverage (i.e. number of genes detected per cell; Ren et al., 2018; Tirosh & Suvà, 2019).

One of the ultimate goals of single-cell analyses is to link tumor subpopulations to distinct cell phenotypes, what is often accomplished using RNA sequencing. For example, studies of adult IDH-mutant oligodendrogliomas/astrocytomas (Tirosh, Venteicher, et al., 2016; Venteicher et al., 2017) and H3K27M-mutant pediatric midline gliomas (Filbin et al., 2018) suggest that such tumors harbor a developmental hierarchy, with stem-like cells capable of self-renewal and more differentiated cells that do not cycle. In melanomas, a subset of cells expressing high levels of the receptor tyrosine kinase AXL, a putative marker of drug resistance, and low levels of the master melanocyte transcriptional regulator MITF and its target genes (TYR, PMEL and MLANA), were shown to be resistant to RAF and MEK inhibitors (Tirosh, Izar, et al., 2016). Notably, the proportion of AXL-high cells appeared to increase in both tumors and cell lines upon treatment and recurrence (Tirosh, Izar, et al., 2016). Finally, in head and neck squamous cell carcinoma (HNSCC), cells with a prominent signal for partial epithelial-mesenchymal transition are located at the periphery of tumors and likely compose the invasive edge (Puram et al., 2017).

Networks of cell-to-cell communication

As multicellular organisms evolved, cells acquired diverse modes of cell-to-cell communication that allow the coordinated functioning of tissues (Pires da Silva & Sommer, 2003). Such interactions are critical for early embryonic development (Eichmann et al., 1997), as well as for the maintenance of adult organs (Chow et al., 2011; Festa et al., 2011). Intercellular communication relies on ligand-receptor interactions, where the ligand can either be a secreted soluble factor, or membrane-bounded, requiring physical proximity between the interacting cells (Pires da Silva & Sommer, 2003). Interactions trigger a chain of specific molecular events inside the cell, which ultimately leads to changes in transcription, translation, as well as modifications in protein folding, processing and localization. The specificity of such pathways depends on the

intensity of the signal and the cross-regulatory interactions with overlapping signal transduction cascades (Dumont et al., 2001).

Signaling by secreted molecules are frequently divided into three general categories according to the distance over which signals are transmitted. In endocrine signaling, the molecules (hormones) are secreted by specialized endocrine cells and carried through the circulation to act on target cells at distant body sites (Lodish et al., 2008). In humans, more than 30 different hormones are produced by endocrine glands, including the thyroid, adrenal, pituitary and pineal (Norman & Litwack, 1997). In autocrine and paracrine signaling, molecules act locally, activating receptors on the same cell and adjacent cells, respectively (Lodish et al., 2008). A recent study revealed that most cell types express tens to hundreds of ligands and receptors, creating a highly connected network of intracellular signal transduction (Ramilowski et al., 2015). More importantly, approximately two thirds of soluble ligands seem to be co-expressed with at least one of its cognate receptors in the same cell, revealing the potential extent of autocrine signaling (Ramilowski et al., 2015). Notably, disrupted autocrine/paracrine cell-to-cell interactions are increasingly recognized as major players controlling tumor progression (Butera et al., 2018; Pietras & Östman, 2010).

The soluble fraction of the tumor microenvironment include signaling molecules such as chemokines, interferons, interleukins, growth and angiogenic factors, which are synthesized by tumor, stromal and/or immune cells (Balkwill et al., 2012). Pro-inflammatory interleukins such as IL6 and IL8, produced either by malignant or stromal cells, have been shown to participate in feed-forward loops involving the nuclear factor κB (NFκB) and signal transducer and activator of transcription 3 (STAT3) oncogenic pathways and to promote tumor proliferation, survival, invasion and metastasis (Jayatilaka et al., 2017; Waugh & Wilson, 2008). Moreover, amplified activation of the endothelial growth factor receptor (EGFR), frequently observed in glioblastoma, lung and breast cancer, is a well-known driver of tumorigenesis and results from gene amplification, activating point mutations, and ligand overproduction (Sigismund et al., 2018). There are also factors such as TGF-β that play a complex and paradoxical role, varying by cell type and stage of tumorigenesis (Morikawa et al., 2016). In early stages, TGF-β may act as a tumor suppressor, inhibiting cell cycle progression and promoting apoptosis (Moses et al., 1990). Later, it may enhance invasion and metastasis by inducing epithelial-mesenchymal transition (Roberts & Wakefield, 2003).

Such signaling pathways represent cancer dependencies that can be exploit therapeutically. In this regard, the use of tyrosine kinase inhibitors (TKI) in patients with non-small cell lung cancer has provided the main example of the successes in targeting such oncogenic addiction, while disclosing the challenges of overcoming tumor resistance mechanisms (Murtuza et al., 2019). Tumors with activating EGFR mutations, approximately 15 to 20% of the cases, are sensitive to EGFR tyrosine kinase inhibitors (Pao & Chmielecki, 2010); and a paradigm shift emerged when these compounds showed improved efficacy to chemotherapy as initial therapy (Zhou et al., 2011). However, despite revolutionary advancements, patients who were sensitive to first- and second-line EGFR TKIs eventually progressed after approximately 9 to 11 months, due to acquisition of new EGFR mutations such as T790M (Sequist et al., 2011). Third-generation TKI osimertinib which precisely targets EGFR T790M resistant clones was recently granted full FDA approval, with data that demonstrate significant improvement in clinical endpoints (Soria et al., 2018). Such compounds illustrate the current focus of much anticancer drug development: targeted therapies interfering with specific molecular pathways that are central to particular cancers. Targeted therapies are a cornerstone of precision medicine and aim to provide more biologically-grounded and patient-tailored treatment regimens (Collins & Varmus, 2015).

Extrapineal melatonin and the Immune-Pineal Axis

As analytical methods increased in sensitivity and specificity, it has become apparent that some of the well-known "endocrine hormones" are not exclusively produced by specialized glands and can act as autocrine/paracrine signals in other tissues. For instance, pioneering works have shown that the local production of adrenal glucocorticoids by thymic epithelial cells play an important role in antigen-specific thymocyte development (Vacchio et al., 1994). Evidences also indicate the existence of extrapancreatic sources of insulin (Kojima et al., 2004) and glucagon (Lund & Knop, 2019). Additionally, during the past two decades, considerable attention has been paid to melatonin, the "pineal hormone". Melatonin is an ancient amphiphilic molecule present in a multitude of taxa, from bacteria to plants and animals (Tan et al., 2009). It was first isolated in the bovine pineal tissue in 1958 by Aaron B. Lerner, and named after its ability to lighten the skin of frogs by reversing the effects of melanocyte-stimulating hormone (Lerner et al., 1958). For a

number of years after its discovery, melatonin was considered to be exclusively produced by the pineal gland. Almost two decades later, the presence of melatonin synthesis enzymes was described in the retina and cerebellum of pinealectomized rodents (Bubenik et al., 1974; Cardinali & Rosner, 1971). Since then, diverse non-pineal sources of melatonin have been revealed (Acuña-Castroviejo et al., 2014).

Melatonin produced by the pineal gland during the night is best known for its role as the "hormone of darkness", translating the environmental dark phase to the organism and ensuring the synchronization of circadian and seasonal rhythms (Reiter, 1993). In mammals, melatonin biosynthesis includes four enzymatic steps, beginning with the hydroxylation of tryptophan to 5-hydroxytryptophan, which is then decarboxylated forming serotonin (Zhao et al., 2019). Serotonin is N-acetylated by serotonin N-acetyltransferase (AANAT) to form N-acetylserotonin (NAS). NAS is then converted to melatonin by the enzyme acetylserotonin-O-methyltransferase (ASMT). In the pineal gland, the temporal gating of nocturnal melatonin synthesis is determined by sympathetic innervations controlled by the central biological clock, the hypothalamic suprachiasmatic nuclei (Simonneaux & Ribelayga, 2003). In humans, as well as in rodents, the release of the norepinephrine during the night promotes the phosphorylation of AANAT through a cAMP-dependent, protein kinase A-mediated phosphorylation mechanism (Ackermann & Stehle, 2006). 14-3-3 chaperone proteins bind to PAANAT protecting it against proteasomal degradation, and inducing allosteric changes that result in increased enzymatic activity, and thus enhanced melatonin production (Klein et al., 2002).

Melatonin presumably emerged in primitive unicellular organism as a potent electron donor, detoxifying free radicals generated during the processes of photosynthesis and energetic metabolism (Tan et al., 2009). However, during evolution this indolamine became a pleiotropic molecule, despite its unchanged chemical structure. The broadening of its functional repertoire was accompanied by the emergence of specific binding sites/receptors and associated signaling transduction pathways. In mammals, many of the currently known activities of melatonin are mediated by the high-affinity G-protein coupled receptors MT1 and MT2 located in the plasma membrane (Reppart et al., 1996), although they have recently been detected also in the mitochondrial membrane (Ahluwalia et al., 2018; Suofu et al., 2017). Both receptors are typically coupled to $G_{i/o}$ proteins, inhibiting cAMP/protein kinase A signaling, while MT1 receptors might also be coupled to G_q proteins, activating the phospholipase C pathway (Brydon et al., 1999;

Jockers et al., 2016). In the cytosol, besides reducing oxidative stress, melatonin can also bind to calmodulin (Benítez-King & Antón-Tay, 1993), and to the enzyme quinone reductase 2, often designated as receptor MT3 (Nosjean et al., 2000).

Currently, known extra-pineal sources of melatonin include the brain, retina, lens, cochlea, Harderian gland, airway epithelium, skin, gastrointestinal tract, liver, kidney, thyroid, pancreas, thymus, spleen, carotid body, reproductive tract, immune and endothelial cells (Acuña-Castroviejo et al., 2014). Extra-pineal melatonin is not released into the circulation, acting locally in the maintenance of tissue homeostasis (Venegas et al., 2012). For instance, over the past decade, our group has provided compelling evidences that during acute inflammatory responses there is a transient switch in melatonin production from the pineal gland to peripheral organs/immunocompetent cells (Markus et al., 2013, 2018, 2007; Markus & Ferreira, 2011). This bidirectional communication, named the Immune-Pineal Axis, provides a framework for understanding the role of melatonin in the mounting and resolution of immune responses (de Oliveira Tatsch-Dias et al., 2013; Pontes et al., 2006).

The nocturnal rise of melatonin is known to impair leukocyte transendothelial migration to the site of tissue damage/infection, a fundamental step of innate immunity (Lotufo et al., 2001; Marçola et al., 2013; Tamura et al., 2010). In pinealocytes, pathogen- and danger-associated molecular patterns bind to pattern recognition receptors and promote the nuclear translocation of the transcription factor NFκB, a classical regulator of inflammation (Carvalho-Sousa et al., 2011; Da Silveira Cruz-Machado et al., 2010). In the nucleus, transactivation domain-free NFκB dimers p50/p50 block the expression of *Aanat* and hence the nighttime production of melatonin, facilitating leukocyte rolling and adhesion to the endothelial layer at the site of inflammation (Carvalho-Sousa et al., 2011; Da Silveira Cruz-Machado et al., 2010; Fernandes et al., 2006). During inflammation initiation, simultaneous activation of glucocorticoid receptors (GR) and adrenoceptors α_1 and β_1 in the pineal gland contributes to the blockage of melatonin production (Fernandes et al., 2017). During the resolution phase, on the other hand, as the sympathetic tonus decreases, GR activation (Fernandes et al., 2017), associated with others immune signals such as interferon-gamma (Barbosa Lima et al., 2019), induces *Aanat* transcription and allows the restoration of the nighttime production of melatonin.

At the site of inflammation, activated macrophages start to produce melatonin upon induction of *Aanat* expression by NFκB dimers containing transactivation domains (p50/RelA and cRel/RelA) (Muxel et al., 2016, 2012; Pires-Lapa et al., 2013). In this context, melatonin acts autocrinally/paracrinally reducing oxidative stress, potentiating phagocytoses and inhibiting bacterial proliferation. Similarly, acute neuroinflammation induced by lipopolysaccharide injected directly into the lateral ventricles of adult rats promotes the synthesis of melatonin by astrocytes and microglia in the cerebellum, though not in the cortex or hippocampus (Pinato et al., 2015). Interestingly, lipopolysaccharide treatment leads to neuronal death in the hippocampus and cortex, but not in the cerebellum. This privileged protection of cerebellar cells is abrogated by blocking melatonin receptors, suggesting that the local production of melatonin protects cerebellar neurons from neuroinflammation-induced cytotoxicity (Pinato et al., 2015).

Melatonin and cancer

In 2007, based on robust mechanistic evidence coming from well-designed experimental studies, the International Agency for Research on Cancer Working Group classified night shift work involving circadian disruption as probably carcinogenic to humans (Group 2A) (IARC Monographs Vol 124, 2019). For instance, exposure to constant light was shown to induce the development of metabolic syndrome and spontaneous tumorigenesis, and shorten the life span of both male and female rats, adverse effects shown to be prevented by the administration of melatonin in nocturnal drinking water (Anisimov et al., 2012). In human breast cancer xenografts, exposure to increasing intensities of white fluorescent light during each 12-hour dark phase result in a dose-dependent suppression of nocturnal melatonin blood levels and a stimulation of tumor growth and linoleic acid uptake/metabolism to the mitogenic molecule 13-hydroxyoctadecadienoic acid (Blask et al., 2005). Importantly, human breast cancer xenografts perfused in situ with physiologically melatonin-rich blood collected from health female volunteers during the night exhibited markedly suppressed proliferative activity compared to those perfused with melatonin-depleted blood collected following exposer to light at night (Blask et al., 2005).

Over the past 30 years, accumulating evidence has outlined the relevance of melatonin to human physiology and pathology. Slow release melatonin (Circadin) and several melatonin

analogues (e.g. Ramelteon, Agomelatine and Tasimelteon) are currently used clinically for the resynchronization of circadian rhythms during jet lag and shift work, and for managing insomnia, depression, and non-24-h sleep-wake disorder (Liu et al., 2016). Additionally, the potential of melatonin as an anticancer agent has gained increasing attention, and the growing number of supporting in vitro and in vivo experimental studies include a wide variety of tumors, such as, melanoma, glioma, sarcoma, as well as cancers of breast, ovary, cervix, and prostate (Cutando et al., 2012; Li et al., 2017). As a pleiotropic molecule, melatonin has been documented to act through several biological mechanisms, including: inhibition of glioma cell migration/invasion by direct scavenging intracellular free radicals and impairing the reactive oxygen species-dependent NFκB oncogenic signaling (Wang et al., 2012); induction of apoptosis of colorectal cancer cells through inactivation of calmodulin-dependent protein kinase II, followed by dephosphorylation and nuclear import of histone deacetylase 4 (Wei et al., 2015); and suppression of estrogen receptor alpha mRNA expression and transcriptional activity in breast cancer cells via MT_1 receptor activation (Girgert et al., 2009; Mao et al., 2010).

Despite the extensive list of promising basic research studies conducted in the past decades, at present, completed clinical trials focusing on melatonin and cancer sum up to only 20, 16 of which were carried out at the Institute of Biological Medicine in Milan, Italy (González et al., 2019). Overall, melatonin seems to effectively improve the quality of life of patients receiving radio and/or chemotherapy by normalizing sleep and relieving symptoms such as pain, asthenia, and anorexia (González et al., 2019). Although individual trials with hepatocellular carcinoma (Yan et al., 2002), glioblastomas (Lissoni et al., 1996), colorectal (Cerea et al., 2003), and lung cancers (Lissoni et al., 2003) have suggested that melatonin, given as an adjuvant, can also significantly increase tumor remission rate and patient overall survival, data are still limited and show inconsistencies in more recent studies (Berk et al., 2007; Sookprasert et al., 2014). There is thus a clear necessity for further large-scale and multi-center randomized clinical trials. Additionally, as rational therapies that interfere with specific molecules become the focus of anticancer drug development, the roles of MT1 and MT2 melatonin receptors as relevant targets should be explored.

Objectives

Over the past few years, single-cell RNA-seq (scRNA-seq) studies of different cancer types have highlighted the heterogeneity among malignant cells within single tumors. Thus it is now crucial to establish frameworks to better understand the biological and clinical relevance of such cellular diversity, as well as its underlying molecular mechanisms. In this sense, although human cell lines have been a cornerstones of cancer research, their value as models of intratumoral heterogeneity remains largely unknown. To comprehensively address this issue, we generated scRNA-seq data for 198 cell lines (22 cancer types, 53,513 cells) from the Cancer Cell Line Encyclopedia (CCLE) collection and systematically characterized intra-cell line expression heterogeneity. We uncovered recurrent programs of heterogeneity and i) determined their similarity to programs of intratumoral heterogeneity previously described in clinical samples; ii) evaluated their association with mutations and drug sensitivities; and iii) investigated their dependency on genetic variability. Finally, we select two optimal cell lines to model a recurring program associated with partial epithelial senescence. We demonstrated the dynamics, regulation, and vulnerabilities associated with this program, highlighting its role in driving phenomena such as drug resistance.

Additionally, we aimed to explore autocrine and paracrine signaling mediating the communication among the diverse malignant cells in the tumor ecosystem, thereby looking for new molecular networks that could be exploited clinically. It is now clear that fine-tuning the extrapineal production of melatonin is critical for the maintenance of an internal steady state within tissues, as illustrated by the Immune-Pineal Axis. However, our knowledge of the pathophysiological role of local melatonin in malignant processes remains very limited. Thus, here, we comprehensively characterized the melatonergic system of human gliomas, the most common primary brain tumor in adults and one of the deadliest malignant neoplasms. We investigated the association between the capacity of glioma cells to synthesize and accumulate melatonin in the surrounding microenvironment and their overall malignancy as well as patient survival. We also further elucidated differential effects of MT1 and MT2 receptors activation, highlighting the therapeutic potential of specific melatonergic agonists/antagonist in the treatment of brain cancers.

Chapter 1

The landscape of intratumoral cellular heterogeneity

Pan-cancer single-cell RNA-seq uncovers recurring programs of cellular heterogeneity

Gabriela S Kinker*[1,3], Alissa C Greenwald*[1], Rotem Tal[1], Zhanna Orlova[1], Mike S Cuoco[2], James McFarland[2], Allie Warren[2], Chris Rodman[2], Danielle Dionne[2], Jennifer Roth[2], Samantha Bender[2], Bhavna Kumar[4], James W Rocco[4], Pedro ACM Fernandes[3], Chris C Mader[2], Hadas-Keren-Shaul[5,6], Alexander Plotnikov[5], Haim Barr[5], Aviad Tsherniak[2], Orit Rozenblatt-Rosen[2], Valery Krizhanovsky[1], Sidharth V. Puram[7], Aviv Regev[2], Itay Tirosh[1,#]

[1]Dept. of Molecular Cell Biology, Weizmann Institute of Science, Rehovot, Israel
[2]Broad Institute of MIT and Harvard, Cambridge, MA, USA
[3]Institute of Bioscience, University of Sao Paulo, Sao Paulo, Brazil
[4]The Ohio State University Wexner Medical Center, Columbus, OH USA
[5]The Nancy & Stephen Grand Israel National Center for Personalized Medicine, Weizmann Institute of Science, Rehovot, Israel
[6]Life Science Core Facility, Weizmann Institute of Science, Rehovot, Israel
[7]Department of Otolaryngology, Washington University School of Medicine, St. Louis, USA

* Equal co-authors
# corresponding author: itay.tirosh@weizmann.ac.il

Abstract

Cultured cell lines are the workhorse of cancer research, but it is unclear to what extent they recapitulate the cellular heterogeneity observed among malignant cells in tumors, given the absence of a native microenvironment in vitro. Here, we used multiplexed single-cell RNA-seq to profile ~200 cancer cell lines (53,513 cells, 22 cancer types). We uncovered expression programs that are recurrently heterogeneous within many cancer cell lines and are largely independent of the observed genetic diversity. These programs of heterogeneity are associated with diverse biological processes, including cell cycle, senescence, stress and interferon responses, epithelial-to-mesenchymal transition, and protein maturation/degradation. Notably, some of these recurrent programs recapitulate those seen in human tumors, suggesting a prominent role of intrinsic plasticity in generating intratumoral heterogeneity. Moreover, the data allowed us to prioritize specific cell lines as model systems of cellular plasticity. We used two of such models to demonstrate the dynamics, regulation and vulnerabilities associated with a cancer senescence program observed both in cell lines and in human tumors. Overall, our work describes the landscape of cancer cell diversity, identifying major patterns of expression heterogeneity that are shared between tumors and specific cell lines and can thus be further explored in follow up studies.

Introduction

Cellular plasticity and heterogeneity are fundamental features of human tumors driven by both genetic and epigenetic mechanisms (Chaffer et al., 2016; McGranahan and Swanton, 2015). Malignant cells within a single tumor display diverse patterns of gene expression, which underlie differences in morphology, metabolism, proliferation, invasion and immunogenicity. The existence of cells with multiple phenotypes plays a major role in disease progression and treatment failure, as subpopulations of cells may drive tumor recurrence and metastasis. Thus, it is critical for cancer research to establish frameworks to characterize cellular diversity within tumors, as well as the underlying mechanisms that generate such diversity.

Single-cell RNA sequencing (scRNA-seq) has emerged as a valuable tool to study cell-to-cell heterogeneity within tumors (Chung et al., 2017; Filbin et al., 2018; Kim et al., 2016; Lambrechts et al., 2018; Li et al., 2017; Patel et al., 2014; Puram et al., 2017; Tirosh et al., 2016a; Tirosh et al., 2016b; Venteicher et al., 2017). Several studies identified functionally significant patterns of intratumoral heterogeneity (ITH) within malignant cells, yet their origin and mechanisms were difficult to resolve from observations in patients. In principle, genetic diversity, epigenetic cell-intrinsic plasticity, and interactions with the spatially-variable tumor microenvironment all contribute to the heterogeneity observed across malignant cells. However, since previous studies suggest that major patterns of expression heterogeneity in tumors are linked to their cell-of-origin and recapitulated in cell lines, we hypothesize that they may reflect intrinsic cellular plasticity that exists even in the absence of genetic diversity and a native microenvironment. For example, we previously reported an EMT-like program associated with metastasis in head and neck squamous cell carcinoma (HNSCC) that was partly preserved in one of a number of tested cell lines (Puram et al., 2017). Similarly, drug-resistance melanoma programs identified in tumors were recapitulated and studied in melanoma cell lines (Jerby-Arnon et al., 2018; Shaffer et al., 2017; Tirosh et al., 2016a).

Human cell lines are a mainstay of cancer research and drug discovery, yet our current knowledge of their ability to recapitulate the expression diversity observed in patient samples is limited. Only a few cancer cell lines have been comprehensively profiled by scRNA-seq so far (Ben-David et al., 2018; Jerby-Arnon et al., 2018; Kim et al., 2015; Sharma et al., 2018). Thus, models are often chosen based on their mutational status, historical popularity, and ease of culturing. To address this issue, here, we apply multiplexed scRNA-seq to profile 198 cell lines from 22 tumor types in the Cancer Cell Line Encyclopedia (CCLE) collection (Barretina et al., 2012; Ghandi et al., 2019). Analysis of expression heterogeneity within cell lines revealed patterns of variability that recurred across different cell lines, and spanned diverse biological functions. Strikingly, many of these variable programs observed in vitro matched those previously characterized in fresh tumors. We used these results to select model cell lines and utilize them for follow up studies, demonstrating the dynamics, regulation and drug sensitivities associated with a recurrent expression program linked to cellular senescence. Likewise, this

dataset provides a resource for the rational selection of cancer cell lines as models for exploring the determinants and consequences of ITH.

Results

Pan-cancer scRNA-seq of human cell lines

To effectively profile expression heterogeneity within diverse cancer cell lines, we developed and applied a multiplexing strategy where cells from different cell lines are grown and profiled in pools and then computationally assigned to the corresponding cell line (**Fig. 1A**). We utilized existing pools that were previously generated from the CCLE collection (Barretina et al., 2012; Yu et al., 2016). Each pool consisted of 24-27 cell lines from diverse lineages but with comparable proliferation rates, and was profiled by massively parallel scRNA-seq, for an average of 280 cells per cell line (**Methods**). We profiled eight CCLE pools, along with one smaller custom pool that included HNSCC cell lines.

We assigned profiled cells to cell lines based on consensus between two complementary approaches, using genetic (SNP) and expression profiles (**Fig. 1A**). First, cells were clustered by their global expression profile, and each cluster was mapped to the cell line with most similar bulk RNA-seq profile (Ghandi et al., 2019). Second, by detection of SNPs in the scRNA-seq reads, we assigned cells to the cell line with highest similarity by SNP profiles derived from bulk RNA-seq (Ghandi et al., 2019; Kang et al., 2018). Cell line assignments based on gene expression and SNPs were consistent for 98% of the cells, which were retained for further analysis (e.g. **Fig. 1B**). The few inconsistent assignments were observed primarily in cells with low data quality, resulting in low SNP coverage, which were therefore excluded. Cell lines with less than 50 assigned cells were also excluded from further analyses, as were low-quality cells and suspected doublets.

Overall, following assignment and quality control filters, we studied the expression profiles of 53,513 cells, from 198 cell lines (56-1,990 cells per cell line), reflecting 22 cancer types (**Fig. 1C**; **Table S1**). We detected an average of 19,264 UMIs and 3,802 genes per cell, underscoring the high quality of our dataset.
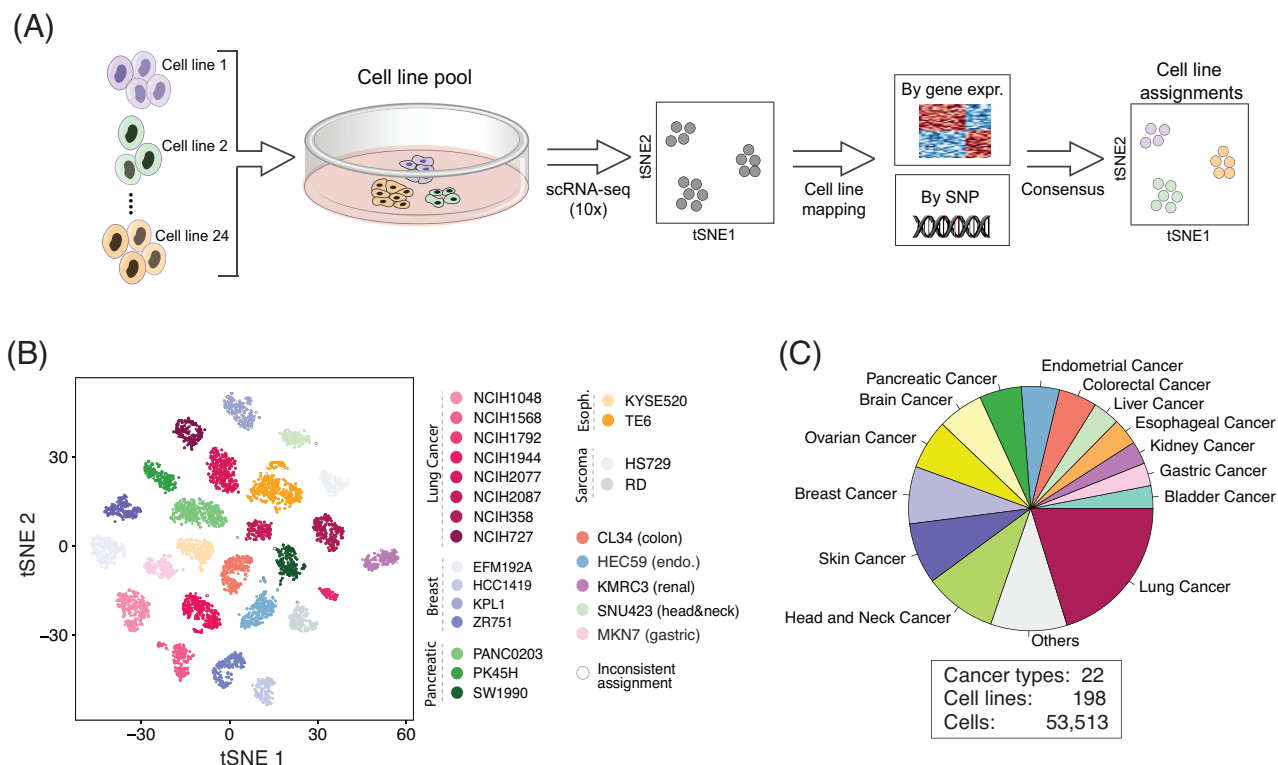
Figure 1. **Characterizing intra-cell line expression heterogeneity by multiplexed scRNA-seq**. (**A**) Workflow of the multiplexing strategy used to profile multiple cell lines simultaneously. Cell lines were pooled and profiled by droplet-based scRNA-seq. We used reference CCLE data to assign cells to the most similar cell line based on their overall gene expression and SNP pattern. (**B**) tSNE plot of a representative pool demonstrating the robustness of cells' assignments to cell lines. Cells with inconsistent assignments (by gene expression and SNPs) were excluded from further analyses. (**C**) Distribution of cancer types profiled.

Discrete and continuous patterns of expression heterogeneity within cell lines

We aimed to characterize the variation in gene expression across cells within individual cell lines, distinguishing between discrete patterns, reflecting highly distinct subpopulations of cells, and continuous patterns, reflecting spectra of cellular states (**Fig. 2A**). To identify discrete subpopulations, we used dimensionality reduction (t-Distributed Stochastic Neighbor Embedding, tSNE) followed by density-based clustering (DBSCAN; **Fig. S1A; Methods**). Discrete clusters of cells within a cell line were found only for a minority (11%) of the cell lines: three cell lines had three or more clusters, three had two clusters of comparable sizes, and 16 had one major and one minor cluster (**Fig. 2B and S1B**). For each such cluster, we identified the top 50 upregulated genes compared to all other cells from the same cell line (**Table S2**). These expression programs showed limited similarities to one another, both within cell lines of the same cancer type and across different cancer types, indicating that discrete subpopulations are typically unique and cell line-

specific (**Fig. 2C**). The main exceptions were seven subpopulations commonly upregulating the expression of cell cycle-related genes, and six subpopulations commonly upregulating the expression of stress response genes. Similar results were obtained using DBSCAN with different parameters (**Fig. S1C-D**).

To also identify continuous variability of cellular states, we applied non-negative matrix factorization (NMF) to each cancer cell line (Puram et al., 2017). We repeated the NMF analysis with distinct parameters to identify robust expression programs (i.e. consistently observed as variable using different parameters), each defined by the top 50 genes based on NMF scores (e.g., **Fig. 2D**; **Methods**). This procedure captures both continuous and discrete programs. Overall, we detected 1,445 robust expression programs across all cell lines, with 4-9 such programs in individual cell lines (**Fig. S1E**; **Table S3**). To identify common expression programs varying within multiple cell lines, we first excluded those with limited similarity to all other programs as well as those associated with the technical confounder of variable cell quality (**Fig. S1F**), retaining 800 programs (0-8 per cell line, **Fig. S1E**). Of these programs, only 4.75% corresponded to the discrete subpopulations described above (**Fig. 2E**).

Hierarchical clustering of the NMF programs based on their shared genes emphasized multiple recurrently heterogeneous programs (RHPs) of gene expression, which are present in multiple cell lines. The two most prominent RHPs reflected the cell cycle, and 10 additional RHPs were associated with other cellular processes (**Fig. 2E**; **Table S4**). The cell cycle RHPs corresponded to the G1/S and the G2/M phases (**Fig. 2E**), as was also observed in clinical tumor samples (**Fig. S2A**). G2/M programs were similar across cell lines, as well as between cell lines and tumors, thus defining a generic mitotic program (**Fig. S2B**). In contrast, G1/S programs differed more both across cell lines and between cell lines and tumors (**Fig. S2B**), indicating that expression programs associated with genome replication are more context-dependent. A central difference in G1/S programs involved the MCM complex genes (MCM2-7) and the linker histone H1 family genes (HIST1H1B-E), which were robustly upregulated only in tumors or cell lines, respectively (**Fig. S2B,D**). This may reflect an in vitro adaptation to rapid growth and loss of the G1 checkpoint in cell lines. Consistent with this possibility, while tumors have a high percentage of apparent G0 cells (i.e., lacking both G1/S and G2/M expression programs), such cells are much less prevalent in cell lines (**Fig. S2E**).
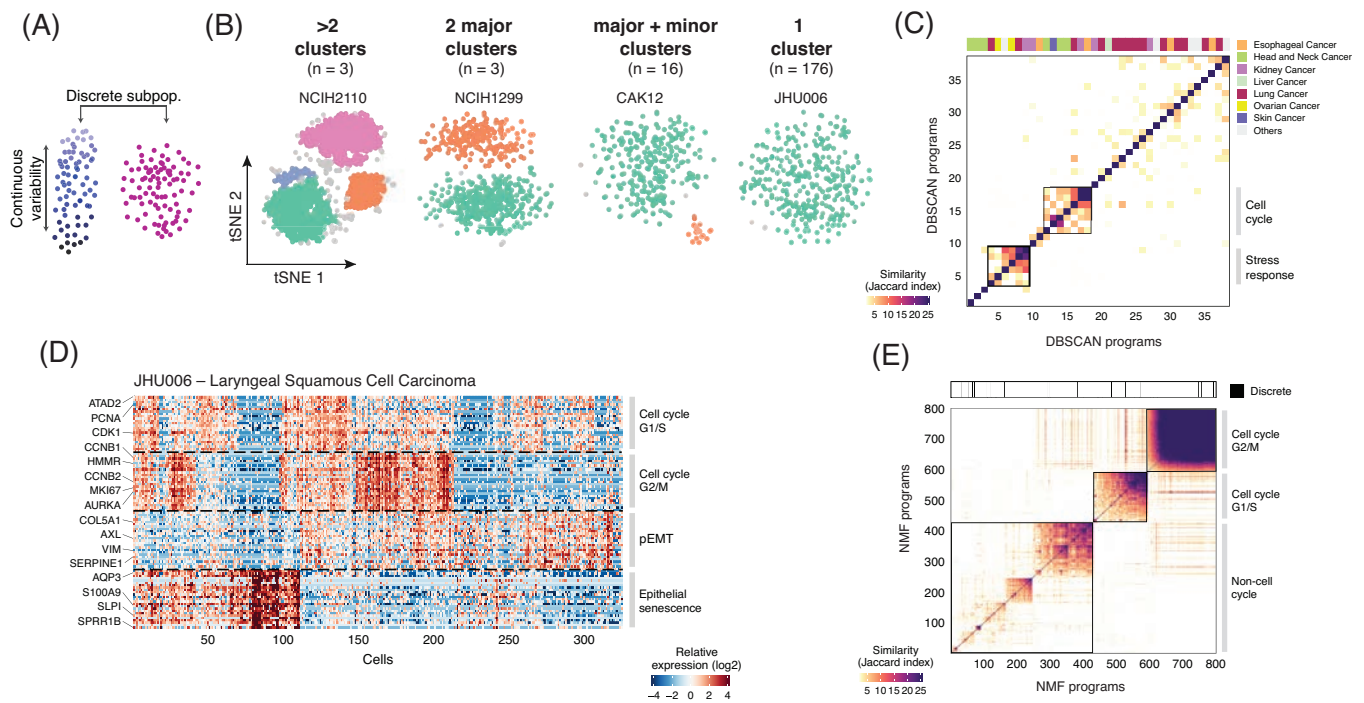
Figure 2. Discrete and continuous patterns of intra-cell line expression heterogeneity. **(A)** Illustration of the two types of expression variability investigated. **(B)** tSNE plots show exemplary cell lines for the four classes defined by the presence and number of discrete subpopulations identified using DBSCAN with optimized parameters (eps = 1.8, MinPts = 5, see **Fig. S2A**). The description of each class and number of cell lines is indicated above the tSNE plots. **(C)** Heatmap depicts pairwise similarities between gene expression programs defined for each of the cell clusters derived from the 22 cell lines identified as having one or more discrete subpopulations. Hierarchical clustering identifies only two coherent groups of programs (metaprograms). Top panel shows assignment to cancer types. **(D)** Continuous programs of heterogeneity identified using NMF in a representative cell line that lacks discrete subpopulations (JHU006; see **Fig. 2B**). Heatmap shows relative expression of genes from four programs across all JHU006 cells. NMF programs are annotated (right) and selected genes are indicated (left). Cells were ordered by hierarchical clustering. **(E)** Pairwise similarities between NMF programs identified across all the cell lines analyzed and ordered by hierarchical clustering. Programs with limited similarity to all other programs as well as those associated with technical confounders were excluded. Top panel indicates the 4% of NMF programs that were consistent with discrete subpopulations identified by DBSCAN.

RHPs reflect distinct biological processes and mirror in vivo cellular states

The 10 additional (non-cell cycle) RHPs reflected diverse biological processes, and are described further below. Importantly, i) the similarity between NMF programs was largely independent of the pools in which they were detected (**Fig. S3A**); ii) RHPs were each detected in

at least four different pools (**Fig. S3B**); and iii) a single cell line had highly similar NMF programs when profiled in two distinct pools (**Fig. S3C**). Thus, the pooling approach had a limited impact on defining heterogeneity within individual cell lines and RHPs are robustly identified across pools.

We characterized these 10 RHPs by functional enrichment of their signature genes, the lineages and mutations of cell lines in which they are observed, as well as their similarity with programs that vary across cells in patient tumor samples (**Fig. 3A-C**). Overall, 7 out of 10 RHPs resemble the heterogeneity observed in human tumor samples, including 5 RHPs with particularly high similarity (**Fig. 3B, S4A,B**), demonstrating the in vivo relevance of cell line RHPs. One of these RHPs (#8) reflected stress response, including DNA damage-induced and immediate early genes (e.g. DDIT3-4 and ATF3). RHP #8 resembles programs of heterogeneity previously observed in melanoma and HNSCC tumors (**Fig. 3B,D**) (Puram et al., 2017; Tirosh et al., 2016a), and may reflect the response to various cellular insults.

RHP (#4) contained interferon (IFN) response genes (e.g., IFT1-3 and ISG15,20) and was depleted in cell lines with mutations in MRE11A (**Fig. S5B**), which recognizes cytosolic dsDNA and activates STING (Kondo et al., 2013). Accordingly, recent studies revealed that IFN response may be triggered by genomic instability through the cGAS-STING pathway (Chen et al., 2016). Two other RHPs (#9 and #10) consisted of genes related to protein folding and maturation (e.g. HSPA1A, RPN2) and to proteasomal degradation (e.g. PSMA3-4), respectively. These RHPs, as well as the IFN response RHP #4, did not resemble the in vivo programs of heterogeneity observed previously among tumor cells. However, it is possible that such programs exist in vivo and have not been detected yet due to the limited number of studies.

RHPs recapitulate in vivo EMT programs and are associated with NOTCH mutations

Three distinct RHPs were related to EMT: two shared across cancer types, and one unique to melanoma cell lines. The melanoma-specific EMT (RHP #2; EMT-I) was negatively correlated with another melanoma-specific RHP (#1) that was enriched with skin pigmentation genes (e.g., MITF and PMEL). Both of these melanoma-specific RHPs, and their negative correlation, recapitulated the patterns of variability previously observed in melanoma tumors (**Fig. 3B,D, S4B,C**), in which they were linked to drug resistance (Shaffer et al., 2017; Tirosh et al., 2016a). Notably, as observed in patient samples, many of the melanoma cell lines (50%; **Table S2**) harbored cells in both of these alternate cellular states, yet our data highlight certain melanoma cell lines as faithful model systems for these in vivo-related RHPs (**Fig. S5A, S4C**).

Two other RHPs, EMT-II (#3) and EMT-III (#5), also reflected EMT-like processes in distinct cell lines. EMT-II was mainly observed in HNSCC cell lines (**Fig. 3A**), although across 7 distinct pools (**Fig. S3B**). It included vimentin (VIM), fibronectin (FN1), the AXL receptor tyrosine kinase, and other genes, closely mirroring the partial EMT (pEMT) state we previously observed in HNSCC tumors (**Fig. 3B,D, S4B,C**), where it was linked to metastasis (Puram et al.,

2017). Cell lines harboring EMT-II were depleted of NOTCH4 mutations (**Fig. S5B**) and were sensitive to inhibitors of NOTCH signaling (**Fig. S5D**), suggesting a potential role of such pathway in enabling EMT-II variability. This is similar to the association we found in glioblastoma between specific mutations and patterns of intratumoral heterogeneity (Neftel et al., 2019). In contrast, EMT-III was enriched among non-cycling cells (**Fig. S5C**) and contained genes involved in cell junction organization such as laminin A3, B3 and C3, and plakoglobin (JUP). Interestingly, JUP was shown to promote collective migration of circulating tumor cells with increased metastatic potential (Aceto et al., 2014). The identification of three distinct EMT programs, two of which are enriched in specific cancer types, highlights EMT as a common, yet context-specific, pattern of cellular heterogeneity, which may have important implications for metastasis and drug responses.

RHPs recapitulate classical and epithelial senescence programs

RHPs #6 and #7 were preferentially observed in G0 cells (**Fig. S5C**) and seem to reflect different expression programs of cellular senescence. RHP #6 was enriched in p53-wild type cell lines and in those sensitive to the pharmacological activation of p53 by the MDM2 inhibitor Nutlin-3a (**Fig. S5B,D**). Moreover, it included the senescence mediator p21 (CDKN1A) and other p53-target genes. Thus, we annotated it as "classical" p53-associated senescence. In contrast, RHP #7 was enriched in HNSCC cell lines, and was highly similar to the senescence program of keratinocytes (Hernandez-Segura et al., 2017) (**Fig. 3A,B**). RHP #7 also contained many secreted factors, such as S100A8/9, SAA1/2, LCN2, SLPI, which are involved in inflammatory responses and are reminiscent of the Senescence-Associated Secretory Phenotype (SASP). To further examine the possibility that RHP #7 reflects a senescence program despite the lack of classical markers (e.g., p16 and p21), we profiled primary lung bronchial cells by bulk RNA-seq after induction of senescence by etoposide. Etoposide-treated cells stained for the senescence marker SA-β-GAL (**Fig. S5E**) and, compared to control, upregulated the expression of genes of both senescence-associated RHPs (#6 and #7) and downregulated the expression of cell cycle genes (**Fig. S5D**).

Hence, RHP #7 resembles the senescence response of both keratinocytes and lung bronchial cells, while it differs from published senescence signatures of fibroblasts and melanocytes (Hernandez-Segura et al., 2017), underscoring the context- and cell type-specificity of senescence expression programs. We therefore denote it as an epithelial senescence (EpiSen) program. Notably, the EpiSen RHP recapitulates a program we previously observed in HNSCC tumors (**Fig. 3B,D, S4B,C**), which was also negatively associated with cell cycle and spatially restricted to the hypoxic tumor core (Puram et al., 2017). We conclude that programs of cell-cycle arrest are observed in subpopulations of cells in tumors and in cell lines, and are associated with distinct expression profiles depending on genetics (e.g., p53 status), lineage (e.g., HNSCC), and possibly other features.
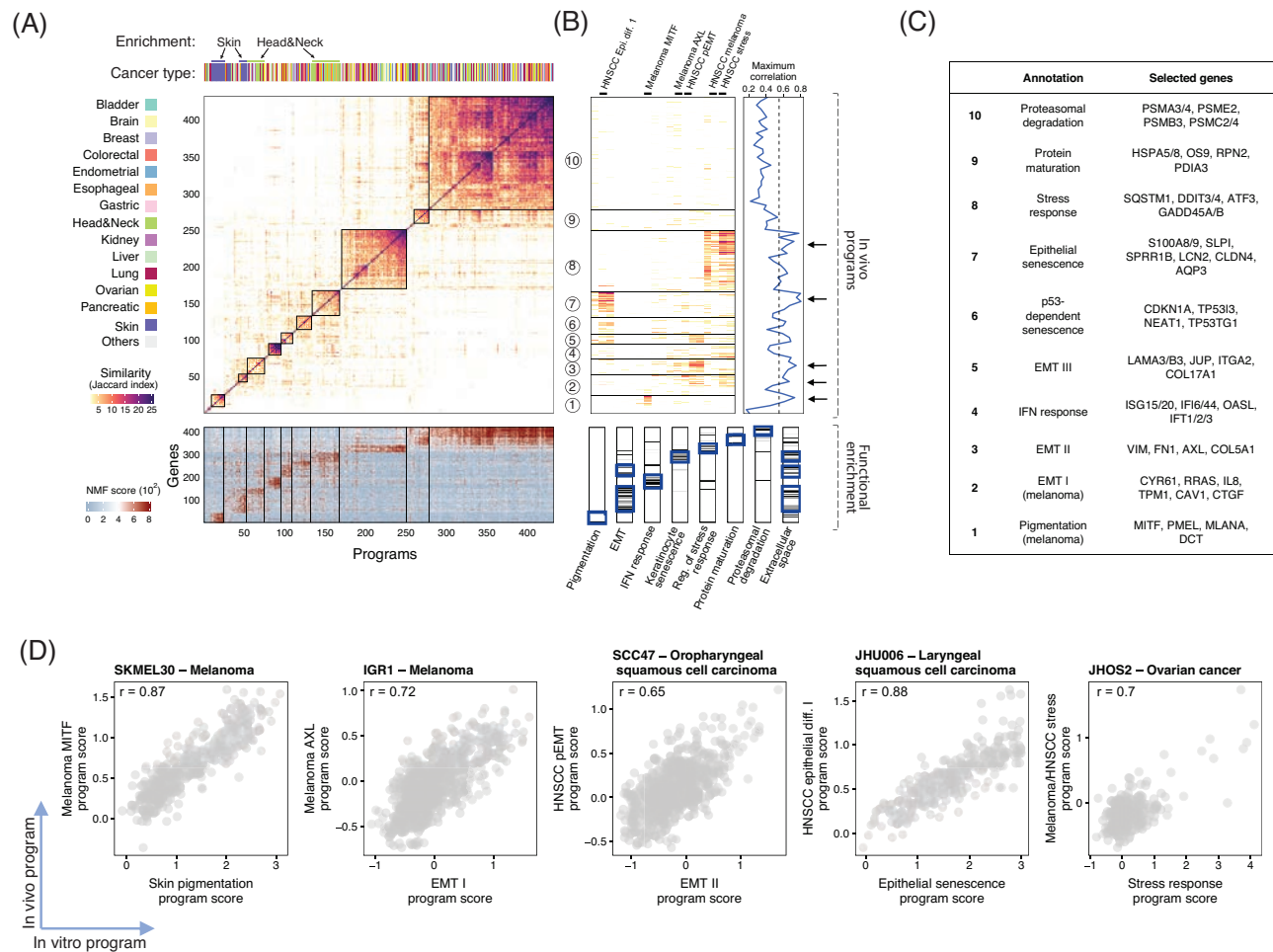
Figure 3. Functional annotation of RHPs. (**A**) The main heatmap depicts pairwise similarities between all NMF programs (except for those linked to the cell cycle, see **Fig. 2E**), ordered by hierarchical clustering. Ten clusters (RHPs) are indicated by squares and by numbers on the right. Top panel shows assignment to cancer types, highlighting significant enrichment (p < 0.05, hypergeometric test) of melanoma and HNSCC cell lines in RHPs #1,2, and #3,7, respectively. Bottom panel shows NMF scores of signature genes of each RHP. (**B**) **Top** heatmap depicts similarities between heterogeneity programs identified in cell lines (in vitro) and those observed in patient samples (in vivo). Line plot on the right shows the maximum correlation between single-cell scores of each in vitro program and the 19 in vivo programs analyzed, emphasizing 5 RHPs (#1, 2, 3, 7 and 8, see **Fig. S5A,B**) that closely recapitulate in vivo programs. Dashed line shows the maximum correlation obtained using 100 permutations. Bottom panel shows enrichment (p < 0.001, hypergeometric test) of RHP genes with eight annotated gene-sets. (**C**) Annotation and selected top genes for each of the 10 RHPs. (**D**) Single-cell scores of in vitro programs (X-axis, RHPs #1, 2, 3, 7 and 8) and the corresponding in vivo programs (Y-axis), in selected model cell lines, demonstrating high Pearson correlations.

Assessing the role of genetic heterogeneity through inference of chromosomal aberrations

Expression heterogeneity within a single cell line could be driven by either genetic or epigenetic mechanisms. To search for the contribution of genetic heterogeneity, we asked if genetic subclones within individual cell lines relate to the discrete/continuous programs of heterogeneity identified. First, to identify genetic subclones, we inferred large-scale copy number aberrations (CNAs) from the gene expression patterns in windows of 100 genes around each locus (Tirosh et al., 2016b). The inferred CNA profiles were consistent with hallmark genomic alterations such as the gain of chromosome 7 and loss of chromosome 10 in most glioblastoma cell lines (**Fig. S6**). Importantly, CNA analysis allowed the robust identification of genetic subclones in 58 cell lines, based on the gain or loss of chromosomes (or chromosome arms) in a subset of cells (**Methods**).

Next, we compared the assignment of cells to genetic subclones with their patterns of expression heterogeneity. Twelve of the 22 cell lines (54%) with discrete expression-based clusters had genetic subclones, and 66% of their expression-based clusters were significantly correlated with genetic subclones (**Fig. 4A**). Thus, 39% of all discrete clusters were significantly associated with identified genetic subclones (**Fig. 4B**). Consistencies between genetic-based and expression-based classifications were much more limited for the continuous patterns of expression variability identified by NMF. Genetic subclones were observed only in 29% of the cell lines with continuous programs. Among these cell lines, only 31% of continuous programs were differentially expressed between genetic subclones. Taken together, only 8% of all continuous programs (compared with 39% for discrete clusters) were significantly associated with identified genetic subclones (**Fig. 4B**). In summary, genetic diversity, as evaluated by CNA-based subclones, partially contributes to expression heterogeneity in cell lines, and this effect is particularly weak for the continuous programs, underscoring the potential role of epigenetic regulation.
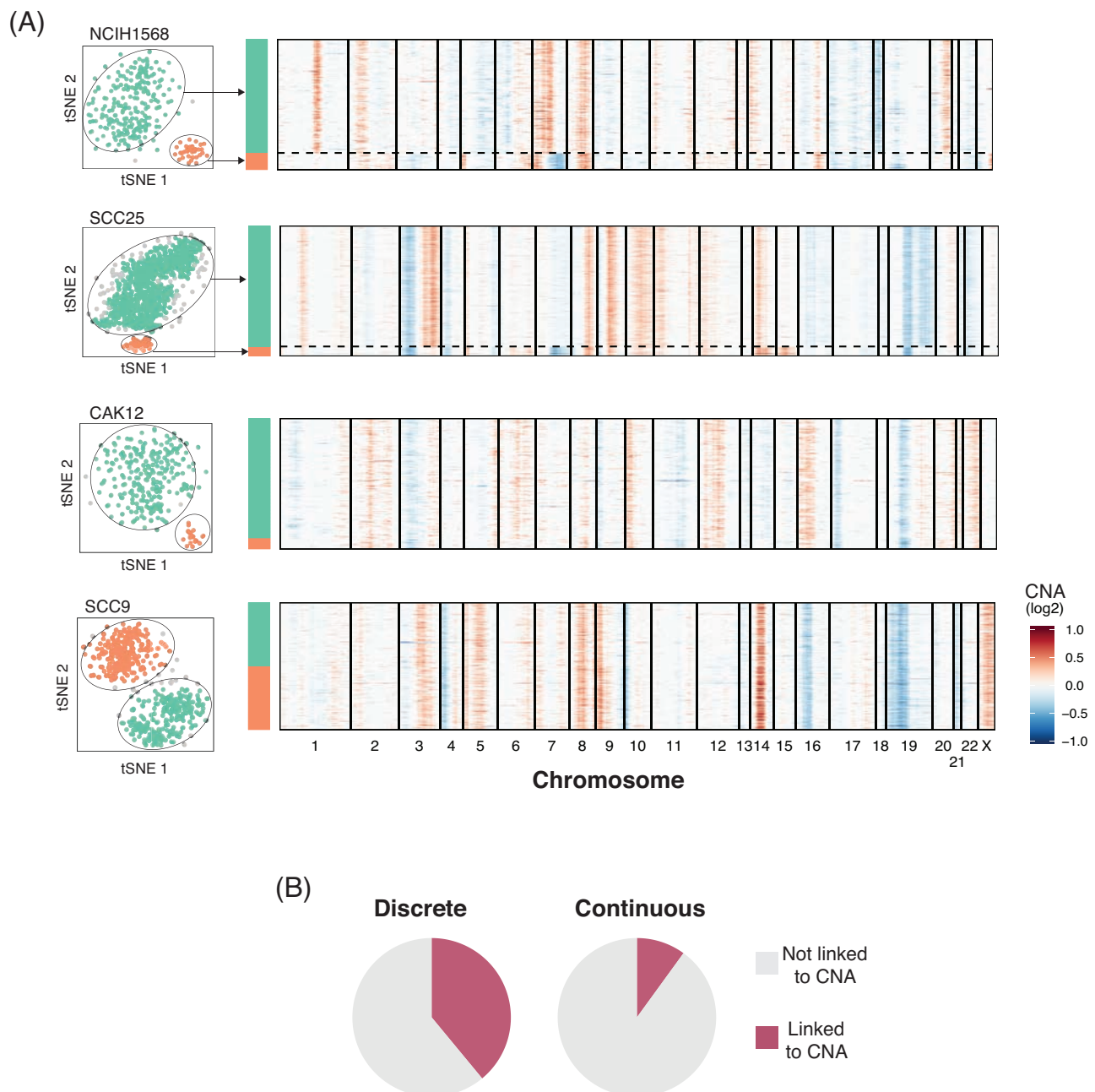
Figure 4. Genetic subclones partially explain intra-cell line expression heterogeneity. (**A**) Representative cell lines showing the association (top two cases) or lack thereof (bottom two cases) between discrete subpopulations and CNA-based subclones. tSNE plots on the left show discrete subpopulations identified using DBSCAN (as in **Fig. 2B** and **S2B**). Heatmaps on the right depict inferred CNAs with cells ordered according to the expression-based clusters. (**B**) Percentage of discrete (left) and continuous (right) heterogeneity programs that are associated with genetic subclones. For discrete programs, associations were assessed by comparing the assignment of cells to CNA subclones and to expression-based subpopulations (Fisher's exact test $p < 0.001$); for continuous programs, we compared NMF cell scores between different clones (t-test $p < 0.001$).

Plasticity of heterogenous cellular states in model cell lines

To assess the role of non-genetic mechanisms in regulating RHPs, we used two cell lines that successfully model both EMT-II (RHP #3) and EpiSen (RHP #7): JHU006, an HPV- laryngeal HNSCC, and SCC47, an HPV+ oropharyngeal HNSCC (**Fig. 3D, S4C**). Notably, EpiSen-high and EpiSen-low cells could be prospectively isolated, but returned to their pre-sorted heterogenous distribution with time. Specifically, we isolated by FACS EpiSen-high ($AXL^-/CLDN4^+$) and EpiSen-low (AXL^+/CLDN4) subpopulations, displaying ~12-fold difference in the expression of the EpiSen program (**Fig. 5A-B**). These sorted subpopulations began to shift by one week in culture and returned to the pre-sorting distribution of cellular states by day 14 (**Fig. 5C; Fig. S7A**). The EpiSen-high subpopulation was enriched for G0/G1 cell cycle phases, consistent with low proliferation (**Fig. 5D; Fig. S7B**). Nevertheless, it still contained cells in the S and G2/M phases, and did not stain for the classical senescence marker SA-β-gal (data not shown). These results suggest that the EpiSen program is dynamically regulated by non-genetic processes, and that it does not represent a permanent exit from cell cycle, consistent with the observation that, in cancer cells, senescence is often an incomplete and reversible state (Lee and Schmitt 2019).

Next, we examined the induction of these programs by tumor microenvironment soluble factors and perturbations (**Fig. 5E**). As expected, TGFβ1 and TGFβ3 induced the expression of genes in the EMT-II program, although the complete program induced had subtle differences from the native EMT-II program observed without perturbations (**Fig. S7C-D**). Interestingly, TGFβ treatments also downregulated the expression of EpiSen genes, underscoring the potential interplay between these two programs. A negative association between EMT and EpiSen was further supported by the single-cell profiles of JHU006 and SCC47 cells (**Fig. S4C**) and by our prior findings in HNSCC clinical samples, in which EMT-high cells were enriched at the invasive edge, while senescent cells were enriched at the core of tumors (Puram et al., 2017). Tumor cores are often associated with increased hypoxia, suggesting a potential mechanism for the spatial enrichment of senescent cells. In accordance with this possibility, the hypoxia mimetic desferrioxamine (DFO) induced the expression of the EpiSen program. A similar effect was observed upon hydrogen peroxide treatment, consistent with oxidative stress and the resultant DNA damage as potent inducers of senescence (te Poele et al., 2002) (**Fig. 5E**).
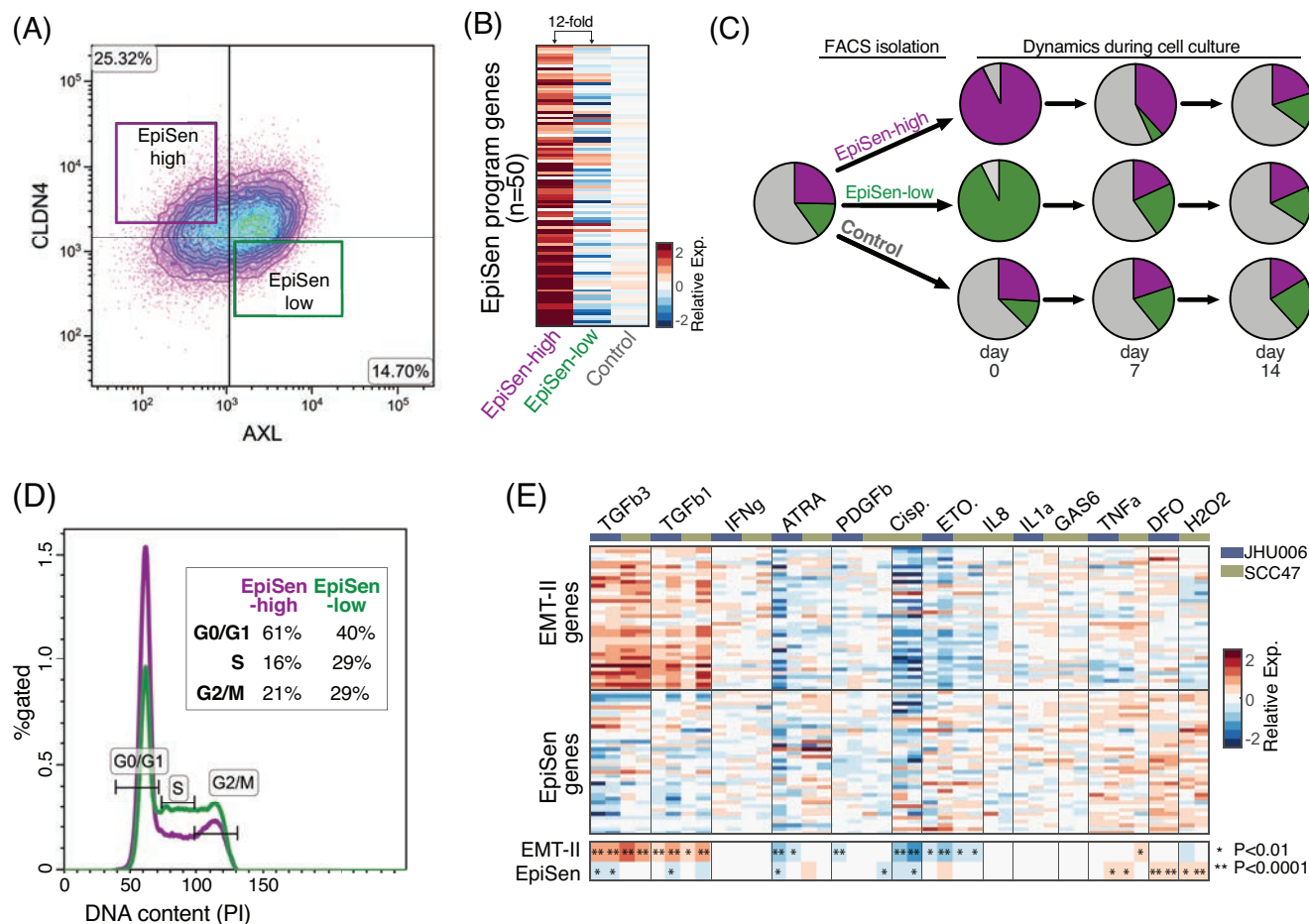
Figure 5. Interrogating the EpiSen expression heterogeneity program in model cell lines. (A) FACS isolation of an EpiSen-high population (AXL-CLDN4+) and an EpiSen-low population (AXL+CLDN4-) from the JHU006 cell line. **(B)** Heatmap shows relative expression of EpiSen genes in the sorted populations. Control corresponds to unsorted cells. **(C)** Pie charts depict relative proportions of the EpiSen-high and EpiSen-low, as determined by FACS based on AXL and Claudin4 expression. Pie charts are shown for an unsorted sample (left, initial distribution) and for sorted subpopulations, all of which were reanalyzed immediately after sorting (day 0) and at two additional time points (at days 7 and 14 in culture). **(D)** Analysis of cell cycle by DNA staining using propidium iodide (PI) on sorted EpiSen-high and EpiSen-low cells from JHU006. **(E)** Main heatmap depicts relative expression of EpiSen genes and EMT-II genes following multiple perturbations in SCC47 and JHU006. Smaller heatmap at the bottom shows the average fold change and asterisks denote significant up or down-regulation (t-test, see thresholds in figure).

Co-existing subpopulations differ in drug sensitivity

An important implication of cellular diversity in cancer is the possibility that distinct subpopulations of cells respond differently to treatments. Thus, we compared the sensitivities of EpiSen-high and EpiSen-low subpopulations sorted from each of the two model cell lines selected (**Fig. 6A**). We initially screened 2,198 bioactive compounds using a CTG-based viability assay performed in simplicate (**Fig. S8A-C).** We identified 200 compounds (9%) as potential hits, defined by differential killing of EpiSen-high and EpiSen-low subpopulations in at least one cell line (**Methods**). There was a significant overlap among compounds that preferentially killed EpiSen-high cells in the two cell lines (p = 0.006, hypergeometric test). Next, these putative hits and an additional group of compounds that killed both populations (n total = 248) were selected for a secondary screen performed in duplicate in each cell line (**Fig. 6B, Table S5**). Such screen identified 113 compounds with differential killing of the subpopulations in at least one cell line. Of the hits preferentially killing the EpiSen-high cells, 15 were shared among both cell lines, representing 41% and 45% of all the corresponding hits in JHU006 and SCC47, respectively. Finally, fourteen compounds with differential sensitivities, including five that were shared between cell lines and nine that were specific to one cell line, were analyzed by a full dose response (**Fig. 6C, Fig. S8D, Table S6**). All five of the shared compounds, and five of the nine cell line-specific compounds (56%), displayed significant differential sensitivity as in the secondary screen (p < 0.05 by paired t-test), supporting the consistency between cell lines as a measure of robustness.

As expected, EpiSen-high cells were more sensitive to the senolytic compound ABT-737 (Yosef et al., 2016). Additional sensitivities included multiple inhibitors of EGFR, AKT, PI3K, DNA-PK, IGF1R, and JAK **(Fig. 6B, Table S5)**. Several of these targets (DNA-PK, IGF1R and AKT) converge on repair of double-strand breaks as part of the DNA repair machinery (Bozulic et al., 2008; Wong et al., 2009). Together with the observation that hydrogen peroxide induces the expression of EpiSen genes (**Fig. 5E**), these results reinforce the role of DNA damage as a potential inducer of such RHP. The PI3K/AKT axis is hyper-activated in HNSCC, and resistance to PI3K inhibition in HNSCC is AXL-dependent (Elkabets et al. 2015). Accordingly, EpiSen-high cells, which are defined by low AXL expression, were more sensitive to inhibitors of PI3K and AKT, as well as those of EGFR and IGF1R that signal via the PI3K/AKT axis.

EpiSen-low cells were more sensitive to inhibitors of cell cycle regulators (CDKs, CHK1 and topoisomerase), consistent with their increased proliferation rate. EpiSen-low sensitivities also included multiple inhibitors of the proteasome and compounds that induce cell death by sensitizing cells to ferroptosis (the GPX4 inhibitor RSL3, Erastin, and the SLC7A11 inhibitor Sorafenib) **(Fig. 6B, Table S5)**. Recent work demonstrated that mesenchymal cells are particularly sensitive to ferroptosis-inducing compounds (Hangauer et al., 2017; Viswanathan et al., 2017). Thus, some of these vulnerabilities may reflect an increased mesenchymal signal of EpiSen-low cells due to the inverse correlation between EpiSen and EMT-II. Taken together, these results suggest that EpiSen-high and EpiSen-low cells are associated with differential vulnerabilities that may be consistent across distinct cellular contexts.
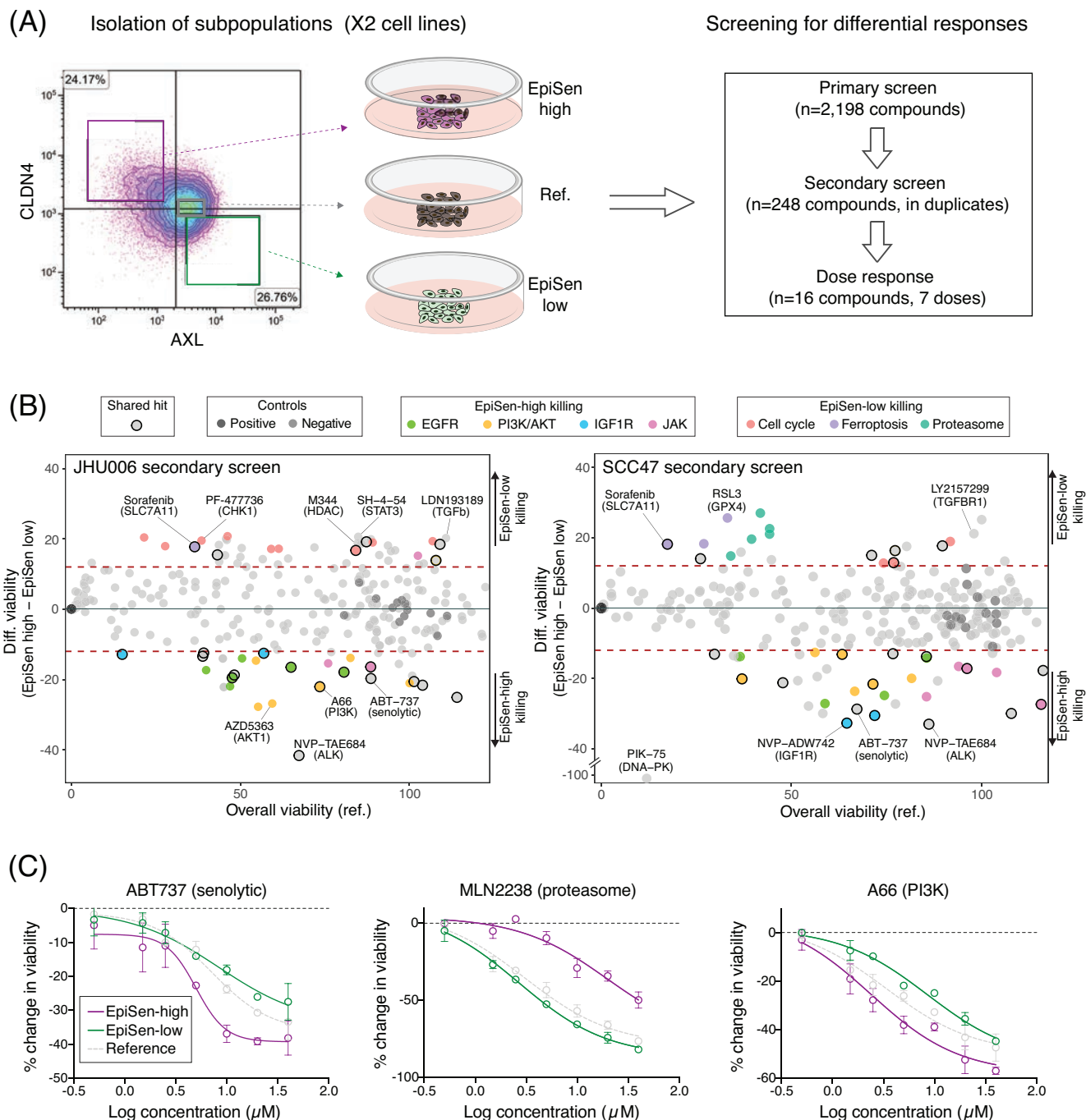
Figure 6. Co-existing cellular states differ in drug sensitivity. (A) Experimental scheme for drug screening: EpiSen-high cells, EpiSen-low cells, and a neutral reference population were isolated by FACS, then treated with a compound library in 384-well format for 48h, and viability was determined by CTG assay. A secondary screen, including drugs that differentially impacted the two populations in the primary screen, was performed in duplicate. **(B)** Viability of the reference population (X-axis) and differential viability of the EpiSen-high vs. EpiSen-low populations (Y-axis) upon treatment with 248 compounds tested in the secondary screen, in

Discussion

Despite widespread interest in tumor heterogeneity and in emerging single-cell technologies, the amount and quality of single-cell tumor datasets remains limited. Moreover, deciphering the function and regulation of the observed heterogeneity requires follow up experiments that are not feasible with clinical samples. Thus, there is a clear need to identify model systems that are proven to recapitulate the cellular diversity within tumors (or certain aspects thereof). One approach towards this goal is the continued effort for developing more realistic models of tumors, such as humanized mouse models and three-dimensional organoids. Such systems benefit from the complex tumor-like microenvironment, yet are expensive and challenging to maintain. An alternative approach might be a more rational utilization of standard culture models, depending on whether or not it is possible to recapitulate important aspects of ITH in such simple model systems. In that respect, cell lines are often criticized and considered inadequate, although to our knowledge no serious attempts have been made to systematically evaluate the heterogeneity of cellular states within them. Notably, recapitulation of aspects of ITH in cell lines would be of interest not only due to the possibility of performing follow up studies, but also due to the implication that such ITH reflects plasticity that is at least partially intrinsic to the cancer cells and observed in the absence of a native microenvironment.

We used a multiplexing strategy to enable labor- and cost-effective scRNA-seq profiling of ~200 cancer cell lines. A caveat of this approach is that individual cell lines may be influenced by other cell lines in their pool, although a previous work demonstrated that cell lines retain their differential drug sensitivities when grown as a pool (Yu et al., 2016). Importantly, in this work we focused exclusively on the variability among cells from the same cell line (rather than on the global expression pattern of each cell line) which is less dependent on the pooling approach (**Fig. S3A**) and is indeed consistent between our scRNA-seq profiles and our follow up experiments with two model cell lines.

Our analysis identified only a few cases of discrete subpopulations within the same cell line, but more widespread continuous variability. While such analysis depends on specific thresholds and computational methods, we argue that the main component of expression heterogeneity in cancer cell lines is continuous rather than discrete. Such gradual patterns contrast with the discrete nature of genetic subclones, suggesting at least a partial decoupling between genetic heterogeneity and the epigenetic heterogeneity that might underlie continuous pattern.

JHU006 (left) and SCC47 (right). Dotted lines represent the thresholds for defining differential sensitivity between the EpiSen-high and EpiSen-low states. Hits are colored by enriched target categories and shared hits between both cells lines are denoted by bold outline. **(C)** Dose response curves of three compounds (ABT-737, MLN2238, and A66) selected for follow-up EC50 studies in SCC47 in each sorted subpopulation (EpiSen-low, EpiSen-high, reference) performed in duplicate. Percent change in viability was calculated at each concentration using the viability normalized to vehicle (DMSO-treated) controls and curves were fit using a three-parameter nonlinear regression model. Error bars represent S.D.

Consistent with this possibility, our analysis of CNAs showed a limited association of genetic subclones with expression heterogeneity, particularly when considering continuous patterns. Moreover, follow up experiments directly demonstrated the dynamic plasticity of the EpiSen program. Thus, cancer cells may harbor variability through two largely distinct processes of genetic and epigenetic mechanisms, both of which may contribute to drug resistance and tumor progression.

Analysis of NMF programs identified cell cycle as well as 10 other recurrent programs (RHPs), each associated with a specific biological process. Importantly, 7 of these were also consistent with ITH patterns observed in tumors in vivo. This consistency has several important implications. First, it indicates that ITH patterns are partially retained even in the absence of a tumor microenvironment and may primarily reflect cell-intrinsic plasticity. Second, as each RHP is observed in a subset of cell lines, we may leverage the extensive cell line annotations to explore the causes and consequences of ITH patterns. This approach identified associations between RHPs and genetic background (p53, MRE11A and NOTCH4), lineage (melanoma and HNSCC), and drug sensitivity (e.g. Nutlin-3a). Third, we can further prioritize particular cell lines that most reliably mirror ITH patterns for follow up experiments. This reflects an important deviation from the traditional focus on historical cell lines that are easy to grow, and provides a resource for custom prioritization of cell lines based on their heterogeneity.

Careful examination of the diversity programs in vivo and in vitro highlights their partial nature compared to their developmental "normal" counterparts. Both EMT and senescence are associated with precise phenotypes and well-defined regulators during development and wound healing, yet in the context of tumors and cancer cell lines, we observe only partial phenotypes and limited dependence on these regulators. The EMT-like profiles we observe include many EMT-related genes and are associated with increased migration, but do not seem to involve EMT hallmarks such as the loss of epithelial markers, a drastic change in morphology, and expression of most EMT transcription factors. Similarly, EpiSen-high cells resemble the senescence response of keratinocytes and lung bronchial cells, are associated with reduced proliferation, and possess markers of SASP, yet they retain some proliferative capacity, harbor p53 mutations and do not express high levels of p16 and p21. Indeed, evidence already exists for incomplete and reversible senescence programs in cancer: low levels of p16 at induction of senescence confers cell cycle re-entry upon p53 inactivation or RAS expression (Beausejour et al. 2003), and loss of Rb in senescent cells leads to renewed proliferation (Sage et al. 2003). We therefore propose that cancer cells often activate partial or distorted programs, possibly not through the canonical developmental mechanisms, and in a context-dependent manner. This could contribute to the difficulties in resolving long-standing debates in the cancer field about the role of EMT and senescence, which are often evaluated through the activity of developmental regulators and markers that may fail to detect certain partial programs.

A partial and reversible epithelial senescence state in tumors could have several implications. First, EpiSen may continue to restrict the growth rate of cancer cells even in established tumors and cell lines. Second, EpiSen cells may be particularly resistant to certain

treatments (**Fig. 6**), such as chemotherapies that target proliferating cells, and thereby may facilitate tumor recurrence. Third, EpiSen could function as a DNA repair program, allowing damaged cells to evade apoptosis and/or ferroptosis. This is consistent with the induction of EpiSen by hydrogen peroxide, the sensitivity of EpiSen-high cells to inhibitors of DNA repair, and the functions of core EpiSen genes in oxidative stress, including the free radical scavengers S100A8/9, the H202 transporter AQP3, and LCN2, a secreted factor that increases ROS levels (Kagoya et al., 2014). Fourth, EpiSen could remodel the tumor microenvironment, influencing cancer, stromal and immune cells through its abundance of secreted factors, including S100A8/A9, SAA1/2, SLPI, CXCL1, and LCN2. While SASP is best characterized in fibroblasts, here we describe a distinct "EpiSASP" whose function will be investigated by future studies.

ITH has long been recognized as a potential source for therapeutic failure. Our analysis supports this notion by demonstrating that subpopulations of cells from the same cell line are associated with distinct drug sensitivities. We ensured the robustness of these results by three approaches: i) Comparing pairs of subpopulations from the same cell line, to control for cell line-specific drug sensitivities; ii) Focusing on effects that were consistent across experiments in two distinct cell lines, i.e. HPV+ and HPV- HNSCC cell lines that differ in many regards; and iii) validating results using a full dose-response analysis. Among others, the differential responses we identified included EGFR inhibitors, which are routinely used in the treatment of HNSCC patients, underscoring the potential clinical relevance of our observations. Our results suggest that EGFR inhibitors (as well as other inhibitors) preferentially eliminate subsets of EpiSen-high cells, providing a rationale for their combination with chemotherapies that target the more proliferative EpiSen-low subpopulations.

In summary, we described here the landscape of diversity across ~200 cell lines of various cancer types, generating a dataset that will be widely useful for the cancer research community. In analyzing this extensive dataset, we found multiple recurrent programs of heterogeneity that recapitulate ITH in vivo, and are associated with continuous epigenetic plasticity. Follow up analysis of one such program demonstrated its dynamics, regulation and vulnerabilities. Further studies of tumors and of the model systems prioritized through this data will provide a better understanding of ITH, which is currently a main barrier for successful cancer therapies.

Methods

Cell lines

Human HNSCC cell lines (laryngeal: JHU006, JHU011, JHU029; oropharyngeal: SCC47, SCC9, SCC90, SCC25, 93-VU-147T) were provided by Dr. James Rocco after confirmation by short tandem repeat analysis. The laryngeal cell lines were grown in RPMI 1640 media (Biological Industries, Kibbutz Beit HaEmek). The oropharyngeal cell lines were grown in a 3:1 mixture of Ham's F12:DMEM (Biological Industries, Kibbutz Beit HaEmek). All growth medias for HNSCC cell lines were supplemented with 10% fetal bovine serum (Biological Industries, Kibbutz Beit HaEmek), 1x penicillin-streptomycin and 1x L-glutamine (Biological Industries, Kibbutz Beit HaEmek). Human primary bronchial epithelial cells (PCS-300-010) were acquired from ATCC and grown in Airway Epithelial Cell Basal Medium (ATCC PCS-300-030) supplemented with the bronchial epithelial cell growth kit (ATCC PCS-300-040). All cell lines screened negative for mycoplasma by the EZ-PCR mycoplasma detection kit (Biological Industries, Kibbutz Beit HaEmek).

Cell line pools

We obtained eight previously generated pools of cell lines (Yu et al., 2016), each containing 24-27 cell lines from diverse cancer types. Cell lines were combined to pools based on growth rates (doubling time), in order to ensure comparable representation over the short-term culturing. Each pool was thawed and cultured in DMEM media for 3 days before generating 3' scRNA-seq libraries with the 10X Genomics Chromium platform. A ninth custom pool was generated by combining the HNSCC cell lines listed above immediately prior to scRNA-seq profiling.

Droplet-based scRNA-seq (10x Genomics)

scRNA-seq libraries were generated using the 10X Chromium Single Cell 3' Kit v2 and the 10x Chromium Controller (10x Genomics) according to the 10X Single Cell 3' v2 protocol. Briefly, we prepared single-cell suspensions (≥95% viability) of each pool in 0.04% PBS-BSA and approximately 10,500 single cells per pool were loaded to the Chromium Controller with a targeted recovery of 6,000 cells. Single cells, reagents and single gel beads containing barcoded oligonucleotides were encapsulated into nanoliter-sized droplets and subjected to reverse transcription. Droplets were broken and the barcoded cDNAs were purified with DynaBeads and amplified by 12 cycles of PCR (98°C for 45 s; [98°C for 20 s, 67°C for 30 s, 72°C for 1 min] x 12; 72°C for 1 min). The amplified cDNA was fragmented, end-repaired, ligated with index adaptors, and size-selected with clean-ups between each step using the SPRIselect Reagent Kit (Beckman Coulter). Quality control of the resulting barcoded libraries was performed with the Agilent

TapeStation and by PCR with primers specific to the P5 and P7 sequence (NEBNext Library Quant Kit for Illumina, New England Biolabs). Final 10x scRNA-seq libraries were diluted to 4 nM, denatured, and further diluted to a final concentration of 2.8 pM for sequencing with the following parameters: Read 1: 26 cycles, i7 index: 8 cycles, i5 index: 0 cycles, Read 2: 58 cycles. Sequencing was performed on the NextSeq500 (Illumina) instrument using the NextSeq 75 cycles High Output Kit (Illumina).

Bulk RNA-seq (SMART-Seq2)

The SMART-Seq2 protocol (Picelli et al., 2014) was adapted as previously described (Rauner et al., 2018). Between 100-200 cells were incubated in lysis buffer at 72°C for 3 min. Reverse transcription and cDNA amplification (17 cycles) were performed using the SMART-Seq V4 Ultra Low Input RNA Kit. Following 1X Agencourt Ampure XP beads cleanup (Beckman Coulter), 200 pg of amplified DNA underwent tagmentation and final amplification (12 cycles) adding unique Illumina barcodes (Nextera XT Library Prep kit, Illumina). Pooled bulk RNA-seq libraries were diluted to 4 nM, denatured, further diluted to 2 pM and sequenced with the following parameters: Read 1: 75bp, Read 2: 15bp, no indices. Sequencing was performed on the NextSeq500 (Illumina) instrument using the NextSeq 75 cycles High Output Kit (Illumina).

Flow cytometry and sorting of cell lines

Sorting of JHU006 and SCC47 cells was performed on a BD FACS Melody using the following antibodies: anti-human AXL-PECy7 (eBioscience) at 1:300, anti-human Claudin-4-APC (Miltenyi) at 1:200, and anti-human ITGA6/CD49f-APC eBioscience) at 1:200. Gating of positive and negative cells was defined by the unstained control. For EpiSen program dynamics experiments, 200,000 cells of each subpopulation (EpiSen-high: AXL^-CLDN4^+; EpiSen-low: AXL^+CLDN4^-; control sort: all cells) were sorted and reanalyzed by FACS immediately post-sorting and at days 7 and 14. Final analysis was performed using Kaluza Analysis Software v2.1 (Beckman Coulter). Similarly, the EMT-II subpopulation was isolated by AXL^+ITGA6^+ (EMT-II-high cells) and AXL^-ITGA6^- (EMT-II-low cells). Experiments were performed three times independently.

Cell cycle analysis by propidium iodide (PI)

Single cells were suspended in ice cold PBS and fixed by adding the cell suspension dropwise to 70% ethanol while vortexing. Fixed cells were stored at 4°C. Following 2x PBS washes, cells were resuspended and incubated in PI/Triton-X-100 staining solution, consisting of 0.1% Triton-X-100 (Sigma), 0.2mg/ml DNAse-free RNAse A (Sigma), and 0.04 mg/ml of 500ug/ml PI (Sigma) in PBS, at 20°C for 30 min. Cells were analyzed in a BD FACS Melody. The experiment was performed three times independently.

Cytokine treatments and perturbations of HNSCC cell lines

For growth factor/drug treatment experiments, JHU006 and SCC47 cells were seeded at 50,000 cells/well in 24 well plates in their standard media and treated in duplicate with drug/cytokine or vehicle (0.1% DMSO with 1ug/mL BSA) 24 hours after seeding. Cells were harvested 24 hours after treatment for bulk expression profiling. Treatments included 10 μM all-trans-retinoic acid (ATRA) (Sigma), 25 ng/ml interferon gamma (Peprotech), 25 ng/ml TNF alpha (Peprotech), 25 ng/ml PDGFBB (Miltenyi), 10 nM etoposide (Sigma), 10 ng/ml TGFβ1 (Peprotech), 10 ng/ml TGFβ3 (Peprotech), 10 μM cisplatin (Sigma), 200 μM hydrogen peroxide (Sigma), 25 ng/ml IL-8/CXCL8 (Peprotech), 25 ng/ml GAS6 (Sino Biological), 50 ng/ml S100A8/A9 (Sino Biological), and 500 μM desferoxamine (DFO) (Sigma).

Senescence induction by etoposide and SA-β-gal staining

Primary bronchial cells were seeded at 50,000 cells/well in 24 well plates and treated with 5-7.5 μM etoposide (Sigma) 24 hours later to induce senescence. After 48 hours, media was replaced and on day 9 etoposide-treated cells and untreated controls were stained with SA-β-gal. Cells were fixed with 0.5% glutaraldehyde solution in PBS pH 7.4 and incubated with X-gal staining solution (0.2M $K_3Fe(CN)_6$, 0.2M $K_4Fe(CN)_6$ $3H_2O$, and 40X X-Gal stock diluted in PBS/$MgCl_2$) for 6 hours protected from light. X-Gal stock consists of 40 mg/ml X Gal (Roche #745740) in N,N-dimethylformamide (Sigma D-4254). Following PBS washes, stained cells were covered with 80% glycerol prior to imaging.

Migration assay

Single-cell suspensions were loaded into Ibidi wound healing inserts (75,000 cells/insert) coupled to 24-well plates and left to attached for 24 h. Inserts were removed and cells were treated with TGFβ3 (Peprotech) or vehicle (PBS). Images were taken 0, 6, 12, 24, and 48 hours post-treatment. The experiment was performed independently three times.

Drug screening - viability assay

The Selleck Bioactive Compound Library (Selleck Chemicals) as well as DMSO-only controls and straurosporine positive (killing) controls were dispensed into 384-well plates with an Echo 550 liquid handler (Labcyte). Drug concentration was 10 μM for the primary screen and 1 μM or 10 μM for the secondary screen (performed in duplicate) depending on hit category. Purity of compounds selected for follow-up by dose response was confirmed by LC/MS (data not shown). For the dose response series, a seven-point two-fold dilution series with an upper limit of 40 μM was performed in duplicate. EpiSen-high (AXL$^-$CLDN4$^+$), EpiSen-low (AXL$^+$CLDN4$^-$), and a third neutral reference population were sorted from JHU006 and SCC47 cell lines as described

above and seeded into the compound-treated plates in their standard media at a concentration of 15,000 cells/ml (750 cells/well) with a Combi Multi-drop (Thermofisher). Plates were incubated at 37°C for 48 hours following sorting and compound treatment and cell viability was determined based on luminescence following addition of CellTiter-Glo (Promega), according to the manufacturer's instructions. Luminescence was measured on a BMG Pherastar plate reader. Data was normalized in Genedata Screener where DMSO (vehicle) is defined as neutral control (i.e. 100% viability) and samples without cells are the inhibitor control (i.e. 0% viability). Compound-centric data was visualized in CDD Vault from Collaborative Drug Discovery (Burligame, CA).

Processing of scRNA-seq data

Cell barcode filtering, alignment of reads and UMI counting were performed using CellRanger 3.0.1 (10x Genomics). Expression levels were quantified as $E_{i,j} = \log_2(1 + CPM_{i,j}/10)$, where $CPM_{i,j}$ refers to $10^6 * UMI_{i,j}/sum[UMI_{1..n,j}]$, for gene i in sample j, with n being the total number of analyzed genes. The average number of UMIs detected per cell was less than 100,000, thus CPM values were divided by 10, to avoid inflating the differences between detected ($E_{i,j} > 0$) and non-detected ($E_{i,j} = 0$) genes, as previously described (Tirosh et al., 2016b). For each cell, we quantified the number of detected genes as a proxy for sample quality. We conservatively retained cells with a number of detected genes ranging from 2,000 to 9,000. When analyzing cell lines individually, we only considered genes expressed at high or intermediate levels ($E_{i,j} > 3.5$) in at least 2% of cells, yielding an average of 6,758 genes analyzed per cell line. Values were then centered per cell line to define relative expression values, by subtracting the average expression of each gene *i* across all k cells: $Er_{i,j} = E_{i,j}$-*average[$E_{i,1...k}$]*. When analyzing cell lines collectively, we selected the top 7,000 expressed genes across all cell lines, resulting in a minimum average expression of 12 CPM. Values were centered by subtracting the average expression across all 53,513 cells analyzed: $ER_{i,j} = E_{i,j}$-*average[$E_{i,1...53,513}$]*.

Processing of bulk RNA-seq data

Single-end reads were aligned to the GHCh38/hg38 human genome using Bowtie and expression values were quantified using RSEM. Data are presented as $E_{i,j} = \log2[(TPM_{i,j}) + 1]$, where $TPM_{i,j}$ refers to transcript-per-million for gene i in sample j, as calculated by RSEM.

Cell line assignment

We used both expression-based and SNP-based methods to assign cells to cell lines. In each of these methods, we compared the single cells to external bulk data of the corresponding cell lines and then either assigned the cells to the most similar cell line or excluded them as potential doublets or low-quality cells. The remaining assignments that were consistent between both

methods were retained for further analysis. Bulk RNA-seq data was obtained from the DepMap portal (https://depmap.org/; 18q3 data release) (Ghandi et al., 2019) for the eight CCLE-based pools and was generated as described above for the eight cell lines in the custom pool.

For SNP based classification, for each cell we determined the cell line from the pool whose SNP profile (based on bulk RNA-seq data) best matched the observed reference and alternate allele reads across a panel of SNP sites, similar to the Demuxlet method (Kang et al., 2018). Specifically, we used a logistic regression model for each cell, where the probability of a read at SNP site i being from the alternate allele is modeled as $P_i = \sigma(\beta_0 + \beta_j * X_{i,j})$, where σ is the logistic function, $X_{i,j}$ is the allelic fraction of cell line j at site i (estimated from bulk RNA-sequencing data), and the β are parameters estimated for each single cell and reference cell line by maximizing the data likelihood under a binomial model. Models were fit using the R package glmnet (Friedman et al., 2010), and the cell line whose SNP profile produced the highest likelihood under this model was selected. Goodness-of-fit was quantified by the model deviance relative to the null-model deviance. We used a reference panel of 100k SNPs that were frequently detected across a panel of 200 cancer cell lines (based on bulk RNA-seq data), and that were detected in 10x scRNA-seq data from the same cell lines.

We used a broadly similar approach to classify single cells based on their gene expression profiles. We applied a local 'smoothing' to the normalized and centered single-cell expression profiles (*ER*), using a Gaussian kernel applied to the cell-cell distances in tSNE embedding space. We used the Rtsne R package to estimate 3 tSNE embedding dimensions for each cell. The Gaussian kernel bandwidth was set using the method 'sigest' from the R package kernlab. We also subsetted the gene expression data to genes that were expressed in at least half of all cells or had a maximal expression (measured by the 98th percentile of that gene's expression across all cells) greater than 3. Finally, for each cell we identified the reference cell line from the pool with the most similar bulk RNA-seq gene expression profile (using $\log_2$(CPM) data mean-subtracted across samples per gene, and Pearson correlation similarity).

Detection of putative 'doublets', where pairs of cells get labeled with the same barcode during droplet-based library preparation, was done based on the SNP data, using the same generalized linear modeling approach to identify a mixture of two reference cell lines whose combined SNP profiles best explained the SNP data from a given cell. To efficiently estimate the best-fitting reference cell line pair we used a Lasso-regularized generalized linear model. After determining the best-fitting 'singlet' and 'doublet' models for each putative cell, we then determined whether each putative cell was a singlet, doublet, or a 'low-quality' cell based on several statistics. To identify low quality cells we took the max of the deviance explained by the singlet model and the deviance explained by the doublet model. We observed that the max deviances formed a bimodal distribution. We thus used the local minimum between the two distributions as a threshold and classified all cells with a max deviance below this threshold as 'low quality'. To separate putative doublets from singlets, we then fit a two-component Gaussian mixture model using three variables: i) the amount of deviance explained by the singlet model, ii) the (log-transformed) deviance-improvement of the doublet model over the singlet model, and iii)

the fraction of genes detected in that cell. Cells with a probability greater than 0.75 of belonging to the cluster with higher average doublet improvement were classified as doublets. Lastly, cell lines with less than 50 high quality assigned cells were excluded.

Systematic characterization of transcriptional heterogeneity

For each of the 198 cell lines passing QC, we applied two distinct approaches to identify discrete and continuous patterns of expression heterogeneity. First, to identify discrete (highly distinct) subpopulations within cell lines, we used tSNE followed by DBSCAN, which assumes that clusters are contiguous regions with high density of cells. tSNE was applied to each cell line individually using relative expression values (Er) and perplexity of 30. To identify dense regions, DBSCAN classifies each point according to a minimum points (minPts) threshold, defined as the minimum number of neighbors within a user-defined radius (eps) around core points. To optimize this parameter selection, we tested the ability of DBSCAN to correctly distinguish cells from two distinct cell lines. We combined cells from two different cell lines and tested the classification accuracy of DBSCAN using different eps (0.6 – 3) and minPts thresholds (5 and 10). DBSCAN classification was evaluated using Fisher's exact test and considered correct if $p < 0.001$. Such procedure was repeated 1,000 times and in each iteration we randomly selected the cell lines, the total number of cells (56 – 898) and the number of cells selected per cell line (2-98 % of total). The parameter combination yielding the highest rate of correct classification (eps = 1.8, minPts = 5) was used in further analyses. We also applied DBSCAN with additional, less stringent eps values (1.2 and 1.5) to show the robustness of the results. To define gene signatures that characterize the discrete subpopulations identified, we compared gene expression of cells in a given cluster to all other cells within the same cell line using t-test. Genes with fold change >= 2 and $p < 0.001$ were selected and the top 50 (by fold change) were defined as the gene signature. Clusters containing above 90% of the cells of a given cell line were excluded from this analysis.

Second, we analyzed each cell line using NMF to identify both discrete and continuous programs of expression heterogeneity. NMF was applied to the relative expression values (Er), by transforming all negative values to zero, as previously described (Puram et al., 2017). We performed NMF with k (the number of factors) ranging from 6-9, and initially defined expression programs as the top 50 genes (by NMF score) for each k. For each cell line, we sought robust expression programs by selecting those with an overlap of at least 70% (35 out of 50 genes) with a program obtained using a different value of k. To avoid redundancies, from each set of overlapping programs from a single cell line, we only kept one program, selected based on having the highest overlap with a NMF program identified in another cell line. The association between programs and technical artifacts was inspected by calculating, for each cell line, Pearson's correlation coefficient between the number of genes detected in a cell (complexity) and the respective NMF program score. This approach identified a cluster of NMF programs (based on 50 minus the number of overlapping genes across expression programs) that share negative correlations with complexity. This cluster appeared to reflect technical artifacts (based also on

manual inspection and inclusion of many mitochondrial genes and pseudogenes) and was excluded from further analysis.

In order to identify RHPs across cell lines, we compared expression programs derived from DBSCAN and NMF, separately, by hierarchical clustering, using 50 minus the number of overlapping genes as a distance metric. Given the high number of NMF programs, clustering was restricted to programs with at least a minimum overlap of 20% (10 out of 50 genes) with a program observed in another cell line. Twelve clusters were defined by manual inspection of the hierarchical clustering results. For each cluster of NMF programs, a RHP was then defined as all genes included in at least 25% of the constituent programs. We then used hypergeometric test to assess the enrichment of RHP signatures with H and C5:BP gene-sets from MSigDB (Liberzon, 2014), and $p < 0.001$ were considered significant.

Pool effect analysis

To evaluate the impact of the pooling procedure on the cell lines we used three different approaches. First, we determined the proportion of the similarity observed among the global expression profiles of cell lines and among expression heterogeneity patterns that was dependent on the pool of origin. We calculated pairwise correlations between global expression profiles, defined as the average expression, by gene, of all cells from each given cell line, and used one-way ANOVA to computed the proportion of the total variance (η^2) explained by whether or not cell lines were in the same CCLE pool. This same procedure was applied to evaluate the pairwise correlations between NMF programs across gene scores. Second, we inspected the distribution of the RHP across all CCLE pools, to ensure no pool-specific bias. Finally, we applied NMF (factor = 6) to scRNA-seq data of the tongue squamous cell carcinoma cell line SCC25 profiled in two different conditions: as part of the CCLE pool ID #19 and as part of the custom HNSCC pool. We compared programs by hierarchical clustering using one minus Pearson correlation coefficient across NMF gene scores as a distance metric.

Defining program scores in each cell

Program scores were calculated for each cell individually in order to evaluate the degree to which they express a given RHP. Cells with higher complexity (i.e. number of genes detected) would be expected to have higher cell scores for any gene-set. To account for this effect, for each gene-set analyzed, we created a control gene-set to be used in the calculation of a normalization factor, as previously described (Tirosh et al., 2016b). Control gene-sets are selected in a way that ensures similar properties (distribution of expression levels) to that of the input gene-set. First, all genes analyzed are ordered by average expression across all cell lines and divided into 75 bins. Next, for each gene in the given gene-set, we randomly select 100 genes from the same expression bin. Finally, given an input set of genes (G_j), we defined a score, $SC_j(i)$, for each cell i, as the average relative expression of the genes in G_j. We then calculate a similar cell score for the

respective control gene-set and subtract it from the initial cell scores: $SC_j(i) = average[ER(G_j,i)] - average[ER(G_j^{cont},i)]$.

Comparison of in vitro and in vivo programs

In vivo programs of expression heterogeneity were previously defined (Puram et al., 2017; Tirosh et al., 2016a) or generated using published single cell data (Chung et al., 2017; Lambrechts et al., 2018) and the NMF-based strategy described above. For each in vivo program we calculated the maximum similarity (Jaccard index) and maximum single cell score (SC) correlation with in vitro programs. Correlations were calculated using the cell lines harboring the respective in vitro program. Next, we identified the overall maximum similarity and maximum correlation obtained by permutating each in vitro program 100 times. To generate permutated gene sets, we first ordered all genes by average expression across all cell lines and divided them into 75 bins. Each gene in a given gene set was then replaced by a randomly select gene from the same expression bin. In vivo programs presenting both maximum similarity and maximum correlation above the permutation threshold were selected. Among selected programs we focused on the top 10 with highest correlation, and manually identified 5 main groups: melanoma MITF, melanoma AXL, HNSCC epithelial differentiation, HNSCC pEMT, and melanoma/HNSCC stress. We defined which in vitro RHP most closely recapitulate the 5 selected in vivo programs based on the average similarity and correlation of the constituent programs.

Computational cell cycle analysis

Scoring cells for the G1/S and G2/M RHPs reveals a circle-like structure, reflecting different phases of the cell cycle (Fig. S3C). This pattern recurs across cell lines, and was also previously described for different human cancers and mouse hematopoietic stem cells (Kowalczyk et al., 2015; Tirosh et al., 2016a; Tirosh et al., 2016b). Since these patterns are continuous, borders between cell cycle phases are unclear and by manual inspection we conservatively defined a classification into four patterns (Fig. S3C): non-cycling ($SC_{G1/S} < -0.75$ and $SC_{G2/M} < -0.5$), G1 ($SC_{G1/S} > -0.5$ and $SC_{G2/M} < 0$), S ($SC_{G1/S} > 0.25$ and $SC_{G2/M} > 0$), and G2/M cycling ($SC_{G1/S} < 0.25$ and $SC_{G2/M} > 0.5$).

Defining program variability in each cell line

To evaluate the degree of heterogeneity of RHPs in each cell line, we examined the variability of cell scores. First, given a program j and cell line i, we defined program variability, $PV_j(i)$, by first ranking cells according to the program score (SC_j) and comparing the average signal of the top vs. bottom 10% cells: $PV(j) = average[SC_j(top10\%)] - average[SC_j(bottom10\%)]$. Next, to control for the potential association between mean and variability of program scores, we applied a local polynomial regression with smoothing span of 0.8 to infer the relationship between

program variability and mean in each cell line, and used the residuals of the model as the corrected program variability score: *PVc(j) = PV(j) - RG(mean(SCj))*, where RG represents the local regression model for PV based on the average program scores, SC.

Association between program variability and mutations or drug responses

Mutation calls (coding region, germline filtered) were downloaded from the CCLE portal (https://portals.broadinstitute.org/ccle), and drug response data (CTRP v2, area under the curve, AUC) were downloaded from the CTD[2] portal (https://ocg.cancer.gov/programs/ctd2/data-portal). We restricted the analysis to non-silent mutations and compounds tested in at least 160 out of the 198 cell lines analyzed. We compared program variability scores of mutated and wild-type cell lines using two-sided t-test. The association between drug sensitivity (1-AUC) and program variability scores was assessed using multiple linear regression, with cancer type as a covariate: *Yd ∼ cancer type + PVj,* for drug *d* and program *j*.

CNA estimation

Initial values (CNA$_0$) were estimated by first sorting the analyzed genes by their chromosomal location and calculating a moving average of relative expression values (*ER*), with sliding window of 100 genes, as previously described (Tirosh et al., 2016b). To avoid considerable impact of any particular gene on the moving average, in this analysis, we limited relative expression values to [−3,3]. In order to define proper CNA reference values to be used as the baseline, we downloaded gene level copy number data (Affymetrix SNP6.0 arrays, log2(copy number/2)) from the CCLE portal (https://portals.broadinstitute.org/ccle) and calculated, for each cell line, the average copy number signal by chromosome arm. Next, for each chromosome arm we selected a set of reference cell lines, defined as those presenting an average copy number signal ranging from -0.2 to 0.2. For a given CNA window, in a given chromosome arm, we then calculated the average CNA estimates of the respective reference cell lines and define the minimum (BaseMin) and maximum (BaseMax) values obtained as the lower and upper baseline limits. The final CNA estimate of cell *i* at position *j* was defined as:

$$CNA_f(i,j) = \begin{cases} CNA_0(i,j) - BaseMax(j), & if\ CNA_0(i,j) > BaseMax(j) + 0.1 \\ CNV_0(i,j) - BaseMin(j), & if\ CNA_0(i,j) < BaseMin(j) - 0.1 \\ 0, & if\ BaseMin(j) - 0.1 < CNA_0(i,j) < BaseMax(j) + 0.1 \end{cases}$$

CNA subclones detection within cell lines

To identify CNA-based subclones with high confidence we focused on CNAs encompassing whole chromosome arms, as these are more reliable than focal CNAs. We reasoned that the presence of multiple subclones in a single cell line would translate into a multimodal distribution of CNA signal for at least one chromosome arm, across cells from a given cell line. Thus, we first calculated for each cell and each chromosome arm, the average CNA_0 estimate across all loci in the chromosome arm. Next, we examined, for each cell line, if the distribution of arm-level CNA values was multimodal for any chromosome arm. To this end, we fitted each distribution to a Gaussian mixture model (GMM) and calculated the probability for each cell to belong to each mode by an expectation-maximization algorithm, implemented by the R function Mclust. A cell line was defined as having subclones if, for at least one chromosome arm, a minimum of 20 cells were classified into a second mode with at least 99% confidence. Cells were then assigned to subclones based on their mode for all chromosome arms with a multimodal distribution. CNA_0 were used instead of CNA_f since the normalization procedure introduces a bias (zero inflation) in signal distribution.

Association between programs of variability and CNA subclones

In cell lines presenting discrete programs of variability and CNA subclones, we evaluated the association between the expression-based classification of cells into subpopulations, as defined by DBSCAN, and the subclone-based classification, as defined by GMM, using Fisher's exact test In cell lines presenting continuous programs of variability and CNA subclones, we compared NMF cell scores of each program between clones using t-test. $P < 0.001$ were considered statistically significant.

Drug screen analysis

In order to define potential hits from the primary screen for follow-up in the secondary screen, we considered the differential viability between the EpiSen-high and EpiSen-low states for each compound in each cell line. In order to define hits that were differentially sensitive for only one cell line, we used 2.5 standard deviations from the mean of the difference in viability of the vehicle (DMSO-treated) controls between states as the threshold. In order to define shared hits that were differentially sensitive between the EpiSen-high and EpiSen-low states in both cell lines we used a threshold of 2 standard deviations from the mean of the difference in viability of the vehicle controls between states. Statistical significance of enrichment for shared hits was evaluated by hypergeometric test ($p = 0.006$, significant for EpiSen-high, $p = 0.943$ n.s. for EpiSen-low). A third category of compounds that killed cells in both the EpiSen-high and EpiSen-low states at 10 μM (defined as $\leq$ 10% viability) was also selected for follow-up in the secondary screen at lower concentration (1 μM).

The secondary screen was performed in duplicates. In order to determine the differential viability between the EpiSen-high and EpiSen-low states, we compared the mean of each duplicate measurements. To avoid an impact from outlier measurements, in each case where the difference between duplicates was larger than 20%, we calculated three potential values for differential viability between EpiSen-high and EpiSen-low populations: one value based on the mean of the two duplicate measurements and two additional values based on each measurement alone. We then conservatively used the minimal value of differential viability to ensure that individual outlier measurements will not lead to the appearance of differential viability. In order to define hits in the secondary screen, the threshold was defined by the upper and lower bounds of the adjusted control values over replicates between states.

A subset of compounds that were differentially sensitive between the EpiSen-high and EpiSen-low cell lines were selected for follow-up dose response studies in SCC47 in each sorted subpopulation (EpiSen-low, EpiSen-high, reference). To generate dose response curves, viability at each concentration of the seven-point dose response series was averaged over replicates and normalized to the viability of vehicle (DMSO) controls. Percent change in viability was calculated at each concentration using the normalized viability and curves were fit using these values with a three-parameter nonlinear regression model in GraphPad Prism 8 (GraphPad Software, La Jolla CA, USA). A paired t-test was performed using the aggregated differences in viability at each concentration to determine statistical significance ($P \leq 0.05$) of differential viability between curves (**Table S6).**

Acknowledgements

References

Aceto, N., Bardia, A., Miyamoto, D.T., Donaldson, M.C., Wittner, B.S., Spencer, J.A., Yu, M., Pely, A., Engstrom, A., Zhu, H.*, et al.* (2014). Circulating tumor cell clusters are oligoclonal precursors of breast cancer metastasis. Cell *158*, 1110-1122.

Barretina, J., Caponigro, G., Stransky, N., Venkatesan, K., Margolin, A.A., Kim, S., Wilson, C.J., Lehar, J., Kryukov, G.V., Sonkin, D.*, et al.* (2012). The Cancer Cell Line Encyclopedia enables predictive modelling of anticancer drug sensitivity. Nature *483*, 603-607.

Beauséjour, C.M., Krtolica, A., Galimi, F., Narita, M., Lowe, S. W., Yaswen, P., and Campisi, J. (2003). Reversal of human cellular senescence: roles of the p53 and p16 pathways. The EMBO journal *22*, 4212-4222.

Ben-David, U., Siranosian, B., Ha, G., Tang, H., Oren, Y., Hinohara, K., Strathdee, C.A., Dempster, J., Lyons, N.J., Burns, R.*, et al.* (2018). Genetic and transcriptional evolution alters cancer cell line drug response. Nature *560*, 325-330.

Bozulic, L., Surucu, B., Hynx, D., and Hemmings, B.A. (2008). PKBalpha/Akt1 acts downstream of DNA-PK in the DNA double-strand break response and promotes survival. Mol Cell *30*, 203-213.

Chaffer, C.L., San Juan, B.P., Lim, E., and Weinberg, R.A. (2016). EMT, cell plasticity and metastasis. Cancer metastasis reviews *35*, 645-654.

Chen, Q., Sun, L., and Chen, Z.J. (2016). Regulation and function of the cGAS-STING pathway of cytosolic DNA sensing. Nature immunology *17*, 1142-1149.

Chung, W., Eum, H.H., Lee, H.O., Lee, K.M., Lee, H.B., Kim, K.T., Ryu, H.S., Kim, S., Lee, J.E., Park, Y.H.*, et al.* (2017). Single-cell RNA-seq enables comprehensive tumour and immune cell profiling in primary breast cancer. Nature communications *8*, 15081.

Elkabets, M., Pazarentzos, E., Juric, D., Sheng, Q., Pelossof, R. A., Brook, S., *et al.* (2015). AXL mediates resistance to PI3Kα inhibition by activating the EGFR/PKC/mTOR axis in head and neck and esophageal squamous cell carcinomas. Cancer cell *27*, 533-546.

Filbin, M.G., Tirosh, I., Hovestadt, V., Shaw, M.L., Escalante, L.E., Mathewson, N.D., Neftel, C., Frank, N., Pelton, K., Hebert, C.M.*, et al.* (2018). Developmental and oncogenic programs in H3K27M gliomas dissected by single-cell RNA-seq. Science *360*, 331-335.

Friedman, J., Hastie, T., and Tibshirani, R. (2010). Regularization Paths for Generalized Linear Models via Coordinate Descent. J Stat Softw *33*, 1-22.

Ghandi, M., Huang, F.W., Jane-Valbuena, J., Kryukov, G.V., Lo, C.C., McDonald, E.R., 3rd, Barretina, J., Gelfand, E.T., Bielski, C.M., Li, H.*, et al.* (2019). Next-generation characterization of the Cancer Cell Line Encyclopedia. Nature *569*, 503-508.

Hangauer, M.J., Viswanathan, V.S., Ryan, M.J., Bole, D., Eaton, J.K., Matov, A., Galeas, J., Dhruv, H.D., Berens, M.E., Schreiber, S.L.*, et al.* (2017). Drug-tolerant persister cancer cells are vulnerable to GPX4 inhibition. Nature *551*, 247-250.

Hernandez-Segura, A., de Jong, T.V., Melov, S., Guryev, V., Campisi, J., and Demaria, M. (2017). Unmasking Transcriptional Heterogeneity in Senescent Cells. Current biology : CB *27*, 2652-2660 e2654.

Jerby-Arnon, L., Shah, P., Cuoco, M.S., Rodman, C., Su, M.J., Melms, J.C., Leeson, R., Kanodia, A., Mei, S., Lin, J.R.*, et al.* (2018). A Cancer Cell Program Promotes T Cell Exclusion and Resistance to Checkpoint Blockade. Cell *175*, 984-997 e924.

Kagoya, Y., Yoshimi, A., Tsuruta-Kishino, T., Arai, S., Satoh, T., Akira, S., and Kurokawa, M. (2014). JAK2V617F+ myeloproliferative neoplasm clones evoke paracrine DNA damage to adjacent normal cells through secretion of lipocalin-2. Blood *124*, 2996-3006.

Kang, H.M., Subramaniam, M., Targ, S., Nguyen, M., Maliskova, L., McCarthy, E., Wan, E., Wong, S., Byrnes, L., Lanata, C.M.*, et al.* (2018). Multiplexed droplet single-cell RNA-sequencing using natural genetic variation. Nature biotechnology *36*, 89-94.

Keren-Shaul, H., Kenigsberg, E., Jaitin, D.A., David, E., Paul, F., Tanay, A., and Amit, I. (2019). MARS-seq2.0: an experimental and analytical pipeline for indexed sorting combined with single-cell RNA sequencing. Nat Protoc *14*, 1841-1862.

Kim, K.T., Lee, H.W., Lee, H.O., Kim, S.C., Seo, Y.J., Chung, W., Eum, H.H., Nam, D.H., Kim, J., Joo, K.M.*, et al.* (2015). Single-cell mRNA sequencing identifies subclonal heterogeneity in anti-cancer drug responses of lung adenocarcinoma cells. Genome biology *16*, 127.

Kim, K.T., Lee, H.W., Lee, H.O., Song, H.J., Jeong da, E., Shin, S., Kim, H., Shin, Y., Nam, D.H., Jeong, B.C.*, et al.* (2016). Application of single-cell RNA sequencing in optimizing a combinatorial therapeutic strategy in metastatic renal cell carcinoma. Genome biology *17*, 80.

Kondo, T., Kobayashi, J., Saitoh, T., Maruyama, K., Ishii, K.J., Barber, G.N., Komatsu, K., Akira, S., and Kawai, T. (2013). DNA damage sensor MRE11 recognizes cytosolic double-stranded DNA and induces type I interferon by regulating STING trafficking. Proceedings of the National Academy of Sciences of the United States of America *110*, 2969-2974.

Kowalczyk, M.S., Tirosh, I., Heckl, D., Rao, T.N., Dixit, A., Haas, B.J., Schneider, R.K., Wagers, A.J., Ebert, B.L., and Regev, A. (2015). Single-cell RNA-seq reveals changes in cell cycle and differentiation programs upon aging of hematopoietic stem cells. Genome Res *25*, 1860-1872.

Lambrechts, D., Wauters, E., Boeckx, B., Aibar, S., Nittner, D., Burton, O., Bassez, A., Decaluwe, H., Pircher, A., Van den Eynde, K.*, et al.* (2018). Phenotype molding of stromal cells in the lung tumor microenvironment. Nature medicine *24*, 1277-1289.

Lee, S., and Schmitt, C.A. (2019). The dynamic nature of senescence in cancer. Nature cell biology *21*, 94.

Li, H., Courtois, E.T., Sengupta, D., Tan, Y., Chen, K.H., Goh, J.J.L., Kong, S.L., Chua, C., Hon, L.K., Tan, W.S.*, et al.* (2017). Reference component analysis of single-cell transcriptomes elucidates cellular heterogeneity in human colorectal tumors. Nature genetics *49*, 708-718.

Liberzon, A. (2014). A description of the Molecular Signatures Database (MSigDB) Web site. Methods Mol Biol *1150*, 153-160.

McGranahan, N., and Swanton, C. (2015). Biological and therapeutic impact of intratumor heterogeneity in cancer evolution. Cancer cell *27*, 15-26.

Neftel, C., Laffy, J., Filbin, M.G., Hara, T., Shore, M.E., Rahme, G.J., Richman, A.R., Silverbush, D., Shaw, M.L., Hebert, C.M.*, et al.* (2019). An Integrative Model of Cellular States, Plasticity, and Genetics for Glioblastoma. Cell *178*, 835-849 e821.

Patel, A.P., Tirosh, I., Trombetta, J.J., Shalek, A.K., Gillespie, S.M., Wakimoto, H., Cahill, D.P., Nahed, B.V., Curry, W.T., Martuza, R.L.*, et al.* (2014). Single-cell RNA-seq highlights intratumoral heterogeneity in primary glioblastoma. Science *344*, 1396-1401.

Picelli, S., Faridani, O.R., Björklund, Å.K., Winberg, G., Sagasser, S., and Sandberg, R. (2014). Full-length RNA-seq from single cells using Smart-seq2. Nature protocols *9*, 171.

Puram, S., Tirosh, I., Parikh, A., Patel, A., Yizhak, K., Gillespie, S., Rodman, R., Luo, C., Mroz, E., Emerick, K.*, et al.* (2017). Single-cell transcriptomic analysis of primary and metastatic tumor ecosystems in head and neck cancer. Cell *171*, 1611-1624.

Rauner, G., Kudinov, T., Gilad, S., Hornung, G., and Barash, I. (2018). High Expression of CD200 and CD200R1 Distinguishes Stem and Progenitor Cell Populations within Mammary Repopulating Units. Stem Cell Reports *11*, 288-302.

Sage, J., Miller, A.L., Pérez-Mancera, P.A., Wysocki, J.M., and Jacks, T. (2003). Acute mutation of retinoblastoma gene function is sufficient for cell cycle re-entry. Nature *424*, 223.

Shaffer, S.M., Dunagin, M.C., Torborg, S.R., Torre, E.A., Emert, B., Krepler, C., Beqiri, M., Sproesser, K., Brafford, P.A., Xiao, M.*, et al.* (2017). Rare cell variability and drug-induced reprogramming as a mode of cancer drug resistance. Nature *546*, 431-435.

Sharma, A., Cao, E.Y., Kumar, V., Zhang, X., Leong, H.S., Wong, A.M.L., Ramakrishnan, N., Hakimullah, M., Teo, H.M.V., Chong, F.T.*, et al.* (2018). Longitudinal single-cell RNA sequencing of patient-derived primary cells reveals drug-induced infidelity in stem cell hierarchy. Nature communications *9*, 4931.

te Poele, R.H., Okorokov, A.L., Jardine, L., Cummings, J., and Joel, S.P. (2002). DNA damage is able to induce senescence in tumor cells in vitro and in vivo. Cancer Res *62*, 1876-1883.

Tirosh, I., Izar, B., Prakadan, S.M., Wadsworth, M.H., 2nd, Treacy, D., Trombetta, J.J., Rotem, A., Rodman, C., Lian, C., Murphy, G.*, et al.* (2016a). Dissecting the multicellular ecosystem of metastatic melanoma by single-cell RNA-seq. Science *352*, 189-196.

Tirosh, I., Venteicher, A.S., Hebert, C., Escalante, L.E., Patel, A.P., Yizhak, K., Fisher, J.M., Rodman, C., Mount, C., Filbin, M.G.*, et al.* (2016b). Single-cell RNA-seq supports a developmental hierarchy in human oligodendroglioma. Nature *539*, 309-313.

Venteicher, A.S., Tirosh, I., Hebert, C., Yizhak, K., Neftel, C., Filbin, M.G., Hovestadt, V., Escalante, L.E., Shaw, M.L., Rodman, C.*, et al.* (2017). Decoupling genetics, lineages, and microenvironment in IDH-mutant gliomas by single-cell RNA-seq. Science *355*.

Viswanathan, V.S., Ryan, M.J., Dhruv, H.D., Gill, S., Eichhoff, O.M., Seashore-Ludlow, B., Kaffenberger, S.D., Eaton, J.K., Shimada, K., Aguirre, A.J.*, et al.* (2017). Dependency of a therapy-resistant state of cancer cells on a lipid peroxidase pathway. Nature *547*, 453-457.

Wong, R.H., Chang, I., Hudak, C.S., Hyun, S., Kwan, H.Y., and Sul, H.S. (2009). A role of DNA-PK for the metabolic gene regulation in response to insulin. Cell *136*, 1056-1072.

Yosef, R., Pilpel, N., Tokarsky-Amiel, R., Biran, A., Ovadya, Y., Cohen, S., Vadai, E., Dassa, L., Shahar, E., Condiotti, R.*, et al.* (2016). Directed elimination of senescent cells by inhibition of BCL-W and BCL-XL. Nature communications *7*, 11190.

Yu, C., Mannan, A.M., Yvone, G.M., Ross, K.N., Zhang, Y.L., Marton, M.A., Taylor, B.R., Crenshaw, A., Gould, J.Z., Tamayo, P.*, et al.* (2016). High-throughput identification of genotype-specific cancer vulnerabilities in mixtures of barcoded tumor cell lines. Nature biotechnology *34*, 419-423.
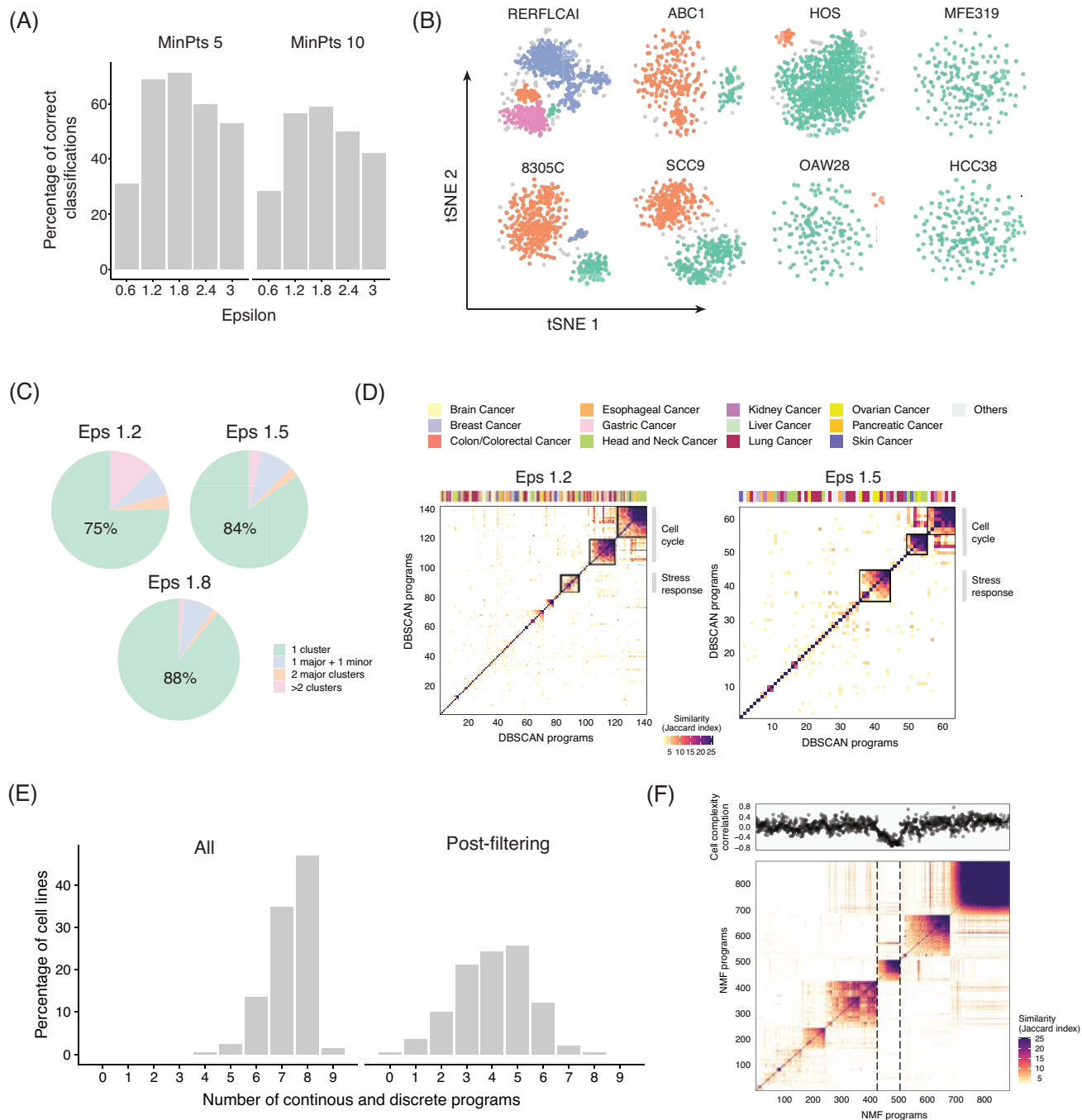
Supplementary Figures

(A)

(B)

(C)

(D)

(E)

(F)

Figure S1. Identifying discrete and continuous programs of heterogeneity. (**A**) Performance of DBSCAN using different sizes of epsilon neighborhood (eps) and minimum numbers of points required to form a dense region (MinPts). We randomly selected cells from two different cell lines and tested the ability of DBSCAN to distinguish between them using different parameter combinations. The procedure was repeated 1,000 times and the combination yielding the highest rate of correct classification was applied in the subsequent analyses. (**B**) tSNE plots for two additional examples of cell lines from each of the four classes defined by presence and number of discrete subpopulations identified by DBSCAN (as in **Fig. 2B**). (**C**)-(**D**) Identification of discrete programs of heterogeneity, as in **Fig. 2B-C**, using less stringent eps (1.2 and 1.5) highlights common trends. (**E**) Number of heterogeneity programs identified per cell line using NMF. NMF was applied to each cell line using k (number of factors) of 6-9, and gene programs identified as variable with 2 or more values of k were retained (left panel). To identify common expression programs varying within multiple cell lines, we excluded programs with limited similarity to all other programs as well as those associated with technical confounders (right panel). (**D**) Pairwise similarities between programs identified by NMF across all the cell lines analyzed, with cell lines ordered by hierarchical clustering. Programs with limited similarity to all other programs were excluded. Top panel indicates correlations between program scores and cell complexity (i.e. number of genes detected per cell). The group of programs that correlates with complexity (indicated by dashed lines) was excluded from subsequent analyses.
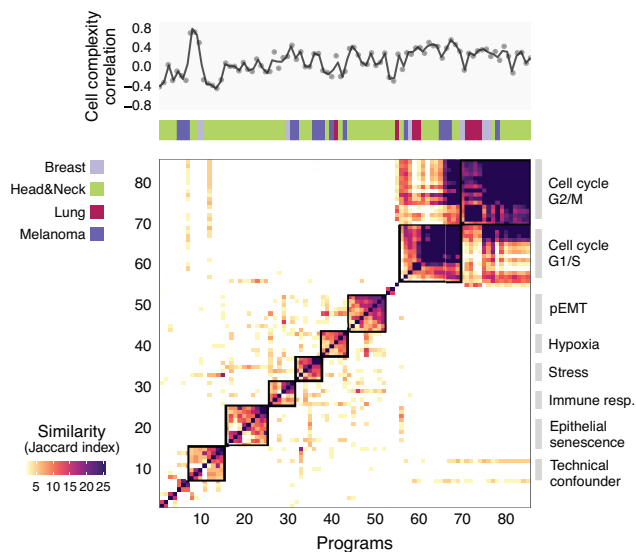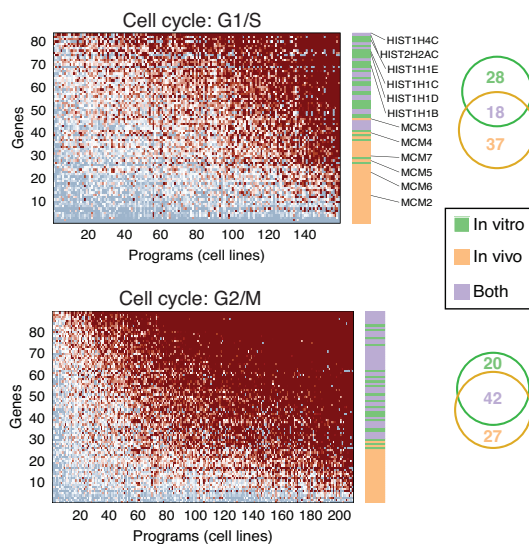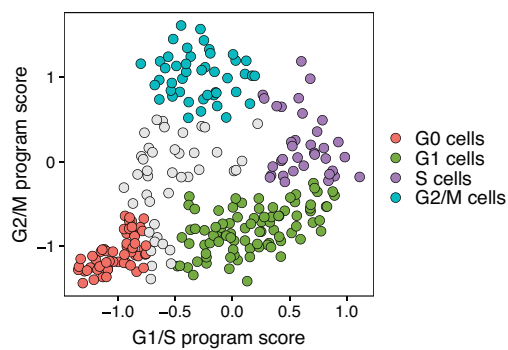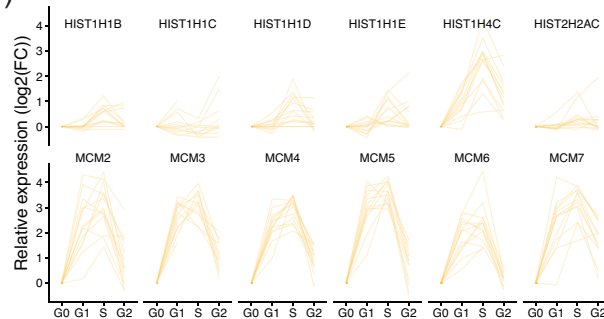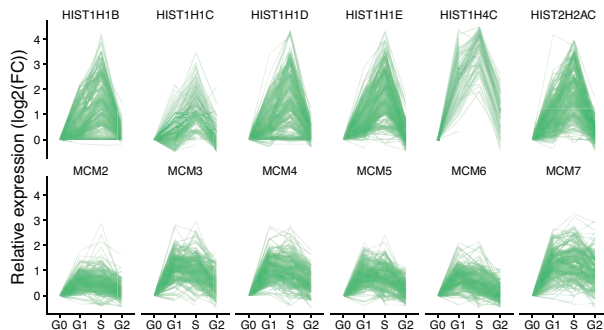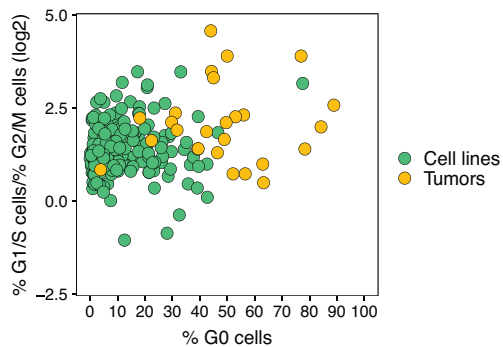
Figure S2. Comparison between cell cycle in vitro and in vivo. (**A**) Heatmap depicts pairwise similarities between programs identified in fresh tumor samples using NMF. NMF was applied to each tumor with *k* (number of factors) of 6-9 and gene programs identified as variable with 2 or more values of *k* were retained. To identify common expression programs varying within multiple tumors, we excluded programs with limited similarity to all other programs. Top panel shows tumor type and correlations between program scores and cell complexity (i.e. number of genes detected per cell). Hierarchical clustering emphasizes multiple metaprograms (shown by squares), one of which is correlated with cell complexity and thus excluded as a potential technical artifact. (**B**) NMF scores of G1/S genes (top panel) and G2/M genes (bottom panel) genes across cell lines with corresponding cell cycle programs. Genes are ranked in each panel by average scores, and their assignment to in vitro and in vivo cell cycle programs is indicated on the right, demonstrating that G1/S programs differ both across cell lines and between cell lines and tumors, while G2/M programs are more consistent. Venn diagrams (right) illustrate the overlap between in vivo and in vitro RHPs. (**C**) Single-cell profiles showing G1/S and G2/M program score thresholds used to assign cells to different cell cycle phases. (**D**) Examples of genes with distinct cell cycle induction in vitro and in vivo. Expression of HIST genes (preferentially induced in vitro) and MCM genes (preferentially induced in vivo) is shown along the cell cycle (relative to cells in G0) in cell lines (C, green lines) and tumors (D, yellow lines). (**E**) Comparison of cell cycle phase distribution in vitro and in vivo. Scatterplot shows the percentage of cells in G0 (x-axis) and the ratio between the percentage of cells in G1/S and G2/M (y-axis) for each cell line (green) and tumor (yellow) analyzed. Cell lines display a significantly lower percentage of cells in G0 cells (p = $2e^{-10}$, t-test).
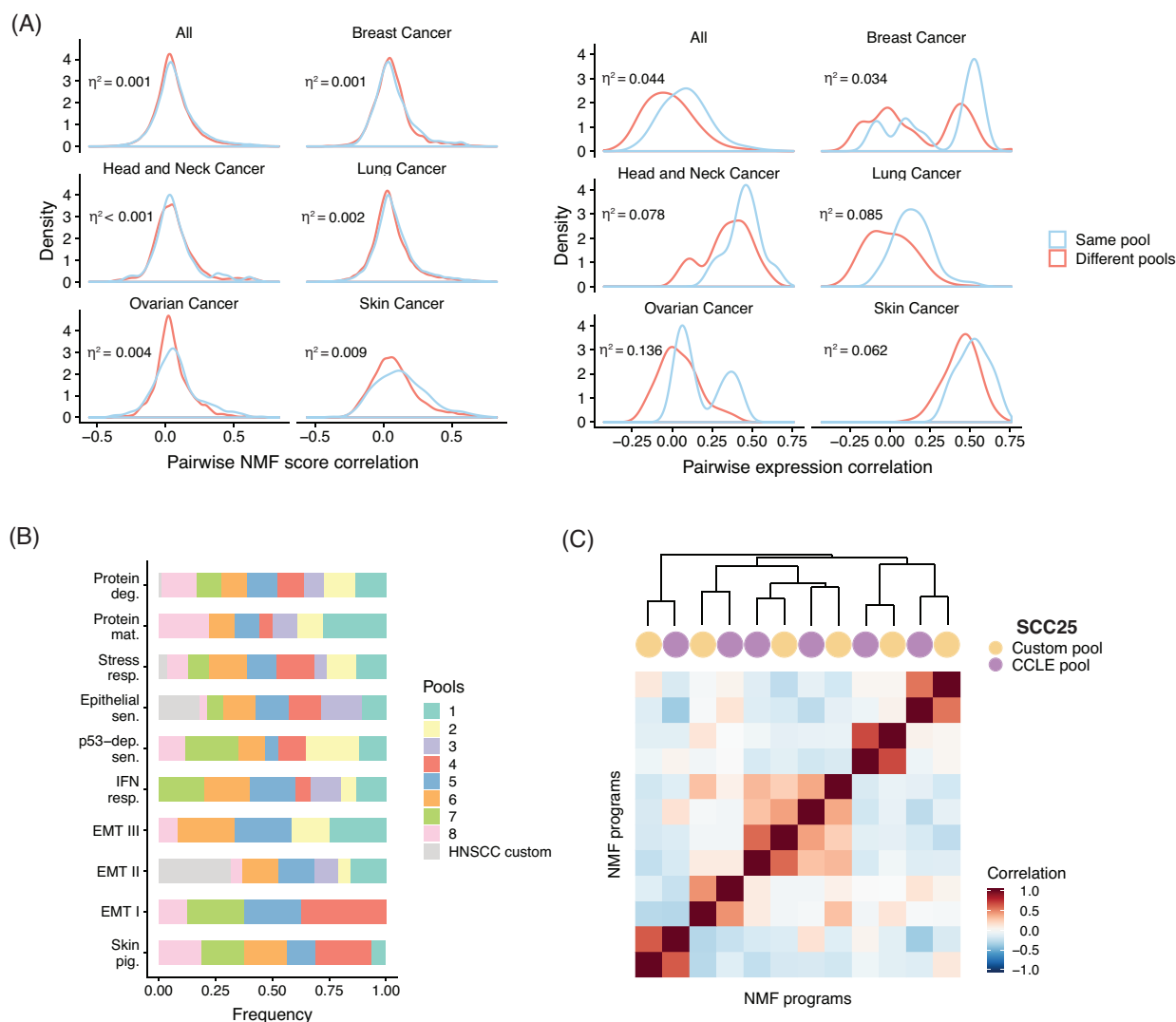
Figure S3. The pooling procedure has a limited impact on intra-cell line expression heterogeneity. (A) Distribution of pairwise similarities between expression patterns of cell lines in the same (blue) and in different (red) pools. Left: The comparison was done for all NMF programs detected in the corresponding cell lines, by correlation of the NMF gene scores (for all analyzed genes). Right: The comparison was done between the average expression profiles of the cell lines, by correlation across all analyzed genes. Comparisons were performed across all cell lines or separated by cancer type (only most abundant types are shown). The proportion of total variance (η^2) explained by whether or not programs/cell lines were in the same pool, calculated using one-way ANOVA, suggests that patterns of expression heterogeneity (left) are largely unaffected by the pool microenvironment, while the average expression profiles (right) are more affected. **(B)** Distribution of the pool of origin of RHPs. Each RHP was observed in multiple pools, underscoring the lack of pool-specific effects. **(C)** Pairwise correlations between NMF programs obtained for the HNSCC cell line SCC25, which is the only cell line that was profiled in two different pools. Hierarchical clustering reveals highly concordant programs in the two pools.
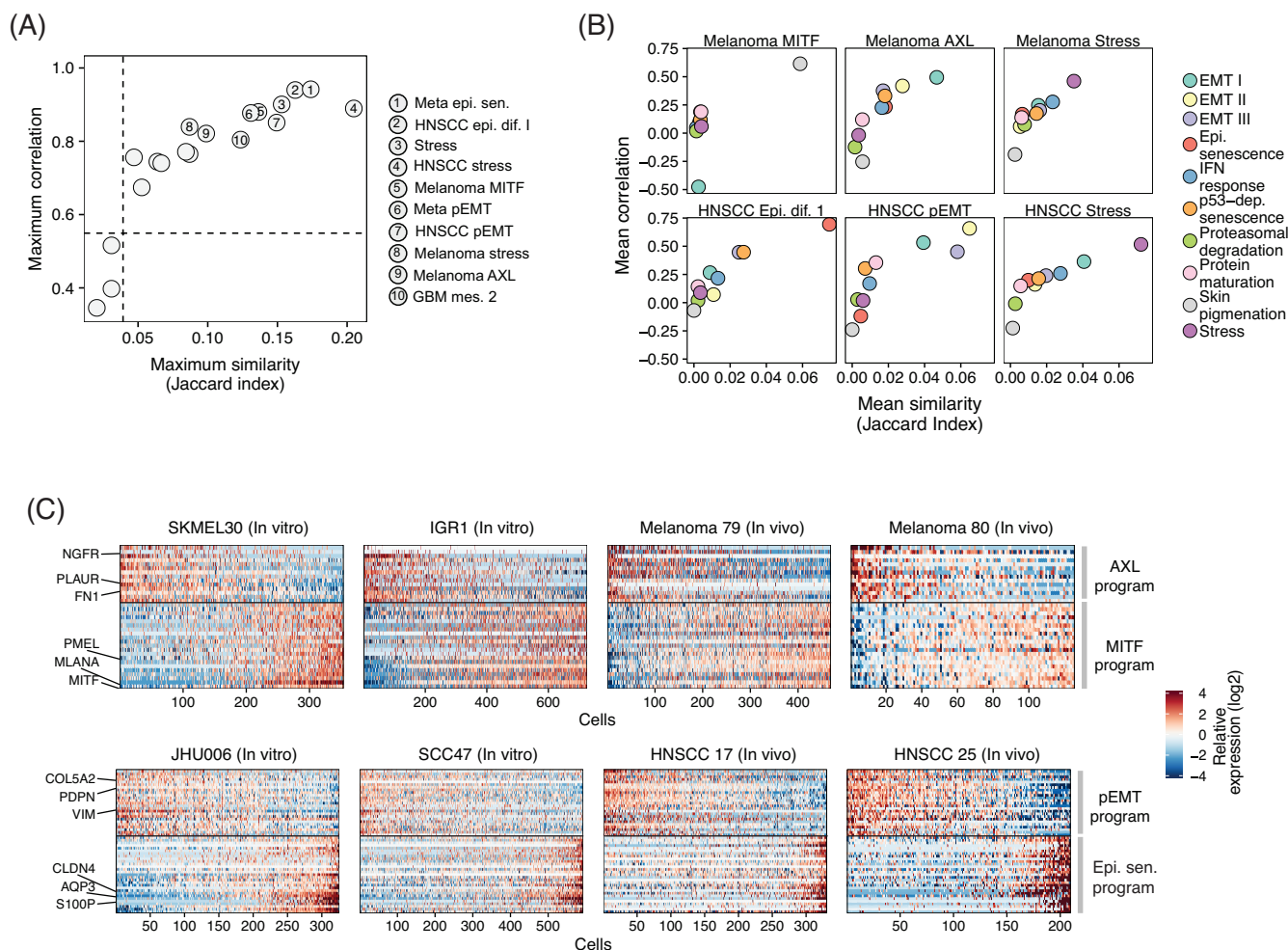
Figure S4. Cell lines recapitulate programs of heterogeneity observed in tumor samples. (A) Scatterplot shows maximum single-cell score correlation (X-axis) and overlap (Y-axis) between each in vivo program and the in vitro programs shown in **Fig. 3A**. The top 10 in vivo programs with highest correlations are annotated, and relevant ones are also highlighted in **Fig. 3B top**. **(B)** Scatterplots show mean single-cell score correlations (X-axis) and mean similarities (Y-axis) between relevant in vivo programs and the 10 in vitro RHPs. The five RHPs with highest correlations/similarities are marked in **Fig. 3B right**. **(C)** Heatmap shows relative expression of genes shared by paired in vivo and in vitro programs in selected melanoma and HNSCC cell lines and tumors, highlighting similar patterns of variability in vivo and in vitro. Cells are sorted according to the relative average expression of genes in each program, showing the negative correlation between the AXL and MITF programs in melanomas and the pEMT and EpiSen programs in HNSCC. Programs are annotated (right) and selected genes are indicated (left).

(A)

(B)

(C)

(D)

(E)

(F)
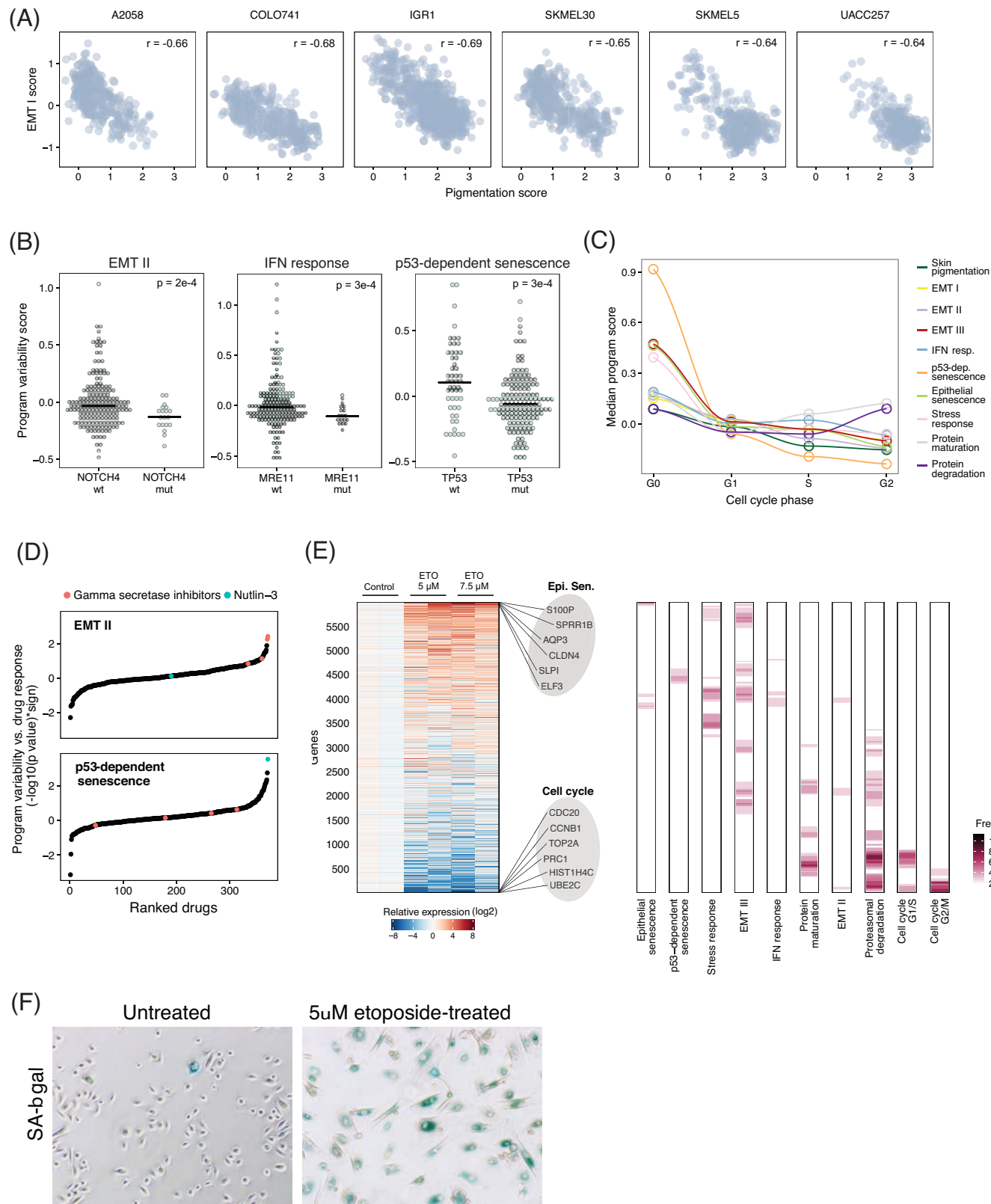
Figure S5. Determinants and consequences of cellular heterogeneity. (**A**) Single-cell profiles show a negative correlation between the skin pigmentation and the EMT-I RHPs within each of six melanoma cell lines. (**B**) Association between RHP variability scores and somatic non-silent mutations. We compared the variability score of each program in mutated and non-mutated cell lines using t-test. Model cell lines (high variability score) of EMT-II, IFN response and p53-dependent senescence RHPs are depleted of NOTCH4, MRE11 and TP53 mutations, respectively. Association between drug response (CTRP database) and program variability calculated using linear regression including tumor type and program variability as independent variables. Increased sensitivity to NOTCH inhibition (gamma secretase inhibitors), MDM2 inhibition (Nutlin-3) were observed in model cell lines (high program variability) of the EMT-II, and p53-dependent senescence respectively. (**C**) Median RHP scores of cells in each phase of the cell cycle, emphasizing the high expression of the senescence, stress and EMT-III metaprograms in non-cycling cells (G0). Cell cycle state was estimated for each individual cell based on the relative expression of the G1/S and G2/M metaprograms. For each RHP we only considered the respective model cell lines. (**D**) Heatmap depicts relative expression of the 6,000 top highly expressed genes (rows) in primary lung bronchial cells 9 days after induction of senescence by etoposide treatment for 48 h in two concentrations. Bars on the right show the frequency of RHP signature genes within sliding windows of 300 genes. RHPs are sorted from left to right by their enrichment with upregulated and downregulated genes, respectively. EpiSen and cell cycle programs were the two extreme programs, and selected genes from these programs are labeled. (**E**) Induction of senescence confirmed by SA-β-gal staining.
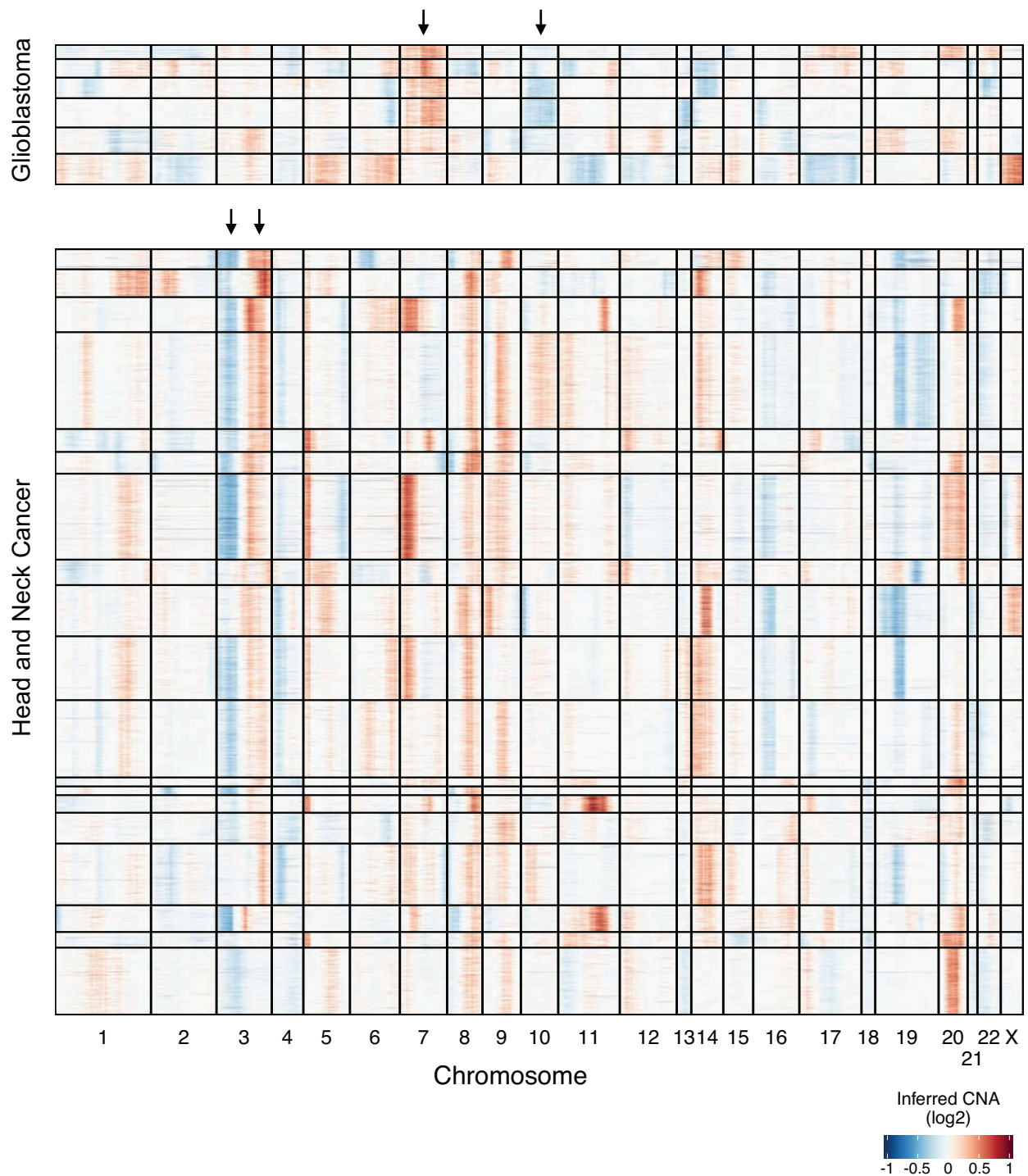
Figure S6. Inferred CNAs are consistent with expected chromosomal aberrations. Heatmap depicts inferred CNAs for individual cells (rows) from 6 glioblastoma (top) and 19 HNSCC (bottom) cell lines, based on the average expression of sliding windows of 100 genes. Arrows highlight expected hallmark alterations - the gain of chromosome 7 and loss of chromosome 10 in glioblastoma, and the loss of chromosome 3p and gain of chromosome 3q in HNSCCs.
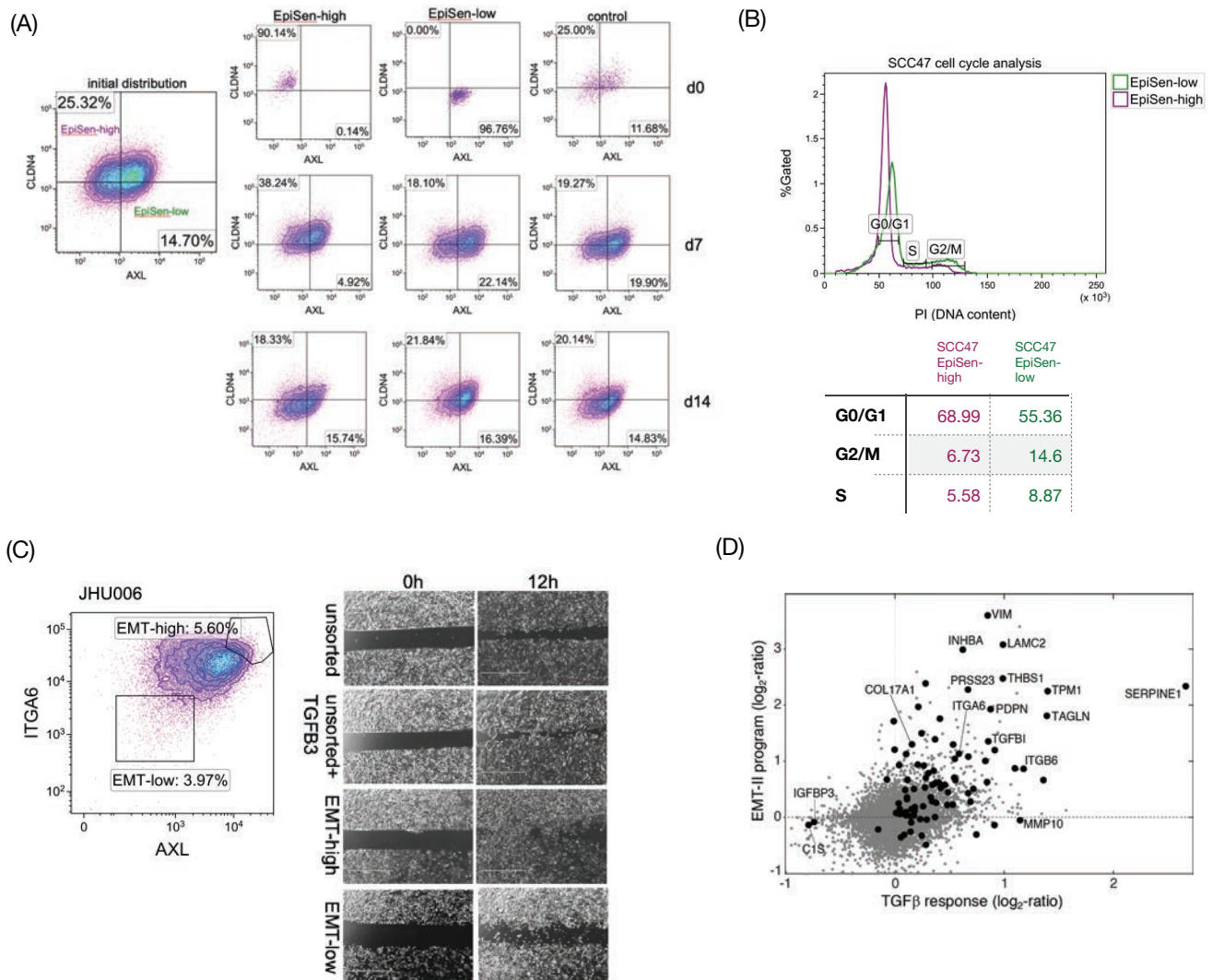
Figure S7. Interrogating EpiSen and EMT-II in model cell lines, refers to Fig. 5. (A) Isolation by FACS of the EpiSen-high population (AXL$^-$CLDN4$^+$), the EpiSen-low population (AXL$^+$CLDN4$^-$) and a third unsorted control population based on AXL and Claudin4 expression analyzed immediately after sorting (day 0) and at two additional time points in culture (day 7 and 14) in JHU006. The density plots correspond to the pie charts depicting dynamics in **Fig. 5c**. Gating was determined by the unstained control at each time point. **(B)** FACS analysis of cell cycle by the DNA binding dye propidium iodide (PI) on sorted EpiSen-high and EpiSen-low cells in SCC47. The table (lower inset) summarizes cell cycle analysis for both SCC47 and JHU006 (shown in Fig. 6D). **(C)** Isolation by FACS of the EMT-II-high population (AXL$^+$ITGA6$^+$) and the EMT-II-low population (AXL$^-$ITGA6$^-$) in JHU006 and images of subsequent gap closure (migration) assay on unsorted, unsorted TGFβ3-treated, EMT-II-high, and EMT-II-low cells at 0 h and 12 h following gap generation. **(D)** Comparison of EMT program induced upon TGFβ treatment of unsorted JHU006 and SCC47 vs. the EMT-II cell line metaprogram.

61

(A)

JHU006   SCC47

- EpiSen-high sensitive (strict)
- EpiSen-low sensitive (strict)
- EpiSen-high sensitive (shared)
- EpiSen-low sensitive (shared)
- Killed all
- No differential sensitivity

(B)

Primary screen

Diff. viability JHU006 (EpiSen-high minus EpiSen-low)

Prednisolone (Glucocorticoid Rc)
Bendamustine HCL (DNA Synthesis)
Albamycin (Topoisomerase)
Etodolac (COX)

WHI−P154 (EGFR,JAK)
S−Ruxolitinib (JAK)
NVP−TAE226 (FAK, IGF1R)
NVP−ADW742 (IGF1R)
Tofacitinib (JAK)
PIK−93 (PI3K)
PIK−93 (PI3K)

Shared hits:
- EpiSen-high
- EpiSen-low

Diff. viability SCC47
(EpiSen-high minus EpiSen-low)

(C)

JHU006 primary screen

Diff. viability (EpiSen-high minus EpiSen-low)

Overall drug response (viability ref.)

SCC47 primary screen

Overall drug response (viability ref.)

- DNA synthesis/cell cycle
- steroid/anti−inflammatory
- TGFBR/VEGFR/PDGFR
- EGFR/PI3K/Akt
- IGF1R
- JAK
- killed all
- positive control
- veh control

(D)

NVP-ADW742 (IGF1-R)

% change in viability

log concentration (μM)

Paroxetine HCl (5HT, SSRI)

log concentration (μM)

AC480 (HER2/EGFR)

log concentration (μM)

Oprozomib (proteasome)

log concentration (μM)

- EpiSen-high
- EpiSen-low
- Reference

Figure S8. Co-existing cellular states differ in drug sensitivity (primary drug screen, refers to Fig. 6). EpiSen-high cells, EpiSen-low cells, and a neutral reference population were isolated by FACS in JHU006 and SCC47, then treated with a compound library in 384-well format for 48 h and viability was determined by CTG assay (n = 2198 compounds screened per state, per cell line). **(A)** Pie charts depicting the relative proportions of hits by type in the primary screen for both JHU006 and SCC47. **(B)** Shared hits between SCC47 and JHU006 for compounds that were differentially sensitive in the EpiSen-high state (green) and EpiSen-low state (orange). Thresholds are cell line-dependent. Significance of overlap of hits between cell lines for EpiSen-high: p = 0.006 (significant), for EpiSen-low: p = 0.943 (not significant) by hypergeometric test. **(C)** Viability of the reference population (X-axis) and differential viability of the EpiSen-high vs. EpiSen-low populations (Y-axis) upon treatment with 2198 compounds in JHU006 (left) and SCC47 (right). Dotted lines represent the thresholds for defining differential sensitivity between the EpiSen-high and EpiSen-low states, hits are colored by enriched target categories. **(D)** Dose response curves of selected compounds (continued from Fig. 6C) for follow-up EC50 studies in SCC47 in each sorted subpopulation (EpiSen-low, EpiSen-high, reference) performed in duplicate. Percent change in viability was calculated at each concentration using the viability normalized to vehicle (DMSO-treated) controls and curves were fit using these values with a three-parameter nonlinear regression model. Error bars represent S.D.

Supplementary Tables S2,3,5,6 were omitted/modified due to limited space

Table S1. Cell lines profiled.

Name	Primary Disease	Cells Analyzed Post QC	Pool ID
YD38_UPPER_AERODIGESTIVE_TRACT	Head and Neck Cancer	624	6
NCIH1299_LUNG	Lung Cancer	534	6
IGR37_SKIN	Skin Cancer	347	6
BFTC909_KIDNEY	Kidney Cancer	379	6
NCIH460_LUNG	Lung Cancer	837	6
IGR1_SKIN	Skin Cancer	725	6
PANC1_PANCREAS	Pancreatic Cancer	159	6
VMCUB1_URINARY_TRACT	Bladder Cancer	478	6
JHOC5_OVARY	Ovarian Cancer	145	6
42MGBA_CENTRAL_NERVOUS_SYSTEM	Brain Cancer	518	6
DAOY_CENTRAL_NERVOUS_SYSTEM	Brain Cancer	281	6
SNU1077_ENDOMETRIUM	Endometrial/Uterine Cancer	172	6
HT1080_SOFT_TISSUE	Sarcoma	516	6
LI7_LIVER	Liver Cancer	196	6
A375_SKIN	Skin Cancer	593	6
SBC5_LUNG	Lung Cancer	102	6
FTC133_THYROID	Thyroid Cancer	140	6
OVK18_OVARY	Ovarian Cancer	178	6
ACCMESO1_PLEURA	Lung Cancer	162	6
HMC18_BREAST	Breast Cancer	293	6
TOV112D_OVARY	Ovarian Cancer	78	6
SJSA1_BONE	Bone Cancer	110	6
JHH6_LIVER	Liver Cancer	206	6
A2058_SKIN	Skin Cancer	294	6
TCCSUP_URINARY_TRACT	Bladder Cancer	316	9
TOV21G_OVARY	Ovarian Cancer	305	9
VMRCRCZ_KIDNEY	Kidney Cancer	300	9
PK59_PANCREAS	Pancreatic Cancer	174	9
HUH6_LIVER	Liver Cancer	338	9
MSTO211H_PLEURA	Lung Cancer	297	9
HS852T_SKIN	Skin Cancer	162	9
SKMEL30_SKIN	Skin Cancer	353	9
T47D_BREAST	Breast Cancer	221	9
CALU6_LUNG	Lung Cancer	258	9
NCIH522_LUNG	Lung Cancer	208	9
DANG_PANCREAS	Pancreatic Cancer	143	9
LMSU_STOMACH	Gastric Cancer	255	9
SNUC4_LARGE_INTESTINE	Colon/Colorectal Cancer	467	9
RVH421_SKIN	Skin Cancer	239	9
OVSAHO_OVARY	Ovarian Cancer	227	9
MFE280_ENDOMETRIUM	Endometrial/Uterine Cancer	217	9
HS939T_SKIN	Skin Cancer	236	9
GOS3_CENTRAL_NERVOUS_SYSTEM	Brain Cancer	191	9
SNU738_CENTRAL_NERVOUS_SYSTEM	Brain Cancer	379	9
PC3_PROSTATE	Prostate Cancer	169	9
PATU8988S_PANCREAS	Pancreatic Cancer	244	9

JHOS2_OVARY	Ovarian Cancer	213	9
OVTOKO_OVARY	Ovarian Cancer	209	9
TE1_OESOPHAGUS	Esophageal Cancer	206	9
NCIH2087_LUNG	Lung Cancer	219	10
HEC59_ENDOMETRIUM	Endometrial/Uterine Cancer	385	10
EFM192A_BREAST	Breast Cancer	333	10
HS729_SOFT_TISSUE	Fibroblast	215	10
SNU423_LIVER	Liver Cancer	212	10
KPL1_BREAST	Breast Cancer	276	10
NCIH727_LUNG	Lung Cancer	270	10
NCIH358_LUNG	Lung Cancer	336	10
COLO792_SKIN	Skin Cancer	271	10
NCIH2077_LUNG	Lung Cancer	445	10
KYSE520_OESOPHAGUS	Esophageal Cancer	323	10
KMRC3_KIDNEY	Kidney Cancer	245	10
MKN7_STOMACH	Gastric Cancer	258	10
NCIH1944_LUNG	Lung Cancer	414	10
HCC1419_BREAST	Breast Cancer	221	10
NCIH1568_LUNG	Lung Cancer	287	10
NCIH1048_LUNG	Lung Cancer	400	10
TE6_OESOPHAGUS	Esophageal Cancer	551	10
ZR751_BREAST	Breast Cancer	309	10
PANC0203_PANCREAS	Pancreatic Cancer	506	10
SW1990_PANCREAS	Pancreatic Cancer	307	10
RD_SOFT_TISSUE	Sarcoma	261	10
CL34_LARGE_INTESTINE	Colon/Colorectal Cancer	378	10
NCIH1792_LUNG	Lung Cancer	111	10
PK45H_PANCREAS	Pancreatic Cancer	271	10
LS180_LARGE_INTESTINE	Colon/Colorectal Cancer	361	15
RERFLCAI_LUNG	Lung Cancer	763	15
CAMA1_BREAST	Breast Cancer	291	15
SNU449_LIVER	Liver Cancer	282	15
A204_SOFT_TISSUE	Sarcoma	250	15
HUCCT1_BILIARY_TRACT	Bile Duct Cancer	241	15
MKN45_STOMACH	Gastric Cancer	118	15
SNU1196_BILIARY_TRACT	Bile Duct Cancer	286	15
HEP3B217_LIVER	Liver Cancer	118	15
HOS_BONE	Bone Cancer	829	15
SKMES1_LUNG	Lung Cancer	144	15
EBC1_LUNG	Lung Cancer	186	15
NCIH292_LUNG	Lung Cancer	213	15
OUMS23_LARGE_INTESTINE	Colon/Colorectal Cancer	107	15
HEC151_ENDOMETRIUM	Endometrial/Uterine Cancer	250	15
MDAMB436_BREAST	Breast Cancer	281	15
ABC1_LUNG	Lung Cancer	311	15
NCIH1373_LUNG	Lung Cancer	164	15
TE9_OESOPHAGUS	Esophageal Cancer	248	15
HCC56_LARGE_INTESTINE	Colon/Colorectal Cancer	99	15
HT55_LARGE_INTESTINE	Colon/Colorectal Cancer	211	15
RT4_URINARY_TRACT	Bladder Cancer	106	15
SKES1_BONE	Bone Cancer	91	15
NCIH1435_LUNG	Lung Cancer	267	15

CCK81_LARGE_INTESTINE	Colon/Colorectal Cancer	127	16
NCIH2110_LUNG	Lung Cancer	1990	16
NCIH650_LUNG	Lung Cancer	271	16
EFE184_ENDOMETRIUM	Endometrial/Uterine Cancer	86	16
HUPT3_PANCREAS	Pancreatic Cancer	136	16
MDAMB361_BREAST	Breast Cancer	135	16
BCPAP_THYROID	Thyroid Cancer	152	16
PECAPJ49_UPPER_AERODIGESTIVE_TRACT	Head and Neck Cancer	202	16
EKVX_LUNG	Lung Cancer	146	16
2313287_STOMACH	Gastric Cancer	103	16
BICR56_UPPER_AERODIGESTIVE_TRACT	Head and Neck Cancer	81	16
NCIH2170_LUNG	Lung Cancer	142	16
DETROIT562_UPPER_AERODIGESTIVE_TRACT	Head and Neck Cancer	163	16
SW1088_CENTRAL_NERVOUS_SYSTEM	Brain Cancer	128	16
BHY_UPPER_AERODIGESTIVE_TRACT	Head and Neck Cancer	145	16
CAS1_CENTRAL_NERVOUS_SYSTEM	Brain Cancer	133	16
HCC1428_BREAST	Breast Cancer	127	16
HDQP1_BREAST	Breast Cancer	64	16
OSRC2_KIDNEY	Kidney Cancer	126	16
RERFLCKJ_LUNG	Lung Cancer	87	16
HUPT4_PANCREAS	Pancreatic Cancer	56	16
NCIH2126_LUNG	Lung Cancer	264	18
SW579_THYROID	Thyroid Cancer	217	18
C32_SKIN	Skin Cancer	554	18
NCIH446_LUNG	Lung Cancer	196	18
HEC251_ENDOMETRIUM	Endometrial/Uterine Cancer	107	18
MFE319_ENDOMETRIUM	Endometrial/Uterine Cancer	191	18
SKNAS_AUTONOMIC_GANGLIA	Neuroblastoma	226	18
NCIH2452_PLEURA	Lung Cancer	538	18
COLO741_SKIN	Skin Cancer	329	18
WM88_SKIN	Skin Cancer	242	18
JHH7_LIVER	Liver Cancer	198	18
KNS42_CENTRAL_NERVOUS_SYSTEM	Brain Cancer	172	18
MCF7_BREAST	Breast Cancer	143	18
HT1197_URINARY_TRACT	Bladder Cancer	74	18
SNU899_UPPER_AERODIGESTIVE_TRACT	Head and Neck Cancer	83	18
HCC38_BREAST	Breast Cancer	200	18
HEC108_ENDOMETRIUM	Endometrial/Uterine Cancer	172	18
HT1376_URINARY_TRACT	Bladder Cancer	120	18
SNU308_BILIARY_TRACT	Gallbladder Cancer	94	18
TYKNU_OVARY	Ovarian Cancer	117	18
SW1271_LUNG	Lung Cancer	115	18
TM31_CENTRAL_NERVOUS_SYSTEM	Brain Cancer	116	18
NCIH747_LARGE_INTESTINE	Colon/Colorectal Cancer	80	18
KPNSI9S_AUTONOMIC_GANGLIA	Neuroblastoma	129	18
8305C_THYROID	Thyroid Cancer	459	19
NCIH2228_LUNG	Lung Cancer	367	19
TE10_OESOPHAGUS	Esophageal Cancer	219	19
ASPC1_PANCREAS	Pancreatic Cancer	290	19
HCC366_LUNG	Lung Cancer	202	19

BICR16_UPPER_AERODIGESTIVE_TRACT	Head and Neck Cancer	212	19
HEC6_ENDOMETRIUM	Endometrial/Uterine Cancer	161	19
KALS1_CENTRAL_NERVOUS_SYSTEM	Brain Cancer	288	19
NCIH2444_LUNG	Lung Cancer	237	19
SNU46_UPPER_AERODIGESTIVE_TRACT	Head and Neck Cancer	236	19
OAW28_OVARY	Ovarian Cancer	161	19
SNU1214_UPPER_AERODIGESTIVE_TRACT	Head and Neck Cancer	188	19
NCIH2073_LUNG	Lung Cancer	176	19
SKMEL5_SKIN	Skin Cancer	297	19
OVCAR4_OVARY	Ovarian Cancer	283	19
UACC257_SKIN	Skin Cancer	239	19
ONCODG1_OVARY	Ovarian Cancer	270	19
HUH28_BILIARY_TRACT	Bile Duct Cancer	139	19
IM95_STOMACH	Gastric Cancer	185	19
TE14_OESOPHAGUS	Esophageal Cancer	474	19
U118MG_CENTRAL_NERVOUS_SYSTEM	Brain Cancer	244	19
CAKI2_KIDNEY	Kidney Cancer	278	19
SU8686_PANCREAS	Pancreatic Cancer	82	19
SQ1_LUNG	Lung Cancer	238	22
CAOV3_OVARY	Ovarian Cancer	221	22
IALM_LUNG	Lung Cancer	322	22
BT474_BREAST	Breast Cancer	125	22
DKMG_CENTRAL_NERVOUS_SYSTEM	Brain Cancer	271	22
BT549_BREAST	Breast Cancer	266	22
BICR6_UPPER_AERODIGESTIVE_TRACT	Head and Neck Cancer	286	22
SH10TC_STOMACH	Gastric Cancer	351	22
UMUC1_URINARY_TRACT	Bladder Cancer	197	22
LS1034_LARGE_INTESTINE	Colon/Colorectal Cancer	146	22
CCFSTTG1_CENTRAL_NERVOUS_SYSTEM	Brain Cancer	246	22
NCIH226_LUNG	Lung Cancer	235	22
LNCAPCLONEFGC_PROSTATE	Prostate Cancer	129	22
RCC10RGB_KIDNEY	Kidney Cancer	233	22
NCIH2347_LUNG	Lung Cancer	145	22
TEN_ENDOMETRIUM	Endometrial/Uterine Cancer	316	22
RERFLCAD1_LUNG	Lung Cancer	243	22
COLO680N_OESOPHAGUS	Esophageal Cancer	523	22
SKMEL2_SKIN	Skin Cancer	276	22
BICR31_UPPER_AERODIGESTIVE_TRACT	Head and Neck Cancer	248	22
SKMEL3_SKIN	Skin Cancer	194	22
RCM1_LARGE_INTESTINE	Colon/Colorectal Cancer	128	22
COV434_OVARY	Ovarian Cancer	88	22
SNU1079_BILIARY_TRACT	Bile Duct Cancer	73	22
SCC47_UPPER_AERODIGESTIVE_TRACT	Head and Neck Cancer	592	custom
JHU029_UPPER_AERODIGESTIVE_TRACT	Head and Neck Cancer	797	custom
SCC25_UPPER_AERODIGESTIVE_TRACT	Head and Neck Cancer	898	custom
SCC9_UPPER_AERODIGESTIVE_TRACT	Head and Neck Cancer	475	custom
JHU011_UPPER_AERODIGESTIVE_TRACT	Head and Neck Cancer	717	custom
93VU_UPPER_AERODIGESTIVE_TRACT	Head and Neck Cancer	572	custom
SCC90_UPPER_AERODIGESTIVE_TRACT	Head and Neck Cancer	258	custom
JHU006_UPPER_AERODIGESTIVE_TRACT	Head and Neck Cancer	325	custom

Table S3. Cell lines harboring each of the non-cell cycle recurrently heterogeneous expression programs (RHP).

Skin Pigmentation	C32_SKIN, COLO741_SKIN, WM88_SKIN, SKMEL2_SKIN, SKMEL3_SKIN, IGR1_SKIN, A2058_SKIN, SKMEL30_SKIN, RVH421_SKIN, HS939T_SKIN, COLO792_SKIN, SKMEL5_SKIN, UACC257_SKIN
EMT I	C32_SKIN, COLO741_SKIN, WM88_SKIN, IGR1_SKIN, A2058_SKIN, SKMEL30_SKIN, SKMEL5_SKIN, UACC257_SKIN,
EMT II	93VU_UPPER_AERODIGESTIVE_TRACT, BCPAP_THYROID, BICR31_UPPER_AERODIGESTIVE_TRACT, CAMA1_BREAST, DKMG_CENTRAL_NERVOUS_SYSTEM, BT549_BREAST, EFM192A_BREAST, NCIH1048_LUNG, EKVX_LUNG, VMRCRCZ_KIDNEY, JHU006_UPPER_AERODIGESTIVE_TRACT, JHU011_UPPER_AERODIGESTIVE_TRACT, NCIH2073_LUNG, NCIH2228_LUNG, OVCAR4_OVARY, RD_SOFT_TISSUE, SCC25_UPPER_AERODIGESTIVE_TRACT, SCC47_UPPER_AERODIGESTIVE_TRACT
IFN Response	42MGBA_CENTRAL_NERVOUS_SYSTEM, A204_SOFT_TISSUE, BCPAP_THYROID, BICR56_UPPER_AERODIGESTIVE_TRACT, COLO680N_OESOPHAGUS, DKMG_CENTRAL_NERVOUS_SYSTEM, FTC133_THYROID, JHH6_LIVER, KALS1_CENTRAL_NERVOUS_SYSTEM, LS1034_LARGE_INTESTINE, NCIH2073_LUNG, NCIH2452_PLEURA, PANC0203_PANCREAS, RD_SOFT_TISSUE, UACC257_SKIN
EMT III	ASPC1_PANCREAS, BICR6_UPPER_AERODIGESTIVE_TRACT, BICR16_UPPER_AERODIGESTIVE_TRACT, HUCCT1_BILIARY_TRACT, JHOS2_OVARY, KYSE520_OESOPHAGUS, MKN7_STOMACH, NCIH2347_LUNG, RERFLCAD1_LUNG, SW1990_PANCREAS, TE9_OESOPHAGUS, TE10_OESOPHAGUS
p53-Dependent Senescence	A375_SKIN, HEC151_ENDOMETRIUM, HT1080_SOFT_TISSUE, IM95_STOMACH, KPNSI9S_AUTONOMIC_GANGLIA, LS180_LARGE_INTESTINE, MCF7_BREAST, NCIH292_LUNG, NCIH460_LUNG, NCIH1373_LUNG, NCIH1944_LUNG, OVK18_OVARY, RCC10RGB_KIDNEY, SNUC4_LARGE_INTESTINE, SW1990_PANCREAS, TEN_ENDOMETRIUM, TOV21G_OVARY
Epithelial Senescence	BICR16_UPPER_AERODIGESTIVE_TRACT, BICR31_UPPER_AERODIGESTIVE_TRACT, COLO680N_OESOPHAGUS, DETROIT562_UPPER_AERODIGESTIVE_TRACT, EKVX_LUNG, HT1376_URINARY_TRACT, HUPT3_PANCREAS, HUPT4_PANCREAS, JHU006_UPPER_AERODIGESTIVE_TRACT, JHU011_UPPER_AERODIGESTIVE_TRACT, JHU029_UPPER_AERODIGESTIVE_TRACT, NCIH358_LUNG, NCIH747_LARGE_INTESTINE, NCIH1048_LUNG, NCIH2126_LUNG, PANC0203_PANCREAS, PK59_PANCREAS, RERFLCKJ_LUNG, SCC25_UPPER_AERODIGESTIVE_TRACT, SCC47_UPPER_AERODIGESTIVE_TRACT, SNU899_UPPER_AERODIGESTIVE_TRACT, SNU1214_UPPER_AERODIGESTIVE_TRACT, TE10_OESOPHAGUS, TE14_OESOPHAGUS, UMUC1_URINARY_TRACT, VMCUB1_URINARY_TRACT, YD38_UPPER_AERODIGESTIVE_TRACT
Stress Response	42MGBA_CENTRAL_NERVOUS_SYSTEM, 93VU_UPPER_AERODIGESTIVE_TRACT, ASPC1_PANCREAS, BCPAP_THYROID, BFTC909_KIDNEY, CAOV3_OVARY, CAS1_CENTRAL_NERVOUS_SYSTEM, COLO680N_OESOPHAGUS, DKMG_CENTRAL_NERVOUS_SYSTEM, EBC1_LUNG, GOS3_CENTRAL_NERVOUS_SYSTEM, HCC56_LARGE_INTESTINE, HEC59_ENDOMETRIUM, HEC251_ENDOMETRIUM, HOS_BONE, HT1376_URINARY_TRACT, HUPT3_PANCREAS, JHOS2_OVARY,

	JHU006_UPPER_AERODIGESTIVE_TRACT, KALS1_CENTRAL_NERVOUS_SYSTEM, KNS42_CENTRAL_NERVOUS_SYSTEM, KYSE520_OESOPHAGUS, MDAMB436_BREAST, MFE280_ENDOMETRIUM, MKN45_STOMACH, NCIH226_LUNG, NCIH727_LUNG, NCIH747_LARGE_INTESTINE, NCIH1299_LUNG, NCIH1435_LUNG, NCIH2077_LUNG, NCIH2126_LUNG, NCIH2347_LUNG, OAW28_OVARY, ONCODG1_OVARY, PC3_PROSTATE, PK45H_PANCREAS, RCC10RGB_KIDNEY, RD_SOFT_TISSUE, RERFLCAD1_LUNG, SNU46_UPPER_AERODIGESTIVE_TRACT, SNU738_CENTRAL_NERVOUS_SYSTEM, SNU1077_ENDOMETRIUM, SNU1079_BILIARY_TRACT, SW1271_LUNG, SW1990_PANCREAS, TE9_OESOPHAGUS, TEN_ENDOMETRIUM, TM31_CENTRAL_NERVOUS_SYSTEM, TYKNU_OVARY, U118MG_CENTRAL_NERVOUS_SYSTEM, VMCUB1_URINARY_TRACT
Protein Maturation	C32_SKIN, DETROIT562_UPPER_AERODIGESTIVE_TRACT, HS729_SOFT_TISSUE, HUCCT1_BILIARY_TRACT, LMSU_STOMACH, MSTO211H_PLEURA, NCIH1568_LUNG, NCIH2087_LUNG, OUMS23_LARGE_INTESTINE, OVTOKO_OVARY, PATU8988S_PANCREAS, PECAPJ49_UPPER_AERODIGESTIVE_TRACT, SNU423_LIVER, TEN_ENDOMETRIUM, UACC257_SKIN, UMUC1_URINARY_TRACT
Proteasomal Degradation	42MGBA_CENTRAL_NERVOUS_SYSTEM, 8305C_THYROID, 2313287_STOMACH, A204_SOFT_TISSUE, A375_SKIN, A2058_SKIN, ABC1_LUNG, BCPAP_THYROID, BFTC909_KIDNEY, BHY_UPPER_AERODIGESTIVE_TRACT, BICR6_UPPER_AERODIGESTIVE_TRACT, BICR16_UPPER_AERODIGESTIVE_TRACT, BICR31_UPPER_AERODIGESTIVE_TRACT, BICR56_UPPER_AERODIGESTIVE_TRACT, BT549_BREAST, C32_SKIN, CAKI2_KIDNEY, CALU6_LUNG, CAMA1_BREAST, CAOV3_OVARY, CAS1_CENTRAL_NERVOUS_SYSTEM, CL34_LARGE_INTESTINE, COLO680N_OESOPHAGUS, COLO741_SKIN, DANG_PANCREAS, DAOY_CENTRAL_NERVOUS_SYSTEM, DETROIT562_UPPER_AERODIGESTIVE_TRACT, DKMG_CENTRAL_NERVOUS_SYSTEM, EBC1_LUNG, EFM192A_BREAST, FTC133_THYROID, GOS3_CENTRAL_NERVOUS_SYSTEM, HCC1419_BREAST, HCC1428_BREAST, HDQP1_BREAST, HEC59_ENDOMETRIUM, HEC108_ENDOMETRIUM, HEC151_ENDOMETRIUM, HEC251_ENDOMETRIUM, HEP3B217_LIVER, HMC18_BREAST, HOS_BONE, HS729_SOFT_TISSUE, HS852T_SKIN, HS939T_SKIN, HT55_LARGE_INTESTINE, HT1080_SOFT_TISSUE, HT1197_URINARY_TRACT, HT1376_URINARY_TRACT, HUCCT1_BILIARY_TRACT, HUH6_LIVER, HUH28_BILIARY_TRACT, HUPT3_PANCREAS, IALM_LUNG, IGR1_SKIN, IM95_STOMACH, JHH7_LIVER, JHOS2_OVARY, KALS1_CENTRAL_NERVOUS_SYSTEM, KMRC3_KIDNEY, KNS42_CENTRAL_NERVOUS_SYSTEM, KPL1_BREAST, LI7_LIVER, LMSU_STOMACH, LNCAPCLONEFGC_PROSTATE, LS180_LARGE_INTESTINE, MCF7_BREAST, MDAMB436_BREAST, MFE280_ENDOMETRIUM, MFE319_ENDOMETRIUM, MKN7_STOMACH, MKN45_STOMACH, MSTO211H_PLEURA, NCIH226_LUNG, NCIH292_LUNG, NCIH358_LUNG, NCIH446_LUNG, NCIH460_LUNG, NCIH522_LUNG, NCIH650_LUNG, NCIH727_LUNG, NCIH747_LARGE_INTESTINE, NCIH1048_LUNG, NCIH1299_LUNG, NCIH1373_LUNG, NCIH1435_LUNG, NCIH1568_LUNG, NCIH1944_LUNG, NCIH2073_LUNG, NCIH2077_LUNG, NCIH2170_LUNG, NCIH2228_LUNG, NCIH2347_LUNG, NCIH2444_LUNG, NCIH2452_PLEURA, OAW28_OVARY, ONCODG1_OVARY, OSRC2_KIDNEY, OVCAR4_OVARY, OVSAHO_OVARY, OVTOKO_OVARY, PANC0203_PANCREAS, PANC1_PANCREAS, PATU8988S_PANCREAS, PC3_PROSTATE, PECAPJ49_UPPER_AERODIGESTIVE_TRACT, RCC10RGB_KIDNEY, RD_SOFT_TISSUE, RERFLCAI_LUNG, RT4_URINARY_TRACT, RVH421_SKIN, SCC9_UPPER_AERODIGESTIVE_TRACT, SCC25_UPPER_AERODIGESTIVE_TRACT,

	SH10TC_STOMACH, SKMEL2_SKIN, SKMEL3_SKIN, SKMEL5_SKIN, SKMEL30_SKIN, SKMES1_LUNG, SNU46_UPPER_AERODIGESTIVE_TRACT, SNU308_BILIARY_TRACT, SNU423_LIVER, SNU449_LIVER, SNU738_CENTRAL_NERVOUS_SYSTEM, SNU899_UPPER_AERODIGESTIVE_TRACT, SNU1077_ENDOMETRIUM, SNU1196_BILIARY_TRACT, SNU1214_UPPER_AERODIGESTIVE_TRACT, SNUC4_LARGE_INTESTINE, SQ1_LUNG, SU8686_PANCREAS, SW1088_CENTRAL_NERVOUS_SYSTEM, SW1271_LUNG, SW1990_PANCREAS, T47D_BREAST, TCCSUP_URINARY_TRACT, TE1_OESOPHAGUS, TE6_OESOPHAGUS, TE9_OESOPHAGUS, TE10_OESOPHAGUS, TE14_OESOPHAGUS, TEN_ENDOMETRIUM, TOV21G_OVARY, U118MG_CENTRAL_NERVOUS_SYSTEM, UACC257_SKIN, UMUC1_URINARY_TRACT, VMCUB1_URINARY_TRACT, VMRCRCZ_KIDNEY, WM88_SKIN, YD38_UPPER_AERODIGESTIVE_TRACT, ZR751_BREAST

Table S4. Gene annotation of recurrently heterogeneous expression programs (RHP).

Cell Cycle - G1/S	HIST1H4C, CLSPN, ATAD2, E2F1, HELLS, RRM2, HIST2H2AC, HIST1H1E, FAM111A, GINS2, CENPU, CDCA5, ASF1B, CHAF1A, TCF19, HIST1H1D, KIAA0101, FEN1, HIST1H1B, PCNA, FBXO5, HIST1H1C, CDCA4, MYBL2, PKMYT1, FAM111B, USP1, CDC6, EZH2, PSMC3IP, GMNN, HMGB2, ORC6, TYMS, DNAJC9, CDK1, UBE2T, SLBP, BRCA1, C21orf58, CDT1, ESCO2, TEX30, ATAD5, CCNE1, RAD51AP1
Cell Cycle - G2/M	AURKA, CENPF, PLK1, TOP2A, UBE2C, ASPM, TPX2, CENPA, CKAP2, GTSE1, CCNB1, ARL6IP1, MKI67, CENPE, CKS2, HMMR, DEPDC1, NUSAP1, PRC1, SGOL2, CCNA2, KPNA2, CDCA8, HMGB2, NUF2, KNSTRN, CDCA3, CEP55, KIF20B, FAM83D, PIF1, CDC20, DLGAP5, KIF2C, PRR11, ARHGAP11A, KIF23, AURKB, CDK1, KIF14, FAM64A, CCNB2, PSRC1, NEK2, CDCA2, BIRC5, TACC3, CKAP2L, HJURP, KIF4A, UBALD2, CDC25B, RACGAP1, SGOL1, ECT2, CCNF, UBE2S, ANLN, CDKN3, DBF4, G2E3, PBK
Skin Pigmentation	PHACTR1, DCT, MITF, CHCHD6, MBP, GDF15, MLANA, TBC1D7, TNFRSF14, TRPM1, ASAH1, CAPN3, LINC00518, BIRC7, FXYD3, GPNMB, GPR137B, LGALS3, MXI1, NOV, PMEL, TBC1D16, WIPI1, GYPC, ISG20, PLP1, APOE, AVPI1, C11orf96, DAB2, FAM210B, GJB1, GPR56, HES6, NBL1, RAB27A, RAB38, RAB5B, RRAGD, S100B, SEMA6A, SH3BP5, STX7, TIMP2, TRIM2, ZFYVE16, ZNF106
EMT I	DKK1, PMEPA1, C12orf75, CYR61, IL8, SORBS2, THBS1, TPST1, CAV1, KRT7, LIMA1, LIMCH1, MAP1B, MGLL, MXD4, PRSS23, RRAS, S100A16, TPM1, CCND1, CTGF, DDIT4, FN1, FOSL1, HOXB2, IER3, KRT81, NT5E, PLAUR, PPFIBP1, PTRF, RND3, S100A4, SMURF2, TGFBI, TNFRSF12A, TSC22D1, AC093673.5, ACTG2, CAV2, CCDC107, CD82, CDKN1A, CEBPD, CSRP1, CXCL1, DCBLD2, EVA1A, FAM20C, FHL2, FLNB, FRMD6, GLIPR1, HEBP2, HPCAL1, ITGA3, KDELR3, KRT18, LINC00152, MIR4435-1HG, MYL9, MYLK, NGFR, NME3, NNMT, PDLIM7, PEG10, PNRC1, PRKCDBP, PRNP, PTGES, S100A2, SERPINE2, SFRP1, SPRY2, TGM2, TIMP3, USP53, ZNF655
EMT II	MYL9, SERPINE1, THBS1, FN1, IL32, LAMC2, MYH9, TAGLN, CLIC3, COL5A1, IGFBP3, INHBA, PMEPA1, CDC42EP3, CST6, CYR61, GLIPR1, TPM1, VIM, AKAP12, AXL, EDN1, FLNA, FST, FSTL1, IGFBP7, PRSS23, PTPRF
IFN Response	ISG20, IFIT3, ISG15, OASL, IFIT1, IFIT2, IFI44, PMAIP1, RARRES3, ZC3HAV1, HERC5, SAMD9, WARS, IGFBP6, SAMD9L, CCL5, IFI6, APOL2, HES4, IFIH1, IRF1, PARP14, PSMB9, ZNFX1, HLA-B, IL7R, APOL6, B4GALT5, DDX58, DDX60, FAM46A, JUNB, KLF4, PLAUR, RSAD2, SAR1A, SDC4, SQRDL, ZFP36L2, APOL1, C15orf48, CDKN1A, FGF2, GRB10, HIP1R, IL6, TNIP1, UBE2L6, USP18

EMT III	LAMA3, LAMB3, LAMC2, CDKN1A, FAM83A, ITGA2, PLAU, C15orf48, JUP, MAST4, RHOD, SERPINB1, SERPINE1, AHNAK2, COL17A1, DMKN, ELK3, F3, G0S2, IL32, INHBA, LRRC8A, NDRG1, NEAT1, S100A14, SLPI, TSPAN1, CDA, CDH1, CDH3, CST6, DHRS9, EPCAM, FN1, FXYD3, HBEGF, KLK10, LCN2, LSR, POLD4, PTGS2, SEMA3C, SERPINB2, SLFN5, SMIM22, SOX4, SRCAP, VAMP8, WFDC2
p53-Dependent Senescence	CDKN1A, NEAT1, POLD4, MXD4, MMP24-AS1, PNRC1, HIST1H2BK, SLPI, TP53TG1, IFI27L2, IGBP1, AHNAK2, FDXR, GPRC5A, IFI27, ISG15, KRT19, S100P, TP53I3
Epithelial Senescence	SLPI, LCN2, ELF3, S100A9, S100P, SAA1, C15orf48, SPRR1B, AQP3, LY6D, ASS1, CLDN4, FXYD3, KRT15, S100A14, S100A8, SERPINB1, AGR2, CXCL1, KRT13, KRT16, ADIRF, C9orf169, CD9, CTSD, GSN, MMP7, NEAT1, PI3, PSCA, RARRES3, SAA2, SAMD9, SAT1, SNCG, TACSTD2, TNFAIP2, WFDC2
Stress Response	DDIT3, SNHG12, SLC3A2, PPP1R15A, GADD45B, GADD45A, RSRC2, TXNIP, ATF3, TAF1D, TRIB3, ASNS, EPB41L4A-AS1, KLF10, SNHG15, PDRG1, CARS, SNAPC1, CCNL1, SQSTM1, TSC22D1, DDIT4, XBP1, HERPUD1, IER2, NFKBIA, RAE1, JUN, RELB, BTG1, IRF1, ZNF622, HIST1H2AC, OSER1, SERTAD1, SNHG8
Protein Maturation	HSPA5, RPN2, SLC3A2, PDIA3, LGALS3BP, MCM7, XRCC6, EPRS, VCP, COPB2, EIF4A3, KPNA2, OS9, PRKCSH, UBC, ANXA1, APP, CYR61, HSPA1A, HSPA8, LAPTM4A, NDUFS2, PGK1, APLP2, ATP6AP2, CTSL, GRN, LAMB3, LAMP1, MAGED2, NASP, POLR2B, SDHA, SON
Proteasomal Degradation	PSMA3, PSMC4, PRDX1, PSMC2, EIF4A3, MDH1, PSMA4, ANXA1, MRPL13, PGK1, DCAF13, PSME2, PRMT1, PSMB3, CCT8, SSBP1, CCNB1, CDC123, DPM1, NDUFS2, PDHA1, LAPTM4A, PSMB1, PCMT1, PSMB6, NDUFA9, POLR2G, CCT5, RTCB, HSPA5, DDX39A, MCTS1, SNRPB2, XRCC6, PSMD13, EIF3I, SSB, NUP37, ILF2, EIF4A1, FH, IMPDH2, CCT7, MAGOH, RBM42, SLC3A2

Chapter 2

Glioma-synthesized melatonin as an autocrine inhibitor of disease progression

Melatonergic system-based two-gene index is prognostic in human gliomas

Abstract: Gliomas, the most common primary brain tumors in adults, are classified into four malignancy grades according to morphological features. Recent studies have shown that melatonin treatment induces cytotoxicity in glioma-initiating cells and reduces the invasion and migration of glioma cell lines, inhibiting the nuclear factor κB (NFκB) oncopathway. Given that C6 rat glioma cells produce melatonin, we investigated the correlation between the capacity of gliomas to synthesize/metabolize melatonin and their overall malignancy. We first characterized the melatonergic system of human gliomas cell lines with different grades of aggressiveness (HOG, T98G, and U87MG) and demonstrated that glioma-synthesized melatonin exerts an autocrine antiproliferative effect. Accordingly, the sensitivity to exogenous melatonin was higher for the most aggressive cell line, U87MG, which synthesized/accumulated less melatonin. Using The Cancer Genome Atlas RNAseq data of 351 glioma patients, we designed a predictive model of the content of melatonin in the tumor microenvironment, the ASMT:CYP1B1 index, combining the gene expression levels of melatonin synthesis and metabolism enzymes. The ASMT:CYP1B1 index negatively correlated with tumor grade, as well as with the expression of pro-proliferation and anti-apoptotic NFκB target genes. More importantly, the index was a grade- and histological type-independent prognostic factor. Even when considering only high-grade glioma patients, a low ASMT:CYP1B1 value, which suggests decreased melatonin and enhanced aggressiveness, was strongly associated with poor survival. Overall, our data reveal the prognostic value of the melatonergic system of gliomas and provide insights into the therapeutic role of melatonin.

Gabriela S. Kinker[1], Sueli M. Oba-Shinjo[2], Claudia E. Carvalho-Sousa[1], Sandra M. Muxel[1], Suely K. N. Marie[2,3], Regina P. Markus[1,3] and Pedro A. Fernandes[1]

[1]Department of Physiology, Institute of Bioscience, University of São Paulo, São Paulo, Brazil; [2]Department of Neurology, School of Medicine, University of São Paulo, São Paulo, Brazil; [3]Center for the Convergence of the Life Sciences, Physical Sciences and Engineering for Innovation in Diagnostics & Therapeutics (IDx&T), University of São Paulo, São Paulo, Brazil

Introduction

Gliomas are the most common primary brain tumors in adults and presumably arise from mature glia cells or their less differentiated progenitor cells [1, 2]. The World Health Organization (WHO) morphological classification of gliomas into four grades (I–IV) is a key factor influencing treatment decisions. However, it is subjected to interobserver variability and lacks reproducibility [3, 4]. The detailed molecular characterization of gliomas can complement the WHO grading through the identification of tumor specific subgroups and contribute to the development of new treatment strategies [5]. Glioblastomas (GBMs, glioma grade IV), which account for approximately 50% of gliomas, are still associated with very poor survival (12–15 months), despite macroscopic complete resection combined to radio and chemotherapy [1, 6].

Melatonin (N-acetyl-5-methoxytryptamine) is an indolamine synthesized by the pineal gland during the night, in response to signals from the central biological clock [7]. The production and release of this hormone by the pineal gland translates the dark phase to the organism, ensuring the synchronization of circadian and seasonal rhythms [8, 9]. Melatonin synthesis has a conserved biosynthesis pathway, involving the conversion of serotonin to N-acetylserotonin (NAS) by the enzyme arylalkylamine N-acetyltransferase (AANAT) and the subsequent NAS methylation by the enzyme acetylserotonin O-methyltransferase (ASMT) [7]. In humans, melatonin is metabolized by the hepatic cytochrome P450 1A1/2 (CYP1A1/2) to 6-hydroxymelatonin (6OH-MEL), conjugated with sulfate and excreted in the urine [10]. Cytochrome P450 1B1 (CYP1B1), which is not significantly expressed in the liver, is responsible for the 6-hydroxylation of melatonin in the brain [11].

Melatonin synthesis has been detected in many extrapineal tissues, including retina, skin, gastrointestinal tract, liver, kidney, and brain [12]. Except for some tissues such as retina, the absence of a daily rhythm of extra-pineal melatonin synthesis suggests that it is not regulated by the environmental light–dark cycle [13]. Generally, extrapineal melatonin is poorly released into the circulation, acting locally in an autocrine and paracrine manner [13, 14]. Interestingly, rat astrocytes and C6 glioma cells synthesize melatonin in vitro and have been shown to express the necessary biosynthetic enzymes [15]. Additionally, we have previously demonstrated that melatonin production by rat cerebellar glia cells selectively protects the cerebellum from neuroinflammation toxicity in a receptor-dependent manner [16].

Kinker et al.

It is well established that melatonin exerts oncostatic effects, in both a receptor-dependent and -independent manners, across a wide variety of tumors, including sarcomas, melanomas, and breast cancer [17]. At millimolar concentrations, melatonin inhibits the proliferation of C6 rat glioma cells and the invasion and migration of human GBM cell lines [18, 19]. In both cases, this indolamine decreases the intracellular basal free radical levels, inhibiting the redox-sensitive activation of the nuclear factor κB (NFκB) oncopathway. Additionally, recent studies have demonstrated that melatonin also promotes cytotoxic effects in human glioma-initiating cells, thereby enhancing the efficacy of chemotherapeutic drugs [20, 21].

Although evidence shows the potential therapeutic role of melatonin in glioma treatment [18–21], no previous studies evaluated the pathophysiologic relevance of glioma-synthesized melatonin. Therefore, the present work investigated the correlation between the capacity of human gliomas to synthesize/metabolize melatonin and their overall malignancy, as well as patient survival.

Materials and methods

Cell culture

Human glioma cell lines HOG, T98G, and U87MG were maintained in RPMI 1640 medium (Life Technologies, Carlsbad, CA, USA) supplemented with 10% heat-inactivated fetal bovine serum (FBS) (Life Technologies), 100 IU/mL penicillin, and 100 μg/mL streptomycin (Life Technologies), at 37°C in a humidified atmosphere of 5% CO_2. T98G and U87MG GBM cell lines were purchased from ATCC, while HOG, established from a grade III anaplastic oligodendroglioma [22], was kindly provided by Dr. MC Sogayar (University of São Paulo, São Paulo, Brazil). All cell lines were authenticated by short tandem repeat DNA profiling using the GenePrint 10 System (Promega, Madison, WI, USA).

Immunofluorescence

Cells were fixed with 4% paraformaldehyde (15 min, room temperature), permeabilized with 0.1% Triton X (10 min, room temperature), and blocked with 2% bovine serum albumin (BSA) in PBS (1 hr, room temperature). Next, cells were incubated overnight at 4°C with rabbit anti-AANAT (IM-0450), pAANAT (IM-0451) or ASMT (IM-0441) primary antibodies (Imuny Biotechnology, São Paulo, Brazil). Cells were washed three times with PBS before incubation with FITC-conjugated anti-rabbit IgG antibody (Sigma-Aldrich, St. Louis, MO, USA) for 1 hr at room temperature. After three washes with PBS, the nuclear DNA was stained with DAPI (5 min, room temperature, Santa Cruz Biotechnology, Santa Cruz, CA, USA). In each experiment, images of three randomly chosen fields per well were captured using a fluorescence microscope (Axio Scope A1; Zeiss, Gottingen, Germany) and analyzed with ImageJ 1.41 Software. The mean fluorescence measured in each field was used in the statistical analysis.

Quantitative real-time polymerase chain reaction

Total RNA was extracted using InviTrap Spin Tissue RNA Mini Kit (Invitek GmbH, Berlin, Germany) and RNAs (1 μg) were reverse transcribed into complementary DNA by the SuperScript III First-Strand Synthesis System for RT-PCR (Life Technologies), following the manufacture's instructions. Quantitative real-time polymerase chain reaction (qPCR) was performed using SYBR Green PCR Master Mix (Applied Biosystems, Foster City, CA, USA) and carried out in an Icycler iQ5 machine (BIO-RAD, Hercules, CA, USA). Primer sets were designed using the software Prime-Blast (National Center for Biotechnology Information, Bethesda, MD, USA): GAPDH, sense 5′-GAGTCCACTGGCGTCTTCAC-3′, antisense 5′-ATGACGAACATGGGGGCATC-3′; CYP1B1, sense 5′-CCACTATCACTGACATCTTCGG-3′, antisense 5′-GATCCAATTCTGCCTGCACT-3′. Thermal cycling conditions were 95°C for 10 min followed by 40 cycles at 95°C for 15 s and 60°C for 1 min. Each run was completed with a melting curve analysis to confirm the specificity of amplification and lack of primer dimers. The $2^{-\Delta\Delta CT}$ equation was applied to calculate the expression of CYP1B1 relative to GAPDH; the mean ΔC_T of T98G cells was used as the calibrator.

Melatonin measurement

The content of melatonin in the cell medium after 6 hr of culture was measured through enzyme-linked immunosorbent assays (Melatonin ELISA; IBL, Hamburg, Germany) according to the manufacturer's instructions. Values were normalized per million of cells and the assay has a detection limit of 3 pg/mL.

MTT cell growth assay

Cells (1×10^4 per well) were seeded on 96-well plates overnight and subsequently treated for 48 hr with various concentrations of luzindole (10^{-12}–10^{-9} M), a competitive antagonist of melatonin receptors, and/or melatonin (10^{-9}–10^{-3} M), both obtained from Sigma-Aldrich. Cells were then incubated with methylthiazolyldiphenyl-tetrazolium bromide (MTT; 0.5 mg/mL, Sigma-Aldrich) for 4 hr at 37°C. The reduced crystals of MTT (formazan) were dissolved in isopropanol:DMSO (1:1 v:v, 30 min, room temperature). The absorbance was measured at 570 nm, with background subtraction at 690 nm, in a SpectraMax 250 spectrophotometer (Molecular Devices, Sunnyvale, CA, USA).

TCGA RNAseq dataset

Gene expression data were generated using the Illumina HiSeq 2000 RNA Sequencing platform by the University of North Carolina TCGA genome characterization center. Level 3 interpreted data and clinical information of 101 gliomas grade II, 98 gliomas grade III, and 152 primary GBMs were downloaded from the TCGA data portal (https://tcga-data.nci.nih.gov/tcga/dataAccessMatrix.htm).

Expression levels were RSEM-normalized and $\log_2(x + 1)$-transformed.

ASMT:CYP1B1 index calculation

The *ASMT* and *CYP1B1* RSEM expression levels were used to design a two-gene expression index, as previously described [23], by *z*-normalizing the $\log_2$-transformed values for each gene and calculating the difference between them (ASMT–CYP1B1).

Gene set enrichment analysis

To account for differences among tumor histological types, gene set enrichment analysis (GSEA) was restricted to astrocytomas (grades II–IV). Genes were ranked according to Pearson's correlation coefficient between the ASMT:CYP1B1 index value and the expression levels obtained from the TCGA RNAseq dataset. GSEA of GO biological processes (C5:BP) was performed using GSEA v4.0 (Broad Institute, M.I.T.). Enrichment scores (ESs) were calculated based on a Kolmogorov–Smirnov-like statistic and further normalized (NES) to account for the size of each gene set. The proportion of false positives was determined by calculating the false discovery rate (FDR) corresponding to each NES [24]. We considered a FDR cutoff of less than 25%.

Statistics

The Cutoff Finder survival algorithm was used to identify the optimal cutoff values, defined as the points with the most significant (log-rank test) data split [25]. Further statistical analyses were performed with the GraphPad Prism 6, the JMP 11 or the R software (http://www.r-project.org). Two-group comparisons were analyzed using two-sided Student's *t*-test. Three-group comparisons were analyzed using one-way ANOVA with Tukey's correction or nonparametric Kruskal–Wallis test with Dunn's correction. To determine correlations, we calculated Spearman's rank (r_s) or Pearson's (r) correlation coefficients. Fisher's exact test was used to analyze the associations between various categorical clinicopathological characteristics and the dichotomized ASMT:CYP1B1 index. Univariate analysis of survival was performed using the Kaplan–Meier method and compared by the log-rank test. Multivariate analysis of survival was performed using Cox proportional hazards regression. Hazard ratios (HRs) including 95% confidence intervals were calculated. *P*-values < 0.05 were considered statistically significant.

Results

To investigate the association between the melatonergic system of gliomas and their overall malignancy, we first analyzed three human glioma cell lines with different grades of aggressiveness: HOG, an oligodendroglioma grade III, T98G, a GBM, and U87MG, a highly tumorigenic GBM [26]. HOG, a lower grade glioma, showed an overexpression of ASMT when compared to T98G and U87MG GBM cell lines (Fig. 1A). The most aggressive cell line, U87MG, presented the highest protein levels of total AANAT and the active form, pAANAT (Fig. 1A), as well as an overexpression of the melatonin catabolic enzyme *CYP1B1* (Fig. 1B). Interestingly, as observed for U87MG, lower protein levels of ASMT (Fig. 1A), combined with a higher expression of *CYP1B1* (Fig. 1B), were associated with a reduced content of melatonin detected in the cell culture medium (Fig. 1C). Notably, given that the pineal gland also secretes high levels of NAS, the precursor of melatonin, during the night [27], ASMT would play a major role in the control of melatonin production by gliomas in vivo.

As we sought to determine the functional relevance of glioma-synthesized melatonin, cell lines were treated for 48 hr with increasing concentrations of the competitive antagonist of MT1 and MT2 melatonin receptors, luzindole. Luzindole significantly increased the cell growth of HOG and T98G, whereas no difference was detected for U87MG (Fig. 2A), which accumulates lower levels of melatonin in its microenvironment (Fig. 1C). To further investigate the oncostatic properties of this indolamine, cell lines were cultured in the presence of exogenous melatonin. Interestingly, 1 nM melatonin, acting in a receptor-dependent manner, significantly decreased the cell growth of U87MG but not HOG and T98G after 48 hr (Fig. 2B, C). In fact, both of the latter cell lines produce and accumulate greater amounts of this indolamine (Fig. 1C) probably sufficient to virtually saturate the receptor binding sites and exert an autocrine, antiproliferative effect. Nevertheless, the treatment with a high concentration of melatonin (1 mM), previously shown to inhibit the NFκB pathway of gliomas in a receptor-independent manner [18, 19], reduced the cell growth of all three cell lines by 15–25% (Fig. 2B).

Given our findings that glioma cell lines produce melatonin, which can exert an autocrine antiproliferative effect, we then further investigated the melatonergic system of human gliomas using the publicly available TCGA RNAseq data of 351 patients. *AANAT* was homogeneously expressed among all glioma grades, and *ASMT* had a significantly decreased expression in GBMs, as compared to grade II tumors (Fig. 3A). Furthermore, GBMs presented a significantly higher mRNA expression of *CYP1B1* than gliomas grade II and grade III (Fig. 3A). In accordance with this, each tumor grade presented a distinct profile in the combined analysis of *ASMT* and *CYP1B1* expression. As such, the density map indicates a gradual increase in the proportion of tumors concomitantly expressing high *CYP1B1* and low *ASMT* from grades II to IV (GBM) (Fig. 3B).

Using the TCGA data, we designed a predictive model of melatonin content in the tumor microenvironment, the ASMT:CYP1B1 expression index, which attempts to combine the rates of melatonin synthesis and metabolism. The two-gene index negatively correlated with tumor grade ($r_s = -0.187$, $P = 0.0004$), with the lowest values observed for GBMs. In a way to confirm the biological relevance of this two-gene molecular signature, we performed a GSEA with TCGA RNAseq genes ranked according to Pearson's correlation with the ASMT:CYP1B1 index. Gene sets associated with the positive control of cell proliferation,
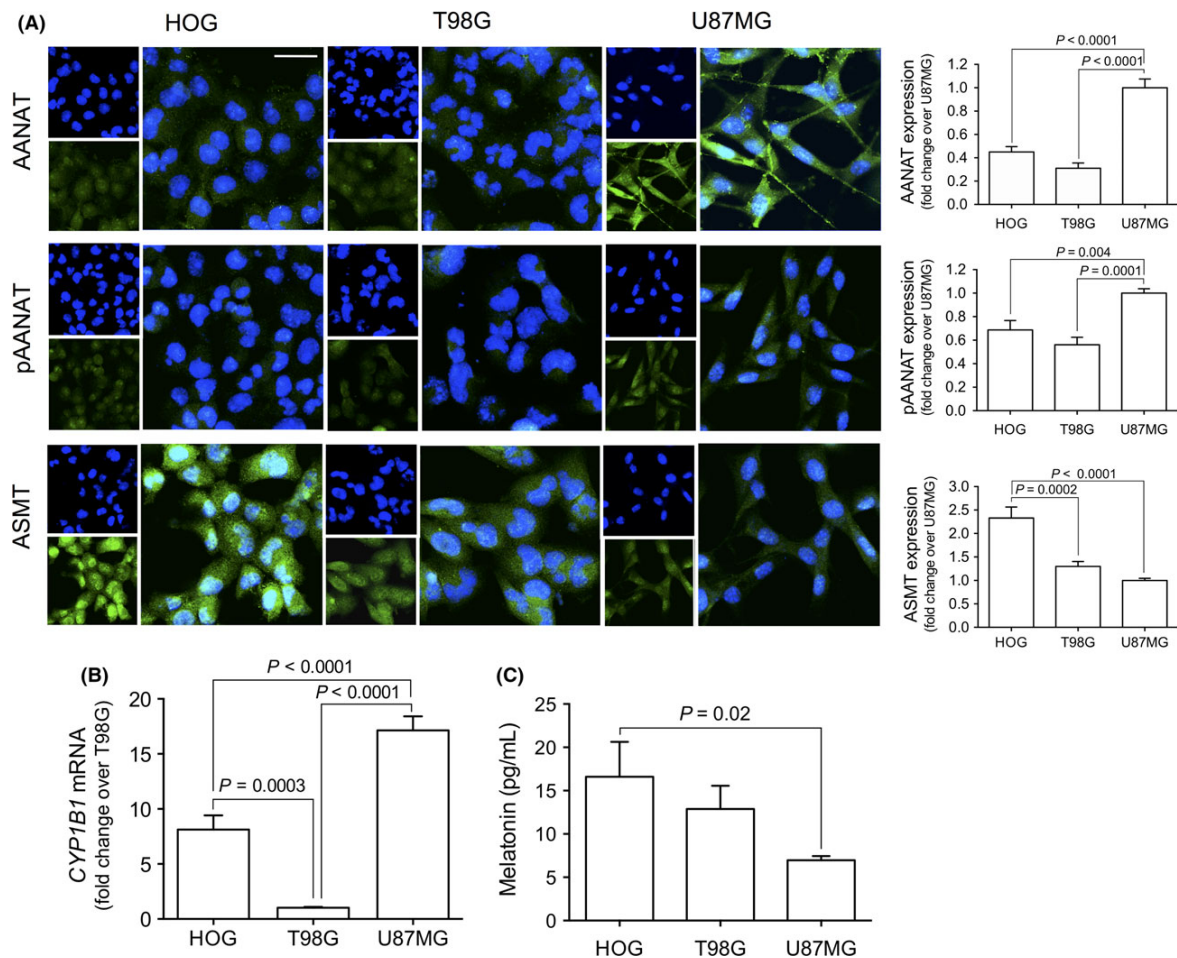
Kinker et al.

Fig. 1. The melatonergic system of glioma cell lines with different grades of aggressiveness (HOG, T98G, and U87MG). (A) Immunofluorescence detection of total AANAT (green), pAANAT (green), and ASMT (green). Nuclear DNA was stained with DAPI (blue). Fluorescence intensity values were normalized by the mean signal detected on U87MG cells. (B) qPCR analysis of *CYP1B1* mRNA expression. The $2^{-\Delta\Delta CT}$ equation was applied to calculate the relative expression; values were normalized by *GAPDH* expression and T98G cells were used as the calibrator. (C) The content of melatonin (per million of cells) in the medium after 6 hr of culture, determined by ELISA assay. Data are shown as mean ± S.E.M. of three independent experiments in triplicate. Comparisons were performed using one-way ANOVA with Tukey's correction (A and B) or nonparametric Kruskal–Wallis test with Dunn's correction (C). Scale bar: 10 μm.

the negative control of apoptosis and the activation of the NFκB were significantly enriched and negatively correlated with the index (Fig. 4A).

The aberrant activation of the NFκB pathway is increasingly recognized as a crucial player in cancer initiation and progression, as well as in chemo- and radiotherapy resistance [28]. In most quiescent cells, NFκB dimers are sequestered in the cytoplasm in an inactive state, complexed with the inhibitory protein IκB [29]. Pro-inflammatory stimulus and genotoxic stress lead to the IκB kinase (IKK)-dependent phosphorylation of IκB and release of NFκB, which translocates to the nucleus where it can activate the transcription of genes associated with cell proliferation, metastasis, angiogenesis, inflammation, and suppression of apoptosis [30, 31]. Accordingly, the ASMT:CYP1B1 index also negatively correlated with the expression of NFκB target genes such as the anti-apoptotic

BCL2A1, *CFLAR*, *TNFAIP3*, *BIRC3,* and *SOD2* (Fig. 4B)*,* as well as the pro-proliferation *INHBA, TNFSF13B, IL6, IL8,* and *RELB* (Fig. 4C).

We next performed survival analyses in regard to the ASMT:CYP1B1 index, using a log-rank test-based algorithm to access the optimal cutoff to dichotomize each dataset (all patients or only high-grade gliomas, HGGs). The index was a significant prognostic factor when considering all patients or only HGGs (astrocytomas grade III–IV). In both cases, a low ASMT:CYP1B1 value, indicative of decreased melatonin, was strongly associated with a poor survival rate (all patients: HR = 1.9, $P = 0.0002$; HGGs: HR = 2.28, $P < 0.0001$) (Fig. 5A,B). The analysis of the relationship between the dichotomized index and clinicopathological features of all patients further confirmed its negative correlation with tumor grade ($P = 0.006$; Table 1). Moreover, patients with a low

Fig. 2. Melatonin inhibits glioma cell growth. HOG, T98G, and U87MG cells were cultured for 48 hr in the presence of (A) various concentration of luzindole (10^{-12}–10^{-9} M), a competitive antagonist of melatonin receptors, or the respective vehicle (10^{-9}–10^{-6}% ethanol); (B) melatonin (1 nM or 1 mM) or the respective vehicle (3×10^{-7} or 3×10^{-1}% ethanol); and (C) melatonin (1 nM) and/or luzindole (1 μM). Cell growth was estimated by the MTT reduction, and values were normalized by the mean absorbance detected on the respective control or vehicle groups. Data are shown as mean ± S.E.M. of three independent experiments in quadruplicates. *$P < 0.05$ and **$P < 0.001$ compared to the respective vehicle group; #$P < 0.05$ compared to the melatonin group. Comparisons were performed using the two-sided Student's *t*-test.
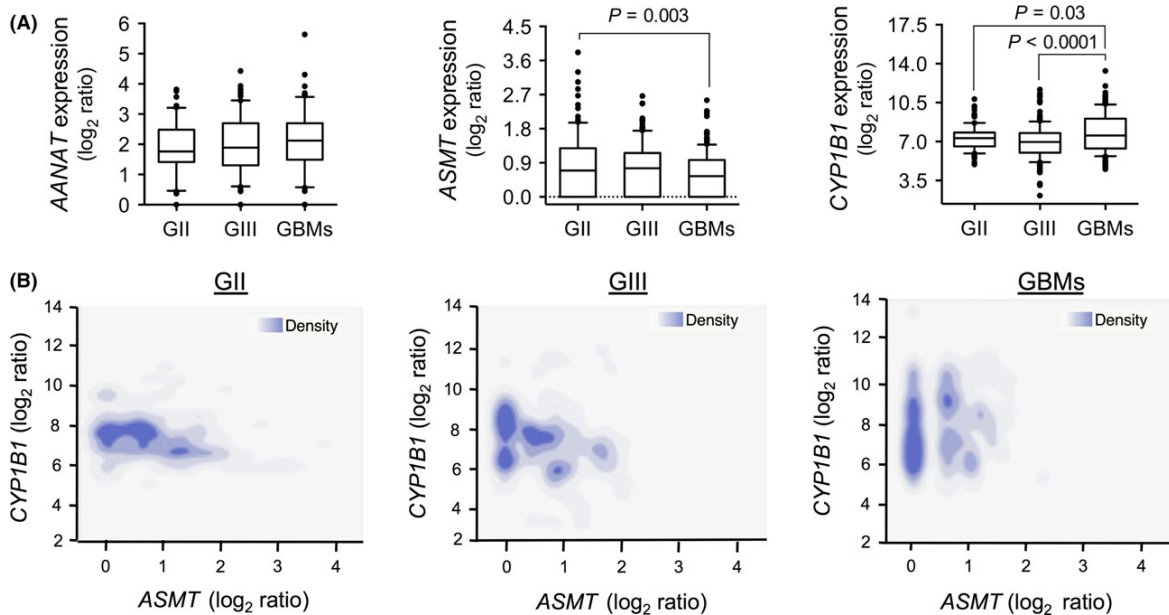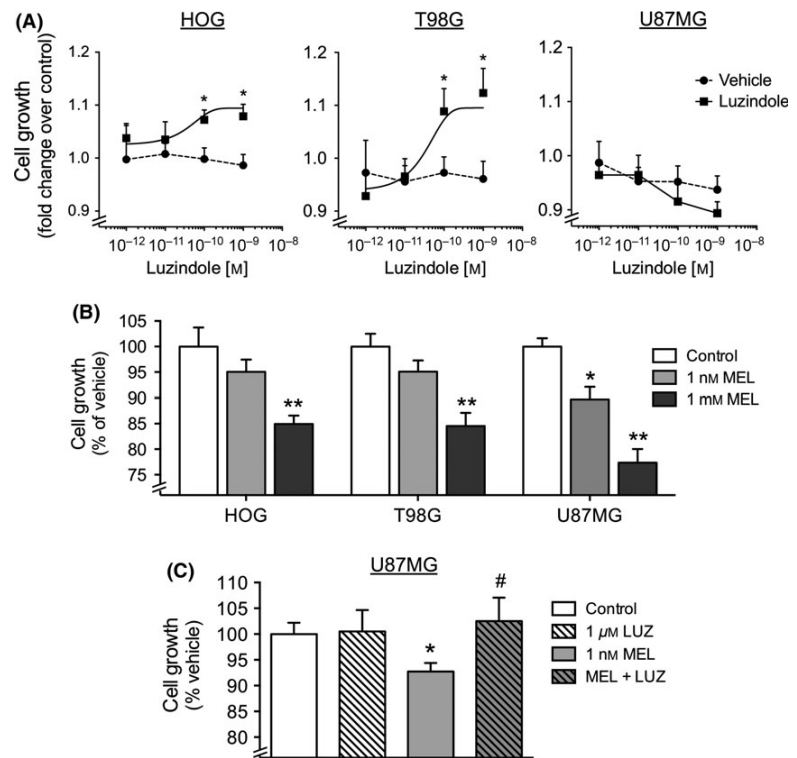

Fig. 3. The melatonergic system of human gliomas (A) RNAseq analysis of *AANAT*, *ASMT* and *CYP1B1* expression in each tumor grade. Values were RSEM-normalized and $\log_2(x + 1)$-transformed. The box extends from the 25th to 75th percentiles, the central bold line shows the median, with whiskers being drawn down to the 10th percentile and up to the 90th. Comparisons were performed using one-way ANOVA with Tukey's correction. (B) Density maps comparing *ASMT* and *CYP1B1* expression for each tumor grade. Color bars on top indicate relative density. GII: glioma grade II, *n* = 101. GIII: glioma grade III, *n* = 98. GBMs: glioblastomas (astrocytomas grade IV), *n* = 152.
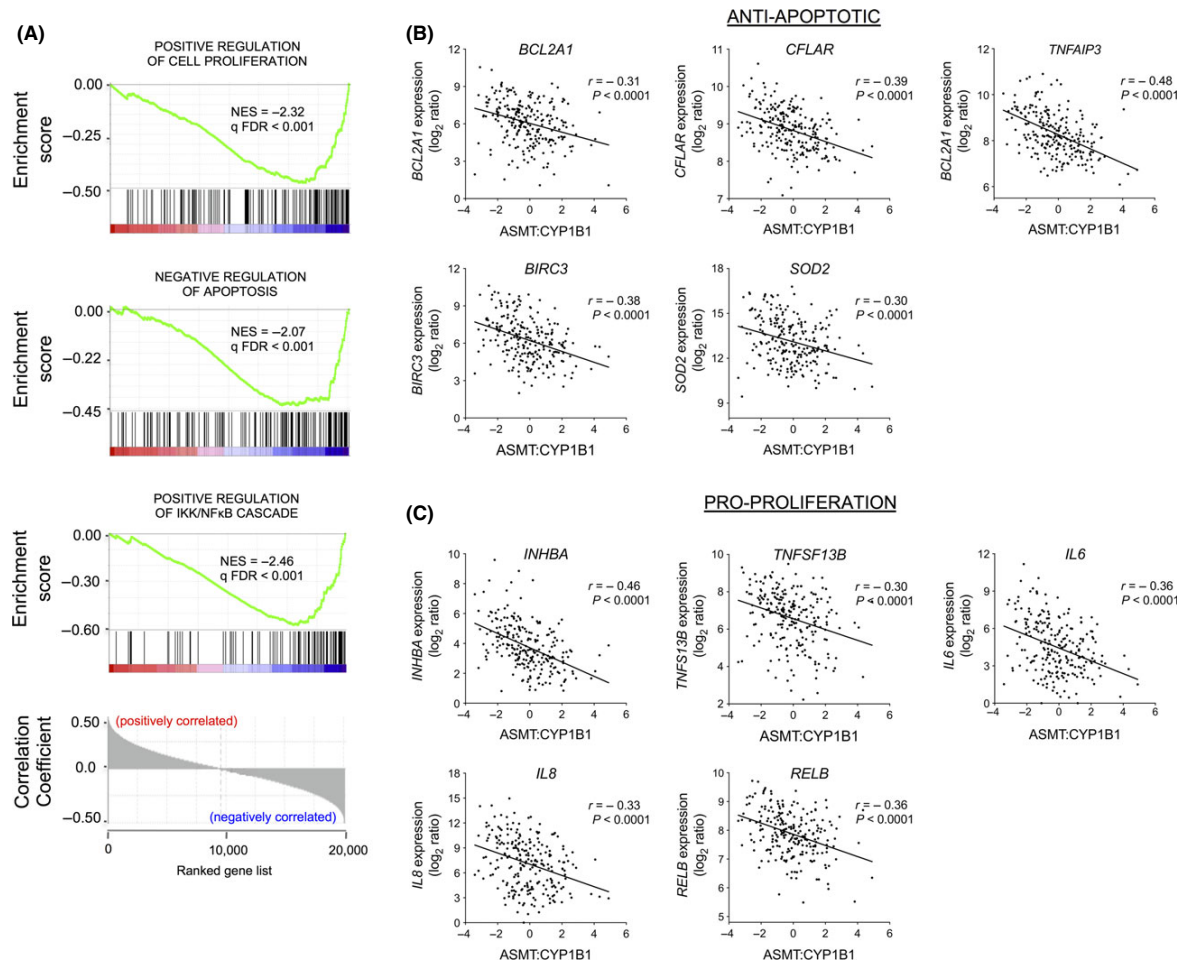
Kinker et al.

Fig. 4. The correlation between the ASMT:CYP1B1 index and the gene expression profile of gliomas. (A) Gene Set Enrichment Analysis (GSEA) on genes ranked according to Pearson's correlation coefficient with the ASMT:CYP1B1 index. Normalized enrichment scores (NES) and false discovery rate (FDR) *q*-values are indicated. Pearson's correlation between ASMT:CYP1B1 and the expression of NFκB target genes involved in the regulation of (B) apoptosis and (C) proliferation.

ASMT:CYP1B1 value were significantly older ($P = 0.001$; Table 1) and more frequently diagnosed with a grade IV GBM tumor ($P = 0.006$; Table 1).

Multivariate Cox analysis adjusting for age, gender, KPS score, histological type, and tumor grade revealed that the ASMT:CYP1B1 index is an independent prognostic factor stronger than either gene alone, being significant for either all patients or only HGGs (Table 2; Fig. S1). As the index and the expression of *CYP1B1* were shown to be grade-independent prognostic factors for HGGs, we further analyzed the survival (log-rank test) of astrocytomas grade III and GBMs patients separately. According to the HGGs cutoff, a low ASMT:CYP1B1 value was again associated with poor survival (astrocytomas grade III: HR = 4.67, $P = 0.001$; GBM: HR = 1.54, $P = 0.026$; Fig. 6A), suggesting an additional prognostic value to the histological diagnosis. Even though a high *CYP1B1* expression was associated with poor survival of GBM patients (HR = 0.56, $P = 0.007$; Fig. 6B), no prognostic value was observed in regard to grade III astrocytomas

(HR = 0.261, $P = 0.498$; Fig. 6B). The analysis of an independent dataset (GSE16011, $n = 264$) confirmed that the two-gene index negatively correlates with tumor grade ($r_s = -0.223$, $P = 0.0003$) and has more power than either gene alone in the multivariate analysis of survival (Fig. S2; Table S1).

Discussion

Previous studies have suggested a potential therapeutic role for exogenous melatonin in the treatment of gliomas [18–21]. However, there are no available data assessing the biological implications of glioma-synthesized melatonin. As such, here we characterized the melatonergic system of human gliomas and demonstrated its relevance in prognosis, providing further insights into the therapeutic role of melatonin. Our findings indicate that the ability of gliomas to synthesize/accumulate melatonin negatively correlates with tumor malignancy. Moreover, we demonstrated that tumor-synthesized melatonin exerts an autocrine
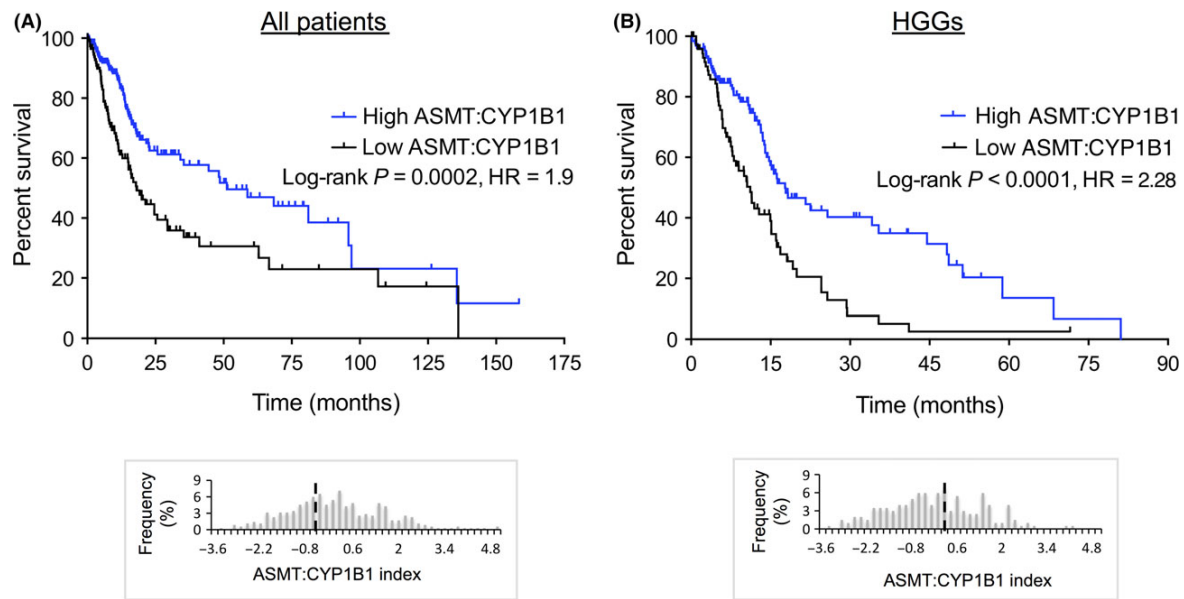
Fig. 5. The ASMT:CYP1B1 index is prognostic in gliomas (TCGA). Kaplan–Meier survival curves comparing (A) all patients or (B) only HGGs with a high vs low ASMT:CYP1B1 index. Comparisons were performed using the log-rank test. Histogram of ASMT:CYP1B1 values denote the cutoff determined for all patients (−0.687) or only HGGs (−0.727). All tumors, $n = 351$. HGGs: high-grade gliomas (astrocytomas grade III and grade IV), $n = 202$. HR: hazard ratio.

Table 1. Association between the ASMT:CYP1B1 index and clinicopathological features of glioma patients (TCGA)

	ASMT:CYP1B1 index		
Variables	Low ($n = 116$)	High ($n = 235$)	P-value*
Age, yr			
Mean (S.D.)	53.7 (1.4)	48.1 (1.1)	0.002
KPS			
Mean (S.D.)	80.5 (1.5)	82.7 (1.2)	0.301
Gender, %			
Male	57.8	59.6	0.817
Female	42.2	40.4	
Histological type, %			
Astrocytoma	75.9	58.7	0.006
Oligodendroglioma	14.6	23.0	
Oligoastrocytoma	9.5	18.3	
Histological grade, %			
II	21.5	32.3	0.006
III	23.3	30.2	
GBM	55.2	37.5	

*Two-sided Student's *t*-test (continuous variables) or Fisher's exact test (categorical variable).

antiproliferative effect. Thus, a more aggressive glioma, which synthesized/accumulated less melatonin, was more sensitive to the treatment with exogenous melatonin. Additionally, we designed a predictive model of the content of melatonin in the tumor microenvironment, the ASMT:CYP1B1 index, which negatively correlated with tumor grade, as well as with the expression of anti-apoptotic and pro-proliferation genes. More importantly, the ASMT:CYP1B1 index was revealed to be an independent prognostic factor, even when considering only HGG patients.

To our knowledge, there is a single investigation that assessed the relationship of tumor-synthesized melatonin and cell malignancy [32]. It was shown that cholangiocarcinoma cells synthesize significantly less melatonin than nonmalignant cholangiocytes and that patients with intrahepatic cholangiocarcinomas have decreased levels of melatonin in bile compared to healthy subjects. Moreover, the overexpression of AANAT reduced tumor growth in vitro, corroborating the idea that an increased production/accumulation of melatonin by malignant cells is associated with a less aggressive phenotype. Thus, measuring the content of melatonin in tumor microenvironment and modulating its production by malignant cells may have a role in the prognosis and treatment of melatonin-synthesizing tumors, such as cholangiocarcinomas and gliomas.

Melatonin has been shown to act through several biological mechanisms, ranging from antioxidant properties, binding to calmodulin and acting through its membrane receptors [33]. Oncostatic mechanisms of this indolamine include: modulation of cell cycle, apoptosis, and differentiation; inhibition of angiogenesis, invasion, and telomerase activity; and activation of the immune system [17]. Taken together with previous studies [18, 19], our data indicate that melatonin decreases glioma cell growth in both a receptor-dependent and independent manner, similarly to what was reported for other malignant neoplasms such as melanoma, prostate, and breast cancer [34–36]. Accordingly, the overexpression of the G protein-coupled melatonin receptor MT1 in melanoma and breast cancer cell lines was shown to enhance the growth suppressive effects of melatonin, both in vitro and in vivo [34, 37, 38]. Moreover, a recent study with ductal breast carcinomas revealed that the expression of MT1, which negatively correlates

Table 2. Multivariate Cox regression analysis of overall survival in glioma patients (TCGA)

| Variables | Overall Survival | | | |
| | All patients | | HGGs | |
	HR (95% CI)	*P*-value	HR (95% CI)	*P*-value
Age	1.038 (1.015–1.061)	0.0008	1.029 (1.005–1.053)	0.014
Gender				
Female	1		1	
Male	0.858 (0.539–1.364)	0.518	0.833 (0.513–1.350)	0.458
KPS score	0.974 (0.957–0.992)	0.004	0.975 (0.958–0.994)	0.008
Histological type				
Astrocytoma	1			
Oligodendroglioma	0.302 (0.089–1.027)	0.055		
Oligoastrocytoma	0.354 (0.078–1.594)	0.176		
Tumor grade				
II	1			
III	1.671 (0.544–5.128)	0.369	1	
Glioblastoma	4.587 (1.270–16.567)	0.020	2.968 (1.253–7.033)	0.013
ASMT:CYP1B1 index				
High	1		1	
Low	1.571 (1.020–2.421)	**0.040**	1.85 (1.165–2.936)	**0.009**
Age	1.040 (1.018–1.063)	0.0003	1.034 (1.010–1.058)	0.005
Gender				
Female	1		1	
Male	0.916 (0.575–1.461)	0.714	0.755 (0.453–1.258)	0.281
KPS score	0.975 (0.957–0.993)	0.006	0.977 (0.959–0.995)	0.016
Histological type				
Astrocytoma	1			
Oligodendroglioma	0.33 (0.092–1.177)	0.087		
Oligoastrocytoma	0.415 (0.091–1.901)	0.257		
Tumor grade				
II	1			
III	1.584 (0.499–5.024)	0.434	1	
Glioblastoma	4.514 (1.205–16.913)	0.025	3.124 (1.322–7.386)	0.009
ASMT				
High	1		1	
Low	2.733 (0.617–12.085)	**0.185**	0.884 (0.534–1.465)	**0.634**
CYP1B1				
High	1		1	
Low	0.675 (0.347–1.314)	**0.248**	0.496 (0.289–0.851)	**0.011**

HGGs, high-grade gliomas (astrocytomas grades III and IV); HR, hazard ratio; CI, confidence interval. Bold text indicates *P*-values calculated for the ASMT:CYP1B1 index or for the expression of ASMT and CYP1B1.

with tumor grade, is an independent prognostic factor, indicating a potential prognostic and therapeutic significance for the melatonergic system of such tumors [39].

The melatonin catabolic enzyme CYP1B1 is a tumor-associated antigen overexpressed in a wide range of human malignant neoplasms including breast, prostate, lung, esophagus, and skin cancer [40, 41]. In accordance with our data, the expression of CYP1B1 has been previously shown to negatively correlate with glioma grade and overall malignancy [42]. As CYP1B1 has a relatively restricted expression profile in normal tissues, it has been exploited as a target for immunotherapy [41, 43]. Interestingly, a phase I clinical trial of a CYP1B1 DNA vaccine demonstrated that all patients with solid and hematologic tumors who increased anti-CYP1B1 immunity presented clinical benefits [44]. The expression of the melatonin synthesis enzyme ASMT, on the other hand, was only detected in few types of cancer, such as human retinoblastoma, melanoma, and cholangiocarcinoma, besides rat C6 glioma [15,

32, 45, 46]. Additionally, as observed in gliomas, ASMT levels also decrease with the grade of pineal parenchymal tumors, reinforcing its potential role as a prognostic indicator [47].

Gene expression profiling of gliomas can contribute to the identification of gene signatures that accurately distinguish different cellular phenotypes, providing a molecular basis for the WHO grading [48, 49]. As such, given the role of ASMT and CYP1B1 in melatonin synthesis and metabolism, as well as their differential expression among glioma grades, we designed a two-gene index, ASMT: CYP1B1, revealed to be an independent prognostic factor that negatively correlates with tumor grade. Models combining two or three prognostically relevant genes have been shown to provide robust classifiers with small error rates [50]. Thus, simple models, such as the ASMT: CYP1B1 index, have the potential to translate high-throughput transcriptome data into practical diagnostic assays for clinical use.
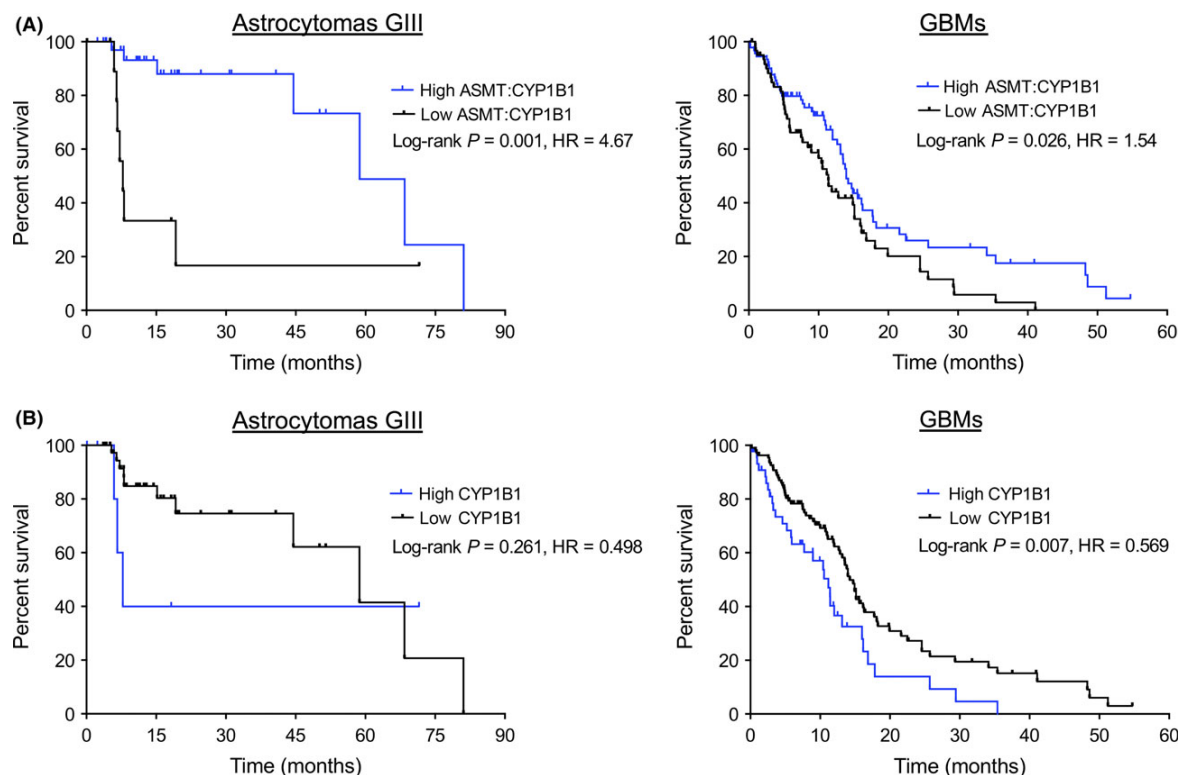
Fig. 6. The ASMT:CYP1B1 index has additional prognostic value to the histological diagnosis (TCGA). Kaplan–Meier survival curves comparing astrocytomas GIII and GBM patients with (A) high vs. low ASMT:CYP1B1 index (cutoff −0.727) and (B) high vs. low *CYP1B1* expression (cutoff 8.710). Patients were segregated according to the cutoff value calculated for high-grade gliomas. Comparisons were performed using the log-rank test. Astrocytomas GIII, $n = 50$. GBMs: glioblastomas, $n = 152$. HR: hazard ratio.

Understanding the basic biology and pathogenesis of gliomas plays a major role not only in classification and prognosis, but also in the stratification of patients in treatment-specific subgroups [5]. In this sense, the ASMT:CYP1B1 index was shown to decrease with the expression of many NFκB target genes involved in tumor development and progression. Levels of NFκB activity in gliomas are higher than in normal brain tissue and positively correlate with tumor grade [51, 52]. Moreover, the inhibition of NFκB attenuates the malignant phenotype of GBM cell lines, enhancing the effect of chemotherapeutic drugs [53]. Accordingly, individuals with tumors presenting a low ASMT:CYP1B1 index, which suggests enhanced NFκB activity, could greatly benefit from the treatment with melatonin, previously shown to act as a free radical scavenger, inhibiting the reactive oxygen species (ROS)/NFκB pathway of glioma cells [18,19]. Thus, the detailed molecular characterization of such tumors can contribute to the development of personalized, more effective, target therapies.

In conclusion, the present findings are the first to reveal the prognostic value of the melatonergic system of gliomas, highlighting the potential use of ASMT and CYP1B1 as clinically relevant biomarkers and pharmaceutical targets. Overall, our data indicate that glioma-synthesized melatonin has a role in tumor progression and thus lays some groundwork for further investiga-tions of the autocrine anticancer effects of this indola-mine. Challenges in the treatment of gliomas include the difficulty of drug delivery across the blood–brain barrier and their neurotoxicity associated side effects [54, 55]. In this sense, melatonin is soluble in both water and lipid and therefore readily crosses the blood–brain barrier [56]. Additionally, it exerts neuroprotective effects in many brain pathologies, including Parkinson's and Alz-heimer's disease [57]. Thus, as melatonin inhibited glioma cell growth also in a receptor-dependent manner, our data reinforce the therapeutic potential of this indola-mine and analogous in the treatment of gliomas, especially those with a reduced production/accumulation of melatonin.

Acknowledgements

Kinker et al.

design, data collection/analysis, decision to publish or manuscript preparation

Conflict of interest

The authors declare that they have no conflict of interest.

Author contributions

GSK, SKNM, RPM, and PAF conceived and designed the experiments; GSK, CEC, SMM, and SMO performed the experiments; SKNM, RPM, and PAF contributed with reagents, material, and analysis tools; GSK, SKNM, RPM, and PAF analyzed the data and wrote the manuscript. All authors critically revised the manuscript.

References

1. Ostrom QT, Gittleman H, Liao P et al. CBTRUS statistical report: primary brain and central nervous system tumors diagnosed in the United States in 2007–2011. Neuro Oncol 2014; **16**:iv1–iv63.

2. Jiang Y, Uhrbom L. On the origin of glioma. Ups J Med Sci 2012; **117**:113–121.

3. Louis DN, Ohgaki H, Wiestler OD et al. The 2007 WHO classification of tumours of the central nervous system. Acta Neuropathol 2007; **114**:97–109.

4. van den Bent MJ. Interobserver variation of the histopathological diagnosis in clinical trials on glioma: a clinician's perspective. Acta Neuropathol 2010; **120**:297–304.

5. Huse JT, Holland EC. Targeting brain cancer: advances in the molecular pathology of malignant glioma and medulloblastoma. Nat Rev Cancer 2010; **10**:319–331.

6. Johnson DR, O'Neill BP. Glioblastoma survival in the United States before and during the temozolomide era. J Neurooncol 2012; **107**:359–364.

7. Simonneaux V, Ribelayga C. Generation of the melatonin endocrine message in mammals: a review of the complex regulation of melatonin synthesis by norepinephrine, peptides, and other pineal transmitters. Pharmacol Rev 2003; **55**:325–395.

8. Hardeland R, Madrid JA, Tan DX et al. Melatonin, the circadian multioscillator system and health: the need for detailed analyses of peripheral melatonin signaling. J Pineal Res 2012; **52**:139–166.

9. Barrett P, Bolborea M. Molecular pathways involved in seasonal body weight and reproductive responses governed by melatonin. J Pineal Res 2012; **52**:376–388.

10. Young IM, Leone RM, Francis P et al. Melatonin is metabolized to N-acetyl serotonin and 6-hydroxymelatonin in man. J Clin Endocrinol Metab 1985; **60**:114–119.

11. Ma X, Idle JR, Krausz KW et al. Metabolism of melatonin by human cytochromes p450. Drug Metab Dispos 2005; **33**:489–494.

12. Acuña-Castroviejo D, Escames G, Venegas C et al. Extrapineal melatonin: sources, regulation, and potential functions. Cell Mol Life Sci 2014; **71**:2997–3025.

13. Venegas C, García JA, Escames G et al. Extrapineal melatonin: analysis of its subcellular distribution and daily fluctuations. J Pineal Res 2012; **52**:217–227.

14. Anderson G, Maes M. Local melatonin regulates inflammation resolution: a common factor in neurodegenerative, psychiatric and systemic inflammatory disorders. CNS Neurol Disord Drug Targets 2014; **13**:817–827.

15. Liu YJ, Zhuang J, Zhu HY et al. Cultured rat cortical astrocytes synthesize melatonin: absence of a diurnal rhythm. J Pineal Res 2007; **43**:232–238.

16. Pinato L, Da Silveira Cruz-Machado S, Franco DG et al. Selective protection of the cerebellum against intracerebroventricular LPS is mediated by local melatonin synthesis. Brain Struct Funct 2015; **220**:827–840.

17. Mediavilla MD, Sanchez-Barcelo EJ, Tan DX et al. Basic mechanisms involved in the anti-cancer effects of melatonin. Curr Med Chem 2010; **17**:4462–4481.

18. Martín V, Herrera F, Carrera-Gonzalez P et al. Intracellular signaling pathways involved in the cell growth inhibition of glioma cells by melatonin. Cancer Res 2006; **66**:1081–1088.

19. Wang J, Hao H, Yao L et al. Melatonin suppresses migration and invasion via inhibition of oxidative stress pathway in glioma cells. J Pineal Res 2012; **53**:180–187.

20. Martin V, Sanchez-Sanchez AM, Herrera F et al. Melatonin-induced methylation of the ABCG2/BCRP promoter as a novel mechanism to overcome multidrug resistance in brain tumour stem cells. Br J Cancer 2013; **108**:2005–2012.

21. Martín V, Sanchez-Sanchez AM, Puente-Moncada N et al. Involvement of autophagy in melatonin-induced cytotoxicity in glioma-initiating cells. J Pineal Res 2014; **57**:308–316.

22. Dubois-Dalcq M, Behar T, Hudson L et al. Emergence of three myelin proteins in oligodendrocytes cultured without neurons. J Cell Biol 1986; **102**:384–392.

23. Ma XJ, Wang Z, Ryan PD et al. A two-gene expression ratio predicts clinical outcome in breast cancer patients treated with tamoxifen. Cancer Cell 2004; **5**:607–616.

24. Subramanian A, Tamayo P, Mootha VK et al. Gene set enrichment analysis: a knowledge-based approach for interpreting genome-wide expression profiles. Proc Natl Acad Sci USA 2005; **102**:15545–15550.

25. Budczies J, Klauschen F, Sinn BV et al. Cutoff Finder: a comprehensive and straightforward web application enabling rapid biomarker cutoff optimization. PLoS ONE 2012; **7**: e51862.

26. Fogh J, Fogh JM, Orfeo T. One hundred and twenty-seven cultured human tumor cell lines producing tumors in nude mice. J Natl Cancer Inst 1997; **59**:221–226.

27. Liu T, Borjigin J. N-acetyltransferase is not the rate-limiting enzyme of melatonin synthesis at night. J Pineal Res 2005; **39**:91–96.

28. Karin M, Cao Y, Greten FR et al. NF-κB in cancer: from innocent bystander to major culprit. Nat Rev Cancer 2002; **2**:301–310.

29. Gilmore TD. Introduction to NF-κB: players, pathways, perspectives. Oncogene 2006; **25**:6680–6684.

30. Pahl HL. Activators and target genes of Rel/NF-kappaB transcription factors. Oncogene 1999; **18**:6853–6866.

31. Baud V, Karin M. Is NF-κB a good target for cancer therapy? Hopes and pitfalls. Nat Rev Drug Discov 2009; **8**:33–40.

32. Han Y, Demorrow S, Invernizzi P et al. Melatonin exerts by an autocrine loop antiproliferative effects in cholangiocarcinoma; its synthesis is reduced favoring cholangiocarcinoma growth. Am J Physiol Gastrointest Liver Physiol 2011; **301**: G623–G633.

33. Hardeland R, Cardinali DP, Srinivasan V et al. Melatonin – a pleiotropic, orchestrating regulator molecule. Prog Neurobiol 2011; **93**:350–384.

34. Kadekaro AL, Andrade LN, Floeter-Winter LM et al. MT-1 melatonin receptor expression increases the antiprolif-

erative effect of melatonin on S-91 murine melanoma cells. J Pineal Res 2004; **36**:204–211.

35. Grant SG, Melan MA, Latimer JJ et al. Melatonin and breast cancer: cellular mechanisms, clinical studies and future perspectives. Expert Rev Mol Med 2009; **11**:e5.

36. Xi SC, Tam PC, Brown GM et al. Potential involvement of mt1 receptor and attenuated sex steroid-induced calcium influx in the direct anti-proliferative action of melatonin on androgen-responsive LNCaP human prostate cancer cells. J Pineal Res 2000; **29**:172–183.

37. Yuan L, Collins AR, Dai J et al. MT 1 melatonin receptor overexpression enhances the growth suppressive effect of melatonin in human breast cancer cells. Mol Cell Endocrinol 2002; **192**:147–156.

38. Collins A, Yuan L, Kiefer TL et al. Overexpression of the MT1 melatonin receptor in MCF-7 human breast cancer cells inhibits mammary tumor formation in nude mice. Cancer Lett 2003; **189**:49–57.

39. Jablonska K, Pula B, Zemla A et al. Expression of melatonin receptor MT1 in cells of human invasive ductal breast carcinoma. J Pineal Res 2013; **54**:334–345.

40. Maecker B, Sherr DH, Vonderheide RH et al. The shared tumor-associated antigen cytochrome P 450 1B1 is recognized by specific cytotoxic T cells. Blood 2003; **102**:3287–3294.

41. Murray GI, Taylor MC, McFadyen MC et al. Tumor-specific expression of cytochrome P450 CYP1B1. Cancer Res 1997; **57**:3026–3031.

42. Barnett JA, Urbauer DL, Murray GI et al. Cytochrome P450 1B1 expression in glial cell tumors: an immunotherapeutic target. Clin Cancer Res 2007; **13**:3559–3567.

43. Luby TM, Cole G, Baker L et al. Repeated immunization with plasmid DNA formulated in poly (lactide-co-glycolide) microparticles is well tolerated and stimulates durable T cell responses to the tumor-associated antigen cytochrome P450 1B1. Clin Immunol 2004; **112**:45–53.

44. Gribben JG, Ryan DP, Boyajian R et al. Unexpected association between induction of immunity to the universal tumor antigen CYP1B1 and response to next therapy. Clin Cancer Res 2005; **11**:4430–4436.

45. Bernard M, Donohue SJ, Klein DC. Human hydroxyindole-O-methyltransferase in pineal gland, retina and Y79 retinoblastoma cells. Brain Res 1995; **696**:37–48.

46. Slominski A, Pisarchik A, Semak I et al. Serotoninergic and melatoninergic systems are fully expressed in human skin. FASEB J 2002; **16**:896–898.

47. Fukuda T, Akiyama N, Ikegami M et al. Expression of hydroxyindole-O-methyltransferase enzyme in the human central nervous system and in pineal parenchymal cell tumors. J Neuropathol Exp Neurol 2010; **69**:498–510.

48. Phillips HS, Kharbanda S, Chen R et al. Molecular subclasses of high-grade glioma predict prognosis, delineate a pattern of disease progression, and resemble stages in neurogenesis. Cancer Cell 2006; **9**:157–173.

49. Verhaak RG, Hoadley KA, Purdom E et al. Integrated genomic analysis identifies clinically relevant subtypes of glioblastoma characterized by abnormalities in PDGFRA, IDH1, EGFR, and NF1. Cancer Cell 2010; **17**:98–110.

50. Kim S, Dougherty ER, Shmulevich I et al. Identification of combination gene sets for glioma classification. Mol Cancer Ther 2002; **1**:1229–1236.

51. Wang H, Zhang W, Huang HJ et al. Analysis of the activation status of Akt, NF-κB, and Stat3 in human diffuse gliomas. Lab Invest 2004; **84**:941–951.

52. Korkolopoulou P, Levidou G, Saetta AA et al. Expression of nuclear factor-κB in human astrocytomas: relation to pI κ Ba, vascular endothelial growth factor, Cox-2, microvascular characteristics, and survival. Hum Pathol 2008; **39**:1143–1152.

53. Zanotto-Filho A, Braganhol E, Schröder R et al. NFκB inhibitors induce cell death in glioblastomas. Biochem Pharmacol 2011; **81**:412–424.

54. Deeken JF, Löscher W. The blood-brain barrier and cancer: transporters, treatment, and Trojan horses. Clin Cancer Res 2007; **13**:1663–1674.

55. Froklage FE, Oosterbaan LJ, Sizoo EM et al. Central neurotoxicity of standard treatment in patients with newly-diagnosed high-grade glioma: a prospective longitudinal study. J Neurooncol 2014; **116**:387–394.

56. Reiter RJ, Tan DX, Kim SJ et al. Delivery of pineal melatonin to the brain and SCN: role of canaliculi, cerebrospinal fluid, tanycytes and Virchow-Robin perivascular spaces. Brain Struct Funct 2014; **219**:1873–1887.

57. Polimeni G, Esposito E, Bevelacqua V et al. Role of melatonin supplementation in neurodegenerative disorders. Front Biosci (Landmark Ed) 2014; **19**:429–446.

Supporting Information

Additional Supporting Information may be found in the online version of this article:

Data S1. Materials and methods

Table S1. Multivariate Cox regression analysis of overall survival in glioma patients (GSE16011)

Figure S1. Single-gene based analysis of survival (TCGA).

Figure S2. The ASMT:CYP1B1 index is prognostic in gliomas (GSE16011).

Kinker et al. Supplemental Data

Supplemental Materials and Methods

Gene Expression Omnibus (GEO) validation dataset

GSE16011 HG-U133 Plus 2 (Affymetrix) microarray dataset was downloaded from the public repository GEO (http://www.ncbi.nlm.nih.gov/geo/). Raw data (.CEL files) from 264 gliomas were normalized by the robust multiarray averaging (RMA) method and probesets were annotated using Affymetrix library files. The probesets 210551_s_at and 202436_s_at were chosen to represent *ASMT* and *CYP1B1* expression, respectively. Raw data processing was performed using Bioconductor R Packages (http://www.bioconductor.org/). Clinical data were obtained from the related article [1].

Supplemental Table

Table S1. Multivariate Cox regression analysis of overall survival in glioma patients (GSE16011)

| | Overall Survival | | | |
| | All patients | | HGGs | |
Variables	HR (95% CI)	*P*-value	HR (95% CI)	*P*-value
Age	1.036 (1.024 – 1.048)	<0.0001	1.035 (1.021 – 1.049)	<0.0001
Gender				
Female	1		1	
Male	1.231 (0.923 – 1.642)	0.157	1.180 (0.841 – 1.658)	0.337
KPS score	0.977 (0.970 – 0.985)	<0.0001	0.967 (0.960 – 0.980)	<0.0001
Histological type				
Astrocytoma	1			
Oligodendroglioma	0.266 (0.145 – 0.491)	<0.0001		
Oligoastrocytoma	0.569 (0.293 – 1.104)	0.096		
Histological grade				
II	1			
III	1.475 (0.784 – 2.774)	0.228	1	
Glioblastoma	2.008 (1.130 – 3.567)	0.018	1.131 (0.636 – 2.010)	0.675
ASMT:CYP1B1 index				
High	1		1	
Low	1.841 (1.203 – 2.818)	**0.005**	1.619 (1.030 – 2.544)	**0.037**
Age	1.034 (1.022 – 1.046)	<0.0001	1.034 (1.020 – 1.048)	<0.0001
Gender				
Female	1		1	
Male	1.200 (0.876 – 1.645)	0.255	1.161 (0.824 – 1.636)	0.393
KPS score	0.977 (0.970. – 0.985)	<0.0001	0.968 (0.958 – 0.978)	<0.0001
Histological type				
Astrocytoma	1			
Oligodendroglioma	0.273 (0.147 – 0.505)	<0.0001		
Oligoastrocytoma	0.570 (0.293 – 1.108)	0.097		
Histological grade				
II	1			
III	1.468 (0.777 – 2.772)	0.237	1	
Glioblastoma	2.050 (1.136 – 3.701)	0.017	3.124 (1.322 – 7.386)	0.009
ASMT				
High	1		1	
Low	1.043 (0.777 – 1.400)	**0.776**	0.957 (0.681 – 1.347)	**0.804**
CYP1B1				
High	1		1	
Low	0.916 (0.665 – 1.263)	**0.593**	0.501 (0.265 – 0.948)	**0.034**

HGGs, high-grade gliomas (astrocytomas grade III and IV); HR, hazard ration; CI, confidence interval.

Kinker et al.   Supplemental Data
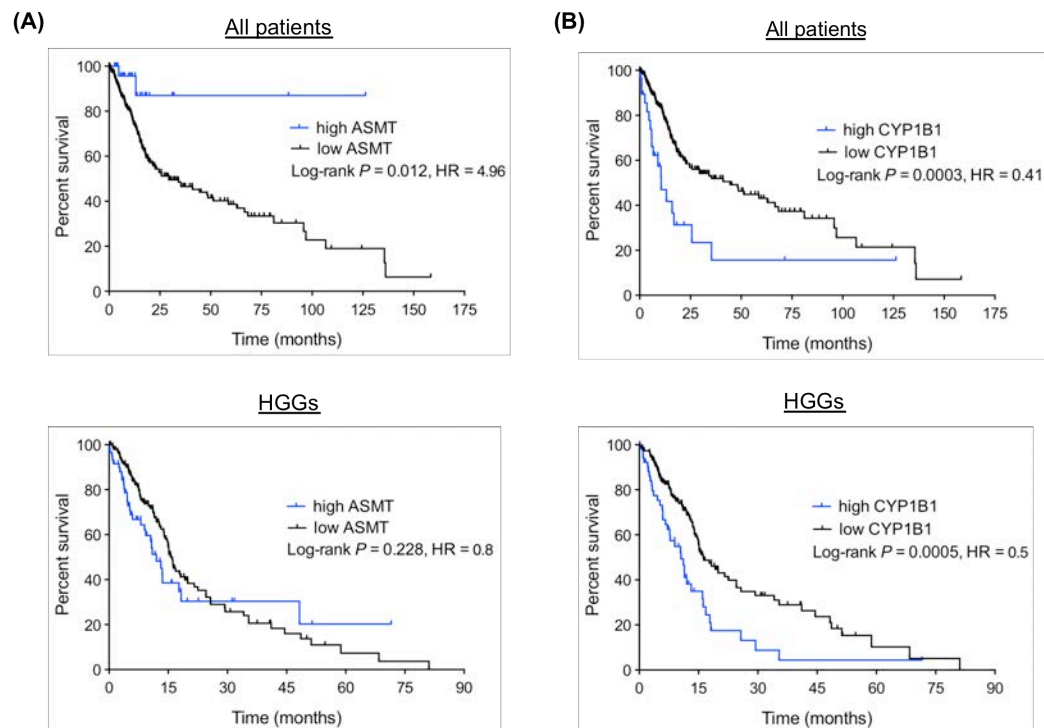
Supplemental Figures

Figure S1. Single-gene based analysis of survival (TCGA). Kaplan-Meier survival curves comparing patients with (A) high vs. low *ASMT* expression (all patients, cutoff 1.662; HGGs, cutoff 0.919) and (B) high vs. low *CYP1B1* expression (all patients, cutoff 10.20; HGGs, cutoff 8.710). Comparisons were performed using the long-rank test. All patients, n = 351. HGGs: high-grade gliomas (astrocytomas grade III and IV), n = 202. HR: hazard ratio.

Figure S2. The ASMT:CYP1B1 index is prognostic in gliomas (GSE16011). Kaplan-Meier survival curves comparing patients with (A) high vs. low *ASMT* expression (all patients, cutoff 4.697; HGGs, cutoff 4.677); (B) high vs. low *CYP1B1* expression (all patients, cutoff 8.572; HGGs, cutoff 10.940) and (C) high vs. low ASMT:CYP1B1 index (all patients, cutoff -1.808; HGGs, cutoff -1.808). Comparisons were performed using the long-rank test. All patients, n = 264. HGGs: high-grade gliomas (astrocytomas grade III and IV), n = 171. HR: hazard ratio.

Kinker et al.   Supplemental Data

References

1. GRAVENDEEL LA, KOUWENHOVEN MC, GEVAERT O, et al. Intrinsic gene expression profiles of gliomas are a better predictor of survival than histology. Cancer Res 2009; 69:9065-9072.

Chapter 3

The role of melatonin receptors in brain cancer

MT1 and MT2 melatonin receptors play opposite roles in brain cancer progression

Kinker GS[1#], Ostrowski LH[1], Ribeiro PAC[2], Chanoch R[3], Muxel SM[1], Tirosh I[3], Spadoni G[4], Rivara S[5], Martins VR[2,6], Santos TG[2,6], Markus RP[1], Fernandes PA[1#].

[1]Dep. of Physiology, Institute of Bioscience, University of Sao Paulo, Sao Paulo, Brazil.
[2]International Research Center, A.C. Camargo Cancer Center, Sao Paulo, Brazil.
[3]Dep. of Molecular Cell Biology, Weizmann Institute, Israel.
[4]Dep. of Biomolecular Sciences, University of Urbino "Carlo Bo", Urbino, Italy
[5]Dep. of Food and Drug, University of Parma, Parma, Italy.
[6]National Institute for Science and Technology in Oncogenomics and Therapeutic Innovation – INCITO-INOTE.

Corresponding author.

Abstract
Introduction: Primary brain tumors remain among the deadliest of all cancers. Glioma grade IV (glioblastoma), the most common and malignant type of brain cancer, is associated with a 5-year survival rate <5%. Melatonin has been widely reported as an anticancer molecule and we have recently demonstrated that the ability of gliomas to synthesize and accumulate this indolamine in the surrounding microenvironment negatively correlates with tumor malignancy. However, our understanding of the specific effects mediated through the activation of melatonin membrane receptors remains limited. Thus, here we investigated the specific roles of MT1 and MT2 in gliomas and medulloblastomas. **Methods and Results:** Using the MT2-selective antagonist DH97 we showed that MT1 activation has a negative impact on the proliferation of human glioma and medulloblastoma cell lines, while MT2 activation has an opposite effect. Accordingly, gliomas have a decreased mRNA expression of *MT1* (also known as *MTNR1A*) and an increased mRNA expression of *MT2* (also known as *MTNR1B*) compared to normal brain cortex. Moreover, the MT1/MT2 expression ratio negatively correlates with the expression of cell cycle-related genes and is a positive prognostic factor in gliomas. Notably, we showed that functional-selective drugs that simultaneously activate MT1 and inhibit MT2 exert robust anti-tumor effects in vivo and in vitro, downregulating the expression of cell cycle and energy metabolism genes in glioma stem-like cells. **Discussion:** Overall, we provided the first evidence regarding the differential roles of MT1 and MT2 in brain tumor progression, highlighting their relevance as druggable targets.

Introduction

Despite decades of research progress, brain tumors remain among the cancers that hold the poorest prognosis. Glioma grade IV (glioblastoma), the most common and malignant type of brain cancer, is associated with a median survival of approximately 15 months in adults (Chinot et al., 2014; Gilbert et al., 2014). Brain tumors are also the most common solid tumors affecting children and adolescents, and survivors often display neurocognitive impairment in adulthood due to the exposure of the developing brain to diverse medical interventions (Smith & Reaman, 2015). Challenges in the treatment of such tumors include their invasive nature and cellular heterogeneity, as well as the difficulty of drug delivery across the blood-brain barrier (Aldape et al., 2019). Recently, the World Health Organization Classification of Central Nervous System Tumors has incorporated biologically and clinically relevant molecular features to the traditional histological diagnosis (Louis et al., 2016; Reifenberger, Wirsching, Knobbe-Thomsen, & Weller, 2017). Diffuse gliomas in adults are now divided into three main groups with progressively worse prognosis: isocitrate dehydrogenase (IDH)-mutant and 1p/19q co-deleted tumors with oligodendroglial morphology; IDH-mutant and non-1p/19q co-deleted tumors with astrocytic morphology; and IDH-wild type glioblastomas. New entities also include diffuse midline pediatric glioma with H3 K27M–mutations, RELA fusion–positive ependymoma, medulloblastoma WNT-activated, and medulloblastoma SHH-activated (Louis et al., 2016; Reifenberger et al., 2017).

Melatonin synthesized by the pineal gland at night translates the environmental dark phase to the organism and ensures the synchronization of circadian and seasonal rhythms (Hardeland, Madrid, Tan, & Reiter, 2012; Reiter, 1993). The production of melatonin has also been detected in many extrapineal tissues, including retina, gastrointestinal tract and brain (Acuña-Castroviejo et al., 2014; Markus, Fernandes, Kinker, da Silveira Cruz-Machado, & Marçola, 2018). Generally, extra-pineal melatonin is poorly released into the circulation, acting locally in autocrine and paracrine manners (Bubenik, 2002; Pinato et al., 2015; Venegas et al., 2012). Melatonin acts through several mechanisms, including activating G protein-coupled receptors in the cytoplasmic and mitochondrial membranes (Jockers et al., 2016), binding to calmodulin in the cytoplasm (Benítez-King & Antón-Tay, 1993), and directly scavenging free radicals (Tan et al., 2002). Human MT1 and MT2 melatonin receptors share 55% of amino acid sequence similarity and bind melatonin with high affinity (Reppart, Weaver, & Godson, 1996). Both are typically coupled to Gi/o proteins, while MT1 can also be couple to Gq, evoking phospholipase-c calcium-dependent signaling (Brydon et al., 1999; Jockers et al., 2016). Melatonin receptors are widely expressed throughout the central nervous system (Klosen et al., 2019) and play a role in circadian entrainment, synaptic function and neurodevelopment (Ng, Leong, Liang, & Paxinos, 2017). Interestingly, altered expression of melatonin receptors has been reported in different neurodegenerative conditions such as Alzheimer's and Parkinson's diseases (Adi et al., 2010; Savaskan et al., 2005, 2002).

Exogenous melatonin has been shown to exert oncostatic effects, in both receptor-dependent and -independent manners, across a wide variety of tumors (Cutando, López-Valverde, Arias-Santiago, DE Vicente, & DE Diego, 2012; Li et al., 2017). In the mM concentration range, this indolamine impairs the invasion and migration of human glioma cell lines and reduces the viability of glioma-initiating cells (Martín et al., 2014; Wang et al., 2012; Zheng et al., 2017). Additionally, we have recently demonstrated that the ability of gliomas to synthesize and accumulate melatonin negatively correlates with their overall malignancy (Kinker et al., 2016). High-grade gliomas have a decreased expression of acetylserotonin O-methyltransferase (*ASMT*), the final enzyme of melatonin biosynthesis, combined with a high expression of cytochrome P450 1B1 (*CYP1B1*), the main enzyme of melatonin extra-hepatic metabolism. Remarkably, we designed a predictive model of the content of melatonin in the tumor microenvironment, the ASMT:CYP1B1 expression index, which was shown to be a positive prognostic factor, independent of glioma grade and histological subtype (Kinker et al., 2016).

Here, to provide further support for the use of melatonin and analogous in brain cancer therapy, we investigated the specific roles of melatonin receptors MT1 and MT2 in the oncostatic actions of this indolamine. Using a MT2-selective antagonist we showed that MT1 impairs, while MT2 promotes, the proliferation of glioma and medulloblastoma cell lines. Accordingly, patients expressing high *MT1* (also known as *MTNR1A*) and low *MT2* (also known as *MTNR1B*) presented a significantly better prognosis. These results suggest that, in glioma and medulloblastomas, the balance between MT1 and MT2 levels in tumor cells might limit the therapeutic effects of melatonin. Notably, we show that functional-selective drugs displaying MT1 agonist and MT2 antagonist properties exert robust anti-tumor effects in vivo and in vitro, and likely interfere with the proliferation and metabolism of glioma stem cells.

Materials and methods

Cell lines

Human glioma cell lines HOG, T98G, U87MG, U87MG-luc (expressing a luciferase reporter gene), and human medulloblastoma cell line DAOY were cultured in RPMI 1640 medium (Thermo Fisher Scientific) supplemented with 10% heat-inactivated fetal bovine serum (Thermo Fisher Scientific), 100 IU/mL penicillin (Thermo Fisher Scientific), and 100 μg/mL streptomycin (Thermo Fisher Scientific). T98G, U87MG and DAOY were purchased from ATCC, HOG was kindly provided by Dr. Suely K. N. Marie (University of Sao Paulo, Brazil), and U87MG-luc was kindly provided by Dr. Andrew L. Kung (Memorial Sloan Kettering Cancer Center, New York, USA). Cancer stem cell-enriched cultures MGG23 and MGH143 were derived from glioblastoma specimens at the Massachusetts General Hospital and kindly provided by Dr. Mario Suvà (Dana-Farber Cancer Institute, USA). MGG23 and MGH143 cells were grown as neurospheres and maintained in neurobasal medium (Thermo Fisher Scientific) supplemented with L-glutamine

(Thermo Fisher Scientific), B27 supplement (Thermo Fisher Scientific), N2 supplement (Thermo Fisher Scientific), 100 IU/mL penicillin (Thermo Fisher Scientific), 100 µg/mL streptomycin (Thermo Fisher Scientific), 20 ng/mL EGF (Sigma), and 20 ng/mL FGF2 (Peprotec). All cell lines were cultured at 37°C in a humidified atmosphere of 5% CO_2.

Drugs

Melatonin was purchased from Sigma, and DH97, a MT2-selective antagonist ($pKi_{MT2}=$ 8.03, 89-fold selectivity over MT1), was purchased from Tocris. Melatonin receptor ligands that act as MT1 agonist and MT2 antagonist, 5-HEAT (Nonno et al., 2000) and N-{2-[(3-methoxyphenyl)benzylamino]ethyl}acetamide (UCM799) (Rivara et al., 2007), were synthesized at Dr. Gilberto Spadoni laboratory (University of Urbino, Italy). DH97 was solubilized to 40 mM in DMSO. Melatonin, 5-HEAT and UCM799 were solubilized to 50 mM also in DMSO.

Flow cytometry

Cells were detached with 0.2% EDTA (10 min, room temperature), fixed with 2% PFA PBS (20 min, on ice), permeabilized with 0.1% TritonX-100 PBS (10 min, room temperature), blocked with 2% BSA PBS (1h, room temperature) and incubated overnight at 4°C with goat anti-MT1 (1:100, sc-13186, Santa Cruz Biotechnology) or goat anti-MT2 (1:100, sc-13177, Santa Cruz Biotechnology) primary antibodies. Cells were washed twice with 2% BSA PBS before incubation with FITC-conjugated anti-goat IgG secondary antibody (1:200, sc-2777, Santa Cruz Biotechnology) for 1 h at room temperature. Cells stained with the secondary antibody alone were used as the isotype control. Data were acquired on a Amnis FlowSight flow cytometer (Merck Millipore) and analyses were carried on using the IDEAS software (Merck Millipore) and FlowJo v9.

MTT proliferation assay

Cells (4 x 10^3 per well) were seeded on 96-well plates, left to attach overnight and treated with DH97 (3 x 10^{-10} – 10^{-6} M), 5-HEAT (10^{-9} – 10^{-6} M), UCM799 (10^{-9} – 10^{-6} M), or the appropriate vehicle for 48 h. Culture media was then replaced with a MTT solution (0.5 mg/mL in PBS, Sigma) and cells were maintained in the incubator for 4 hr. Reduced MTT crystals (formazan) were dissolved in isopropanol:DMSO (1v:1v) for 10 minutes at room temperature. Absorbance was measured at 570 nm, with background subtraction at 690 nm, in a SpectraMax 250 spectrophotometer (Molecular Devices).

U87MG-luc orthotopic xenograft model

U87MG-luc cells (5×10^5) suspended in 5 μL PBS were injected into the right striatum of female/male 8–10-week-old Balb/C nude mice (Charles River International) using a 10 μL Hamilton syringe attached to a Harvard 22 syringe pump (Harvard Apparatus), as previously describe (Lopes et al., 2015; Wasilewska-Sampaio, Santos, Lopes, Cammarota, & Martins, 2014). Two weeks after tumor implantation, animals were randomly assigned to four experimental groups: vehicle (0.2% DMSO, n = 7), 10^{-4} M melatonin (n = 5), 10^{-4} M 5-HEAT (n = 5) and 10^{-4} M UCM799 (n = 5). Treatments were continuously infused (0.25 μl/hr) into the right striatum of mice for 14 days using ALZET mini osmotic pumps (model 1002) and the ALZET brain infusion kit 3 (DURECT Corporation). Prior to implantation, pre-filled pumps were primed in sterile 0.9% saline overnight at 37°C, according to manufacturer's instructions. For in vivo bioluminescence imaging, animals were anesthetized with isoflurane, injected intraperitoneally with D-luciferin (50 μg/g, PerkinElmer) and placed into an In Vivo FX PRO imaging system (Bruker). Analyses were performed using the MI Software (Bruker). Fourteen days post-treatment mice were euthanized by deep anesthesia and encapsulated tumors were resected. Tumor volume (mm^3) was determined using width (a) and length (b) measurements ($V = (a^2 \times b)/2$, where $a \leq b$). Institutional guidelines for animal welfare and experimental conduct were followed. The study was approved by the Animal Ethics Committee of the A. C. Camargo Cancer Center (process 076/17), and by the Animal Ethics Committee of the Institute of Bioscience, University of Sao Paulo (process 284/2017).

TCGA and GTEx data

The Cancer Genome Atlas (TCGA) RNA-seq and clinical data from 662 primary gliomas (509 lower grade gliomas and 153 glioblastomas) and Genotype-Tissue Expression (GTEx) RNA-seq data from 283 normal brain cortex were downloaded from the UCSC XENA Browser (Goldman et al., 2018). RNA-seq data were generated using the Illumina HiSeq 2000 RNA sequencing platform and quantified by RSEM. Estimated counts were upper quartile normalized, $\log_2$(*normalized counts* + 1) transformed and converted to z-score.

Survival analysis

We evaluated the association between the MT1/MT2 expression ratio and patient 10-year survival using tumors expressing MT1 and/or MT2 (331 lower grade gliomas and 91 glioblastomas). Cutoffs used for patient dichotomization were defined using a log-rank test-based approach that identifies the most statistically significant data split, as previously described (Budczies et al., 2012). Univariate analyses of survival were performed using Kaplan-Meier curves and the log-rank test. Multivariate analyses of survival adjusting for clinically significant

parameters were performed using Cox proportional hazards regression. Hazard ratios including 95% confidence intervals were calculated.

Predictive model of the content of melatonin in the microenvironment

The concentration of melatonin synthesized and accumulated by tumor cells in the microenvironment was estimated using gene expression data by calculating the ASMT:CYP1B1 index, as previously described (Kinker et al., 2016). The index reflects the ratio between the expression of *ASMT*, the final enzyme in the biosynthetic pathway of melatonin, and *CYP1B1*, the main enzyme of melatonin metabolism in the brain. Tumors were classified as having low or high melatonin using the median ASMT:CYP1B1 index value as the split point.

RNA-seq

MGH143 and MGG23 cells (1,000 per well) were seeded in 96-well plates, left to rest overnight and treated with 5-HEAT (10^{-6} M) or vehicle (2 x 10^{-3} % DMSO) for 48 h. Culture media was removed after centrifugation and 10 µL of RNasin lysis buffer (SMART-Seq V4 Ultra Low Input RNA Kit; Clontech) was added to each well. Samples were incubated for 5 min at room temperature and transferred to −80°C. Once samples were thawed, reverse transcription and cDNA amplification (17 cycles) were performed with the SMART-Seq V4 Ultra Low Input RNA Kit according to the manufacturer's protocol. Following Agencourt Ampure XP beads cleanup (Beckman Coulter), 200 pg of amplified DNA were used for library preparation, as previously described (Blecher-Gonen et al., 2013). Individual barcodes were ligated to each sample to allow multiplexing. Between 10 and 12 million single-end reads were sequenced per sample using Sequencing was performed on the Illumina NextSeq500 instrument using the Illumina NextSeq High Output Kit (75 cycles). Reads were aligned to the GHCh38/hg38 human genome using Bowtie and expression values were quantified using RSEM. Data are presented as log2(TPM +1).

GSEA

For the TCGA RNA-seq data analysis, we selected tumors expressing MT1 and/or MT2 (331 lower grade gliomas and 91 glioblastomas), and used Pearson's correlation coefficient with the MT1/MT2 expression ratio as the ranking metric. For the glioma stem-like cells RNA-seq data analysis, genes were ranked according to the average log2(fold change) observed across samples treated with 5-HEAT compared to the vehicle group. GSEA was performed using the GSEA desktop application v3.0 (Subramanian et al., 2005) and Reactome pathways (Fabregat et al., 2016). Enrichment scores (ES) were calculated based on a weighted Kolmogorov–Smirnov-like statistic and normalized (NES) to account for gene set size. P-values corresponding to each NES were calculated using 1,000 gene set permutations and corrected for multiple comparisons with the false discovery rate (FDR) procedure. Adjusted p-values < 0.1 were considered statistically

significant. The Cytoscape plug-in EnrichmentMap was used to generate network-based enrichment maps of significantly enriched gene sets (Merico, Isserlin, Stueker, Emili, & Bader, 2010).

Additional statistical analysis

We used two-sided Student's t test to perform two-group comparisons and Pearson's correlation to assess associations between continuous variable. Where specified, p values were corrected for multiple comparisons using the FDR procedure and combined using Fisher's method. Sample size and number of experimental and technical replicates are reported in Figure Legends. P-values < 0.05 were considered statistically significant. Analyses were performed with GraphPad Prism 6 and R (www.r-project.org).

Results

Melatonin receptors MT1 and MT2 differentially control the proliferation of glioma and medulloblastoma cell lines

To explore the biological role of melatonin receptors in brain tumors, we first showed the expression of MT1 and MT2 in three human glioma cell lines (HOG, an oligodendroglioma grade III; T98G, a glioblastoma; and U87MG, a tumorigenic glioblastoma; **Fig. 1A**). The less aggressive cell lines HOG and T98G synthesize and accumulate significant amounts of melatonin in their microenvironment (Kinker et al., 2016). Using luzindole, a non-selective antagonist of melatonin receptors, we have previously demonstrated that this glioma-synthesized melatonin exerts an autocrine anti-proliferative effect in a receptor-dependent manner (Kinker et al., 2016). Thus, to elucidate the specific roles of MT1 and MT2, we treated cells with the MT2 antagonist DH97, which display 89-fold selectivity over MT1. Surprisingly, the selective blockage of MT2 by 10^{-8} M DH97 significantly decreased the proliferation of HOG and T98G (**Fig. 1B**). This effect was reverted, in a concentration dependent manner (DH97 $10^{-7} - 10^{-6}$ M), probably by the concomitant inhibition of both melatonin receptors, suggesting opposite roles for MT1 and MT2 (**Fig. 1B**). Indeed, the treatment with 10^{-6} M DH97 mimicked the effects of the non-selective antagonist luzindole and stimulated the proliferation of HOG and T98G (Kinker et al., 2016). Similar results were obtained using the medulloblastoma cell line DAOY, which expresses MT1, MT2, and the enzymes involved in melatonin synthesis aralkylamine N-acetyltransferase (AANAT), its active form PAANAT, and ASMT. DAOY also accumulates significant amounts of melatonin (9.8 ± 0.7 pg/mL, n = 6, 6 h incubation) in the culture media (**Fig. S1A-B**). No difference was observed for the glioma cell line U87MG (**Fig. 1A**), which produces low levels of melatonin, and is also unaffected by luzindole (Kinker et al., 2016).
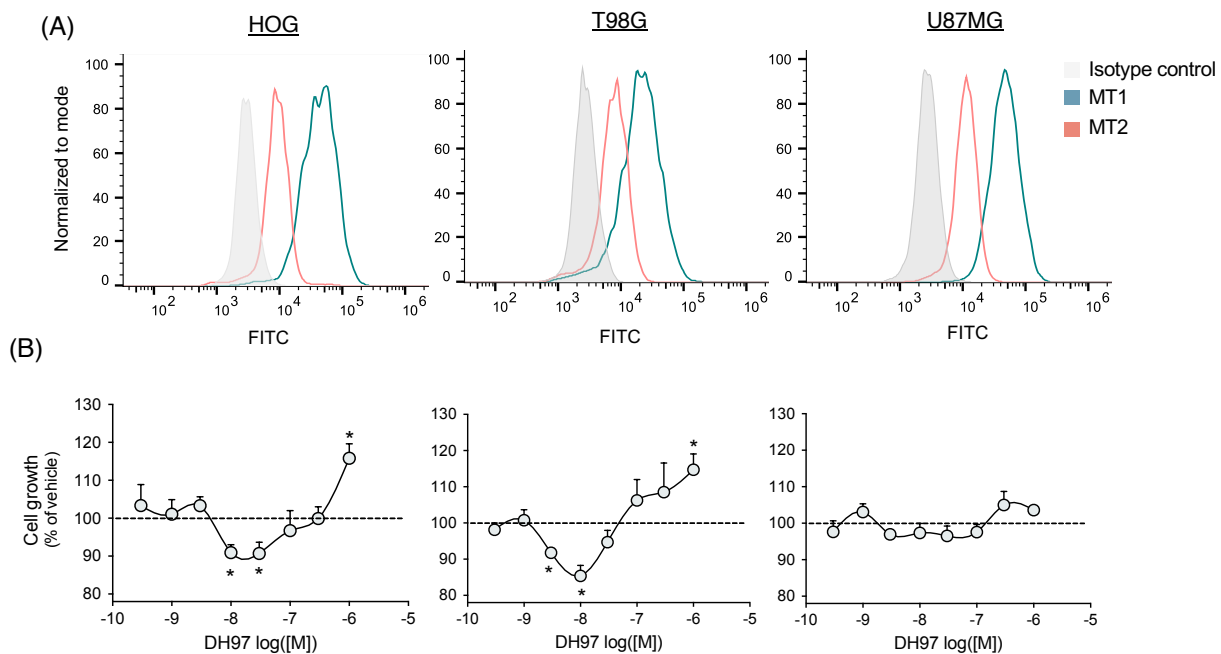
Figure 1. The activation of MT1 and MT2 receptors play opposite roles in the control of glioma proliferation. (A) Detection of melatonin receptors by indirect immunofluorescence using flow cytometry. Isotype control corresponds to cells stained with secondary antibody alone. **(B)** High- (HOG and T98G) and low-melatonin (U87MG) glioma cell lines were cultured for 48 h in the presence of DH97 ($3 \times 10^{-10} - 10^{-6}$ M), an MT2-selective antagonist (pKi = 8.03, 89-fold selectivity over MT1), or the respective vehicle ($7 \times 10^{-7} - 2 \times 10^{-3}$ % DMSO). Cell number was estimated by MTT assay and values were normalized by the mean absorbance detected in the respective vehicle group. Data are shown as mean ± SEM of four independent experiments in quadruplicates. * Significantly different from the respective vehicle group ($p < 0.05$) using the two-sided Student's t test.

Clinical relevance of MT1 and MT2 expression in glioma

Analysis of TCGA and GTEx RNAseq data revealed that lower grade gliomas and glioblastomas have a decreased expression of *MT1* and an increased expression of *MT2* compared to normal brain cortex (**Fig. 2A**). Moreover, gliomas simultaneously expressing high *MT1* and low *MT2* (high MT1/MT2 ratio) were associated with significantly better 10-year survival **(Fig. 2B).** Such effect was especially relevant in gliomas predicted to synthesize and accumulate more melatonin, for which the MT1/MT2 ratio was a positive prognostic factor of 10-year survival independent of age, gender, IDH mutation and 1p/19q co-deletion (**Table 1**). Similar results were obtained for 5-year survival (**Table S1**). Next, in a way to assess whether a high MT1/MT2 ratio translates into enhanced MT1-induced Gq activation, using GSEA we showed that the ratio

97

positively correlates with the expression of gene sets associated with calcium-dependent signaling (**Fig. 2C, Table S2**). Moreover, in accordance with the in vitro results suggesting that MT1 has a negative and MT2 a positive impact on glioma growth, the MT1/MT2 ratio also negatively correlated with the expression of cell cycle-related gene sets (**Fig. 2C, Table S2**).
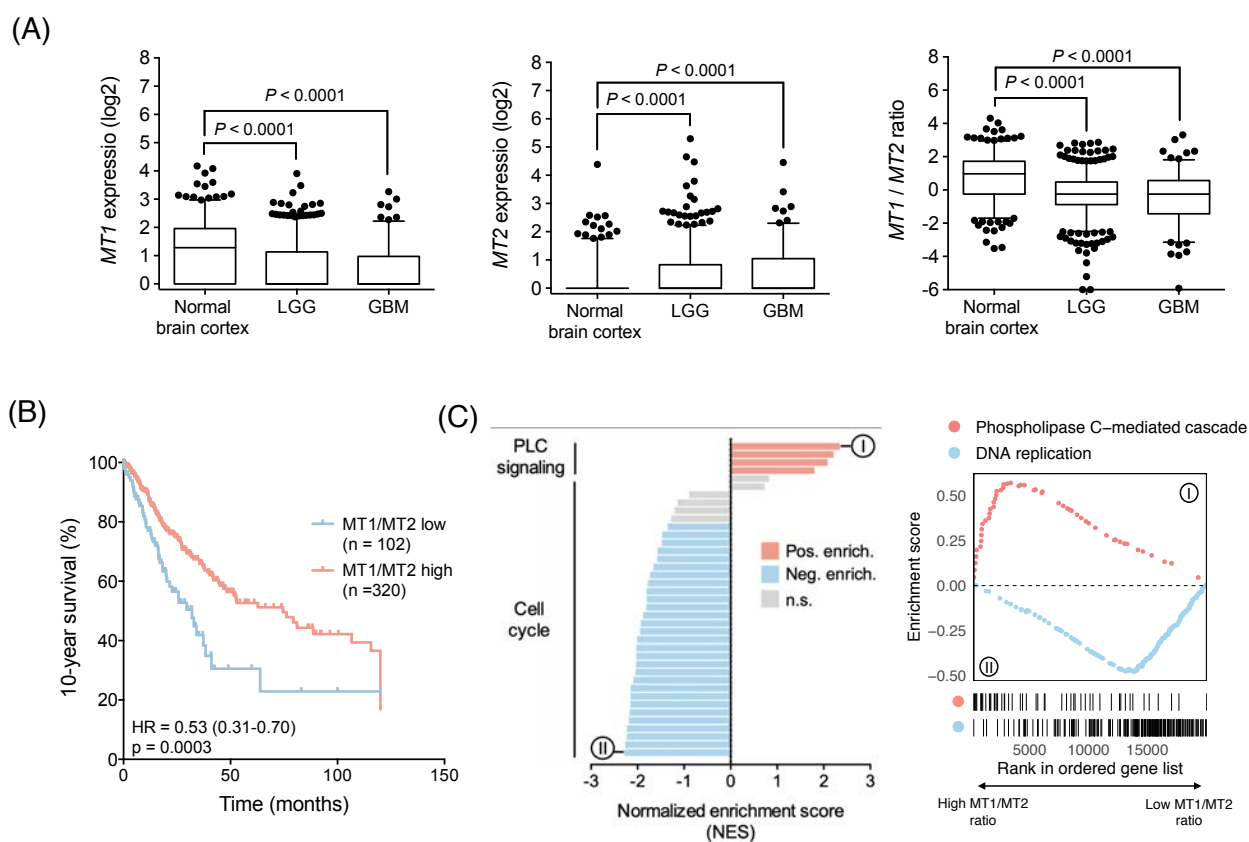

Figure 2. Expression of *MT1* and *MT2* differentially impact glioma patient survival. (A) Expression of *MT1* and *MT2* and the MT1/MT2 ratio in normal brain cortexes (n = 283) from GTEx and primary lower grade gliomas (n = 509) and glioblastomas (n = 153) from TCGA. Boxes extend from the 25th to the 75th percentile, the central bold line shows the median, and whiskers are drawn from the 5th to the 95th percentile. Comparisons were performed using the two-sided Student's t test. **(B)** Kaplan-Meier survival curves of gliomas patients with high vs. low MT1/MT2 expression ratios. Comparisons were performed using the log-rank test. **(C)** Gene set enrichment analysis testing the correlation between the MT1/MT2 expression ratio and the expression of genes related to the cell cycle and phospholipase C signaling in gliomas. Bar plots show normalized enrichment scores of the Reactome gene sets analyzed. FDR adjusted p values < 0.1 were considered statistically significant.

Table 1. Multivariate Cox analysis of 10-year survival in gliomas.

	10-year survival							
	Low melatonin gliomas*				High melatonin gliomas*			
	Univariate		Multivariate		Univariate		Multivariate	
Variable	HR (95% CI)	P value	HR (95% CI)	P value	HR (95% CI)	P value	HR (95% CI)	P value
Gender (male vs. female)	0.79 (0.52-1.22)	0.297	1 (0.64-1.56)	0.984	1.75 (1.06-2.9)	0.03	1.46 (0.87-2.45)	0.156
Age	1.07 (1.05-1.09)	<0.001	1.05 (1.03-1.06)	<0.001	1.07 (1.05-1.09)	<0.001	1.04 (1.02-1.06)	<0.001
IDH mutation (yes vs. no)	0.12 (0.07-0.2)	<0.001	0.16 (0.08-0.32)	<0.001	0.15 (0.09-0.25)	<0.001	0.32 (0.16-0.64)	0.001
1p/19q codel (yes vs. no)	0.29 (0.14-0.6)	0.001	0.62 (0.26-1.49)	0.285	0.21 (0.09-0.49)	<0.001	0.38 (0.15-0.97)	0.043
MT1/MT2 ratio (high vs. low)	0.61 (0.38-0.97)	0.035	1.03 (0.63-1.69)	0.897	0.48 (0.27-0.86)	0.013	0.48 (0.27-0.87)	0.015

HR: hazard ratio. CI: confidence interval
*As predicted by the ASMY:CYP1B1 index

Functional-selective drugs that simultaneously activate MT1 and inhibit MT2 exert robust anti-tumor effects

Given the opposite roles of melatonin receptors suggested by our data, we reasoned that drugs able to activate MT1 while inhibiting MT2 would have promising therapeutic potential. We tested two high affinity compounds that act as agonists of MT1 and antagonists of MT2: 5-HEAT, that bears an hydroxyethoxy group on the C5-indole position of melatonin (Nonno et al., 2000), and UCM799, which is a N-anilinoethylamide derivative carrying a benzyl substituent on the aniline nitrogen (Rivara et al., 2007). 5-HEAT and UCM799 inhibited the in vitro proliferation of all four cell lines analyzed (HOG, T98G, U87MG, DAOY; **Fig. 3A-B, S1C**), including the low-melatonin cell line U87MG. Next, we tested the therapeutic efficiency of such compounds in vivo using the U87MG-luc orthotopic xenograft model. We expect 5-HEAT and UCM799 to be effective regardless of the content of melatonin in the tumor microenvironment. For instance, given the limited capacity of U87MG cells to produce and accumulate melatonin, we postulate that in vivo, during the day, such compounds would act mainly by activating MT1, while at night they would antagonize the binding of pineal melatonin to MT2. Notably, continuous brain infusion of 5-HEAT or UCM799 for 14 days reduced tumor growth by approximately 75% compared to

vehicle, a robust therapeutic effect that likely reflects the complementary mechanisms of action of these functional-selective drugs (**Fig. 3C**). Moreover, the fact that the N-anilinoethylamide UCM799 reproduces the effect of the indoleamine 5-HEAT implies that the antioxidant activity ascribed to the indole ring of 5-HEAT plays a minor role in its growth suppressive action. Finally, the effect of melatonin was variable and not significant, what could reflect dynamic fluctuations of MT1 and MT2 levels in the tumor bulk.

Cancer stem cells are a small subpopulation within tumors that has enhanced tumorigenicity and is capable of self-renewal and differentiation (Batlle & Clevers, 2017). In glioblastomas, the failure of current gold-standard therapies to eliminate tumor stem cells has been considered a major factor contributing to the inevitable tumor recurrence (Lathia, Mack, Mulkearns-Hubert, Valentim, & Rich, 2015). Thus, to better understand the mechanism of action of the functional-selective melatonergic compounds, we used glioma stem cell-enriched neurosphere cultures MGG23 and MGH143, previously shown to maintain primary tumor phenotype and genotype (Neftel et al., 2019; Wakimoto et al., 2012). Neurospheres were treated with vehicle or 5-HEAT for 48 h and profiled by RNA-seq. We then used GSEA to explore gene sets differentially expressed upon treatment in both cell lines. We identified 73 gene sets negatively enriched compared to the vehicle group, whereas no gene sets were positively enriched (**Fig. 4A, Table S3**). In both cell lines 5-HEAT inhibited the expression of cell cycle genes including CCND1, CDK4, CKD9, regulators of DNA replication RPA2, GINS2 and RFC2/5, as well as tubulins (**Fig. 4B, Table S4**). 5-HEAT also impaired the expression of multiple RNA processing and translation genes, and important regulators of cellular metabolism such as the glycolysis enzymes GAPDH and ENO1, translocases of inner mitochondrial membrane TOMM22, TIMM17B/22/50, and CYC1, which encodes a subunit of the cytochrome bc1 complex, the third complex in the electron transport chain of the mitochondrial (**Fig. 4B, Table S4**). The 48h treatment did not induce apoptosis/necrosis (**Fig. S2**), suggesting that, in glioma stem cells, the oncostatic effects of 5-HEAT likely involve cell cycle arrest .
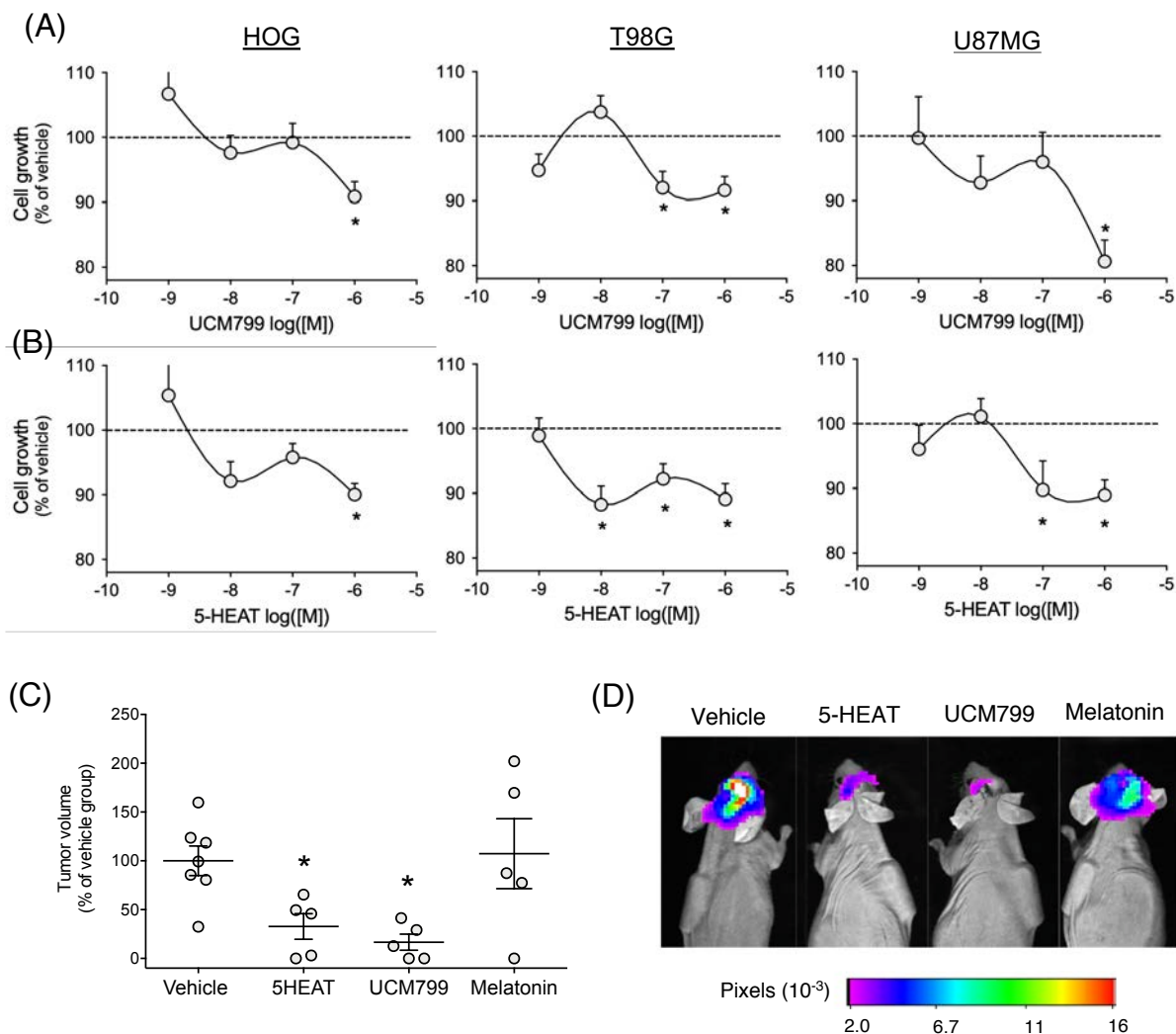
Figure 3. The simultaneous activation of MT1 and inhibition of MT2 by functional-selective drugs impairs glioma growth in vitro and in vivo. (A)-(B) High- (HOG and T98G) and low-melatonin (U87MG) glioma cell lines were cultured for 48 h with drugs that simultaneously activate MT1 and inhibit MT2, 5-HEAT ($10^{-9} - 10^{-6}$ M) and UCM799 ($10^{-9} - 10^{-6}$ M), or the respective vehicle ($2 \times 10^{-6} - 2 \times 10^{-3}$ % DMSO). Cell number was estimated by MTT assay and values were normalized by the mean absorbance detected in the respective vehicle group. Data are shown as mean ± SEM of four independent experiments in quadruplicates. **(C)** Mice with pre-stablished U87MG-luc orthotopic tumors received continuous brain infusions of vehicle (0.2% DMSO), 10^{-4} M 5-HEAT, 10^{-4} M UCM799 or 10^{-4} M melatonin. Mice were euthanized 14 days post treatment initiation for tumor volume evaluation. Values were normalized by the average tumor volume of the vehicle group. Data are shown as mean ± SEM of five independent experiments. **(D)** In vivo bioluminescence imaging of tumor burden 14 days post-treatment. * Significantly different from the respective vehicle group ($p < 0.05$) using the two-sided Student's t test.
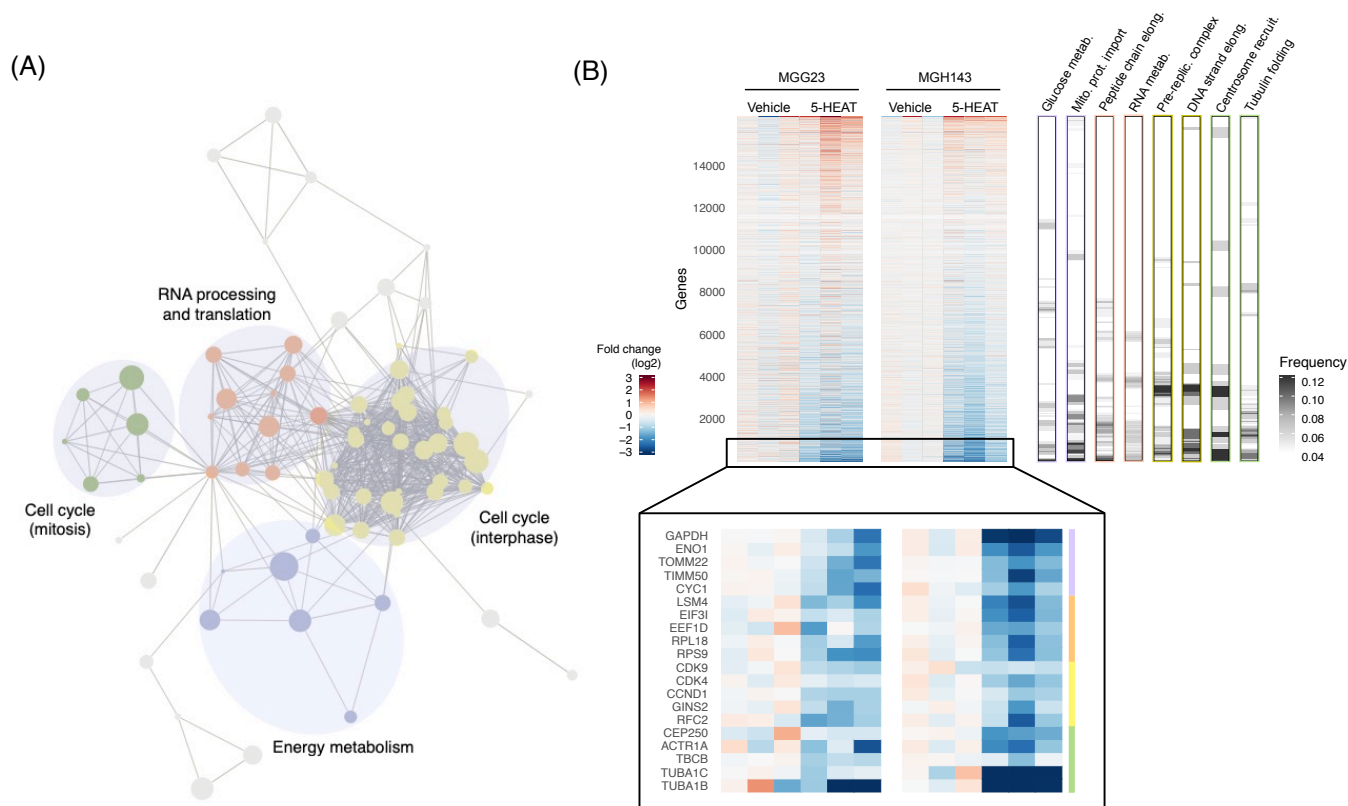
Figure 4. Impact of 5-HEAT on the expression profile of glioma stem-like cells. (A) MGG23 and MGH143 stem cell-enriched neurosphere cultures were incubated with 10^{-6} M 5-HEAT or vehicle (2 x 10^{-3} % DMSO) for 48 h and profiled by RNA-seq. Reactome gene sets differentially expressed in 5-HEAT treated cells compared to vehicle were identified using GSEA. Enrichment map shows negatively enriched gene sets (FDR adjusted $p < 0.1$) composing 4 main modules. Each gene set is a node and edges represent the similarity between gene sets. Node size shows enrichment significance (-log10(FDR-adjusted p)) and edge thickness is proportional to the overlap coefficient between gene sets. **(B)** Heatmap depicts the expression profile of 5-HEAT treated cells. Genes are ranked according to their average log2(expression fold change) in the 5-HEAT group compared to the vehicle. Bars on the right show the frequency of genes from selected gene sets within sliding windows of 500 genes. Relevant genes from each of the four gene set modules are highlighted in the bottom. Data correspond to three independent experiments.

Discussion

The detailed characterization of the biological roles of melatonin receptors is essential for a rational clinical application of melatonin and other melatonergic compounds (Cecon, Liu, & Jockers, 2019). Despite the widespread interest in using melatonin as an adjuvant anticancer therapy, our understanding of the specific effects mediated through MT1 and MT2 receptor activation remains limited. Importantly, although accumulating studies have supported the anticancer properties of melatonin in different tumor types, in vitro and in vivo animal models experiments often involve millimolar concentrations of this indolamine (Li et al., 2017), which likely trigger diverse receptor-independent mechanisms, masking the impact of MT1 and MT2 activation. In this respect, here we demonstrated that in glioma and medulloblastoma the receptor-dependent anti-proliferative effect of melatonin is mediated by the activation of MT1, whereas MT2 seems to play a pro-tumor role, displaying a significantly higher mRNA expression in tumors compared to the normal brain cortex. Accordingly, the ratio between MT1/MT2 expression is a positive prognostic factor of patient survival, being particularly relevant when considering tumors predicted to have higher concentrations of melatonin in the microenvironment. Finally, we also showed the potential of MT1 and MT2 receptors as druggable targets, as the simultaneous activation of MT1 and inhibition of MT2 promotes a decrease in the expression of cell cycle-, metabolism- and translation-related genes in glioma stem-like cells, besides impairing tumor growth in vitro and in vivo.

Notably, MT1 has often been recognized as the mediator of receptor-dependent antitumor actions of melatonin (Li et al., 2017). Studies with melanoma and breast cancer cell lines demonstrated that MT1 overexpression potentiates the growth suppressive effects of melatonin (Collins et al., 2003; Kadekaro et al., 2004; Yuan, Collins, Dai, Dubocovich, & Hill, 2002). In glioblastoma stem cells, MT1 activation has been recently shown to inhibit the expression of nestin, p-c-Myc(S62), and c-Myc, suppressing neurosphere formation and inducing G2/M arrest (H. Lee, Lee, Jung, Shin, & Kim, 2018). In estrogen receptor positive ductal breast carcinomas, MT1 protein levels decrease with tumor grade and positively correlates with patient overall survival (Jablonska et al., 2013). Moreover, mRNA expression of MT1 is significant decreased in colorectal cancer compared to the adjacent mucosa (Nemeth et al., 2011).

In contrast, in the brain, activation of MT2 receptors has been linked to the neuroprotection conferred by melatonin following ischemic strokes (Chern, Liao, Wang, & Shen, 2012; C. H. Lee et al., 2010). Treatment with melatonin enhances endogenous neurogenesis and cell proliferation in the peri-infarct regions in a MT2-dependent manner, improving survival rates and the neural functioning of mice (Chern et al., 2012). Under high glucose conditions, melatonin has also been shown to prevent neuronal cell apoptosis via a MT2/Akt/NF-κB pathway (Onphachanh et al., 2017). Importantly, in Alzheimer's disease patients, the hippocampal expression of MT1 is up and of MT2 is downregulated (Savaskan et al., 2005, 2002). Moreover, MT2 activation prevents the disruption of dendritic complexity and spine induced by amyloid β in hippocampal neuron cultures (Tang et al., 2019). All together, these findings corroborate the idea that MT1 and MT2 have

opposite roles controlling cell proliferation in the brain, a pattern that seems to be preserved in brain tumor cells, as revealed by our data.

Recent studies using subtype selective receptor ligands and knockout mice suggest that MT1 and MT2 also play differential roles in process such control of sleep and body temperature (Gobbi & Comai, 2019; López-Canul et al., 2019). Activation of MT1 receptors seems to be implicated in the regulation of rapid eye movement (REM) sleep, whereas MT2 receptors selectively increase non-REM (NREM) sleep (Gobbi & Comai, 2019). MT1 knockout mice have an increase in NREM sleep and a decrease in REM sleep, while MT2 knockout mice have a decrease in NREM sleep. Regarding thermal regulation, administration of the MT1-selective partial agonist UCM871 and the MT2-selective partial agonist UCM924 have been shown to impact body temperature at different times of the dark phase and with opposite magnitude. UCM871 enhances body temperature just after the light–dark transition, whereas UCM924 decreases body temperature just before the dark–light transition (López-Canul et al., 2019).

The current mainstay treatment of glioblastomas (i.e. maximal surgical resection, concurrent chemoradiation and adjuvant chemotherapy) offers only palliation and is normally followed by tumor recurrence (Stupp et al., 2009). In this regard, the clinical significance of glioma stem cells is supported by studies showing their ability to promote radioresistance by preferential activation of the DNA damage responses (Bao et al., 2006), and to propagate tumor growth after chemotherapy (Chen et al., 2012). Single-cell RNA-seq characterization of different types of glioma, including glioblastomas, have also shown that cycling cells within human tumors are enriched in stem-like subpopulation (Filbin et al., 2018; Neftel et al., 2019; Tirosh et al., 2016). Notably, the MT1 agonist and MT2 antagonist 5-HEAT suppressed the expression of multiple cell cycle and translation related genes in stem cell-enriched cultures, as well as seemed to interfere with their energy metabolism; mechanisms that likely contribute the robust growth suppressive effect of 5-HEAT observed in vivo. Additionally, the ability of 5-HEAT to downregulate the expression of both glycolysis enzymes and mitochondrial proteins might be specially beneficial given the capacity of glioblastoma stem cells to rely on both oxidative and non-oxidative glucose metabolism, depending on the environment conditions (Marin-Valencia et al., 2012; Vlashi et al., 2011).

Overall, here we provided the first evidences regarding the differential role of MT1 and MT2 in brain tumor progression, supporting further investigations of the specific signaling pathways, as well as the relevance of melatonin receptors homo (MT1/MT1 and MT2/MT2) and heterodimers (MT1/MT2) (Ayoub et al., 2002). Our findings suggest that melatonin antitumor effects mediated by MT1 can be counterbalanced by the pro-tumor MT2 activation, what could be especially relevant in tumors expressing low MT1 and high MT2. Accordingly, we lay a substantial groundwork for the use of functional-selective melatonergic compounds that activate MT1 and/or inhibit MT2 receptors in brain cancer therapy.

Author contributions

G.S.K, L.H.O, S.M.M., T.G.S., R.P.M, and P.A.F. designed the study. G.S.K., L.H.O., P.A.C.R. and R.C. performed the experiments. S.M.M., I.T. G.S, S.R., V.R.M, T.G.S, R.P.M, P.A.F contributed with reagents, material, and analysis tools. All authors analyzed the data and G.S.K wrote the manuscript. All authors critically revised the manuscript. R.P.M and P.A.F supervised the project.

Conflict of interest

The authors declare no conflict of interest.

References

Acuña-Castroviejo, D., Escames, G., Venegas, C., Díaz-Casado, M. E., Lima-Cabello, E., López, L. C., Rosales-Corral, S., Tan, D.-X., & Reiter, R. J. (2014). Extrapineal melatonin: sources, regulation, and potential functions. *Cellular and Molecular Life Sciences*, *71*(16), 2997–3025. https://doi.org/10.1007/s00018-014-1579-2

Adi, N., Mash, D. C., Ali, Y., Singer, C., Shehadeh, L., & Papapetropoulos, S. (2010). Melatonin MT1 and MT2 receptor expression in Parkinson's disease. *Medical Science Monitor*, *16*(2), 61–67.

Aldape, K., Brindle, K. M., Chesler, L., Chopra, R., Gajjar, A., Gilbert, M. R., et al. (2019). Challenges to curing primary brain tumours. *Nature Reviews Clinical Oncology*, *16*(8), 509–520. https://doi.org/10.1038/s41571-019-0177-5

Ayoub, M. A., Couturier, C., Lucas-Meunier, E., Angers, S., Fossier, P., Bouvier, M., & Jockers, R. (2002). Monitoring of ligand-independent dimerization and ligand-induced conformational changes of melatonin receptors in living cells by bioluminescence resonance energy transfer. *The Journal of Biological Chemistry*, *277*(24), 21522–21528. https://doi.org/10.1074/jbc.M200729200

Bao, S., Wu, Q., McLendon, R. E., Hao, Y., Shi, Q., Hjelmeland, A. B., Dewhirst, M. W., Bigner, D. D., & Rich, J. N. (2006). Glioma stem cells promote radioresistance by preferential activation of the DNA damage response. *Nature*, *444*(7120), 756–760. https://doi.org/10.1038/nature05236

Batlle, E., & Clevers, H. (2017). Cancer stem cells revisited. *Nature Medicine*, *23*(10), 1124–1134. https://doi.org/10.1038/nm.4409

Benítez-King, G., & Antón-Tay, F. (1993). Calmodulin mediates melatonin cytoskeletal effects. *Experientia*, *49*(8), 635–641. https://doi.org/10.1007/BF01923944

Blecher-Gonen, R., Barnett-Itzhaki, Z., Jaitin, D., Amann-Zalcenstein, D., Lara-Astiaso, D., & Amit, I. (2013). High-throughput chromatin immunoprecipitation for genome-wide mapping of in vivo protein-DNA interactions and epigenomic states. *Nature Protocols*, *8*(3), 539–554. https://doi.org/10.1038/nprot.2013.023

Brydon, L., Roka, F., Petit, L., de Coppet, P., Tissot, M., Barrett, P., Morgan, P. J., Nanoff, C., Strosberg, A. D., & Jockers, R. (1999). Dual Signaling of Human Mel1a Melatonin Receptors via G_{i2}, G_{i3}, and

G $_{q/11}$ Proteins. *Molecular Endocrinology*, *13*(12), 2025–2038. https://doi.org/10.1210/mend.13.12.0390

Bubenik, G. A. (2002). REVIEW: Gastrointestinal Melatonin: Localization, Function, and Clinical Relevance. *Digestive Diseases and Sciences*, *47*(10), 2336–2348. https://doi.org/10.1023/A:1020107915919

Budczies, J., Klauschen, F., Sinn, B. V, Győrffy, B., Schmitt, W. D., Darb-Esfahani, S., & Denkert, C. (2012). Cutoff Finder: a comprehensive and straightforward Web application enabling rapid biomarker cutoff optimization. *PloS One*, *7*(12), e51862. https://doi.org/10.1371/journal.pone.0051862

Cecon, E., Liu, L., & Jockers, R. (2019). Melatonin receptor structures shed new light on melatonin research. *Journal of Pineal Research*. https://doi.org/10.1111/jpi.12606

Chen, J., Li, Y., Yu, T.-S., McKay, R. M., Burns, D. K., Kernie, S. G., & Parada, L. F. (2012). A restricted cell population propagates glioblastoma growth after chemotherapy. *Nature, 488*(7412), 522–526. https://doi.org/10.1038/nature11287

Chern, C.-M., Liao, J.-F., Wang, Y.-H., & Shen, Y.-C. (2012). Melatonin ameliorates neural function by promoting endogenous neurogenesis through the MT2 melatonin receptor in ischemic-stroke mice. *Free Radical Biology and Medicine*, *52*(9), 1634–1647. https://doi.org/10.1016/J.FREERADBIOMED.2012.01.030

Chinot, O. L., Wick, W., Mason, W., Henriksson, R., Saran, F., Nishikawa, R., Carpentier, A. F., Hoang-Xuan, K., Kavan, P., Cernea, D., Brandes, A. A., Hilton, M., Abrey, L., & Cloughesy, T. (2014). Bevacizumab plus Radiotherapy–Temozolomide for Newly Diagnosed Glioblastoma. *New England Journal of Medicine*, *370*(8), 709–722. https://doi.org/10.1056/NEJMoa1308345

Collins, A., Yuan, L., Kiefer, T. L., Cheng, Q., Lai, L., & Hill, S. M. (2003). Overexpression of the MT1 melatonin receptor in MCF-7 human breast cancer cells inhibits mammary tumor formation in nude mice. *Cancer Letters*, *189*(1), 49–57. https://doi.org/10.1016/S0304-3835(02)00502-5

Cutando, A., López-Valverde, A., Arias-Santiago, S., DE Vicente, J., & DE Diego, R. G. (2012). Role of melatonin in cancer treatment. *Anticancer Research*, *32*(7), 2747–2753. Retrieved from http://www.ncbi.nlm.nih.gov/pubmed/22753734

Fabregat, A., Sidiropoulos, K., Garapati, P., Gillespie, M., Hausmann, K., Haw, R., et al. (2016). The Reactome pathway Knowledgebase. *Nucleic Acids Research*, *44*(D1), D481–D487. https://doi.org/10.1093/nar/gkv1351

Filbin, M. G., Tirosh, I., Hovestadt, V., Shaw, M. L., Escalante, L. E., Mathewson, N. D., et al. (2018). Developmental and oncogenic programs in H3K27M gliomas dissected by single-cell RNA-seq. *Science, 360*(6386), 331–335. https://doi.org/10.1126/science.aao4750

Gilbert, M. R., Dignam, J. J., Armstrong, T. S., Wefel, J. S., Blumenthal, D. T., Vogelbaum, M. A., et al. (2014). A Randomized Trial of Bevacizumab for Newly Diagnosed Glioblastoma. *New England Journal of Medicine*, *370*(8), 699–708. https://doi.org/10.1056/NEJMoa1308573

Gobbi, G., & Comai, S. (2019). Differential Function of Melatonin MT1 and MT2 Receptors in REM and NREM Sleep. *Frontiers in Endocrinology*, *10*, 87. https://doi.org/10.3389/fendo.2019.00087

Goldman, M., Craft, B., Kamath, A., Brooks, A., Zhu, J., & Haussler, D. (2018). The UCSC Xena Platform for cancer genomics data visualization and interpretation. *BioRxiv*, 326470. https://doi.org/10.1101/326470

Hardeland, R., Madrid, J. A., Tan, D.-X., & Reiter, R. J. (2012). Melatonin, the circadian multioscillator system and health: the need for detailed analyses of peripheral melatonin signaling. *Journal of Pineal Research*, *52*(2), 139–166. https://doi.org/10.1111/j.1600-079X.2011.00934.x

Jablonska, K., Pula, B., Zemla, A., Owczarek, T., Wojnar, A., Rys, J., Ambicka, A., Podhorska-Okolow, M., Ugorski, M., & Dziegiel, P. (2013). Expression of melatonin receptor MT1 in cells of human invasive ductal breast carcinoma. *Journal of Pineal Research*, *54*(3), 334–345. https://doi.org/10.1111/jpi.12032

Jockers, R., Delagrange, P., Dubocovich, M. L., Markus, R. P., Renault, N., Tosini, G., Cecon, E., & Zlotos, D. P. (2016). Update on melatonin receptors: IUPHAR Review 20. *British Journal of Pharmacology*,

173(18), 2702–2725. https://doi.org/10.1111/bph.13536

Kadekaro, A. L., Andrade, L. N. S., Floeter-Winter, L. M., Rollag, M. D., Virador, V., Vieira, W., & Castrucci, A. M. de L. (2004). MT-1 melatonin receptor expression increases the antiproliferative effect of melatonin on S-91 murine melanoma cells. *Journal of Pineal Research*, *36*(3), 204–211. https://doi.org/10.1111/j.1600-079X.2004.00119.x

Kinker, G. S., Oba-Shinjo, S. M., Carvalho-Sousa, C. E., Muxel, S. M., Marie, S. K. N., Markus, R. P., & Fernandes, P. A. (2016). Melatonergic system-based two-gene index is prognostic in human gliomas. *Journal of Pineal Research*, *60*(1), 84–94. https://doi.org/10.1111/jpi.12293

Klosen, P., Lapmanee, S., Schuster, C., Guardiola, B., Hicks, D., Pevet, P., & Felder-Schmittbuhl, M. P. (2019). MT1 and MT2 melatonin receptors are expressed in nonoverlapping neuronal populations. *Journal of Pineal Research*, *67*(1), e12575. https://doi.org/10.1111/jpi.12575

Lathia, J. D., Mack, S. C., Mulkearns-Hubert, E. E., Valentim, C. L. L., & Rich, J. N. (2015). Cancer stem cells in glioblastoma. *Genes & Development*, *29*(12), 1203–1217. https://doi.org/10.1101/gad.261982.115

Lee, C. H., Yoo, K.-Y., Choi, J. H., Park, O. K., Hwang, I. K., Kwon, Y.-G., Kim, Y.-M., & Won, M.-H. (2010). Melatonin's protective action against ischemic neuronal damage is associated with up-regulation of the MT2 melatonin receptor. *Journal of Neuroscience Research*, *88*(12), n/a-n/a. https://doi.org/10.1002/jnr.22430

Lee, H., Lee, H.-J., Jung, J. H., Shin, E. A., & Kim, S.-H. (2018). Melatonin disturbs SUMOylation-mediated crosstalk between c-Myc and nestin via MT1 activation and promotes the sensitivity of paclitaxel in brain cancer stem cells. *Journal of Pineal Research*, *65*(2), e12496. https://doi.org/10.1111/jpi.12496

Li, Y., Li, S., Zhou, Y., Meng, X., Zhang, J.-J., Xu, D.-P., & Li, H.-B. (2017). Melatonin for the prevention and treatment of cancer. *Oncotarget*, *8*(24), 39896–39921. https://doi.org/10.18632/oncotarget.16379

Lopes, M. H., Santos, T. G., Rodrigues, B. R., Queiroz-Hazarbassanov, N., Cunha, I. W., Wasilewska-Sampaio, A. P., Costa-Silva, B., Marchi, F. A., Bleggi-Torres, L. F., Sanematsu, P. I., Suzuki, S. H., Oba-Shinjo, S. M., Marie, S. K. N., Toulmin, E., Hill, A. F., & Martins, V. R. (2015). Disruption of prion protein–HOP engagement impairs glioblastoma growth and cognitive decline and improves overall survival. *Oncogene*, *34*(25), 3305–3314. https://doi.org/10.1038/onc.2014.261

López-Canul, M., Min, S. H., Posa, L., De Gregorio, D., Bedini, A., Spadoni, G., Gobbi, G., Comai, S., López-Canul, M., Min, S. H., Posa, L., De Gregorio, D., Bedini, A., Spadoni, G., Gobbi, G., & Comai, S. (2019). Melatonin MT1 and MT2 Receptors Exhibit Distinct Effects in the Modulation of Body Temperature across the Light/Dark Cycle. *International Journal of Molecular Sciences*, *20*(10), 2452. https://doi.org/10.3390/ijms20102452

Louis, D. N., Perry, A., Reifenberger, G., von Deimling, A., Figarella-Branger, D., Cavenee, W. K., Ohgaki, H., Wiestler, O. D., Kleihues, P., & Ellison, D. W. (2016). The 2016 World Health Organization Classification of Tumors of the Central Nervous System: a summary. *Acta Neuropathologica*, *131*(6), 803–820. https://doi.org/10.1007/s00401-016-1545-1

Marin-Valencia, I., Yang, C., Mashimo, T., Cho, S., Baek, H., Yang, X.-L., et al. (2012). Analysis of Tumor Metabolism Reveals Mitochondrial Glucose Oxidation in Genetically Diverse Human Glioblastomas in the Mouse Brain In Vivo. *Cell Metabolism*, *15*(6), 827–837. https://doi.org/10.1016/j.cmet.2012.05.001

Markus, R. P., Fernandes, P. A., Kinker, G. S., da Silveira Cruz-Machado, S., & Marçola, M. (2018). Immune-pineal axis - acute inflammatory responses coordinate melatonin synthesis by pinealocytes and phagocytes. *British Journal of Pharmacology*, *175*(16), 3239–3250. https://doi.org/10.1111/bph.14083

Martín, V., Sanchez-Sanchez, A. M., Puente-Moncada, N., Gomez-Lobo, M., Alvarez-Vega, M. A., Antolín, I., & Rodriguez, C. (2014). Involvement of autophagy in melatonin-induced cytotoxicity in glioma-initiating cells. *Journal of Pineal Research*, *57*(3), 308–316. https://doi.org/10.1111/jpi.12170

Merico, D., Isserlin, R., Stueker, O., Emili, A., & Bader, G. D. (2010). Enrichment Map: A Network-Based Method for Gene-Set Enrichment Visualization and Interpretation. *PLoS ONE*, *5*(11).

https://doi.org/10.1371/JOURNAL.PONE.0013984

Neftel, C., Laffy, J., Filbin, M. G., Hara, T., Shore, M. E., Rahme, G. J., et al. (2019). An Integrative Model of Cellular States, Plasticity, and Genetics for Glioblastoma. *Cell*, *178*(4), 835-849.e21. https://doi.org/10.1016/J.CELL.2019.06.024

Nemeth, C., Humpeler, S., Kallay, E., Mesteri, I., Svoboda, M., Rögelsperger, O., Klammer, N., Thalhammer, T., & Ekmekcioglu, C. (2011). Decreased expression of the melatonin receptor 1 in human colorectal adenocarcinomas. *Journal of Biological Regulators and Homeostatic Agents*, *25*(4), 531–542. Retrieved from http://www.ncbi.nlm.nih.gov/pubmed/22217986

Ng, K. Y., Leong, M. K., Liang, H., & Paxinos, G. (2017). Melatonin receptors: distribution in mammalian brain and their respective putative functions. *Brain Structure and Function*, *222*(7), 2921–2939. https://doi.org/10.1007/s00429-017-1439-6

Nonno, R., Lucini, V., Spadoni, G., Pannacci, M., Croce, A., Esposti, D., Balsamini, C., Tarzia, G., Fraschini, F., & Stankov, B. M. (2000). A new melatonin receptor ligand with mt1-agonist and MT2-antagonist properties. *Journal of Pineal Research*, *29*(4), 234–240. https://doi.org/10.1034/j.1600-0633.2002.290406.x

Onphachanh, X., Lee, H. J., Lim, J. R., Jung, Y. H., Kim, J. S., Chae, C. W., Lee, S. J., Gabr, A. A., & Han, H. J. (2017). Enhancement of high glucose-induced PINK1 expression by melatonin stimulates neuronal cell survival: Involvement of MT 2 /Akt/NF-κB pathway. *Journal of Pineal Research*, *63*(2), e12427. https://doi.org/10.1111/jpi.12427

Pinato, L., da Silveira Cruz-Machado, S., Franco, D. G., Campos, L. M. G., Cecon, E., Fernandes, P. A. C. M., Bittencourt, J. C., & Markus, R. P. (2015). Selective protection of the cerebellum against intracerebroventricular LPS is mediated by local melatonin synthesis. *Brain Structure & Function*, *220*(2), 827–840. https://doi.org/10.1007/s00429-013-0686-4

Reifenberger, G., Wirsching, H.-G., Knobbe-Thomsen, C. B., & Weller, M. (2017). Advances in the molecular genetics of gliomas — implications for classification and therapy. *Nature Reviews Clinical Oncology*, *14*(7), 434–452. https://doi.org/10.1038/nrclinonc.2016.204

Reiter, R. J. (1993). The melatonin rhythm: both a clock and a calendar. *Experientia*, *49*(8), 654–664. https://doi.org/10.1007/BF01923947

Reppart, S. M., Weaver, D. R., & Godson, C. (1996). Melatonin receptors step into the light: cloning and classification of subtypes. *Trends in Pharmacological Sciences*, *17*(3), 100–102. https://doi.org/10.1016/0165-6147(96)10005-5

Rivara, S., Lodola, A., Mor, M., Bedini, A., Spadoni, G., Lucini, V., Pannacci, M., Fraschini, F., Scaglione, F., Sanchez, R. O., Gobbi, G., & Tarzia, G. (2007). *N* -(Substituted-anilinoethyl)amides: Design, Synthesis, and Pharmacological Characterization of a New Class of Melatonin Receptor Ligands. *Journal of Medicinal Chemistry*, *50*(26), 6618–6626. https://doi.org/10.1021/jm700957j

Savaskan, E., Ayoub, M. A., Ravid, R., Angeloni, D., Fraschini, F., Meier, F., Eckert, A., Muller-Spahn, F., & Jockers, R. (2005). Reduced hippocampal MT2 melatonin receptor expression in Alzheimer's disease. *Journal of Pineal Research*, *38*(1), 10–16. https://doi.org/10.1111/j.1600-079X.2004.00169.x

Savaskan, E., Olivieri, G., Meier, F., Brydon, L., Jockers, R., Ravid, R., Wirz-Justice, A., & Muller-Spahn, F. (2002). Increased melatonin 1a-receptor immunoreactivity in the hippocampus of Alzheimer's disease patients. *Journal of Pineal Research*, *32*(1), 59–62. https://doi.org/10.1034/j.1600-079x.2002.00841.x

Smith, M. A., & Reaman, G. H. (2015). Remaining challenges in childhood cancer and newer targeted therapeutics. *Pediatric Clinics of North America*, *62*(1), 301. https://doi.org/10.1016/J.PCL.2014.09.018

Stupp, R., Hegi, M. E., Mason, W. P., van den Bent, M. J., Taphoorn, M. J., Janzer, R. C., et al. (2009). Effects of radiotherapy with concomitant and adjuvant temozolomide versus radiotherapy alone on survival in glioblastoma in a randomised phase III study: 5-year analysis of the EORTC-NCIC trial. *The Lancet Oncology*, *10*(5), 459–466. https://doi.org/10.1016/S1470-2045(09)70025-7

Subramanian, A., Tamayo, P., Mootha, V. K., Mukherjee, S., Ebert, B. L., Gillette, M. A., Paulovich, A.,

Pomeroy, S. L., Golub, T. R., Lander, E. S., & Mesirov, J. P. (2005). Gene set enrichment analysis: a knowledge-based approach for interpreting genome-wide expression profiles. *Proceedings of the National Academy of Sciences of the United States of America*, *102*(43), 15545–15550. https://doi.org/10.1073/pnas.0506580102

Tan, D., Reiter, R., Manchester, L., Yan, M., El-Sawi, M., Sainz, R., Mayo, J., Kohen, R., Allegra, M., & Hardelan, R. (2002). Chemical and Physical Properties and Potential Mechanisms: Melatonin as a Broad Spectrum Antioxidant and Free Radical Scavenger. *Current Topics in Medicinal Chemistry*, *2*(2), 181–197. https://doi.org/10.2174/1568026023394443

Tang, H., Ma, M., Wu, Y., Deng, M.-F., Hu, F., Almansoub, H. a. m. m., Huang, H.-Z., Wang, D.-Q., Zhou, L.-T., Wei, N., Man, H., Lu, Y., Liu, D., & Zhu, L.-Q. (2019). Activation of MT2 receptor ameliorates dendritic abnormalities in Alzheimer's disease via C/EBPα/miR-125b pathway. *Aging Cell*, *18*(2), e12902. https://doi.org/10.1111/acel.12902

Tirosh, I., Venteicher, A. S., Hebert, C., Escalante, L. E., Patel, A. P., Yizhak, K., et al. (2016). Single-cell RNA-seq supports a developmental hierarchy in human oligodendroglioma. *Nature*, *539*(7628), 309–313. https://doi.org/10.1038/nature20123

Venegas, C., García, J. A., Escames, G., Ortiz, F., López, A., Doerrier, C., García-Corzo, L., López, L. C., Reiter, R. J., & Acuña-Castroviejo, D. (2012). Extrapineal melatonin: analysis of its subcellular distribution and daily fluctuations. *Journal of Pineal Research*, *52*(2), 217–227. https://doi.org/10.1111/j.1600-079X.2011.00931.x

Vlashi, E., Lagadec, C., Vergnes, L., Matsutani, T., Masui, K., Poulou, M., Popescu, R., Della Donna, L., Evers, P., Dekmezian, C., Reue, K., Christofk, H., Mischel, P. S., & Pajonk, F. (2011). Metabolic state of glioma stem cells and nontumorigenic cells. *Proceedings of the National Academy of Sciences of the United States of America*, *108*(38), 16062–16067. https://doi.org/10.1073/pnas.1106704108

Wakimoto, H., Mohapatra, G., Kanai, R., Curry, W. T., Yip, S., Nitta, M., Patel, A. P., Barnard, Z. R., Stemmer-Rachamimov, A. O., Louis, D. N., Martuza, R. L., Rabkin, S. D., & Rabkin, S. D. (2012). Maintenance of primary tumor phenotype and genotype in glioblastoma stem cells. *Neuro-Oncology*, *14*(2), 132–144. https://doi.org/10.1093/neuonc/nor195

Wang, J., Hao, H., Yao, L., Zhang, X., Zhao, S., Ling, E.-A., Hao, A., & Li, G. (2012). Melatonin suppresses migration and invasion via inhibition of oxidative stress pathway in glioma cells. *Journal of Pineal Research*, *53*(2), 180–187. https://doi.org/10.1111/j.1600-079X.2012.00985.x

Wasilewska-Sampaio, A. P., Santos, T. G., Lopes, M. H., Cammarota, M., & Martins, V. R. (2014). The growth of glioblastoma orthotopic xenografts in nude mice is directly correlated with impaired object recognition memory. *Physiology & Behavior*, *123*, 55–61. https://doi.org/10.1016/J.PHYSBEH.2013.09.012

Yuan, L., Collins, A. R., Dai, J., Dubocovich, M. L., & Hill, S. M. (2002). MT1 melatonin receptor overexpression enhances the growth suppressive effect of melatonin in human breast cancer cells. *Molecular and Cellular Endocrinology*, *192*(1–2), 147–156. https://doi.org/10.1016/S0303-7207(02)00029-1

Zheng, X., Pang, B., Gu, G., Gao, T., Zhang, R., Pang, Q., & Liu, Q. (2017). Melatonin Inhibits Glioblastoma Stem-like cells through Suppression of EZH2-NOTCH1 Signaling Axis. *International Journal of Biological Sciences*, *13*(2), 245–253. https://doi.org/10.7150/ijbs.16818

Supplementary materials and methods

Melatonin quantification

Cells (5 x 10^5 per well) were seeded on 24-well plates and left to attach overnight. Next, culture media was replaced and melatonin accumulated following 6 h of incubation was measured through enzyme-linked immunosorbent assays (Melatonin ELISA; IBL, Hamburg, Germany) according to the manufacturer's instructions. Values are shown per millions of cells. The assay has a detection limit of 3 pg/mL.

Immunofluorescence microscopy

Cells (3 x 10^4 per well) were seeded on 8-well chamber slides (Merck) and left to attach overnight. Next, culture media was removed and cells were washed with PBS prior to fixation with 4% paraformaldehyde (15 min, room temperature). Cells were then permeabilized with 0.1% Triton X (10 min, room temperature), blocked with 2% BSA (1 h, room temperature) and incubated overnight at 4°C with rabbit anti-AANAT (1:200, IM-0450), pAANAT (1:200, IM-0451) or ASMT (1:200, IM-0441) primary antibodies (Imuny Biotechnology). Cells were washed three times with PBS before incubation with FITC-conjugated anti-rabbit IgG antibody (1:200, Sigma-Aldrich) for 1 hr at room temperature. After three washes with PBS, nuclear DNA was stained with DAPI (5 min, room temperature, Santa Cruz Biotechnology. Images were captured using an Axio Scope A1 (Zeiss, Gottingen) fluorescence microscope.

Cell death assay

MGH143 and MGG23 cells (1,000 per well) were seeded in 96-well plates, left to rest overnight and treated with 5-HEAT (10^{-6} M) or vehicle (2 x 10^{-3} % DMSO) for 48 h. Cell death was assessed using the Annexin V APC Apoptosis Detection Kit from Biogems, according to manufacturer's instruction. Briefly, cells were washed twice with PBS, incubated with APC-conjugated annexin V and 7AAD for 15 min at room temperature, and analyzed using the LSD II (BD Biosciences) and the FCS Express v.6 software.
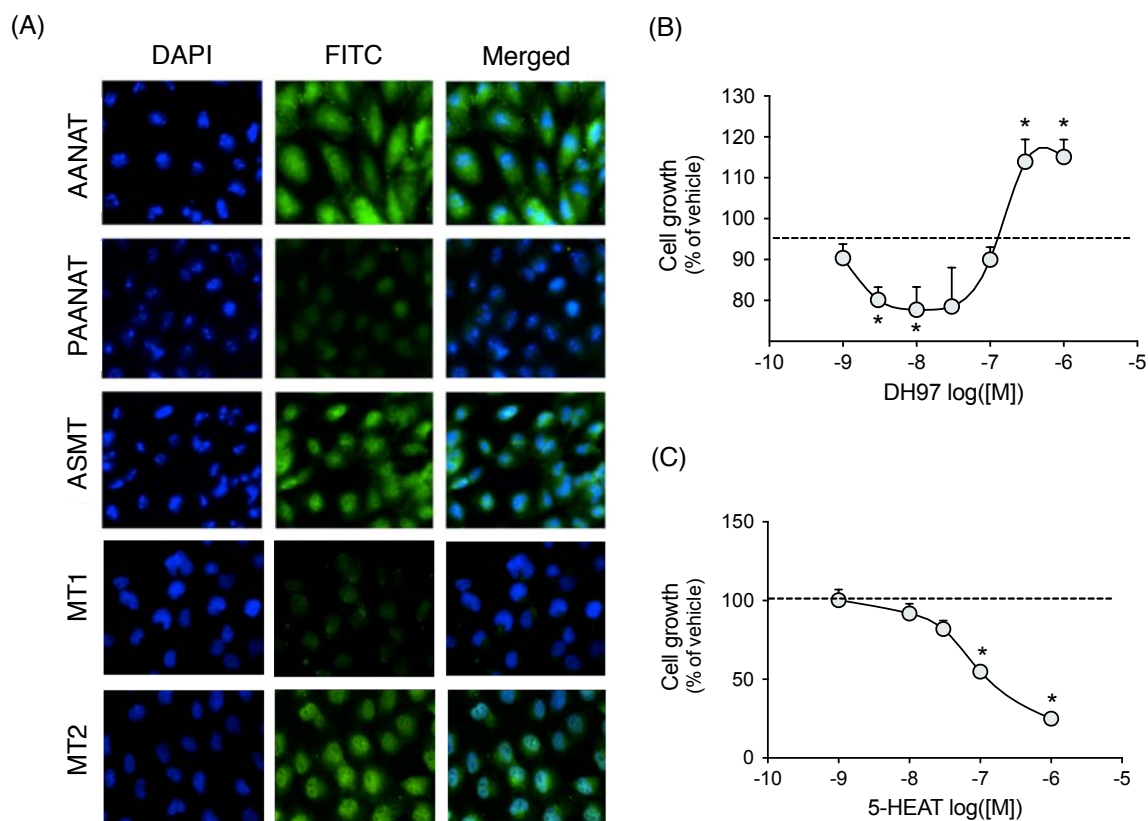
Supplementary Figures

Figure S1. Biological relevance of MT1 and MT2 melatonin receptors in medulloblastoma.
(A) Immunofluorescence detection of AANAT, PAANAT, ASMT, MT1 and MT2 in the human
medulloblastoma cell line DAOY. Nuclear DNA was stained with DAPI (blue). **(B)-(C)** DAOY
cell lines were cultured for 48 h with the MT2-selective antagonist DH97 ($3 \times 10^{-10} - 10^{-6}$ M) and
with the MT1 agonist and MT2 antagonist 5-HEAT ($10^{-9} - 10^{-6}$ M). Cell number was estimated
by MTT assay and values were normalized by the mean absorbance detected in the respective
vehicle group. Data are shown as mean ± SEM of four independent experiments in quadruplicates.
* Significantly different from the respective vehicle group ($p < 0.05$) using the two-sided Student's
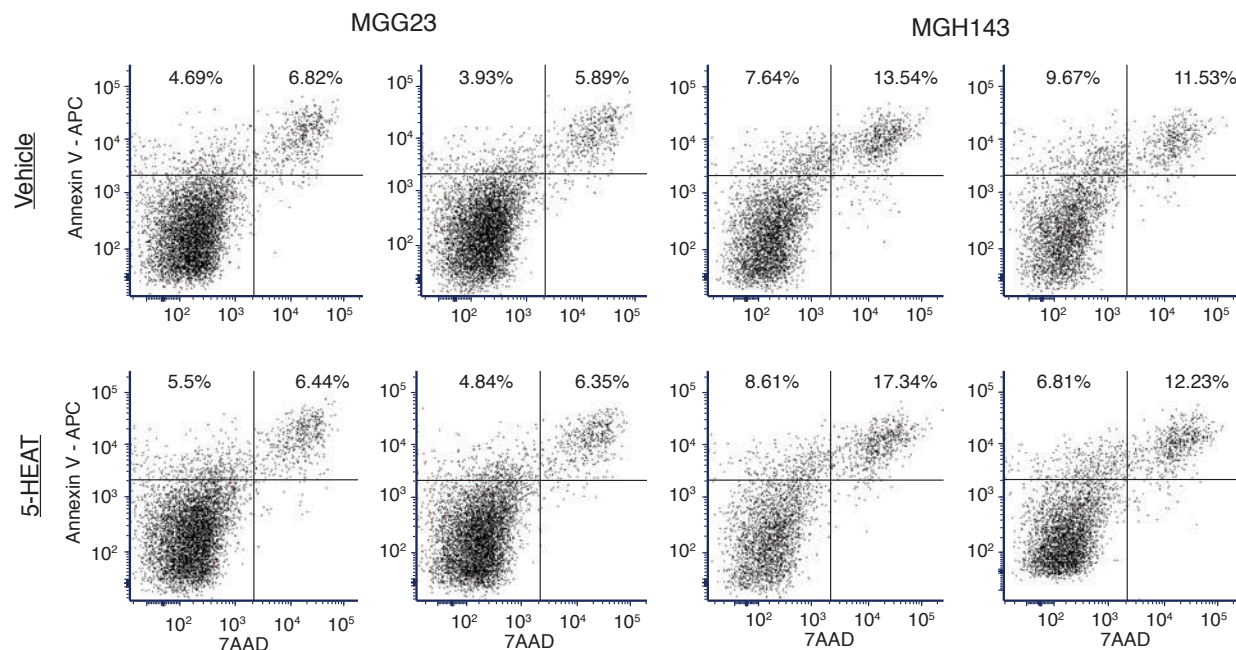t test.

Figure S2. 5-HEAT does not induce cell death in glioma stem-like cells. MGG23 (left) and MGH143 (right) stem cell-enriched neurosphere cultures were incubated with 10^{-6} M 5-HEAT or vehicle (2 x 10^{-3} % DMSO) for 48 h and cell death was assessed by measuring annexin V (APC) and 7AAD staining using flow cytometry. Data correspond to two independent experiments.

Supplementary Tables (Tables S2-4 were omitted due to limited space)

Table S1. Multivariate Cox analysis of 5-year survival in gliomas.

	5-year survival							
	Low melatonin gliomas*				High melatonin gliomas*			
	Univariate		Multivariate		Univariate		Multivariate	
Variable	HR (95% CI)	P value	HR (95% CI)	P value	HR (95% CI)	P value	HR (95% CI)	P value
Gender (male vs. female)	0.82 (0.52-1.3)	0.397	0.97 (0.6-1.55)	0.889	1.78 (1.05-3.04)	0.033	1.4 (0.81-2.41)	0.232
Age	1.07 (1.05-1.09)	<0.001	1.05 (1.03-1.07)	<0.001	1.07 (1.05-1.09)	<0.001	1.04 (1.02-1.07)	<0.001
IDH mutation (yes vs. no)	0.08 (0.05-0.15)	<0.001	0.23 (0.11-0.46)	<0.001	0.13 (0.08-0.23)	<0.001	0.34 (0.16-0.72)	0.005
1p/19q codel (yes vs. no)	0.16 (0.06-0.43)	<0.001	0.28 (0.09-0.88)	0.029	0.16 (0.06-0.45)	<0.001	0.34 (0.11-1.02)	0.054
MT1/MT2 ratio (high vs. low)	0.56 (0.35-0.91)	**0.019**	0.83 (0.51-1.36)	0.459	0.48 (0.27-0.86)	**0.013**	0.49 (0.27-0.88)	**0.017**

HR: hazard ratio. CI: confidence interval

*As predicted by the ASMY:CYP1B1 index

Conclusions

Causes and consequences of tumor cell plasticity and heterogeneity

Tumor cell plasticity and heterogeneity are key mechanism underlying disease progression and therapeutic resistance (Dagogo-Jack & Shaw, 2018). Recent advances of single-cell technologies have allowed the profiling of tumors at unprecedented depth, enabling the dissection of potential cell trajectories associated with changes in phenotypes (Neftel et al., 2019; Peng et al., 2019; Puram et al., 2017; Tirosh, Izar, et al., 2016; Tirosh, Venteicher, et al., 2016; Venteicher et al., 2017; Zhang et al., 2019). Nevertheless, the molecular mechanisms underlying such changes and ways of modulating it remain poorly understood. Most studies of intratumoral heterogeneity have focused on genetic alterations, as genome instability represents a prominent fuel for cell-to-cell variation and hence selection and evolution (Campbell et al., 2010; de Bruin et al., 2014; Gerlinger et al., 2012; Harbst et al., 2016; Jamal-Hanjani et al., 2017; Yates et al., 2015). However, as evidenced by our work, even genetically homogenous cells show significant expression heterogeneity. Remarkably, by analyzing scRNA-seq data of dozens of cell lines from diverse cancer types we demonstrated that most heterogeneity observed within tumors reflect non-genetic mechanisms that generate continuous programs of expression diversity, characterized by spectra of cellular states.

Expression heterogeneity of genetic homogeneous cellular populations, could reflect, for instance: i) the intrinsic fluctuations due to the randomness inherent to transcription; ii) epigenetic developmental programs; and iii) responses to microenvironmental factors. Interestingly, we showed that many of the continuous programs observed in cell lines are recurrent and recapitulate those seen in fresh human tumors, even though in vitro conditions lack a native and spatially-variable microenvironment. These observations suggest that some cellular developmental hierarchies present in normal tissues, such as those observed during wound-healing and cellular aging, are at least partially preserved in tumors (and cell lines), representing a prominent source of phenotype variability. As illustrated by experiments with the HNSCC cell lines JHU006 and SCC47, which harbor a variability program of epithelial senescence (EpiSen) also seen in clinical

samples of HNSCC, such non-genetic heterogeneity is reversible and dynamic, and could thus more directly regulate cellular phenotypes.

Non-genetic variability can also contribute to therapeutic resistance by multiple different mechanisms. For instance, we demonstrated that cells with high expression of the EpiSen program are more sensitive to inhibitors of the PI3K/AKT pathway and less sensitive to inhibitors of the cell cycle when compared to the EpiSen low population. Thus, epigenetic manipulation of cancer cells that makes expression patterns more uniform could be a powerful therapeutic tool to improve the efficacy of targeted/chemo therapies by reducing the risk of resistant phenotypes. Notably, by showing the relevance of certain cell lines as models of intratumoral heterogeneity, we provided the framework for the scientific community to start testing such innovative hypothesis. In coming years, major challenges will likely involve the transferring of the acquired knowledge "from bench to bedside". More specifically, developing cost- and time-effective ways to assess expression heterogeneity in clinical samples, as well as generating protocols on how to use this information to guide therapeutic decisions.

The melatonergic system in cancer prognosis and treatment

Over the past decades, melatonin, best known as the "hormone of darkness" or the "pineal hormone", has been revealed as a pleiotropic molecule with diverse biological functions: it is produced by multiple tissues (Acuña-Castroviejo et al., 2014); has clinical relevance as a treatment for conditions such as insomnia and Alzheimer's disease (Liu et al., 2016); and even shows anticancer properties (Cutando et al., 2012). Adding to this list, here, we are the first to show the role of glioma-synthesized melatonin as an autocrine/paracrine suppressor of disease progression. Remarkably, analysis of RNA-seq data of more than 4,500 samples from The Cancer Genome Atlas (TCGA) and The Genotype-Tissue Expression (GTEx), revealed that in almost all cancer types the content of melatonin locally produced and accumulated, as predicted by the ASMT:CYP1B1 expression index, is significantly lower than in matched normal tissues (**Fig. 1**). Accordingly, as observed in gliomas, a low index value, indicative of decreased melatonin, is associated with poor prognosis in bladder urothelial carcinoma, colorectal adenocarcinoma, medulloblastoma, metastatic melanoma, lung squamous cell carcinoma, pancreatic adenocarcinoma, pheochromocytoma/paraganglioma, and stomach adenocarcinoma (**Fig. 2**).
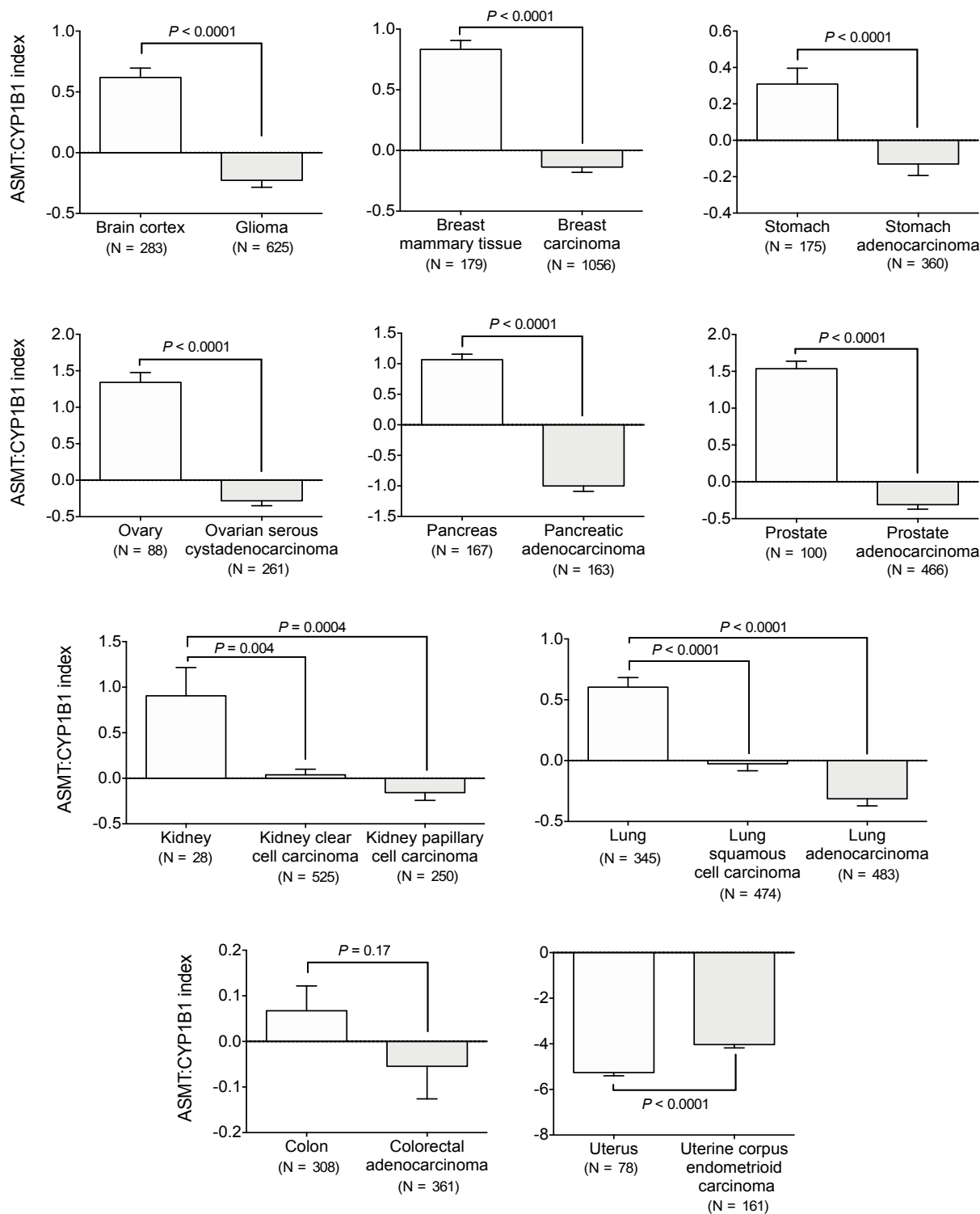
Figure 1. Melatonin levels, as predicted by the ASMT:CYP1B1 expression index, in normal and malignant tissues. The index value was calculated for each sample according to the mRNA levels of melatonin synthesis (ASMT) and metabolism (CYP1B1) enzymes, as previously described (Kinker et al., 2016). Comparisons were performed using the two-sided Students t-test. Gene expression data were downloaded from public databases (GTEx and TCGA).
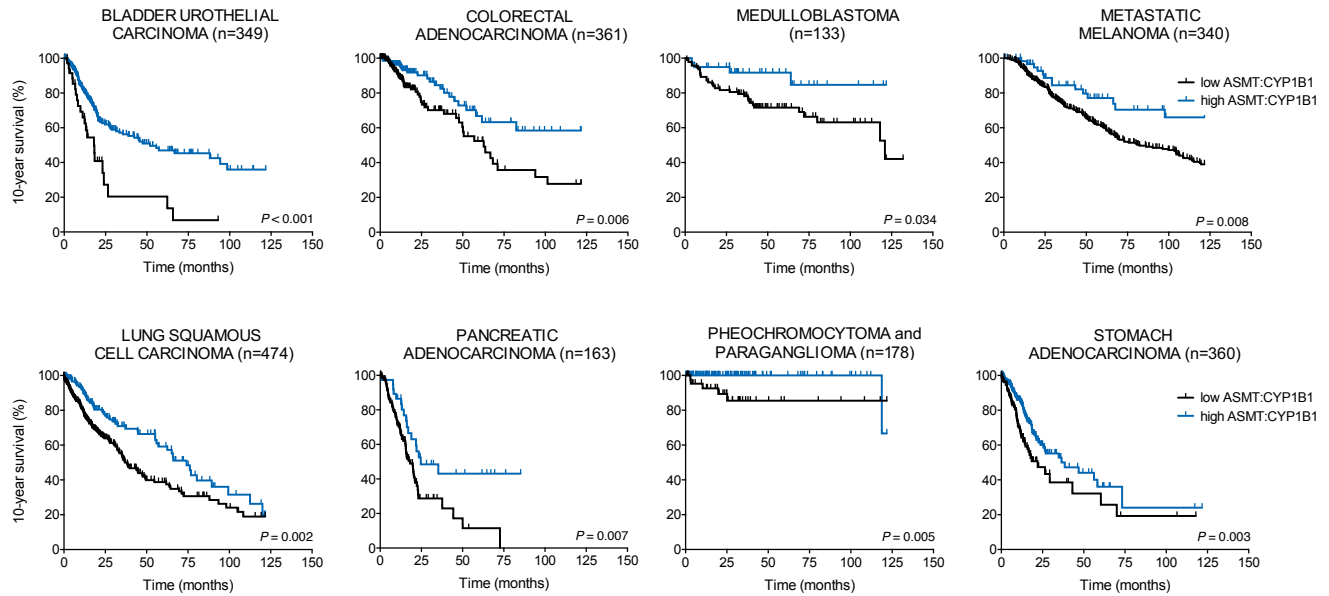
Figure 2. The prognostic value of the ASMT:CYP1B1 index in solid tumors. Kaplan-Meier survival curves of patients with tumors presenting low vs. high ASMT:CYP1B1 index scores. The index value was calculated for each sample based on the mRNA levels of the melatonin synthesis (ASMT) and metabolism (CYP1B1) enzymes, as previously described (Kinker et al., 2016). Gene expression and clinical data were obtained from public database repositories (Cho et al., 2011, for medulloblastomas, and TCGA, for all other tumors).

Although further studies are needed to define if decreased levels of tissue melatonin are a cause or consequence of tumorigenesis, we can speculate about the role of this indolamine as a major modulator of the malignant behavior. Given the tissue- and context- specific effect of melatonin receptors activation, it is possible that this apparent universal trend is linked to the more primitive role of melatonin as a broad-spectrum antioxidant (Tan et al., 2009). Reactive oxygen species (ROS) can be produced from endogenous sources, including organelles such as mitochondria, peroxisomes and endoplasmic reticulum, where the oxygen consumption is high, as well as from pollution, alcohol, tobacco smoke, and UV radiation (Di Meo et al., 2016). Keeping the cellular redox state well-balanced is essential for the maintenance of tissue homeostasis, and it is now clear that ROS have a dual role in cancer (Reczek & Chandel, 2017). Slightly increased levels of ROS can promote genomic instability and activate pro-tumorigenic signaling such as NFκB (A. C. H. Chen et al., 2011). Too high concentrations, on the other hand, can cause excessive oxidative damage and cell death (Y. Chen et al., 2008). Thus, locally produced melatonin might

act, together with others known antioxidant systems (e.g. thioredoxin and glutathione systems), as a buffer, ensuring optimal levels of free radical in the tissues. Of note, recent studies with neuronal cells (Suofu et al., 2017) and oocytes (He et al., 2016) have shown that melatonin can be synthesized in the mitochondria, where it plays a role avoiding electron leakage.

As described earlier, apart from functioning as an elector donor, melatonin can also activate high-affinity G-protein coupled receptors, MT1 and MT2. Although this indolamine is increasingly referred as a potential adjuvant in cancer treatments, few serious attempts have been made to understand the effects associated with the activation of each one of these receptors. Most in vitro studies use concentrations of melatonin that are much higher than those required for the saturation of MT1 and MT2 receptor binding sites, and thus likely trigger many receptor-independent effects. Importantly, in patients, achieving high concentrations of melatonin in the tumor microenvironment through systemic administration might be a challenge, limiting the reproduction of such in vitro observations in the clinics. Moreover, as anticancer drug discovery moves towards the development of more rational and biologically-grounded treatments, it becomes clear that the comprehensive characterization of targeted molecular networks is essential for improving therapeutic efficacy while avoiding adverse effects. In this regard, surprisingly, we showed that in gliomas and medulloblastomas MT1 and MT2 play opposite roles in controlling disease progression. Compounds that activate MT1 and inhibit MT2 displayed a remarkable growth suppressive effect in glioma xenografts, while the therapeutic benefits of melatonin were variable and with no significant trend. All together, we provided the first robust evidence of the therapeutic relevance of MT1 and MT2 receptors as druggable targets in brain cancer, which now must be tested clinically.

References

Ackermann, K., & Stehle, J. H. (2006). Melatonin Synthesis in the Human Pineal Gland: Advantages, Implications, and Difficulties. *Chronobiology International*, *23*(1–2), 369–379. https://doi.org/10.1080/07420520500464379

Acuña-Castroviejo, D., Escames, G., Venegas, C., Díaz-Casado, M. E., Lima-Cabello, E., López, L. C., Rosales-Corral, S., Tan, D.-X., & Reiter, R. J. (2014). Extrapineal melatonin: sources, regulation, and potential functions. *Cellular and Molecular Life Sciences*, *71*(16), 2997–3025. https://doi.org/10.1007/s00018-014-1579-2

Ahluwalia, A., Brzozowska, I. M., Hoa, N., Jones, M. K., & Tarnawski, A. S. (2018). Melatonin signaling in mitochondria extends beyond neurons and neuroprotection: Implications for angiogenesis and cardio/gastroprotection. *Proceedings of the National Academy of Sciences of the United States of America*, *115*(9), E1942–E1943. https://doi.org/10.1073/pnas.1722131115

Anisimov, V. N., Vinogradova, I. A., Panchenko, A. V, Popovich, I. G., & Zabezhinski, M. A. (2012). Light-at-night-induced circadian disruption, cancer and aging. *Current Aging Science*, *5*(3), 170–177. Retrieved from http://www.ncbi.nlm.nih.gov/pubmed/23237593

Balkwill, F. R., Capasso, M., & Hagemann, T. (2012). The tumor microenvironment at a glance. *Journal of Cell Science*, *125*(23), 5591–5596. https://doi.org/10.1242/jcs.116392

Barbosa Lima, L. E., Muxel, S. M., Kinker, G. S., Carvalho-Sousa, C. E., Silveira Cruz-Machado, S., Markus, R. P., & Fernandes, P. A. C. M. (2019). STAT1-NFκB crosstalk triggered by interferon gamma regulates noradrenaline-induced pineal hormonal production. *Journal of Pineal Research*. https://doi.org/10.1111/jpi.12599

Benítez-King, G., & Antón-Tay, F. (1993). Calmodulin mediates melatonin cytoskeletal effects. *Experientia*, *49*(8), 635–641. https://doi.org/10.1007/BF01923944

Berglund, E., Maaskola, J., Schultz, N., Friedrich, S., Marklund, M., Bergenstråhle, J., Tarish, F., Tanoglidi, A., Vickovic, S., Larsson, L., Salmén, F., Ogris, C., Wallenborg, K., Lagergren, J., Ståhl, P., Sonnhammer, E., Helleday, T., & Lundeberg, J. (2018). Spatial maps of prostate cancer transcriptomes reveal an unexplored landscape of heterogeneity. *Nature Communications*, *9*(1), 2419. https://doi.org/10.1038/s41467-018-04724-5

Berk, L., Berkey, B., Rich, T., Hrushesky, W., Blask, D., Gallagher, M., Kudrimoti, M., McGarry, R. C., Suh, J., & Mehta, M. (2007). Randomized Phase II Trial of High-Dose Melatonin and Radiation Therapy for RPA Class 2 Patients With Brain Metastases (RTOG 0119). *International Journal of Radiation Oncology*Biology*Physics*, *68*(3), 852–857. https://doi.org/10.1016/j.ijrobp.2007.01.012

Binnewies, M., Roberts, E. W., Kersten, K., Chan, V., Fearon, D. F., Merad, M., Coussens, L. M., Gabrilovich, D. I., Ostrand-Rosenberg, S., Hedrick, C. C., Vonderheide, R. H., Pittet, M. J., Jain, R. K., Zou, W., Howcroft, T. K., Woodhouse, E. C., Weinberg, R. A., & Krummel, M. F. (2018). Understanding the tumor immune microenvironment (TIME) for effective therapy. *Nature Medicine*, *24*(5), 541–550. https://doi.org/10.1038/s41591-018-0014-x

Blask, D. E., Brainard, G. C., Dauchy, R. T., Hanifin, J. P., Davidson, L. K., Krause, J. A., Sauer, L. A., Rivera-Bermudez, M. A., Dubocovich, M. L., Jasser, S. A., Lynch, D. T., Rollag, M. D., & Zalatan, F. (2005). Melatonin-Depleted Blood from Premenopausal Women Exposed to Light at Night Stimulates Growth of Human Breast Cancer Xenografts in Nude Rats. *Cancer Research*, *65*(23), 11174–11184. https://doi.org/10.1158/0008-5472.CAN-05-1945

Brydon, L., Roka, F., Petit, L., de Coppet, P., Tissot, M., Barrett, P., Morgan, P. J., Nanoff, C.,

Strosberg, A. D., & Jockers, R. (1999). Dual Signaling of Human Mel1a Melatonin Receptors via G $_{i2}$, G $_{i3}$, and G $_{q/11}$ Proteins. *Molecular Endocrinology*, *13*(12), 2025–2038. https://doi.org/10.1210/mend.13.12.0390

Bubenik, G. A., Brown, G. M., Uhlir, I., & Grota, L. J. (1974). Immunohistological localization of N-acetylindolealkylamines in pineal gland, retina and cerebellum. *Brain Research*, *81*(2), 233–242. https://doi.org/10.1016/0006-8993(74)90938-x

Butera, G., Pacchiana, R., & Donadelli, M. (2018). Autocrine mechanisms of cancer chemoresistance. *Seminars in Cell & Developmental Biology*, *78*, 3–12. https://doi.org/10.1016/j.semcdb.2017.07.019

Campbell, P. J., Yachida, S., Mudie, L. J., Stephens, P. J., Pleasance, E. D., Stebbings, L. A., Morsberger, L. A., Latimer, C., McLaren, S., Lin, M.-L., McBride, D. J., Varela, I., Nik-Zainal, S. A., Leroy, C., Jia, M., Menzies, A., Butler, A. P., Teague, J. W., Griffin, C. A., Burton, J., Swerdlow, H., Quail, M. A., Stratton, M. R., Iacobuzio-Donahue, C., & Futreal, P. A. (2010). The patterns and dynamics of genomic instability in metastatic pancreatic cancer. *Nature*, *467*(7319), 1109–1113. https://doi.org/10.1038/nature09460

Cardinali, D. P., & Rosner, J. M. (1971). Retinal Localization of the Hydroxyindole-O-methyl Transferase (HIOMT) in the Rat. *Endocrinology*, *89*(1), 301–303. https://doi.org/10.1210/endo-89-1-301

Carvalho-Sousa, C. E., da Silveira Cruz-Machado, S., Tamura, E. K., Fernandes, P. A. C. M., Pinato, L., Muxel, S. M., Cecon, E., & Markus, R. P. (2011). Molecular basis for defining the pineal gland and pinealocytes as targets for tumor necrosis factor. *Frontiers in Endocrinology*, *2*, 10. https://doi.org/10.3389/fendo.2011.00010

Cerea, G., Vaghi, M., Ardizzoia, A., Villa, S., Bucovec, R., Mengo, S., Gardani, G., Tancini, G., & Lissoni, P. (2003). Biomodulation of cancer chemotherapy for metastatic colorectal cancer: a randomized study of weekly low-dose irinotecan alone versus irinotecan plus the oncostatic pineal hormone melatonin in metastatic colorectal cancer patients progressing on 5-fluorour. *Anticancer Research*, *23*(2C), 1951–1954. Retrieved from http://www.ncbi.nlm.nih.gov/pubmed/12820485

Chen, A. C. H., Arany, P. R., Huang, Y.-Y., Tomkinson, E. M., Sharma, S. K., Kharkwal, G. B., Saleem, T., Mooney, D., Yull, F. E., Blackwell, T. S., & Hamblin, M. R. (2011). Low-Level Laser Therapy Activates NF-kB via Generation of Reactive Oxygen Species in Mouse Embryonic Fibroblasts. *PLoS ONE*, *6*(7), e22453. https://doi.org/10.1371/journal.pone.0022453

Chen, Y., McMillan-Ward, E., Kong, J., Israels, S. J., & Gibson, S. B. (2008). Oxidative stress induces autophagic cell death independent of apoptosis in transformed and cancer cells. *Cell Death & Differentiation*, *15*(1), 171–182. https://doi.org/10.1038/sj.cdd.4402233

Cho, Y. J., Tsherniak, A., Tamayo, P., Santagata, S., Ligon, A., Greulich, H., Berhoukim, R., Amani, V., Goumnerova, L., Eberhart, C. G., Lau, C. C., Olson, J. M., Gilbertson, R. J., Gajjar, A., Delattre, O., Kool, M., Ligon, K., Meyerson, M., Mesirov, J. P., & Pomeroy, S. L. (2011). Integrative genomic analysis of medulloblastoma identifies a molecular subgroup that drives poor clinical outcome. *Journal of Clinical Oncology : Official Journal of the American Society of Clinical Oncology*, *29*(11), 1424–1430. https://doi.org/10.1200/JCO.2010.28.5148

Chow, A., Lucas, D., Hidalgo, A., Méndez-Ferrer, S., Hashimoto, D., Scheiermann, C., Battista, M., Leboeuf, M., Prophete, C., van Rooijen, N., Tanaka, M., Merad, M., & Frenette, P. S. (2011). Bone marrow CD169+ macrophages promote the retention of hematopoietic stem and progenitor cells in the mesenchymal stem cell niche. *The Journal of Experimental Medicine*,

208(2), 261–271. https://doi.org/10.1084/jem.20101688

Collins, F. S., & Varmus, H. (2015). A New Initiative on Precision Medicine. *New England Journal of Medicine*, *372*(9), 793–795. https://doi.org/10.1056/NEJMp1500523

Cutando, A., López-Valverde, A., Arias-Santiago, S., DE Vicente, J., & DE Diego, R. G. (2012). Role of melatonin in cancer treatment. *Anticancer Research*, *32*(7), 2747–2753. Retrieved from http://www.ncbi.nlm.nih.gov/pubmed/22753734

Da Silveira Cruz-Machado, S., Carvalho-Sousa, C. E., Tamura, E. K., Pinato, L., Cecon, E., Fernandes, P. A. C. M., De Avellar, M. C. W., Ferreira, Z. S., & Markus, R. P. (2010). TLR4 and CD14 receptors expressed in rat pineal gland trigger NFKB pathway. *Journal of Pineal Research*, *49*(2), no-no. https://doi.org/10.1111/j.1600-079X.2010.00785.x

Dagogo-Jack, I., & Shaw, A. T. (2018). Tumour heterogeneity and resistance to cancer therapies. *Nature Reviews Clinical Oncology*, *15*(2), 81–94. https://doi.org/10.1038/nrclinonc.2017.166

de Bruin, E. C., McGranahan, N., Mitter, R., Salm, M., Wedge, D. C., Yates, L., Jamal-Hanjani, M., Shafi, S., Murugaesu, N., Rowan, A. J., Gronroos, E., Muhammad, M. A., Horswell, S., Gerlinger, M., Varela, I., Jones, D., Marshall, J., Voet, T., Van Loo, P., Rassl, D. M., Rintoul, R. C., Janes, S. M., Lee, S.-M., Forster, M., Ahmad, T., Lawrence, D., Falzon, M., Capitanio, A., Harkins, T. T., Lee, C. C., Tom, W., Teefe, E., Chen, S.-C., Begum, S., Rabinowitz, A., Phillimore, B., Spencer-Dene, B., Stamp, G., Szallasi, Z., Matthews, N., Stewart, A., Campbell, P., & Swanton, C. (2014). Spatial and temporal diversity in genomic instability processes defines lung cancer evolution. *Science*, *346*(6206), 251–256. https://doi.org/10.1126/science.1253462

de Oliveira Tatsch-Dias, M., Levandovski, R. M., Custódio de Souza, I. C., Gregianin Rocha, M., Magno Fernandes, P. A. C., Torres, I. L. S., Hidalgo, M. P. L., Markus, R. P., & Caumo, W. (2013). The Concept of the Immune-Pineal Axis Tested in Patients Undergoing an Abdominal Hysterectomy. *Neuroimmunomodulation*, *20*(4), 205–212. https://doi.org/10.1159/000347160

Di Meo, S., Reed, T. T., Venditti, P., & Victor, V. M. (2016). Role of ROS and RNS Sources in Physiological and Pathological Conditions. *Oxidative Medicine and Cellular Longevity*, *2016*, 1245049. https://doi.org/10.1155/2016/1245049

Dixon, A. R., Bathany, C., Tsuei, M., White, J., Barald, K. F., & Takayama, S. (2015). Recent developments in multiplexing techniques for immunohistochemistry. *Expert Review of Molecular Diagnostics*, *15*(9), 1171–1186. https://doi.org/10.1586/14737159.2015.1069182

Dumont, J. E., Pécasse, F., & Maenhaut, C. (2001). Crosstalk and specificity in signalling. Are we crosstalking ourselves into general confusion? *Cellular Signalling*, *13*(7), 457–463. Retrieved from http://www.ncbi.nlm.nih.gov/pubmed/11516620

Eichmann, A., Corbel, C., Nataf, V., Vaigot, P., Breant, C., & Le Douarin, N. M. (1997). Ligand-dependent development of the endothelial and hemopoietic lineages from embryonic mesodermal cells expressing vascular endothelial growth factor receptor 2. *Proceedings of the National Academy of Sciences*, *94*(10), 5141–5146. https://doi.org/10.1073/pnas.94.10.5141

Fernandes, P. A., Cecon, E., Markus, R. P., & Ferreira, Z. S. (2006). Effect of TNF-alpha on the melatonin synthetic pathway in the rat pineal gland: basis for a "feedback" of the immune response on circadian timing. *Journal of Pineal Research*, *41*(4), 344–350. https://doi.org/10.1111/j.1600-079X.2006.00373.x

Fernandes, P. A., Tamura, E. K., D'Argenio-Garcia, L., Muxel, S. M., da Silveira Cruz-Machado, S., Marçola, M., Carvalho-Sousa, C. E., Cecon, E., Ferreira, Z. S., & Markus, R. P. (2017).

Dual Effect of Catecholamines and Corticosterone Crosstalk on Pineal Gland Melatonin Synthesis. *Neuroendocrinology, 104*(2), 126–134. https://doi.org/10.1159/000445189

Festa, E., Fretz, J., Berry, R., Schmidt, B., Rodeheffer, M., Horowitz, M., & Horsley, V. (2011). Adipocyte Lineage Cells Contribute to the Skin Stem Cell Niche to Drive Hair Cycling. *Cell, 146*(5), 761–771. https://doi.org/10.1016/J.CELL.2011.07.019

Filbin, M. G., Tirosh, I., Hovestadt, V., Shaw, M. L., Escalante, L. E., Mathewson, N. D., Neftel, C., Frank, N., Pelton, K., Hebert, C. M., Haberler, C., Yizhak, K., Gojo, J., Egervari, K., Mount, C., van Galen, P., Bonal, D. M., Nguyen, Q.-D., Beck, A., Sinai, C., Czech, T., Dorfer, C., Goumnerova, L., Lavarino, C., Carcaboso, A. M., Mora, J., Mylvaganam, R., Luo, C. C., Peyrl, A., Popović, M., Azizi, A., Batchelor, T. T., Frosch, M. P., Martinez-Lage, M., Kieran, M. W., Bandopadhayay, P., Beroukhim, R., Fritsch, G., Getz, G., Rozenblatt-Rosen, O., Wucherpfennig, K. W., Louis, D. N., Monje, M., Slavc, I., Ligon, K. L., Golub, T. R., Regev, A., Bernstein, B. E., & Suvà, M. L. (2018). Developmental and oncogenic programs in H3K27M gliomas dissected by single-cell RNA-seq. *Science, 360*(6386), 331–335. https://doi.org/10.1126/science.aao4750

Gerlinger, M., Rowan, A. J., Horswell, S., Larkin, J., Endesfelder, D., Gronroos, E., Martinez, P., Matthews, N., Stewart, A., Tarpey, P., Varela, I., Phillimore, B., Begum, S., McDonald, N. Q., Butler, A., Jones, D., Raine, K., Latimer, C., Santos, C. R., Nohadani, M., Eklund, A. C., Spencer-Dene, B., Clark, G., Pickering, L., Stamp, G., Gore, M., Szallasi, Z., Downward, J., Futreal, P. A., & Swanton, C. (2012). Intratumor Heterogeneity and Branched Evolution Revealed by Multiregion Sequencing. *New England Journal of Medicine, 366*(10), 883–892. https://doi.org/10.1056/NEJMoa1113205

Girgert, R., Hanf, V., Emons, G., & Gründker, C. (2009). Membrane-bound melatonin receptor MT1 down-regulates estrogen responsive genes in breast cancer cells. *Journal of Pineal Research, 47*(1), 23–31. https://doi.org/10.1111/j.1600-079X.2009.00684.x

González, A. G., Rueda, N. R., & Sánchez-Barceló, E. J. (2019). Clinical uses of melatonin: evaluation of human trials on cancer treatment. *Melatonin Research, 2*(2), 47–69. https://doi.org/10.32794/mr11250021

Hanahan, D., & Coussens, L. M. (2012). Accessories to the Crime: Functions of Cells Recruited to the Tumor Microenvironment. *Cancer Cell, 21*(3), 309–322. https://doi.org/10.1016/J.CCR.2012.02.022

Harbst, K., Lauss, M., Cirenajwis, H., Isaksson, K., Rosengren, F., To rngren, T., Kvist, A., Johansson, M. C., Vallon-Christersson, J., Baldetorp, B., Borg, A., Olsson, H., Ingvar, C., Carneiro, A., & Jo nsson, G. (2016). Multiregion Whole-Exome Sequencing Uncovers the Genetic Evolution and Mutational Heterogeneity of Early-Stage Metastatic Melanoma. *Cancer Research, 76*(16), 4765–4774. https://doi.org/10.1158/0008-5472.CAN-15-3476

He, C., Wang, J., Zhang, Z., Yang, M., Li, Y., Tian, X., Ma, T., Tao, J., Zhu, K., Song, Y., Ji, P., & Liu, G. (2016). Mitochondria Synthesize Melatonin to Ameliorate Its Function and Improve Mice Oocyte's Quality under in Vitro Conditions. *International Journal of Molecular Sciences, 17*(6). https://doi.org/10.3390/ijms17060939

IARC Monographs Vol 124 group, E. M., Germolec, D., Kogevinas, M., McCormick, D., Vermeulen, R., Anisimov, V. N., Aronson, K. J., Bhatti, P., Cocco, P., Costa, G., Dorman, D. C., Fu, L., Garde, A. H., Guénel, P., Hansen, J., Härmä, M. I., Kawai, K., Khizkhin, E. A., Knutsson, A., Lévi, F., Moreno, C. R., Pukkala, E., Schernhammer, E., Travis, R., Waters, M., Yakubovskaya, M., Zeeb, H., Zhu, Y., Zienolddiny, S., Grosse, Y., Hall, A. L., Benbrahim-Tallaa, L., Girschik, J., Bouvard, V., Ghissassi, F. El, Turner, M. C., Diver, W.

R., Herceg, Z., Olson, N., Rowan, E. G., Rumgay, H., Guyton, K. Z., & Schubauer-Berigan, M. K. (2019). Carcinogenicity of night shift work. *The Lancet. Oncology*, *20*(8), 1058–1059. https://doi.org/10.1016/S1470-2045(19)30455-3

Jamal-Hanjani, M., Wilson, G. A., McGranahan, N., Birkbak, N. J., Watkins, T. B. K., Veeriah, S., Shafi, S., Johnson, D. H., Mitter, R., Rosenthal, R., Salm, M., Horswell, S., Escudero, M., Matthews, N., Rowan, A., Chambers, T., Moore, D. A., Turajlic, S., Xu, H., Lee, S.-M., Forster, M. D., Ahmad, T., Hiley, C. T., Abbosh, C., Falzon, M., Borg, E., Marafioti, T., Lawrence, D., Hayward, M., Kolvekar, S., Panagiotopoulos, N., Janes, S. M., Thakrar, R., Ahmed, A., Blackhall, F., Summers, Y., Shah, R., Joseph, L., Quinn, A. M., Crosbie, P. A., Naidu, B., Middleton, G., Langman, G., Trotter, S., Nicolson, M., Remmen, H., Kerr, K., Chetty, M., Gomersall, L., Fennell, D. A., Nakas, A., Rathinam, S., Anand, G., Khan, S., Russell, P., Ezhil, V., Ismail, B., Irvin-Sellers, M., Prakash, V., Lester, J. F., Kornaszewska, M., Attanoos, R., Adams, H., Davies, H., Dentro, S., Taniere, P., O'Sullivan, B., Lowe, H. L., Hartley, J. A., Iles, N., Bell, H., Ngai, Y., Shaw, J. A., Herrero, J., Szallasi, Z., Schwarz, R. F., Stewart, A., Quezada, S. A., Le Quesne, J., Van Loo, P., Dive, C., Hackshaw, A., Swanton, C., & TRACERx Consortium. (2017). Tracking the Evolution of Non–Small-Cell Lung Cancer. *New England Journal of Medicine*, *376*(22), 2109–2121. https://doi.org/10.1056/NEJMoa1616288

Jayatilaka, H., Tyle, P., Chen, J. J., Kwak, M., Ju, J., Kim, H. J., Lee, J. S. H., Wu, P.-H., Gilkes, D. M., Fan, R., & Wirtz, D. (2017). Synergistic IL-6 and IL-8 paracrine signalling pathway infers a strategy to inhibit tumour cell migration. *Nature Communications*, *8*(1), 15584. https://doi.org/10.1038/ncomms15584

Jockers, R., Delagrange, P., Dubocovich, M. L., Markus, R. P., Renault, N., Tosini, G., Cecon, E., & Zlotos, D. P. (2016). Update on melatonin receptors: IUPHAR Review 20. *British Journal of Pharmacology*, *173*(18), 2702–2725. https://doi.org/10.1111/bph.13536

Kinker, G. S., Oba-Shinjo, S. M., Carvalho-Sousa, C. E., Muxel, S. M., Marie, S. K. N., Markus, R. P., & Fernandes, P. A. (2016). Melatonergic system-based two-gene index is prognostic in human gliomas. *Journal of Pineal Research*, *60*(1), 84–94. https://doi.org/10.1111/jpi.12293

Klein, D. C., Ganguly, S., Coon, S., Weller, J. L., Obsil, T., Hickman, A., & Dyda, F. (2002). 14-3-3 Proteins and photoneuroendocrine transduction: role in controlling the daily rhythm in melatonin. *Biochemical Society Transactions*, *30*(4), 365–373. https://doi.org/10.1042/bst0300365

Kojima, H., Fujimiya, M., Matsumura, K., Nakahara, T., Hara, M., & Chan, L. (2004). Extrapancreatic insulin-producing cells in multiple organs in diabetes. *Proceedings of the National Academy of Sciences*, *101*(8), 2458–2463. https://doi.org/10.1073/pnas.0308690100

Lerner, A. B., Case, J. D., Takahashi, Y., Lee, T. H., & Mori, W. (1958). ISOLATION OF MELATONIN, THE PINEAL GLAND FACTOR THAT LIGHTENS MELANOCYTES [1]. *Journal of the American Chemical Society*, *80*(10), 2587–2587. https://doi.org/10.1021/ja01543a060

Li, Y., Li, S., Zhou, Y., Meng, X., Zhang, J.-J., Xu, D.-P., & Li, H.-B. (2017). Melatonin for the prevention and treatment of cancer. *Oncotarget*, *8*(24), 39896–39921. https://doi.org/10.18632/oncotarget.16379

Lissoni, P., Chilelli, M., Villa, S., Cerizza, L., & Tancini, G. (2003). Five years survival in metastatic non-small cell lung cancer patients treated with chemotherapy alone or chemotherapy and melatonin: a randomized trial. *Journal of Pineal Research*, *35*(1), 12–15.

Retrieved from http://www.ncbi.nlm.nih.gov/pubmed/12823608

Lissoni, P., Meregalli, S., Nosetto, L., Barni, S., Tancini, G., Fossati, V., & Maestroni, G. (1996). Increased Survival Time in Brain Glioblastomas by a Radioneuroendocrine Strategy with Radiotherapy plus Melatonin Compared to Radiotherapy Alone. *Oncology*, *53*(1), 43–46. https://doi.org/10.1159/000227533

Liu, J., Clough, S. J., Hutchinson, A. J., Adamah-Biassi, E. B., Popovska-Gorevski, M., & Dubocovich, M. L. (2016). MT1 and MT2 Melatonin Receptors: A Therapeutic Perspective. *Annual Review of Pharmacology and Toxicology*, *56*, 361–383. https://doi.org/10.1146/annurev-pharmtox-010814-124742

Lodish, H. F., Berk, A., Kaiser, C., Krieger, M., Scott, M. P., Bretscher, A., Ploegh, H. L., & Matsudaira, P. T. (2008). *Molecular cell biology*. Retrieved from http://125.234.102.146:8080/dspace/handle/DNULIB_52011/2575

Lotufo, C. M. ., Lopes, C., Dubocovich, M. L., Farsky, S. H. ., & Markus, R. P. (2001). Melatonin and N-acetylserotonin inhibit leukocyte rolling and adhesion to rat microcirculation. *European Journal of Pharmacology*, *430*(2–3), 351–357. https://doi.org/10.1016/S0014-2999(01)01369-3

Lund, A., & Knop, F. K. (2019). Extrapancreatic glucagon: Present status. *Diabetes Research and Clinical Practice*, *147*, 19–28. https://doi.org/10.1016/J.DIABRES.2018.06.013

Macosko, E. Z., Basu, A., Satija, R., Nemesh, J., Shekhar, K., Goldman, M., Tirosh, I., Bialas, A. R., Kamitaki, N., Martersteck, E. M., Trombetta, J. J., Weitz, D. A., Sanes, J. R., Shalek, A. K., Regev, A., & McCarroll, S. A. (2015). Highly Parallel Genome-wide Expression Profiling of Individual Cells Using Nanoliter Droplets. *Cell*, *161*(5), 1202–1214. https://doi.org/10.1016/j.cell.2015.05.002

Mao, L., Cheng, Q., Guardiola-Lemaître, B., Schuster-Klein, C., Dong, C., Lai, L., & Hill, S. M. (2010). In vitro and in vivo antitumor activity of melatonin receptor agonists. *Journal of Pineal Research*, *49*(3), 210–221. https://doi.org/10.1111/j.1600-079X.2010.00781.x

Marçola, M., da Silveira Cruz-Machado, S., Fernandes, P. A. C. M., Monteiro, A. W. A., Markus, R. P., & Tamura, E. K. (2013). Endothelial cell adhesiveness is a function of environmental lighting and melatonin level. *Journal of Pineal Research*, *54*(2), 162–169. https://doi.org/10.1111/j.1600-079X.2012.01025.x

Markus, R. P., Cecon, E., & Pires-Lapa, M. (2013). Immune-Pineal Axis: Nuclear Factor κB (NF-kB) Mediates the Shift in the Melatonin Source from Pinealocytes to Immune Competent Cells. *International Journal of Molecular Sciences*, *14*(6), 10979–10997. https://doi.org/10.3390/ijms140610979

Markus, R. P., Fernandes, P. A., Kinker, G. S., da Silveira Cruz-Machado, S., & Marçola, M. (2018). Immune-pineal axis - acute inflammatory responses coordinate melatonin synthesis by pinealocytes and phagocytes. *British Journal of Pharmacology*, *175*(16), 3239–3250. https://doi.org/10.1111/bph.14083

Markus, R. P., & Ferreira, Z. S. (2011). The Immune-Pineal Axis: the Role of Pineal and Extra-Pineal Melatonin in Modulating Inflammation. *Advances in Neuroimmune Biology*, *1*(1), 95–104. https://doi.org/10.3233/NIB-2011-009

Markus, R. P., Ferreira, Z. S., Fernandes, P. A. C. M., & Cecon, E. (2007). The Immune-Pineal Axis: A Shuttle between Endocrine and Paracrine Melatonin Sources. *Neuroimmunomodulation*, *14*(3–4), 126–133. https://doi.org/10.1159/000110635

Marusyk, A., Almendro, V., & Polyak, K. (2012). Intra-tumour heterogeneity: a looking glass for cancer? *Nature Reviews Cancer*, *12*(5), 323–334. https://doi.org/10.1038/nrc3261

McGranahan, N., & Swanton, C. (2015). Biological and Therapeutic Impact of Intratumor Heterogeneity in Cancer Evolution. *Cancer Cell*, *27*(1), 15–26. https://doi.org/10.1016/J.CCELL.2014.12.001

Morikawa, M., Derynck, R., & Miyazono, K. (2016). TGF-β and the TGF-β Family: Context-Dependent Roles in Cell and Tissue Physiology. *Cold Spring Harbor Perspectives in Biology*, *8*(5), a021873. https://doi.org/10.1101/cshperspect.a021873

Moses, H. L., Yang, E. Y., & Pietenpol, J. A. (1990). TGF-β stimulation and inhibition of cell proliferation: New mechanistic insights. *Cell*, *63*(2), 245–247. https://doi.org/10.1016/0092-8674(90)90155-8

Murtuza, A., Bulbul, A., Shen, J. P., Keshavarzian, P., Woodward, B. D., Lopez-Diaz, F. J., Lippman, S. M., & Husain, H. (2019). Novel Third-Generation EGFR Tyrosine Kinase Inhibitors and Strategies to Overcome Therapeutic Resistance in Lung Cancer. *Cancer Research*, *79*(4), 689–698. https://doi.org/10.1158/0008-5472.CAN-18-1281

Muxel, S. M., Laranjeira-Silva, M. F., Carvalho-Sousa, C. E., Floeter-Winter, L. M., & Markus, R. P. (2016). The RelA/cRel nuclear factor- κ B (NF- κ B) dimer, crucial for inflammation resolution, mediates the transcription of the key enzyme in melatonin synthesis in RAW 264.7 macrophages. *Journal of Pineal Research*, *60*(4), 394–404. https://doi.org/10.1111/jpi.12321

Muxel, S. M., Pires-Lapa, M. A., Monteiro, A. W. A., Cecon, E., Tamura, E. K., Floeter-Winter, L. M., & Markus, R. P. (2012). NF-κB Drives the Synthesis of Melatonin in RAW 264.7 Macrophages by Inducing the Transcription of the Arylalkylamine-N-Acetyltransferase (AA-NAT) Gene. *PLoS ONE*, *7*(12), e52010. https://doi.org/10.1371/journal.pone.0052010

Neftel, C., Laffy, J., Filbin, M. G., Hara, T., Shore, M. E., Rahme, G. J., Richman, A. R., Silverbush, D., Shaw, M. L., Hebert, C. M., Dewitt, J., Gritsch, S., Perez, E. M., Gonzalez Castro, L. N., Lan, X., Druck, N., Rodman, C., Dionne, D., Kaplan, A., Bertalan, M. S., Small, J., Pelton, K., Becker, S., Bonal, D., Nguyen, Q.-D., Servis, R. L., Fung, J. M., Mylvaganam, R., Mayr, L., Gojo, J., Haberler, C., Geyeregger, R., Czech, T., Slavc, I., Nahed, B. V., Curry, W. T., Carter, B. S., Wakimoto, H., Brastianos, P. K., Batchelor, T. T., Stemmer-Rachamimov, A., Martinez-Lage, M., Frosch, M. P., Stamenkovic, I., Riggi, N., Rheinbay, E., Monje, M., Rozenblatt-Rosen, O., Cahill, D. P., Patel, A. P., Hunter, T., Verma, I. M., Ligon, K. L., Louis, D. N., Regev, A., Bernstein, B. E., Tirosh, I., & Suvà, M. L. (2019). An Integrative Model of Cellular States, Plasticity, and Genetics for Glioblastoma. *Cell*, *178*(4), 835-849.e21. https://doi.org/10.1016/J.CELL.2019.06.024

Norman, A. W. (Anthony W. ., & Litwack, G. (1997). *Hormones*. Academic Press.

Nosjean, O., Ferro, M., Coge, F., Beauverger, P., Henlin, J. M., Lefoulon, F., Fauchere, J. L., Delagrange, P., Canet, E., & Boutin, J. A. (2000). Identification of the melatonin-binding site MT3 as the quinone reductase 2. *The Journal of Biological Chemistry*, *275*(40), 31311–31317. https://doi.org/10.1074/jbc.M005141200

Pao, W., & Chmielecki, J. (2010). Rational, biologically based treatment of EGFR-mutant non-small-cell lung cancer. *Nature Reviews Cancer*, *10*(11), 760–774. https://doi.org/10.1038/nrc2947

Pedreira, C. E., Costa, E. S., Lecrevisse, Q., van Dongen, J. J. M., & Orfao, A. (2013). Overview of clinical flow cytometry data analysis: recent advances and future challenges. *Trends in Biotechnology*, *31*(7), 415–425. https://doi.org/10.1016/J.TIBTECH.2013.04.008

Peng, J., Sun, B.-F., Chen, C.-Y., Zhou, J.-Y., Chen, Y.-S., Chen, H., Liu, L., Huang, D., Jiang, J., Cui, G.-S., Yang, Y., Wang, W., Guo, D., Dai, M., Guo, J., Zhang, T., Liao, Q., Liu, Y., Zhao, Y.-L., Han, D.-L., Zhao, Y., Yang, Y.-G., & Wu, W. (2019). Single-cell RNA-seq highlights

intra-tumoral heterogeneity and malignant progression in pancreatic ductal adenocarcinoma. *Cell Research*, *29*(9), 725–738. https://doi.org/10.1038/s41422-019-0195-y

Pietras, K., & Östman, A. (2010). Hallmarks of cancer: Interactions with the tumor stroma. *Experimental Cell Research*, *316*(8), 1324–1331. https://doi.org/10.1016/J.YEXCR.2010.02.045

Pinato, L., da Silveira Cruz-Machado, S., Franco, D. G., Campos, L. M. G., Cecon, E., Fernandes, P. A. C. M., Bittencourt, J. C., & Markus, R. P. (2015). Selective protection of the cerebellum against intracerebroventricular LPS is mediated by local melatonin synthesis. *Brain Structure & Function*, *220*(2), 827–840. https://doi.org/10.1007/s00429-013-0686-4

Pires-Lapa, M. A., Tamura, E. K., Salustiano, E. M. A., & Markus, R. P. (2013). Melatonin synthesis in human colostrum mononuclear cells enhances dectin-1-mediated phagocytosis by mononuclear cells. *Journal of Pineal Research*, *55*(3), 240–246. https://doi.org/10.1111/jpi.12066

Pires da Silva, A., & Sommer, R. J. (2003). The evolution of signalling pathways in animal development. *Nature Reviews Genetics*, *4*(1), 39–49. https://doi.org/10.1038/nrg977

Pontes, G. N., Cardoso, E. C., Carneiro-Sampaio, M. M. S., & Markus, R. P. (2006). Injury switches melatonin production source from endocrine (pineal) to paracrine (phagocytes) – melatonin in human colostrum and colostrum phagocytes. *Journal of Pineal Research*, *41*(2), 136–141. https://doi.org/10.1111/j.1600-079X.2006.00345.x

Pribluda, A., de la Cruz, C. C., & Jackson, E. L. (2015). Intratumoral Heterogeneity: From Diversity Comes Resistance. *Clinical Cancer Research : An Official Journal of the American Association for Cancer Research*, *21*(13), 2916–2923. https://doi.org/10.1158/1078-0432.CCR-14-1213

Puram, S. V., Tirosh, I., Parikh, A. S., Patel, A. P., Yizhak, K., Gillespie, S., Rodman, C., Luo, C. L., Mroz, E. A., Emerick, K. S., Deschler, D. G., Varvares, M. A., Mylvaganam, R., Rozenblatt-Rosen, O., Rocco, J. W., Faquin, W. C., Lin, D. T., Regev, A., & Bernstein, B. E. (2017). Single-Cell Transcriptomic Analysis of Primary and Metastatic Tumor Ecosystems in Head and Neck Cancer. *Cell*, *171*(7), 1611-1624.e24. https://doi.org/10.1016/J.CELL.2017.10.044

Quail, D. F., & Joyce, J. A. (2013). Microenvironmental regulation of tumor progression and metastasis. *Nature Medicine*, *19*(11), 1423–1437. https://doi.org/10.1038/nm.3394

Ramilowski, J. A., Goldberg, T., Harshbarger, J., Kloppmann, E., Lizio, M., Satagopam, V. P., Itoh, M., Kawaji, H., Carninci, P., Rost, B., & Forrest, A. R. R. (2015). A draft network of ligand–receptor-mediated multicellular signalling in human. *Nature Communications*, *6*(1), 7866. https://doi.org/10.1038/ncomms8866

Reczek, C. R., & Chandel, N. S. (2017). The Two Faces of Reactive Oxygen Species in Cancer. *Annual Review of Cancer Biology*, *1*(1), 79–98. https://doi.org/10.1146/annurev-cancerbio-041916-065808

Reiter, R. J. (1993). The melatonin rhythm: both a clock and a calendar. *Experientia*, *49*(8), 654–664. https://doi.org/10.1007/BF01923947

Ren, X., Kang, B., & Zhang, Z. (2018). Understanding tumor ecosystems by single-cell sequencing: promises and limitations. *Genome Biology*, *19*(1), 211. https://doi.org/10.1186/s13059-018-1593-z

Reppart, S. M., Weaver, D. R., & Godson, C. (1996). Melatonin receptors step into the light: cloning and classification of subtypes. *Trends in Pharmacological Sciences*, *17*(3), 100–102. https://doi.org/10.1016/0165-6147(96)10005-5

Roberts, A. B., & Wakefield, L. M. (2003). The two faces of transforming growth factor beta in carcinogenesis. *Proceedings of the National Academy of Sciences of the United States of America*, *100*(15), 8621–8623. https://doi.org/10.1073/pnas.1633291100

Sequist, L. V., Waltman, B. A., Dias-Santagata, D., Digumarthy, S., Turke, A. B., Fidias, P., Bergethon, K., Shaw, A. T., Gettinger, S., Cosper, A. K., Akhavanfard, S., Heist, R. S., Temel, J., Christensen, J. G., Wain, J. C., Lynch, T. J., Vernovsky, K., Mark, E. J., Lanuti, M., Iafrate, A. J., Mino-Kenudson, M., & Engelman, J. A. (2011). Genotypic and Histological Evolution of Lung Cancers Acquiring Resistance to EGFR Inhibitors. *Science Translational Medicine*, *3*(75), 75ra26-75ra26. https://doi.org/10.1126/scitranslmed.3002003

Sigismund, S., Avanzato, D., & Lanzetti, L. (2018). Emerging functions of the EGFR in cancer. *Molecular Oncology*, *12*(1), 3–20. https://doi.org/10.1002/1878-0261.12155

Simonneaux, V., & Ribelayga, C. (2003). Generation of the Melatonin Endocrine Message in Mammals: A Review of the Complex Regulation of Melatonin Synthesis by Norepinephrine, Peptides, and Other Pineal Transmitters. *Pharmacological Reviews*, *55*(2), 325–395. https://doi.org/10.1124/pr.55.2.2

Sookprasert, A., Johns, N. P., Phunmanee, A., Pongthai, P., Cheawchanwattana, A., Johns, J., Konsil, J., Plaimee, P., Porasuphatana, S., & Jitpimolmard, S. (2014). Melatonin in patients with cancer receiving chemotherapy: a randomized, double-blind, placebo-controlled trial. *Anticancer Research*, *34*(12), 7327–7337. Retrieved from http://www.ncbi.nlm.nih.gov/pubmed/25503168

Soria, J.-C., Ohe, Y., Vansteenkiste, J., Reungwetwattana, T., Chewaskulyong, B., Lee, K. H., Dechaphunkul, A., Imamura, F., Nogami, N., Kurata, T., Okamoto, I., Zhou, C., Cho, B. C., Cheng, Y., Cho, E. K., Voon, P. J., Planchard, D., Su, W.-C., Gray, J. E., Lee, S.-M., Hodge, R., Marotti, M., Rukazenkov, Y., & Ramalingam, S. S. (2018). Osimertinib in Untreated *EGFR* -Mutated Advanced Non–Small-Cell Lung Cancer. *New England Journal of Medicine*, *378*(2), 113–125. https://doi.org/10.1056/NEJMoa1713137

Suofu, Y., Li, W., Jean-Alphonse, F. G., Jia, J., Khattar, N. K., Li, J., Baranov, S. V, Leronni, D., Mihalik, A. C., He, Y., Cecon, E., Wehbi, V. L., Kim, J., Heath, B. E., Baranova, O. V, Wang, X., Gable, M. J., Kretz, E. S., Di Benedetto, G., Lezon, T. R., Ferrando, L. M., Larkin, T. M., Sullivan, M., Yablonska, S., Wang, J., Minnigh, M. B., Guillaumet, G., Suzenet, F., Richardson, R. M., Poloyac, S. M., Stolz, D. B., Jockers, R., Witt-Enderby, P. A., Carlisle, D. L., Vilardaga, J.-P., & Friedlander, R. M. (2017). Dual role of mitochondria in producing melatonin and driving GPCR signaling to block cytochrome c release. *Proceedings of the National Academy of Sciences of the United States of America*, *114*(38), E7997–E8006. https://doi.org/10.1073/pnas.1705768114

Tamura, E. K., Fernandes, P. A., Marçola, M., Cruz-Machado, S. da S., & Markus, R. P. (2010). Long-Lasting Priming of Endothelial Cells by Plasma Melatonin Levels. *PLoS ONE*, *5*(11), e13958. https://doi.org/10.1371/journal.pone.0013958

Tan, D.-X., Hardeland, R., Manchester, L. C., Paredes, S. D., Korkmaz, A., Sainz, R. M., Mayo, J. C., Fuentes-Broto, L., & Reiter, R. J. (2009). The changing biological roles of melatonin during evolution: from an antioxidant to signals of darkness, sexual selection and fitness. *Biological Reviews*, *85*(3), no-no. https://doi.org/10.1111/j.1469-185X.2009.00118.x

Tang, F., Barbacioru, C., Wang, Y., Nordman, E., Lee, C., Xu, N., Wang, X., Bodeau, J., Tuch, B. B., Siddiqui, A., Lao, K., & Surani, M. A. (2009). mRNA-Seq whole-transcriptome analysis of a single cell. *Nature Methods*, *6*(5), 377–382. https://doi.org/10.1038/nmeth.1315

Tirosh, I., Izar, B., Prakadan, S. M., Wadsworth, M. H., Treacy, D., Trombetta, J. J., Rotem, A.,

Rodman, C., Lian, C., Murphy, G., Fallahi-Sichani, M., Dutton-Regester, K., Lin, J.-R., Cohen, O., Shah, P., Lu, D., Genshaft, A. S., Hughes, T. K., Ziegler, C. G. K., Kazer, S. W., Gaillard, A., Kolb, K. E., Villani, A.-C., Johannessen, C. M., Andreev, A. Y., Van Allen, E. M., Bertagnolli, M., Sorger, P. K., Sullivan, R. J., Flaherty, K. T., Frederick, D. T., Jané-Valbuena, J., Yoon, C. H., Rozenblatt-Rosen, O., Shalek, A. K., Regev, A., & Garraway, L. A. (2016). Dissecting the multicellular ecosystem of metastatic melanoma by single-cell RNA-seq. *Science (New York, N.Y.)*, *352*(6282), 189–196. https://doi.org/10.1126/science.aad0501

Tirosh, I., & Suvà, M. L. (2019). Deciphering Human Tumor Biology by Single-Cell Expression Profiling. *Annu. Rev. Cancer Biol*. https://doi.org/10.1146/annurev-cancerbio-030518

Tirosh, I., Venteicher, A. S., Hebert, C., Escalante, L. E., Patel, A. P., Yizhak, K., Fisher, J. M., Rodman, C., Mount, C., Filbin, M. G., Neftel, C., Desai, N., Nyman, J., Izar, B., Luo, C. C., Francis, J. M., Patel, A. A., Onozato, M. L., Riggi, N., Livak, K. J., Gennert, D., Satija, R., Nahed, B. V., Curry, W. T., Martuza, R. L., Mylvaganam, R., Iafrate, A. J., Frosch, M. P., Golub, T. R., Rivera, M. N., Getz, G., Rozenblatt-Rosen, O., Cahill, D. P., Monje, M., Bernstein, B. E., Louis, D. N., Regev, A., & Suvà, M. L. (2016). Single-cell RNA-seq supports a developmental hierarchy in human oligodendroglioma. *Nature*, *539*(7628), 309–313. https://doi.org/10.1038/nature20123

Vacchio, M. S., Papadopoulos, V., & Ashwell, J. D. (1994). Steroid production in the thymus: implications for thymocyte selection. *Journal of Experimental Medicine*, *179*(6), 1835–1846. https://doi.org/10.1084/jem.179.6.1835

Venegas, C., García, J. A., Escames, G., Ortiz, F., López, A., Doerrier, C., García-Corzo, L., López, L. C., Reiter, R. J., & Acuña-Castroviejo, D. (2012). Extrapineal melatonin: analysis of its subcellular distribution and daily fluctuations. *Journal of Pineal Research*, *52*(2), 217–227. https://doi.org/10.1111/j.1600-079X.2011.00931.x

Venteicher, A. S., Tirosh, I., Hebert, C., Yizhak, K., Neftel, C., Filbin, M. G., Hovestadt, V., Escalante, L. E., Shaw, M. L., Rodman, C., Gillespie, S. M., Dionne, D., Luo, C. C., Ravichandran, H., Mylvaganam, R., Mount, C., Onozato, M. L., Nahed, B. V, Wakimoto, H., Curry, W. T., Iafrate, A. J., Rivera, M. N., Frosch, M. P., Golub, T. R., Brastianos, P. K., Getz, G., Patel, A. P., Monje, M., Cahill, D. P., Rozenblatt-Rosen, O., Louis, D. N., Bernstein, B. E., Regev, A., & Suvà, M. L. (2017). Decoupling genetics, lineages, and microenvironment in IDH-mutant gliomas by single-cell RNA-seq. *Science (New York, N.Y.)*, *355*(6332), eaai8478. https://doi.org/10.1126/science.aai8478

Wang, J., Hao, H., Yao, L., Zhang, X., Zhao, S., Ling, E.-A., Hao, A., & Li, G. (2012). Melatonin suppresses migration and invasion via inhibition of oxidative stress pathway in glioma cells. *Journal of Pineal Research*, *53*(2), 180–187. https://doi.org/10.1111/j.1600-079X.2012.00985.x

Waugh, D. J. J., & Wilson, C. (2008). The Interleukin-8 Pathway in Cancer. *Clinical Cancer Research*, *14*(21), 6735–6741. https://doi.org/10.1158/1078-0432.CCR-07-4843

Wei, J. Y., Li, W. M., Zhou, L. L., Lu, Q.-N., & He, W. (2015). Melatonin induces apoptosis of colorectal cancer cells through HDAC4 nuclear import mediated by CaMKII inactivation. *Journal of Pineal Research*, *58*(4), 429–438. https://doi.org/10.1111/jpi.12226

Yan, J. J., Shen, F., Wang, K., & Wu, M. C. (2002). Patients with advanced primary hepatocellular carcinoma treated by melatonin and transcatheter arterial chemoembolization: a prospective study. *Hepatobiliary & Pancreatic Diseases International : HBPD INT*, *1*(2), 183–186. Retrieved from http://www.ncbi.nlm.nih.gov/pubmed/14607735

Yates, L. R., Gerstung, M., Knappskog, S., Desmedt, C., Gundem, G., Van Loo, P., Aas, T., Alexandrov, L. B., Larsimont, D., Davies, H., Li, Y., Ju, Y. S., Ramakrishna, M., Haugland, H. K., Lilleng, P. K., Nik-Zainal, S., McLaren, S., Butler, A., Martin, S., Glodzik, D., Menzies, A., Raine, K., Hinton, J., Jones, D., Mudie, L. J., Jiang, B., Vincent, D., Greene-Colozzi, A., Adnet, P.-Y., Fatima, A., Maetens, M., Ignatiadis, M., Stratton, M. R., Sotiriou, C., Richardson, A. L., Lønning, P. E., Wedge, D. C., & Campbell, P. J. (2015). Subclonal diversification of primary breast cancer revealed by multiregion sequencing. *Nature Medicine*, *21*(7), 751–759. https://doi.org/10.1038/nm.3886

Zhang, P., Yang, M., Zhang, Y., Xiao, S., Lai, X., Tan, A., Du, S., & Li, S. (2019). Dissecting the Single-Cell Transcriptome Network Underlying Gastric Premalignant Lesions and Early Gastric Cancer. *Cell Reports*, *27*(6), 1934-1947.e5. https://doi.org/10.1016/j.celrep.2019.04.052

Zhao, D., Yu, Y., Shen, Y., Liu, Q., Zhao, Z., Sharma, R., & Reiter, R. J. (2019). Melatonin Synthesis and Function: Evolutionary History in Animals and Plants. *Frontiers in Endocrinology*, *10*, 249. https://doi.org/10.3389/fendo.2019.00249

Zhou, C., Wu, Y.-L., Chen, G., Feng, J., Liu, X.-Q., Wang, C., Zhang, S., Wang, J., Zhou, S., Ren, S., Lu, S., Zhang, L., Hu, C., Hu, C., Luo, Y., Chen, L., Ye, M., Huang, J., Zhi, X., Zhang, Y., Xiu, Q., Ma, J., Zhang, L., & You, C. (2011). Erlotinib versus chemotherapy as first-line treatment for patients with advanced EGFR mutation-positive non-small-cell lung cancer (OPTIMAL, CTONG-0802): a multicentre, open-label, randomised, phase 3 study. *The Lancet Oncology*, *12*(8), 735–742. https://doi.org/10.1016/S1470-2045(11)70184-X

Attachment I - Animal ethics approval certificate - CEUA IBUSP

USP Universidade de São Paulo

Instituto de Biociências

www.ib.usp.br

CERTIFICADO

Certificamos que a proposta intitulada **"Caracterização do sistema melatonérgico de gliomas humanos e sua implicação sobre o grau de malignidade tumoral"**, registrada com o nº 284/2017, sob a responsabilidade da do Prof. Dr. Pedro Augusto Carlos Magno Fernandes e com a participação dos colaboradores Gabriela Sarti Kinker (IB/USP), Regina Pekelmann Markus (IB/USP), Tiago Goss dos Santos (A.C.Camargo Câncer Center/Fundação Antônio Prudente (FAP), e Vilma Regina Martins (A.C.Camargo Câncer Center/Fundação Antônio Prudente (FAP), que envolve a produção, manutenção ou utilização de animais pertencentes ao filo Chordata, subfilo Vertebrata (exceto humanos), para fins de pesquisa científica encontra-se de acordo com os preceitos da Lei nº 11.794, de 08 de outubro de 2008, do Decreto nº 6.899, de 15 de julho de 2009 e com as normas editadas pelo Conselho Nacional de Controle da Experimentação Animal (CONCEA), e foi aprovada pela Comissão de Ética no Uso de Animais – CEUA do Instituto de Biociências da Universidade de São Paulo, em reunião de 09 de maio de 2017.

Vigência da autorização: 09/05/2017 a 08/05/2020

Finalidade: Pesquisa Científica

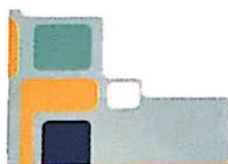**Espécie/linhagem:** Camundongo heterogênico/ Balb/c nude

Nº de animais: 28 (M) e 28 (F)   **Total:** 56 animais
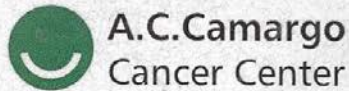
Peso: não informado   **Idade:** não informado

Origem: animais adquiridos do Charles River Laboratories International, as colônicas estão estabelecidas no próprio biotério.

OBS.: Qualquer alteração e/ou intercorrência deverá ser comunicada a CEUA-IB.

Profa. Dra. Maria Vainzof
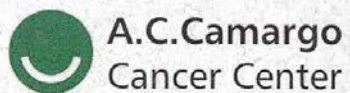Coordenadora da Comissão de Ética no Uso de Animais

Rua do Matão • Travessa 14 • nº 321 • Cidade Universitária • São Paulo • SP • CEP 05508-090 • Brasil

Attachment II - Animal ethics approval certificate - CEUA A.C. Camargo

A.C.Camargo
Cancer Center

CEUA/FAP
COMISSÃO DE ÉTICA NO USO DE ANIMAIS DA
FUNDAÇÃO ANTÔNIO PRUDENTE

PARECER CONSUBSTANCIADO

Ref. Projeto de Pesquisa nº CEUA 076/17

Título: Caracterização do sistema melatonérgico de gliomas humanos e sua implicação sobre o grau de malignidade tumoral

Pesquisador responsável: Tiago Goss dos Santos

Executor: Tiago Goss do Santos (pesquisador proponente), Pedro Augusto Carlos Magno Fernandes (pesquisador colaborador), Gabriela Sarti Kinker (doutoranda colaboradora)

APRECIAÇÃO GERAL

Consultamos o veterinário Bruno Roque, membro suplente do CEUA, sobre as doses de analgésicos pós-cirurgia propostos no projeto. Ele considera que:

Somente o Tramadol seja insuficiente no controle da dor. A manipulação de calota craniana gera edema de meninges que causam desconforto agudo e sinas neurológicos transitórios que variam de ataxia a convulsões. Sugiro que associem a Dexametasona na dose de 1 mg/kg - a ampola apresenta concentração de 2mg/ml. Segue abaixo um exemplo de diluição: 1ml de Dexametasona (2mg) em 9 ml de agua para injeção, criando uma concentração de 0,2mg/ml - peso aproximado do camundongo 0,023kg x 1mg/kg Dexametasona = 0,023mg dividido pela concentração 0,2mg/ml = 0,11ml volume final. Acredito que a analgesia (Tramadol e Dexa) deva ser feita a cada 12 horas por dois dias pelo menos.

Sugerimos que sejam incluídos 9 animais em cada grupo experimental (3 animais por grupo por etapa, totalizando 21 animais por etapa) totalizando 63 animais (sendo 32 machos e 32 fêmeas). O organograma na página 10 do projeto deve ser modificado para refletir essa alteração.
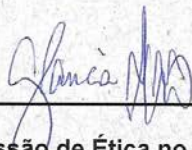
Parecer referente a Reunião da CEUA de

A.C.Camargo Cancer Center

CEUA/FAP
COMISSÃO DE ÉTICA NO USO DE ANIMAIS DA FUNDAÇÃO ANTÔNIO PRUDENTE

De acordo com o parecer supracitado, consideramos o projeto aprovado.

Descrição dos animais aprovados (linhagem/quantidade/sexo):

64 animais Balb/c (nude), 8-10 semanas:
32 machos
32 fêmeas

Coordenadora da Comissão de Ética no Uso de Animais
Dra. Glaucia j Noeli Maroso Hajj

Parecer referente a Reunião da CEUA de